UNIVERSITÀ DEGLI STUDI DI PADOVA

Dipartimento di Ingegneria Civile, Edile e Ambientale - DICEA

Corso di Laurea Magistrale in Environmental Engineering

Michela Carrer

LOCAL SITE SEISMIC RESPONSE IN AN ALPINE VALLEY: SEISMIC MICROZONATION OF THE CASTEL CALDES AREA (NORTH-WESTERN TRENTINO)

A.A. 2012/2013

Relatore:

Prof.ssa Silvana Martin

Correlatori:

Dott. Alfio Viganò

Dott. Jacopo Boaga

Fabio Fedrizzi

To Anna, Daniele and Carla.

Table of contents

I would like to express my very sincere gratitude to my supervisor Professor Silvana Martin.
I also thank Dr. Alfio Viganò, Dr. Jacopo Boaga and Fabio Fedrizzi because with their comments, criticisms and suggestions have contributed to the drafting of this thesis.

Abstract

The purpose of this work is to analyse the local-site seismic response in the Castel Caldes area, located in an alpine valley (Val di Sole) of the north-western Trentino region. The final result is the seismic microzonation map of this area. The seismic microzonation aims to characterize at a small scale two contiguous localities in which the seismic motion is amplified (and how), due to the lithostratigraphic and geomorphological specific characteristics. Seismic microzonation is based on multidisciplinary studies, in order to study a territory in detail, integrating data derived from geology, geomorphology, geophysics and geotechnics.

The following steps were carried out to achieve the aims mentioned above:

1. identification of the geological, geomorphological and structural settings;
2. subsoil schematization by the analysis of stratigraphic and geophysical data;
3. soil geotechnical study for determination of their dynamic response parameters;
4. evaluation of the input seismic motion;
5. numerical modelling to estimate possible amplification effects of the seismic motion at the surface (one-dimensional analysis);
6. presentation of a synthetic map with the obtained results.

The numerical modelling was carried out in two localities (Caldes and Samoclevo), assuming a plane-parallel layer deep structure in each site. Caldes and Samoclevo are located downstream and upstream the Castel Caldes castle, respectively. These two sites show significantly different lithostratigraphy and deep structure. The zone of transition between Caldes and Samoclevo, that cannot be analysed by using one-dimensional analyses, is going to be studied through advanced two-dimensional approaches.

The obtained results, expressed in terms of spectral acceleration, amplification ratio function, and Housner amplification factors, are compared with those obtained according to the simplified approach proposed by the Italian building code. The seismic action (considering local amplification) at the surface determined following the simplified approach is significantly underestimated at low periods ($0.1 - 0.5\ s$). The amplifications obtained are different in the two sites: in Caldes the amplification is high (Housner amplification factor equal to 1.80 at low periods), in Samoclevo there is no amplification.

This study shows how integrated multidisciplinary studies are able to obtain more detailed and site-specific seismic response analyses.

Riassunto

Lo scopo di questo lavoro è quello di analizzare la risposta sismica locale della zona di Castel Caldes, situata in una vallata alpina (Val di Sole) del Trentino nord-occidentale. Il risultato finale è la mappa di microzonazione sismica di questa zona. La microzonazione sismica ha l'obiettivo di caratterizzare a piccola scala due località contigue nelle quali il moto sismico viene amplificato (e come), a causa delle specifiche caratteristiche litostratigrafiche e geomorfologiche. La microzonazione sismica si basa su studi multidisciplinari al fine di caratterizzare un territorio in modo dettagliato, integrando dati geologici, geomorfologici, geofisici e geotecnici.

Lo scopo sopra citato è stato conseguito svolgendo i seguenti passaggi:

1. identificazione degli assetti geologico, geomorfologico e strutturale;
2. schematizzazione del sottosuolo mediante l'analisi dei dati stratigrafici e geofisici;
3. studio geotecnico dei terreni per la determinazione dei loro parametri dinamici;
4. valutazione del moto sismico di input;
5. modellazione numerica per stimare i possibili effetti di amplificazione del moto sismico in superficie (analisi monodimensionale);
6. presentazione di una mappa sintetica con i risultati ottenuti.

La modellazione numerica è stata condotta in due località (Caldes e Samoclevo), ipotizzando in ciascun sito una struttura profonda a strati piano-paralleli. Caldes e Samoclevo si trovano rispettivamente a valle ed a monte di Castel Caldes. Questi due siti sono molto differenti in termini litostratigrafici e di struttura profonda. La zona di transizione tra Caldes e Samoclevo, che non può essere analizzata mediante analisi monodimensionali, sta per essere studiata attraverso avanzati approcci bidimensionali.

I risultati ottenuti, espressi in termini di accelerazione spettrale, funzione del rapporto di amplificazione e fattori di amplificazione di Housner, sono confrontati con quelli ottenuti secondo l'approccio semplificato proposto dalla normativa italiana. L'azione sismica in superficie (considerando l'amplificazione locale) determinata seguendo l'approccio semplificato è significativamente sottostimata a bassi periodi ($0.1 - 0.5\ s$). Le amplificazioni ottenute nei due siti sono diverse: a Caldes l'amplificazione è elevata (fattore di amplificazione di Housner pari a 1.80 a bassi periodi), a Samoclevo non c'è amplificazione.

Questo studio mostra come mediante studi multidisciplinari integrati è possibile ottenere analisi di risposta sismica più dettagliate e specifiche per il sito considerato.

Presentation and outline of the thesis

This thesis evaluates the effects of a possible seismic action in the Castel Caldes area (Val di Sole, Trentino, NE Italy). This problem concerns the study of the local-site seismic response by means of site-specific analyses. Rules and prescriptions established by the Italian building code (DM 14/01/2008) and by the Seismic microzonation addresses and criteria (SM Working Group, 2008) were followed.
The thesis is structured as follows.

Chapter 1: Introduction.
Introduction of the study area from geographical, geomorphological, geological, structural and stratigraphic points of view. A descriptive part concerning the seismic microzonation and regulatory references on which it is based will follow.

Chapter 2: Deep structure and seismic properties.
It regards the modelling of the subsurface starting from geophysical campaigns. The geophysical methods used in the study area and how the subsoil has been schematized on the basis of these data and on the stratigraphies are explained.

Chapter 3: Dynamic properties of soils.
Firstly there is a theoretical introduction concerning the dynamic parameters of the soils (shear modulus and damping). Afterwards the laboratory methods used to determine their decay curves are described.

Chapter 4: Local site response.
It starts with the theoretical treatment of the analyses of the seismic response, and then it describes how they are regulated by the Italian building code. Subsequently there are numerical analyses performed with one-dimensional approach, with discussion of the results. The two-dimensional approach is also sketched out because there are studies on-going.

Chapter 5. Conclusions.
It summarizes the main aspects of the study and the obtained results.

Chapter 1

Introduction

1.1 Geological overview

1.1.1 Geography and geomorphology

Caldes is a municipality of just over 1000 inhabitants in Val di Sole, in the province of Trento, in the Trentino Alto Adige region (north-eastern Italy) (Figure 1.1).

It is located at coordinates $46°22'0"\ N$ and $10°57'0"\ E$, at an altitude of $697\ m$ above sea level and covers an area of 20 km^2.

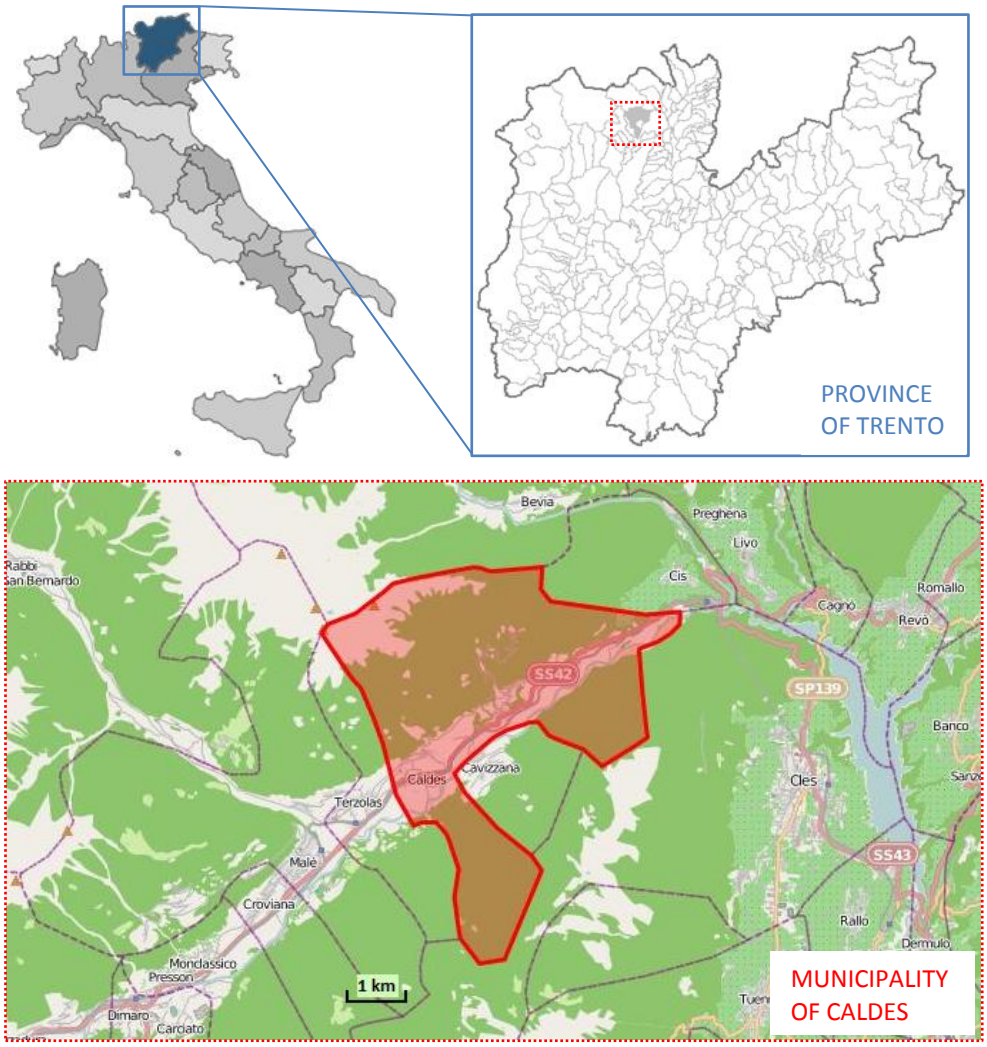

Figure 1.1. Location of the study area.

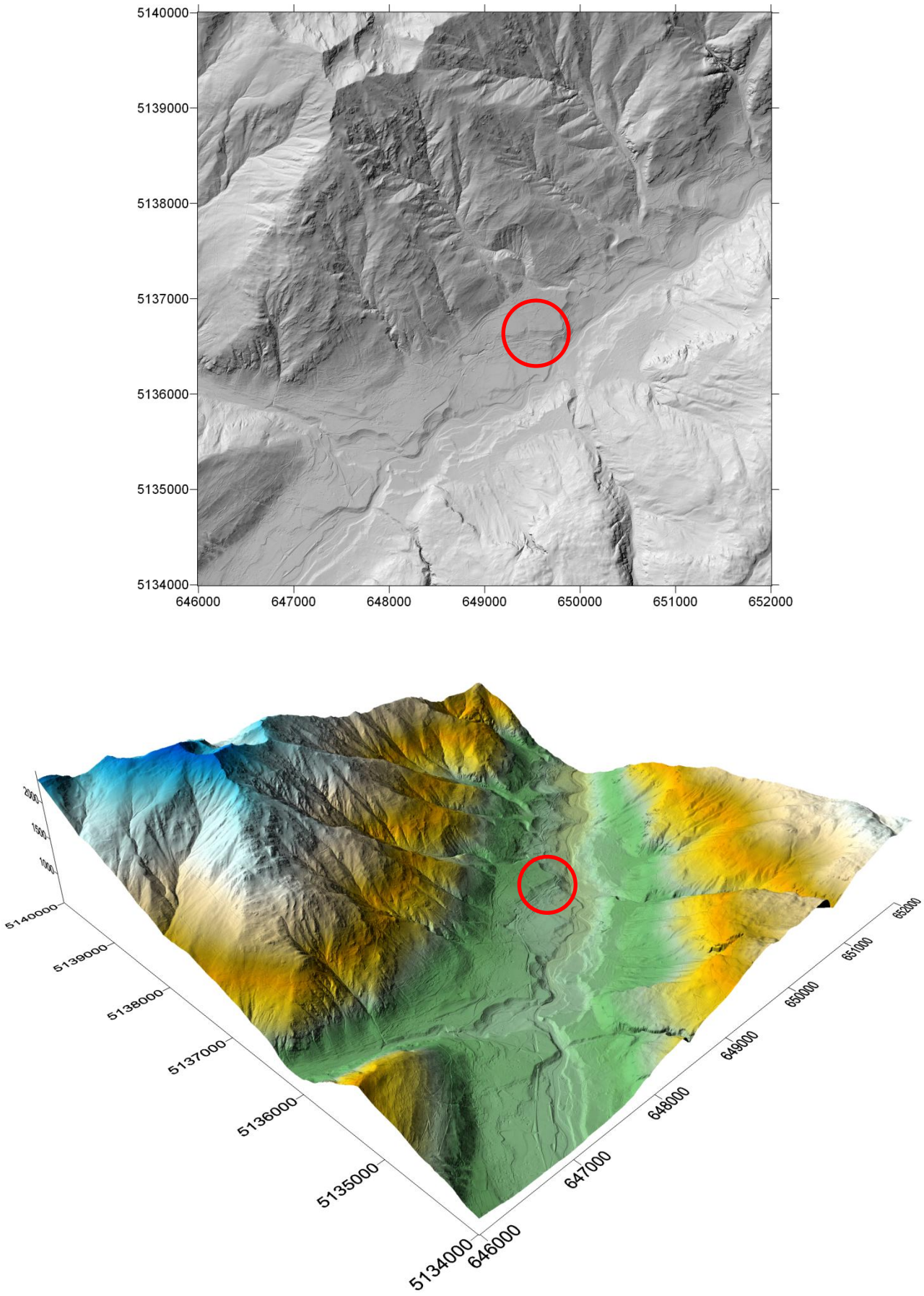

Figure 1.2. Identification of the study area in 2D and 3D georeferenced images (Reference system WGS84).

It includes the localities of Bordiana, Bozzana, Cassana Samoclevo, San Giacono, Tozzaga and is bordered by Bresimo, Cavizzana, Cis, Cles, Male, Terzolas. It is located a few km away from Malè, the main town of the Val di Sole.

The study area is represented in 2D and 3D georeferenced images of the Figure 1.2 and in the Geological Map of Italy at scale 1:50,000 in the Malè sheet (Appendix 1).

In the Malè sheet there are three big mountain Groups: the Group of Cima Mezzana (2,845 m) to the North, the Group of the Brenta Dolomites (Cima di Pietra Grande, 2,937 m) to the East, the northern offshoots of the Adamello-Presanella Group (Cima d'Amola, 3,260 m) to the South-West. They are separated by a hydrographic network quite articulated, characterized by two main valleys of tectonic origin:

- the Val di Sole and its extension to the Tonale Pass (Val Vermiglio), with a prevailing direction ENE-WSW;
- the Val Meledrio and its southern extension in Val di Campiglio, with a prevailing direction NNE-SSW.

Most of the rivers of the region pertains to the hydrographic basin of the Noce torrent (mean discharge $40\ m^3/s$, Martin and Zambotti, 2012), right tributary of the Adige river. Only the torrents that flow to the south, beyond the watershed that ranges from Cima d'Amola to Cima Vagliana, confluence into the torrent Sarca di Campiglio, bringing their waters to the hydrographic basin of the Garda Lake. Are right tributary of the Noce torrent, the Noce Bianco (Val di Peio) and the Rabbies torrent (Val di Rabbi), which reaches the Noce torrent at Malé.

Are present numerous springs, mainly distributed along the fault zones. The average flow of the springs do not exceed $10 - 15\ l/s$. They are sources related to surface aquifers, located in the cortical part of the fractured bedrock or on loose deposits (Martin and Zambotti, 2012).

The erosion of Pleistocene glaciers has certainly helped to shape the slopes and the bottom of the valleys that, in several places, have the typical glacial shape. The Val di Sole, between the valleys here mentioned by name, is the most important for amplitude of the basin, abundance of water and population density. It is a large glacial valley set along the Tonale line. It has steep slopes and wide valley bottom, occupied at the withdrawal of glaciers by large accumulations of alluvial deposits and mass transport. The E-W trending, longitudinally with respect the Alps chain, highlights the morphological and vegetational contrasts of the two sides, with a clear predominance of forest on the southern slope, largely covered by glacial deposits, compared to the opposite slope, where the crops are widespread and the glacial deposits are relatively few.

The annual rainfall in Val di Sole is on average around 1000 mm for the valley bottom, with peaks in spring and autumn. The snow is normally continuous from December to March (Dal Piaz et al., 2007).

1.1.2 Geology

The region included in Malè sheet has a very complex stratigraphic and structural setting characterized by the presence of the tectonic boundary between the sedimentary sequences of the Southern Alps and the Austroalpine domain basement, divided by two segments of the Insubric (or Periadriatic) line (Figure 1.2): the Tonale and the North Giudicarie lines.

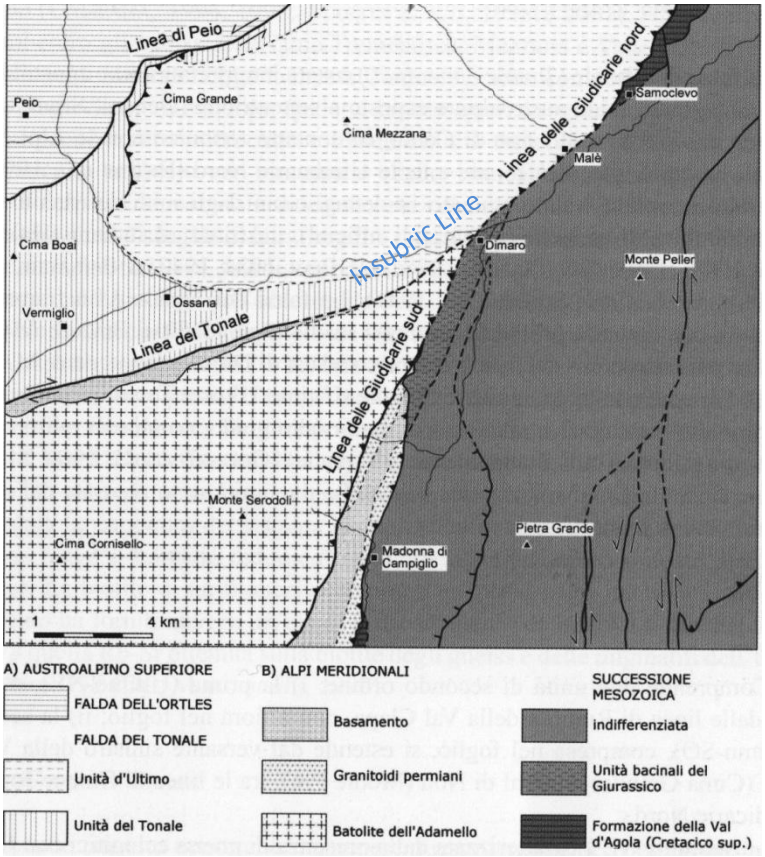

Figure 1.3: tectonic scheme of the Malè sheet. A) Upper Austroalpine, B) Southern Alps (Dal Piaz et al., 2007).

In the north-western part of the region the southern stretch of the collisional Europe-verging chain emerges, represented by tecto-metamorphic units of the Upper Austroalpine system characterized by the crystalline basement. In the south-eastern part of the region, the northern sector of the Southern Alps crops out, characterized by the sedimentary sequences of the Brenta Group (Figure 1.3). In both cases they are derived from the passive margin of the Adriatic microplate, collided

with the European margin during the Alpine orogeny. In particular, the Upper Austroalpine is constituted by units of lower and medium-upper crust. The Southern Alps are composed of a basement with pre-Permian metamorphism of low to medium grade, of Permian igneous rocks, of Meso-Cenozoic succession of the Brenta Dolomites and of the Presanella tonalitic pluton (Oligocene). The line of the South Giudicarie, internal to the Southern Alps, separates the Adamello batholith from the Mesozoic-Cenozoic covers of the Brenta Group (Dal Piaz et al., 2007).

1.1.3 Structural setting

In Trentino region, the Giudicarie fault zone is a first-order deformation zone representing a discontinuity at crustal scale. This zone is characterized by the presence of three main tectonic systems, the ENE-WSW Valsugana, the NNE-SSW Giudicarie and the NW-SE Schio–Vicenza fault systems (Figure 1.4), which acted in different times during the Giudicarie fault zone polyphase deformation history since the Late Permian (Viganò et al., 2013a).
In the Brenta Group, the faults control the evolution of karst networks (Martin and Zambotti, 2012).

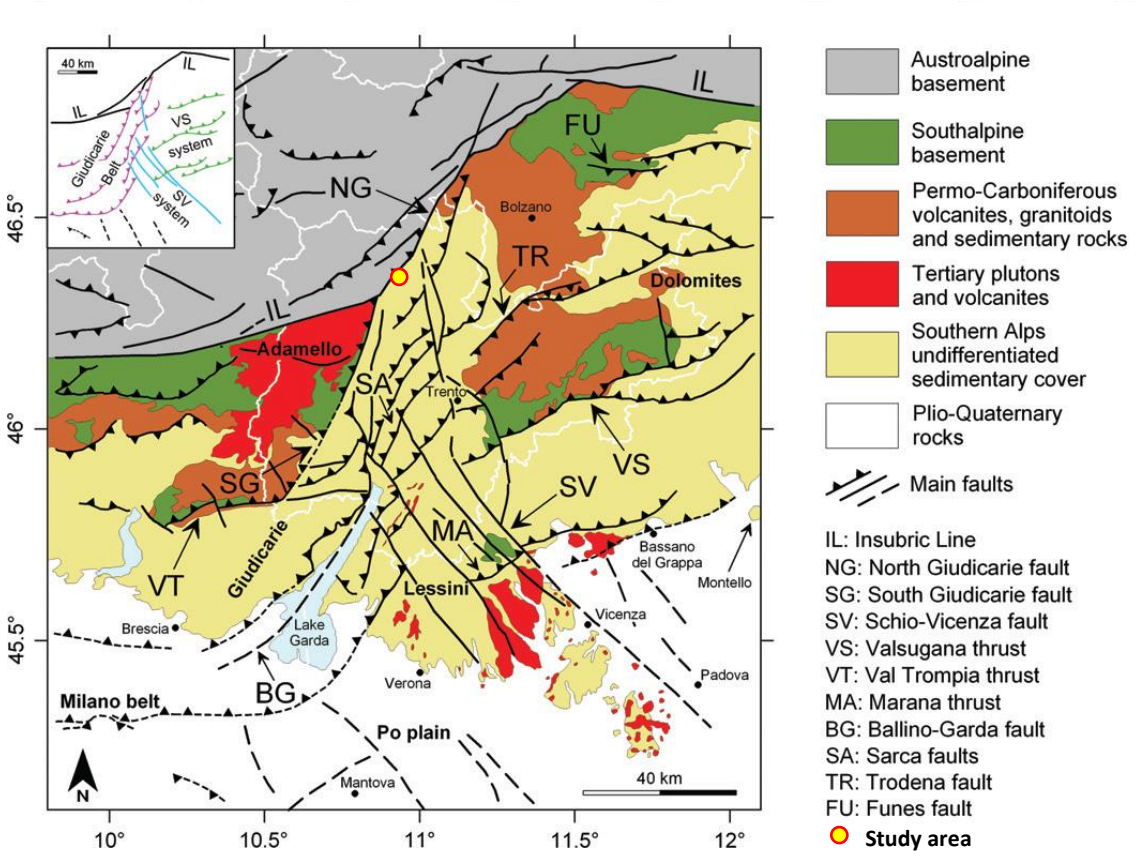

Figure 1.4. Simplified geological and structural map of the Trentino region with identification of the study area. In the upper-left inset, the three Valsugana (VS), Giudicarie and Schio–Vicenza (SV) regional tectonic systems (Viganò et al., 2013a).

The area around Caldes is characterized by the presence of three major fault systems: the Tonale (ENE-WSW orientation), the Giudicarie (NNE-SSW orientation) and the Trento-Cles (N-S orientation) fault system. The study area is located in a strongly deformed zone and near the conjunction of three faults (Tonale, North Giudicarie and South Giudicarie). Moreover, it is close to the separation between the crystalline basement and sedimentary sequences, which implies the presence of edge effects.

The knowledge of these information is so important because the seismic response in a rock mass ridge can be affected by rock mass jointing: adjacent rock masses with significantly different jointing and specific geometries seem to favour trapped wave amplification, if persistency along depth of these characteristics occurs (Martino et al., 2006).

Marzorati et al., 2011, on the occasion of a study on the site effects in a village occurred during the earthquake of L'Aquila (2009), had noted that the amplification effects are increased by the presence of fault zones due to rock mass jointing. Ground motion amplification have been identified in portion of the ridge where the bedrock is affected by open joints and fractures related to the main structural features that affect the area. In particular, the trend of ground motion amplification is parallel to the opening direction of the fractures. These observations suggest that the damage related to the earthquakes can also related to the local geological characteristics of the area and, in particular, to the style of deformation.

Moreover, due to the presence of lithological changes, the same seismic input can have different characteristics in dependence on where it comes from.

1.1.4 Stratigraphy

- **Basement**

The area of Caldes is characterized by sedimentary sequences, mainly of carbonate rocks of Middle Triassic age (Viganò et al., 2013a).

Figure 1.5 shows a section perpendicular to the Val di Sole in order to see the stratigraphic sequence of the basement. Although situated more to the North (between San Giacomo e Tozzaga) it can be considered representative of the study area.

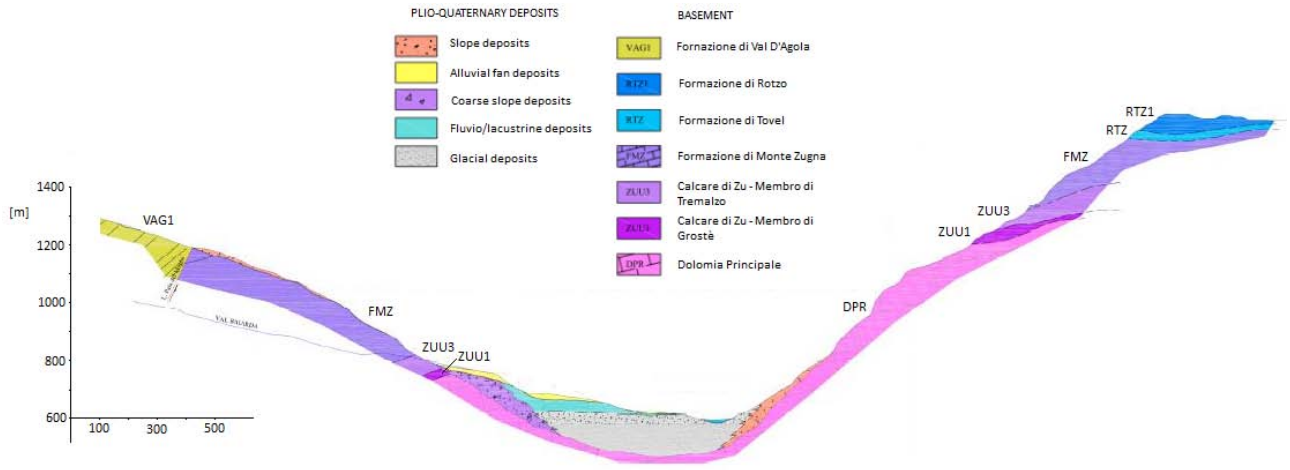

Figure 1.5 Section WSW-ENE between san Giacomo and Tozzaga (Modified from Martin and Zambotti, 2012).

Below the Quaternary deposits, on the eastern side the Formazione di Monte Zugna (FMZ) crops out, it belongs to the group of Calcari Grigi. Below there is the Calcari di Zu (ZUU3, ZUU1) and the Dolomia Principale (DP). The valley bottom is engraved on the Dolomia principale.
Since to the east emerges the complete stratigraphic succession, up to the Scaglia Rossa (SAA) belonging to the Cretaceous-Eocene age (visible in the geological map, not in the section of the Figure 1.5), it means that in the study area the more recent formations have been eroded.

- **Plio-Quaternary deposits**

The presence for long periods of the Pleistocene of extensive glacial areas (Figure 1.6) has strongly influenced the characteristics of the Val di sole Quaternary sediments. In fact, the slopes of the valleys are mostly covered by glacial deposits and more rarely by moraine. The glacial deposits of the Late Glacial and Holocene times are found only at the head of the valleys, in the vicinity of the existing glacier fronts. The first form frontal or lateral moraines, while the latter constitute small alluvial plains or fluvioglacial cones of small extension.
The lower part of the valley slopes is covered with large deposits and debris cones leaning on the flat alluvial plains, constituted by small plains or by extensive alluvial fans which often occupy the entire valley bottom. Most of the alluvial fans was formed because of the mass transport of steep torrents that connect the upper part of the slopes to the valley floor, through deep incisions. The waters have produced extensive colluvial bands that are found both along slightly sloping sides, both on the valley bottom, where they represent a transition between the slopes covered by glacial deposits and the cones, or floodplains. The crioclastic deposits give rise to a nearly continuous coverage at the foot of the rock walls above the treeline, most frequent in the correspondence of the

numerous detritic bands present in the area. The rock glaicer are widespread particularly in upper valleys located on the north-facing slopes of the Presanella Group.

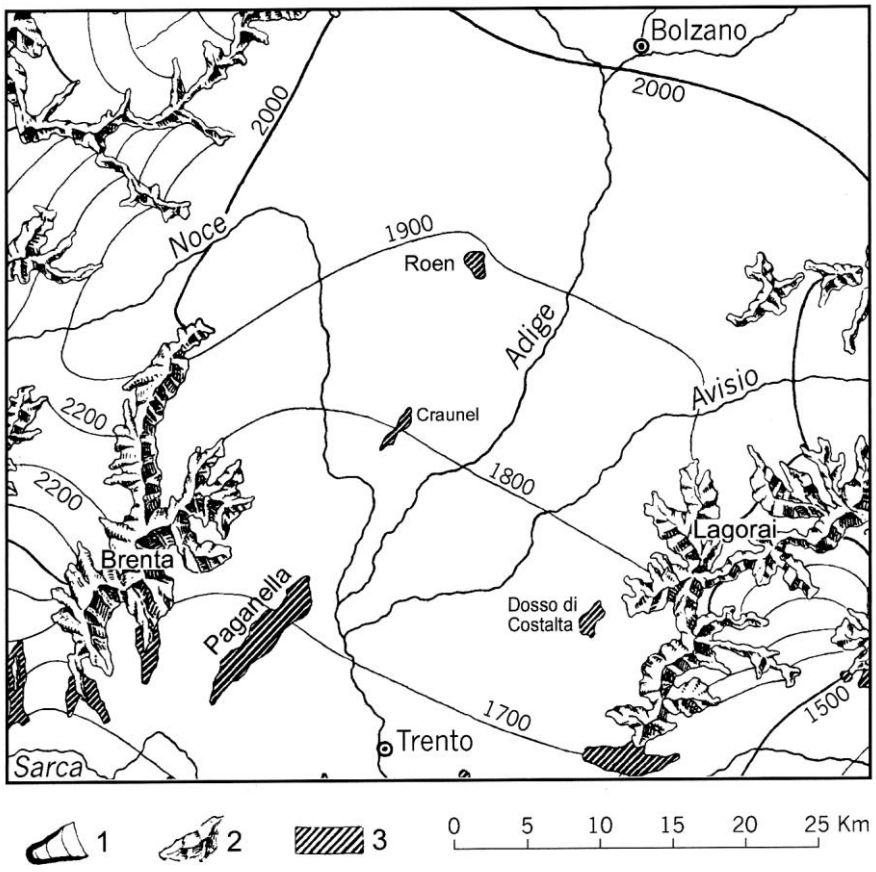

Fig. 54 – *Ricostruzione della posizione raggiunta dai ghiacciai durante il Würm secondo* PENCK *&* BRÜCKNER *(1909, modificato). Legenda: 1) ghiacciai vallivi del Würm (isoipse della superficie glaciale ad intervalli di 100 m); 2) creste spartiacque con copertura nevosa; 3) zone montuose non coperte dai ghiacci.*

Figure 1.6. Reconstruction of the position of the glaciers reached during the Würm (Avanzini et al., 2010).

The glacial valleys typically have the terrace-shaped, often suspended on the main valley and contains short fluvio-glacial plains.

On the base of the ages and shapes, the Quaternary deposits belong mainly to the Late Pleistocene and Holocene, with the presence of some important outcrops of deposits preceding the last glacial expansion. In particular, both sides of the Val di Sole are largely covered, down to the valley bottom, by deposits of the glaciers of the last expansion or those immediately following (Dal Piaz et al., 2007).

The area of Caldes is covered by this type of deposits, as can be seen in the geological map reported in Figure 1.7. These belong to the Malè sub-Synthem (SDG1) of the Garda Synthem (SDG) and to the post-glacial Alpine Synthem (PTG).

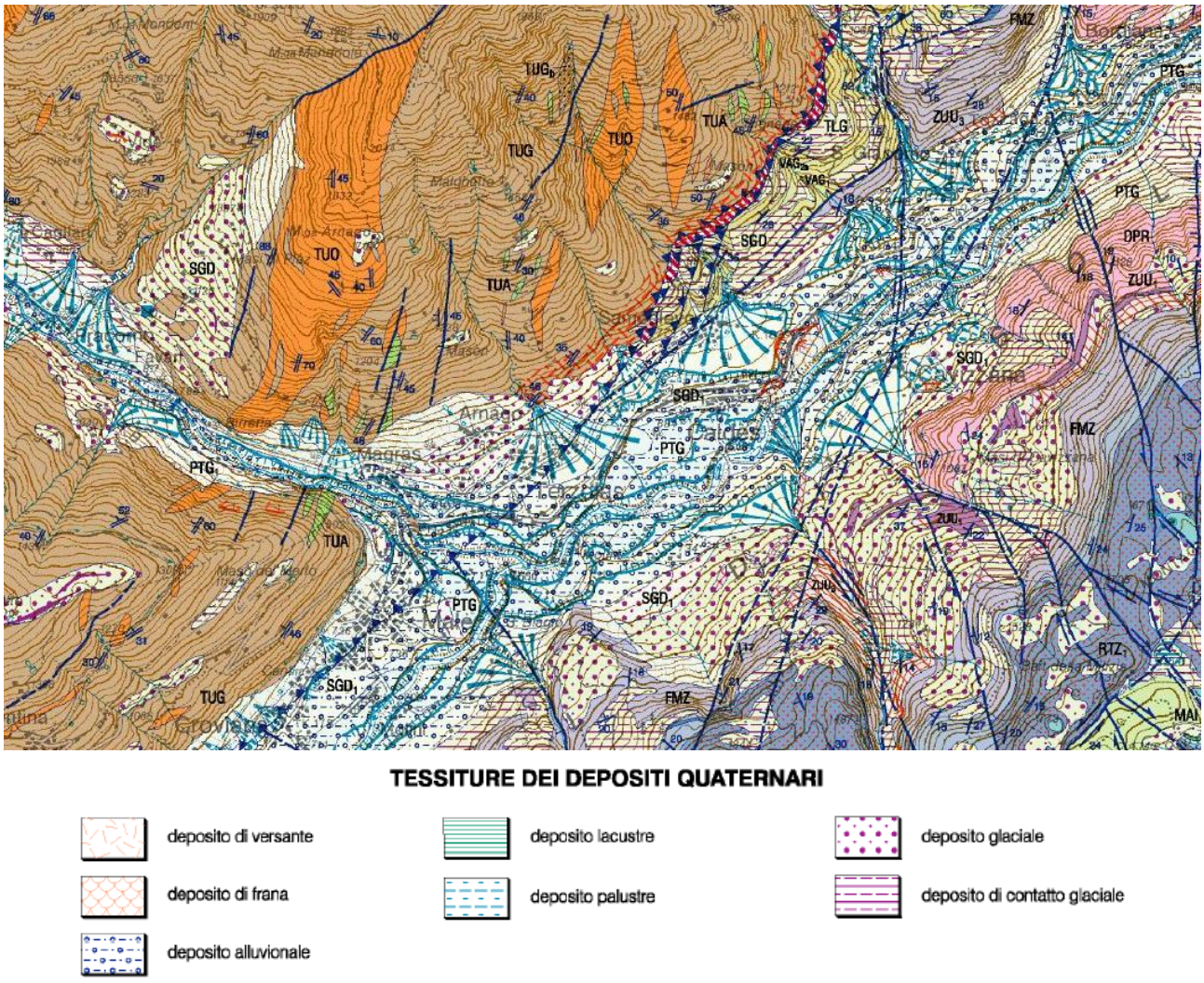

Figure 1.7. Geological map of the area of Caldes (scale 1:50,000) with legend of the Quaternary deposits (Dal Piaz et al., 2007).

The Garda Synthem brings together the deposits related to the last glacial maximum expansion (age: Upper Pleistocene). The northern part of the Val di Sole, near Malé, is characterized by a series of alluvial fans suspended over the valley. The highest suspended alluvial fans show the connection between the Val di Sole glacier (still present) and that of the Val di Rabbi. The cones at lower altitudes highlight a next sedimentary phase.

In the deposits of the valley bottom have been recognized 4 main facies:

- Glacial deposits: diamicton composed mainly of elements centimeter and decimeter dimensions and without clear striae, embedded in a clayey silt matrix, in which emerge larger blocks (4-5 dm). The polygenic nature of the clasts is due to the presence of micaschist coming from the Val di Rabbi and of tonalite coming from the Val di Sole.
- Alluvial deposits and ice-contact deposits: consist of sands and gravels with pebbles and boulders of centimeter and meter in size respectively. Levels of chaotic material and large blocks are alternated, testifying a high energy regime during the deposition. Glacial

deposits, like those previously described, occur at the base. Above the glacial deposits there are alluvial deposits.

The longitudinal profiles of the surfaces of the suspended alluvial fans in the Val di Sole (between Malè and Mostizzolo) are shown in Figure 1.8. During the last stage of the retreat of the Pleistocene glacier, the bottom of the Val di Sole was temporarily occupied by ice. Due to the input of significant amounts of debris derived from the ice-free slopes, the alluvial fans were originated in two successive stages of withdrawal. Some were also originated from debris flow, and are interpreted as ice-contact forms.

- Lacustrine deposits: consist of silt and fine sand, silty sands, well stratified shales. They are unconformably superimposed on the pre-Pleistocene substrate or on the fluvio-glacial deposits of the previous facies. They vary in thickness from a few meters to 40 m.

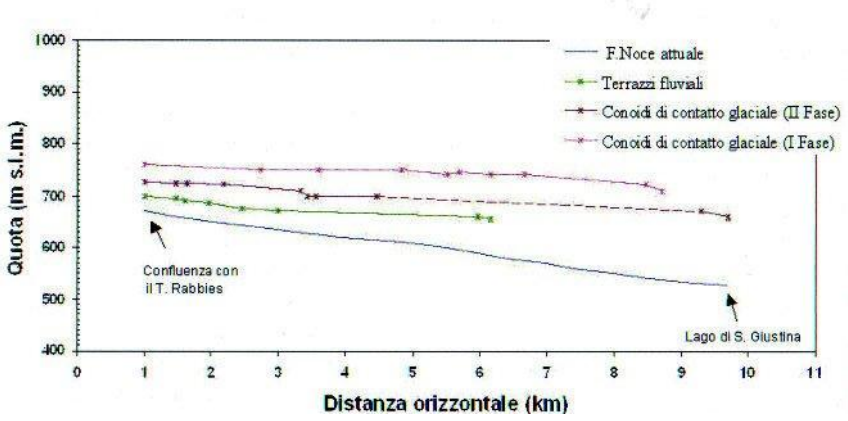

Figure 1.8. Longitudinal profiles across the terraces of the suspended alluvial fans in the Val di Sole, between Malè and Mostizzolo (Dal Piaz et al., 2007).

The post-glacial Alpine Synthem includes the deposits formed in the de-glaciated valleys, often in morphological conditions similar to those described above. The lower limit is defined by the bedrock or, more often, by the previous quaternary units. The upper limit in most cases corresponds to the topographic surface. The sedimentary bodies belonging to this synthem have a younger age at increasing altitude, where the morphogenetic processes were active.

There are several facies: glacial deposits, rock glaciers, alluvial and of mixed origin deposits, slope deposits, landslide deposits, marsh deposits. Among them, the ones present on the site of Caldes are the alluvial deposits. They are made of gravel, pebbles and coarse sands with well developed layering. Gravels, heterogeneous grain size, are interbedded with silt and sand deposits, in lenses of varying thickness and at maximum one decimeter thick. In some places of the Val di Sole they rest on glacial deposits of the sub-synthem Malé. The upper limit is given by the surfaces of the terraces, ranging between 705 and 560 m of altitude, which represent the final stage of an alluvial

deposit filling between Croviara and Mostizzolo. In the nearby areas are also present landslide deposits bounded by landslide scarp. They consist of massive diamicton, in clastic support, of rock fragments with sharp corners. May be due to rockfalls or debris flows (Dal Piaz et al., 2007).

1.2 Seismic microzonation

The observation of damages on constructions and infrastructures after an earthquake often highlights substantial differences in different built-up areas, even at short distance among them. Besides quality of buildings, the damage entity is often linked to the local seismic dangerousness, determined by the different earthquake propagation or by the instability of the soil.

These considerations are part of the studies of *seismic microzonation*, though which it is possible to pick out and characterize (i) stable areas, (ii) stable areas susceptible to local amplification and (iii) areas subjected to instability, such as landslides, surface fractures and soil liquefaction. Seismic microzonation studies are aimed to know the alterations that the seismic shaking may produce at the surface, giving useful information for the government of the territory, for the design, for planning the emergencies and for the reconstruction after the earthquake.

The technical details of execution and application of the seismic microzonation on the Italian territory are defined by the *Seismic microzonation addresses and criteria*, recently approved by the Department of Civil Protection and by the Conference of Regions and Autonomous Provinces (SM Working Group, 2008).

Seismic microzonation studies are conducted according to three levels of analysis, with increasing complexity, moving from level 1 to level 3.

Level 1 has for objective the identification of micro-zones of homogeneous seismic behavior. It is a propaedeutic and mandatory study for deal with successive levels of detail. The results of this level determine the analyses of the next level (level 2 or/and level 3). The elaborate provided at this level is the *map of the homogeneous micro-zones in seismic perspective*. From the evaluation of geological, geomorphological and lithological data already available of the area, this map identifies the micro-zones where it is predictable the occurrence of different types of effects produced by the seismic action (amplification, slope instability, liquefaction, etc..). The use of a seismic input or numerical quantification of the different effects it is not foreseen. The micro-zones are classified into three categories:

A. stable areas: significant local effects are not expected (geological substrate in outcrop with flat or slightly inclined morphology - hills with slopes less than 15°);

B. stable areas susceptible to local amplification: amplification of seismic motion is expected, as an effect of lithostratigraphic and morphological characteristics;
C. areas susceptible to instability: the expected predominant seismic effects are due to the permanent deformation of the territory. The main types of instability are: slope instability, liquefaction, active and capable faults, differential settlements.

Level 2 has two objectives to be achieved in sequence: (i) compensate for some uncertainty of the level 1 with insights, and (ii) provide numerical quantifications of the local change of the seismic motion at the surface and of the permanent deformation phenomena. The result of this level is the *seismic microzonation map*. It is obtained by associating a numerical quantification of the effects with simplified methods (abacuses and empirical laws) to the areas of the *map of the homogeneous micro-zones in seismic perspective*.

The third level of analysis is applied:

- in stable areas susceptible to local amplification, in cases of geological and geotechnical complex situations that cannot be solved with the use of abacuses, or for works of particular importance;
- in areas subject to particularly severe instability that cannot be solved with the use of expeditious methods.

The procedures and the computer codes used, the results of the experimental tests on site and in the laboratory, have to be described in detail. The investigations consist of seismic data acquisition, surveys, tests in the hole and on the surface, geotechnical static and dynamic in situ and laboratory tests, micro-tremors campaigns. The calculations are constituted by 1D and 2D numerical analysis for the quantification of local amplification, and by dynamic analysis for cases of slope instability and liquefaction susceptibility. It is typical of this level the palaeo-sismological study of active and capable faults. The results of this level can modify the *seismic microzonation map* providing the *seismic microzonation map with insights*.

The seismic microzonation study provides a knowledge of the local seismic hazard of the different areas and allows to establish an hazard hierarchy at various scales useful for the planning of interventions to reduce seismic risk. Its realization is a cognitive tool with different potentials, which costs vary according to the level of detail (Gruppo di lavoro MS, 2008).

1.2.1 First level seismic microzonation map of Trentino

For the entire Trentino region, the first level seismic microzonation map was drafted on the base of the criteria defined in the *Seismic microzonation addresses and criteria*. This map (Figure 1.9,

Appendix 2, downloadable from http://www.protezionecivile.tn.it/territorio/) defines a qualitative seismic behavior of homogeneous zones, taking into account possible topographic or stratigraphic amplifications.

The areas defined stable without local amplification are the areas characterized by bedrock outcropping or sub-outcropping in the presence of topography with steepness less than 15°.

The areas that may have local topographic amplifications are characterized by the presence of substrate and steepness larger than 15°. The areas susceptible to local stratigraphic amplification include areas with slope deposits and areas along the valleys with coarse-grained or medium/fine-grained deposits. In the presence of medium/fine-grained deposits the highest local amplification effects are expected.

The areas susceptible to instability are finally characterized by gravitational movements that can be triggered by an earthquake.

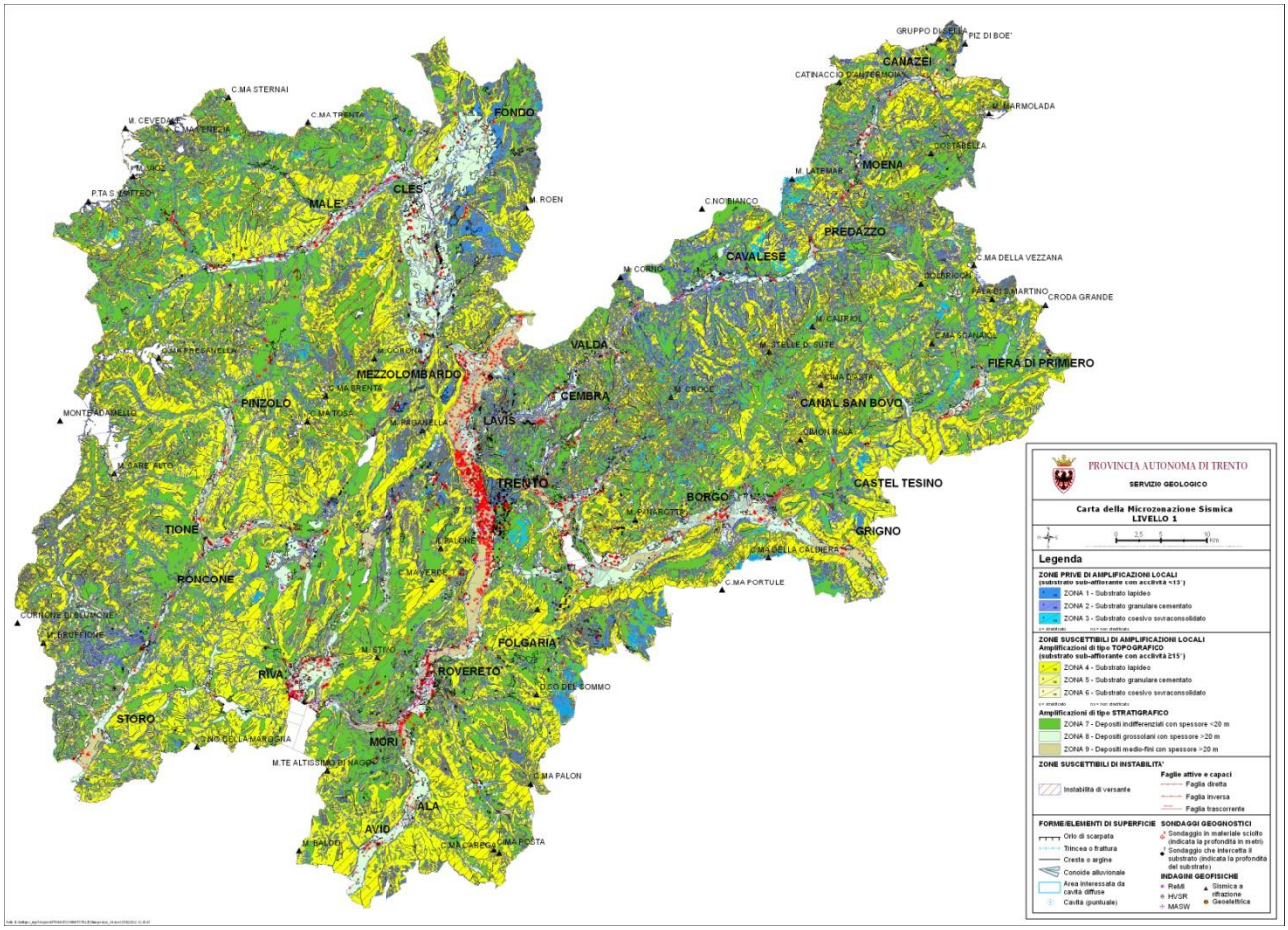

Figure 1.9. First level seismic microzonation map of Trentino (http://www.protezionecivile.tn.it/territorio/).

Chapter 2

Deep structure and seismic properties

2.1 Geophysical investigations

Deep structures and seismic properties of the subsoil were determined by means of geophysical investigations. In the first two sections (2.1.1 and 2.1.2) the geophysical methods used in the study area are described from a purely theoretical point of view. It is necessary to understand the principles on which they are based, the results that each of them offers, the advantages and disadvantages, the required equipment. From the practical point of view, the utilized tests are reported in section 2.1.3. The adopted geophysical methods are the direct current resistivity and the surface-wave seismic methods.

Geophysical methods are commonly used as support for geological modelling (for example to locate fracture zones, to study the groundwater system, to locate abandoned landfills), and to obtain information on the lithology and physical parameters of the ground. Different geophysical methods is available for the investigation of the subsurface: magnetic methods, gravity methods, direct current resistivity, electromagnetic methods, ground penetrating radar, refraction seismic, reflection seismic, surface nuclear magnetic resonance, geophysical borehole logging and geophysical monitoring methods. A necessary condition for a meaningful of a geophysical method is the existence of differences in the values assumed by the physical parameter (density, electrical resistivity, seismic wave velocities, etc.) of the different geological structures. It must be first determined which parameters can be expected to have sufficiently different values at the site before a geophysical survey is conducted (Knödel and Voigt, 2007). Geophysical methods are complementary because they detect different physical properties. For example seismic methods are used to investigate structures and lithology, electrical and electromagnetic methods are used to detect changes in electrolyte concentration in pore water, and so on.

2.1.1 Seismic methods

The *seismic methods* are geophysical methods which are used to investigate the subsurface both controlled generation of elastic (seismic) waves by a seismic source (e.g., explosion, vibrator, weight drop) and passive (e.g. microtremors) seismic sources. During their propagation in the

subsurface seismic waves are reflected, refracted or diffracted at boundaries between layers with different properties (seismic velocity and/or density) or at man-made structures. The seismic response is at the same time detected by a number of receivers (geophones, seismometers) positioned along straight profile lines (2-D seismics) or over an area in 3-D seismic surveying. The signal is then sent via cables to a recorder. The recordings are collected by a seismograph, processed and displayed in seismic sections to image the ground structure. The recording of seismic waves returning from the ground to the surface provides information regarding structures and lithological composition of the subsurface. A geological model of the subsurface can be derived by measuring the traveltimes of seismic waves and determining their material-specific velocities (Knödel and Voigt, 2007).

The classical seismic methods are seismic refraction and seismic reflection. Seismic methods based on surface waves have been great development in recent years.

The main objective of refraction surveys is to determine the depths to rock layers, the refractor topography and layer velocities. These method requires an increase in velocity with depth. If a layer of lower velocity lies beneath a layer of higher velocity, that layer cannot be detected. These conditions can cause ambiguity in the interpretation.

Reflection seismic has become increasingly used for depths lower than 50 m. There are some problems for shallow seismic surveys. Since the traveltimes are short, genuine reflections are masked because source generated noise, surface waves, first arrivals of direct waves and refracted waves dominate. Thus, both acquisition and standard processing of conventional seismic methods cannot be used deep reflection seismic.

The surface wave method is based on analysing the variation of seismic velocities with frequency (dispersion). Dispersion of surface waves is high when near-surface velocity layering occurs (Knödel and Voigt, 2007). This method is widely described below.

Surface-wave methods

The characterization of the subsoil using seismic techniques consists of observing a wavefield, measuring the properties of the propagation, and by means of an interpretation procedure, obtaining the distribution of the subsoil properties which influence the propagation: namely the deformability and the dissipative properties at very low strain (Socco and Strobbia, 2004). This can be achieved using different techniques and acquisition geometries, and analysing the propagation of different kinds of waves (P, S, Rayleigh, Love, etc.) and the related phenomena (reflection, refraction, diffraction, dispersion, etc.). The wavefield is sampled in space and time, and from the record

obtained, the properties of the propagation are deduced. After they are used for an imaging or inversion procedure that leads to the geometrical distribution of the subsoil characteristics and the dynamic behaviour of the site.

More diffused seismic techniques are based on body-wave propagation, in particular P-wave reflection, and in this context, surface waves are a coherent noise to be removed or attenuated. In more recent times, interest in the large amount of information contained in surface waves has increased. Surface waves can be interpreted or even expressly acquired and analysed to characterize the shallow near surface.

Surface waves exist only in media with a free surface. They propagate in a limited layer having a thickness approximately equal to one wavelength close to the surface. Therefore waves of different wavelength affect different depths in the same medium. In not homogeneous medium they propagate with different velocities and different attenuations in different materials. Hence, the velocity of propagation can be strongly frequency-dependent (dispersion) according to the geometric distribution of the soil properties: this behaviour is called *geometric dispersion*. The physical principle on which the surface-wave method test is based is the geometrical dispersion: it is possible to measure the dispersive characteristics at a site and invert them to estimate the soil properties. The surface-wave method consists of three phases: acquisition, processing and inversion, the latter based on forward modelling. Acquisition consists of recording surface waves with high S/N (Signal-to-Noise ratio) in the appropriate band of frequency. Processing consists in determining the properties of surface waves. Inversion estimates the soil properties related to the measured propagation, by means of comparison with the results of a simulation. These phases are described below.

Some intrinsic limits depending on the physics of the propagation exist and have to be considered. Despite that, an accurate testing procedure can improve the quality of the results, taking into account limitation and uncertainties. The critical aspects of the surface wave method are:

- the acquisition, the lack of resolution or sensitivity to a certain target can limit the depth at which reliable information can be obtained;
- most approaches are based on a one-dimensional model. If this hypothesis is not true at the observations scale, model errors can affect the result;
- the propagation is a multimode phenomenon: the presence of different modes and the modal superposition can introduce ambiguity and the interpretation may becomes complex (Socco and Strobbia, 2004).

- **Surface wave dispersion analyses**

In order to summarize the concept behind the use of geometrical dispersion for soil characterization, consider the stratified medium in Fig. 2.1a. It is characterized by increasing stiffness, then increasing shear-wave velocity, with depth. In this situation, a high frequency Rayleigh wave (short wavelength, Fig. 2.1b), travelling in the top layer will have a velocity of propagation slightly lower than the shear wave velocity in the first layer. On the other hand, a low frequency wave (i.e., a long wavelength, Fig. 2.1c) will travel at a higher velocity because it is influenced also by the deeper stiffer materials. This concept can be extended to several frequency components. The phase velocity vs. wavelength plot (Fig. 2.1d) will show an increasing trend for longer wavelengths. Considering the relationship between wavelength and frequency, this information can be represented as a phase velocity versus frequency plot (Fig. 2.1e). This graph is usually called a *dispersion curve*. This example shows that the dispersion curve will be associated with the variation of medium parameters with depth. This is the so-called *forward problem*. It is important, however, to recognize the multimodal nature of surface waves. Several modes of propagation exist and higher modes can play a relevant role in several situations (Foti et al, 2011). Only the fundamental mode dispersion curve is showed in Figure 2.1.

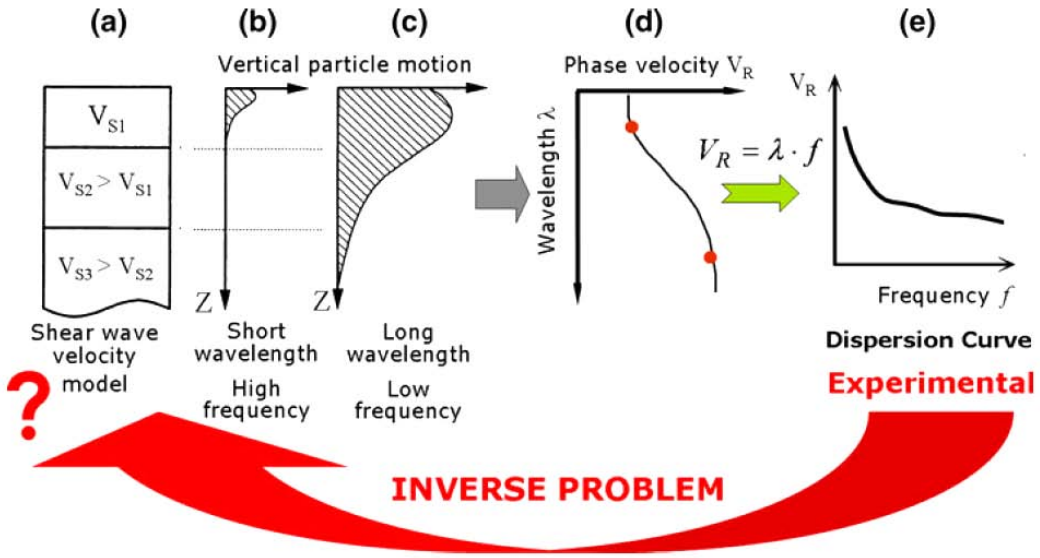

Figure 2.1. Parameter identification on the basis of geometrical dispersion (Foti et al, 2011).

If the dispersion curve is estimated on the basis of experimental data, it is therefore possible to solve the inverse problem. The model parameters are identified on the basis of the experimental data collected on the boundary of the medium.

Figure 2.2 delineates the standard procedure for surface wave tests:

1) Experimental data acquisition;
2) Signal processing in order to obtain the experimental dispersion curve;
3) Inversion process to estimate the shear wave velocity profile.

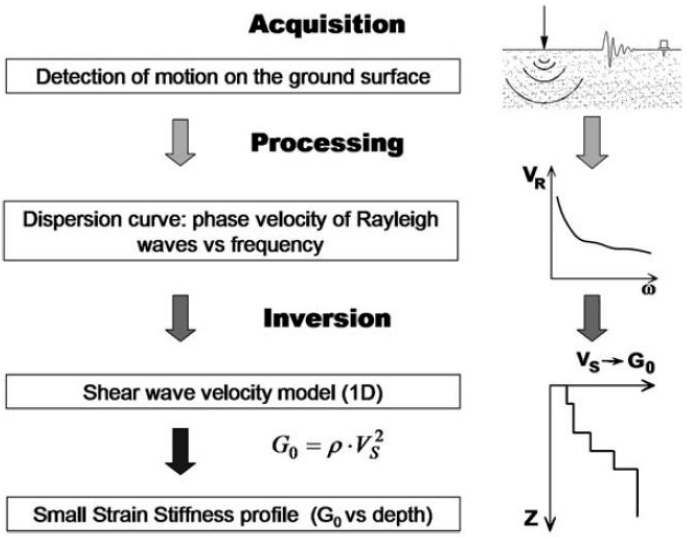

Fig. 2.2 Flow chart of surface wave tests (Foti et al, 2011).

It is important to remember that the above steps are interconnected and their interaction must be considered during the whole interpretation process.

The primary use of surface wave testing is the characterization of the site in terms of shear wave velocity (V_S) profiles. The V_S profile is of fundamental interest for seismic site response, vibration of foundations and vibration transmission in soils (Foti et al, 2011).

1) Acquisition

The choice of equipment and testing configuration is linked to the objective of the test and to the technique to be used in the interpretation. Typically the length of the survey line should be at least double than the depth of the investigation. It is important to remember specific characteristics of Rayleigh waves, such as that they travel in a zone of about one wavelength and then they give information about this zone. Moreover the link between frequency, wavelength and phase velocity makes the frequency range of interest closely linked to the materials to be investigated. Preliminary information related to the considered site can be very useful at this stage.

Independently from subsequent stages, signals are detected in time and space. The information related to wave propagation is incorporated in the signals and can be extracted using different

techniques. It is a good practice to store the original unprocessed signals in time-offset domain, in this manner they can be reinterpreted with different processing techniques (Foti, 2005).

The multichannel approach should be preferred to the two-station approach because it (i) averages and attenuate errors, (ii) improves the possibility of mode separation and identification, (iii) allows for the recognition and the interpretation of other seismic events present in the data, (iv) allows for coherent noise filtering and, (v) does not require complex acquisition procedures. The most usual array is a linear, evenly spaced array of vertical low-frequency geophones (Socco and Strobbia, 2004).

– Testing equipment:

The frequency range of interest is a function of the desired depth of investigation and resolution for shallow layers. The basic testing equipment is composed of receivers (geophones or accelerometers) connected to an acquisition device, that digitizes and stores seismic signals. In active test, the wave is artificially generated using a seismic source with a trigger device connected to the acquisition device to set the starting time of the acquisition (Foti, 2005). Passive arrays techniques usually measure the microtremors, using a two-dimensional array of sensors distributed on the ground surface (Socco and Strobbia, 2004).

Surface wave data are generally collected on the surface using a variable number of receivers. The geometries can be one-dimensional or two-dimensional. The receivers adopted are typically geophones (velocity transducers). The advantage of using geophones instead of accelerometers stems from the fact that geophones do not need a power supply, whereas accelerometers do. Moreover, in cases where surface waves are extracted from seismic noise recordings, accelerometers do not generally have the necessary sensitivity. On the contrary, low frequency geophones (natural frequency less than $2\ Hz$) tend to be cumbersome and very vulnerable because the heavy suspended mass can be easily damaged during deployment on site (Foti et al, 2011). A good compromise is to use $4.5\ Hz$ geophones that are less expensive and do not need particular care to be used on site (Foti, 2005).

Several devices can be used for the acquisition and storage of signals. Its main function is to digitalize and record analog electrical signals generated by the receivers. Any device having an A/D (analog-to-digital) converter and the capability to store the digital data can be adopted. Commercial seismographs for geophysical prospecting are in general the first choice because they are designed to be used in the field, so they are very robust. New generation seismographs are comprised of scalable acquisition blocks to be used in connection with field computers, so allowing preliminary processing of data on site.

For the generation of the wavefield, several different sources can be used, provided they generate sufficient energy in the frequency range of interest. Impact sources are often preferred because they are quite cheap and allow for fast testing (Foti et al, 2011). Heavy sources are needed to produce energy in the low frequency range, whereas lighter sources can be used for shallow characterization (Foti, 2005).

- Testing configuration:

The choice of sampling parameters both in time and space has significant effects. Sampling parameters in time are set on the acquisition device. Sampling parameters in space are determined by the layout geometry and are generally subjected to restrictions due to available receivers and testing space (Foti, 2005).

The typical arrangement for receivers is to have multiple receivers along a straight line and the seismic source acting on one end of the array. Using constant receiver spacing the processing is simplified. However considering the trade-off between depth of penetration and resolution variable receiver spacing acquisition setup have also been proposed. The number of receivers in fact is fixed in relationship to the available equipment so that the total length of the array is determined by the space among the receivers. Wide spacing consent the detection of long wavelength and then a characterization of deeper layers. But the attenuation of high frequency components causes loss of information for the high frequency range and then of resolution for shallow layers. Several strategies can be adopted to overtake these limitations. One important aspect is that using constant spacing it is easier to repeat the test with forward and reverse shot position, by moving the seismic source on the opposite side. This procedure is a good practice in surface wave test. In fact the comparison of experimental dispersion curve obtained for the same receiver array with forward and reverse shots can give indication about the presence of lateral variations, which violates the basic assumption of horizontally stratified medium (Foti, 2005).

Long arrays should be preferred because they improve the modal separation and because they reduce the data uncertainties. Moreover, they produce a better S/N ratio, are less affected by high-frequency attenuation and, given the number of channels, produce less severe spatial aliasing (Socco and Strobbia, 2004).

2) Processing

The field data are processed to estimate the experimental dispersion curve, which is the relationship between phase velocity and frequency. Some equipment allow for a pre-processing of experimental data directly in the field because the simple visual screening of time traces is not always sufficient

(Foti et al, 2011). The objective of the processing is to derive from records all the information about the surface-wave propagation, to estimate the uncertainty, and to test whether the site fits the assumed 1-D model. The processing, in fact, extracts from data the factors to be compare with the simulations within the inversion procedure. It is the link between the real world of acquired data, containing other seismic events and noise, and the ideal world of simulated data containing only surface waves (Socco and Strobbia, 2004).

To increase the reliability of the inversion, the data have to be sampled in order to increase the independent information, without replication, and reducing its uncertainty. Different approaches exist to process surface-wave data, many of these are formally identical or linearly dependent. Wavefield transforms are widespread to analyse the data in domains where surface waves are easily identified and their properties are estimated. Many of these domains are related by linear invertible transforms. The frequency-wavenumber (*f-k*) transform has the advantage of being a natural approach to the analysis of the seismic event. In fact, the ideal wavefield related to the surface can be described with its energy located on the eigenvalues, which are the lines in the *f-k* domain. The observation produces constant a spreading of energy in the whole *f-k* domain. A real wavefield will have the energy of random and coherent noise: this additional energy can be separated in the *f-k* domain. It is then impossible to identify the surface waves as the dominant events. However other transforms can be completely equivalent. The computation of the spectrum needs some attentions to allow proper identification of the maxima: some pre-processing is performed to remove eventual low-quality data. When a good image of the energy density of the propagation is obtained, the analysis of the energy maxima is performed. When maxima have been identified in *f-k*, the velocities are computed simply as $v = 2\pi f/k$.

The set of all the position of the absolute maximum at each frequency, known as the *dispersion curve*, can sometimes have most of the required information. However it is limited to a frequency range, may not be continuous, may not coincide with any branch of the modal curves, and can often be related to higher modes (Socco and Strobbia, 2004).

3) Inversion

The final step of surface wave analysis is the inversion process necessary to estimate soil parameters from the experimental dispersion curve. Usually, a local search algorithms starting from a tentative solution is used. The trial and error method, although very rough, is still sometimes used in particular when higher mode contributions make the interpretation more bulky (Foti, 2005).

The requisites for the inversion derives directly from the properties of the final result resumable in the following statement: the result should be a unique subsoil model with adequate reliability and

resolution down to the depth of interest, and should be presented with the associated uncertainties. The properties of the solution are considered starting from the analysis of the data to be inverted. These data have to be analysed with the goals of (i) increase the amount of the information produced, (ii) reduce the amount of useless data and (iii) select other properties of the propagation, besides the velocity, that can add useful information about the model. The other aspect to be considered are the model in terms of its parametrization, the estimated parameters reliability and the investigation depth (Socco and Strobbia, 2004).

An important aspect is related to the manner in which the forward problem is solved. The easiest way is the use of a fundamental mode approach, assuming that the experimental dispersion curve is representative of the fundamental mode at the site. This approach is correct only if the fundamental Rayleigh mode effectively dominates the propagation phenomenon. But it must be considered that in some situations higher modes plays a relevant role. In these cases the experimental dispersion curve is given by an apparent phase velocity given by modal superposition and influenced by the testing setup. Typical examples are inversely dispersive profiles (i.e. stiff shallow layers) and profile with abrupt variations of soil impedance (Foti, 2005).

The model parameters are generally the physical and geometric properties of the model, i.e. the shear-wave velocity, Poisson's ratio, the damping ratios, the density and the thickness of the layers. The choice of the parametrization of the model depends on the available forward modelling and on the need of a balance among the number of unknowns with the information content and the uncertainty of the data. In the layered model illustrated, the model parameters are the properties of each layer and the characteristics of the layout of acquisition. The acquisition layout is known and has to be introduced into the modelling. The layer properties are the unknowns and have to be chosen according to the sensitivity of their variations on the surface waves propagation. Parametric studies indicate that the shear wave velocity and the thickness of the layers are the parameters to which the propagation is more sensitive. The mass density, having small ranges and influence, can be estimated a priori. For the same reason, Poisson's ratio is also usually assumed a priori or neglected, but the effect of the saturating water of Poisson's ratio is high. So information about the water-table should be used to make a right choice of Poisson's ration values (Socco and Strobbia, 2004). A priori information or constrains given by other tests performed at the site are indispensable (Foti, 2005).

- **Active source methods - Multi-channel Analysis of Surface Waves (MASW)**

The *active source methods* are the methods in which the waves are generated by a source suitably energized during the test. Different active source methods exist (such as Spectral Analysis of Surface Waves method, Continuous Surface Wave method). Only the one used in the field, which is the Multi-channel Analysis of Surface Waves (MASW), is here described.

The use of a multi-station testing setup, characteristic of the MASW method, introduce different advantages in surface wave testing. In this case, the motion generated by the source is detected simultaneously at several receivers, located in line with the source itself.

For surface wave analysis, the experimental data are in general transformed from the time-offset domain to different domains, where the dispersion curve is easily extracted from the spectral maxima. Another method for extracting the surface wave dispersion curve from multistation data is based on the linear regression of phase versus offset at each frequency. Transform-based methods allow the identification of several different Rayleigh modes. When the modal wavenumbers have been estimated for every frequency, they can be used to evaluate the dispersion curve. The possibility of using modal dispersion curves is a great advantage with respect to methods giving only a single dispersion curve (as the two-station method) because have more information is traduced in a better constrained inversion. But, it has to be considered that, in standard practice, the number of receivers is small and the consequent reduced spatial sampling strongly affects the resolution of the surface wave test.

Unfortunately, when a survey has been carried out adopting a certain array configuration, no signal analysis strategies can allow the improvement of the real resolution. So, in the subsequent signal analysis step, it will not be possible anymore to separate modal contributions when more than a single mode exist. If a large number of receivers is used to estimate the *f-k* spectrum, the resolution is very high and the energy peaks are well defined. But, if the number of receivers is low, the resolution is very low. With low resolution it is only possible to locale a single peak in the *f-k* panel, which associated to several superposed modes. The apparent phase velocity denote the velocity of propagation corresponding to this single peak representing several modes. In this case, it is no longer possible to use inversion processes based on the fundamental mode or on modal dispersion, but it is necessary to use an algorithm that takes into account the mode superposition effects and the effective testing configuration. This situation is common when strong impedance contrasts are present in the soil profile or in inversely dispersive profiles, i.e., profiles in which stiff layers are above soft layers.

As mentioned above, the apparent dispersion curve is dependent on the spatial array so if higher modes are relevant, the inversion process will be bulky. But, if the fundamental mode is dominant, the inversion process can be noticeably simplified. However, it is not always clear from the simple inspection of the experimental dispersion curve if higher modes are involved (Foti et al, 2011).

- **Passive source methods - Seismic Noise Horizontal-to-Vertical spectral ratio (HVSR)**

A different perspective is the use of seismic noise analysis. In this case no source is needed, the recording background noise and the test is carried out using a ‘‘passive’’ approach. The seismic noise is rich in low frequency components, as high frequency components are strongly attenuated when they travel through the medium and are typically not detected. This is the great advantage of the passive source methods. So, seismic noise surveys provide useful information for deep characterization (tens or hundreds of meters), but the level of detail close to the surface is typically low. The limitation in resolution close to the surface can be overcome by the combination of active and passive measurements, or with the new low cost systems characterized by a large number of sensors and high sampling rates (Foti et al, 2011). In seismic noise surveys the choice of the appropriate instrument is crucial. In fact, due to the very low environmental seismic noise amplitude, a prerequisite for high quality seismic noise recordings is the selection of A/D converters with adequate dynamic ranges.

Different passive source methods exist (such as Refractor Microtremor, Two-dimensional Arrays) but only the one used in the field, which is the Seismic Noise Horizontal-to-Vertical spectral ratio (HVSR) method, is described below.

HVSR method is based on the principle that average spectral ratios of ambient vibrations in the horizontal and vertical directions could supply information about the seismic properties of the local subsoil. Most researchers agree that the maximum of the H/V ratios vs. frequency (NHV curve) provides a good estimation of the fundamental resonance frequency of a site, at least in the presence simple stratigraphic configurations. This parameter is directly related to the thickness of the soft sedimentary cover and this makes NHV curves an effective exploratory instrument for seismic microzoning studies and geological surveys. Recent studies showed that noise measurements can be used to map the thickness of soft sediments.

The approach is based on the assumption that in the area under investigation, lateral variations of the shear wave velocity are minor and that it principally increases with depth according to a relationship such as:

$$v_s(z) = v_{s0}(1 + Z)^x$$

where v_{s0} is the surface shear wave velocity, $Z = z/z_0$ (with $z_0 = 1\ m$) and x describes the depth dependence of velocity. Considering the well-known relation among f_r (the resonance frequency), the average shear wave velocity of soft sediments $\bar{V}_s$, and its thickness h,

$$f_r = \bar{V}_s/4h$$

the dependency between thickness and f_r becomes

$$h = \left[v_{s0} \frac{(1-x)}{4f_r} + 1 \right]^{1/(1-x)}$$

where f_r is to be given in Hz, v_{s0} in m/s and h in m.

A possible limit of the HVSR method is the presence of thick sedimentary covers. In this case, NHV peaks could occur at very low frequency, also below the minimum frequency that can be detected by the experimental tools. However, the generally available seismological/geophysical equipment allows detection of eventual NHV maxima occurring above 0,1–0,5 Hz (Foti et al, 2011).

2.1.2 Electrical survey

The capacity of the earth to produce and respond to electric fields is at the base of a variety of geophysical exploration procedures. The various electrical methods measure the flow of electric current in the ground. Electric current, which is the movement of charged particles, can take place in three different ways: ohmic conduction in crystalline structure of some materials, electrolytic conduction in groundwater, dielectric conduction in insulator materials. All substances act to retard the flow of electric current. The extent to which a substance retains this movement is described by its *electrical resistivity* (Robinson and Coruh, 1988). It is the reciprocal of the *electrical conductivity*, a material that readily allows the movement of electrons or ions has a low resistivity.

The electrical survey are measurements of electrical resistivity or conductivity at shallow depth by direct current resistivity, induced polarization or electromagnetic methods (Knödel and Voigt, 2007). The first method is widely described below.

Direct current resistivity methods

- **Principle of the methods**

Direct current resistivity methods use artificial sources of current to produce an electrical potential field in the ground. In nearly all resistivity methods, a current is introduced into the ground through point electrodes (C_1, C_2) and the potential field is measured using two other electrodes (the potential electrodes P_1 and P_2), as represented in Figure 2.3. The source current can be direct current or low-frequency (0.1 - 30 Hz) alternating current. The aim of generating and measuring the electrical potential field is to determine the spatial resistivity (or conductivity) distribution in the ground. The resistivity of the ground can be determined as the potential between P_1 and P_2, the current introduced through C_1 and C_2, and the electrode configuration are known (Seidel and Lange, 2007). This is called *apparent resistivity*.

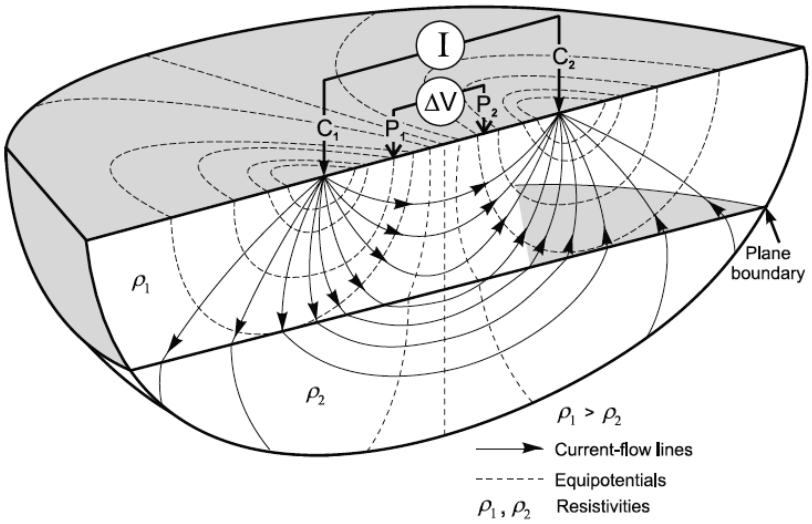

Figure 2.3. Principle of resistivity measurement with a four-electrodes array (Seidel and Lange, 2007).

Resistivity measurements may be made at the Earth's surface, between boreholes or between a single borehole and the surface. The following operating modes can be adopted:

- profiling (mapping),
- vertical electrical sounding (VES),
- combined sounding and profiling (two-dimensional resistivity imaging),
- three-dimensional resistivity survey (3-D resistivity imaging),
- electrical resistivity tomography (ERT).

Profiling methods use fixed electrode spacings to detect changes on lateral resistivity along a profile down to an about constant investigation depth, determined by the electrode spacing. The results are in general interpreted in a qualitative way. Contour maps or profile plots of the measured apparent resistivities allow delineation of lateral boundaries of geogenic structures, anthropogenic features and of hydrogeological conditions.

The objective of sounding methods is to determine the vertical distribution of the resistivity in the ground. Several soundings performed along profiles and/or distributed in the study area can also provide information about the lateral extent of structures. Soundings reach investigation depths up to several hundred meters. The measured data may be interpreted both qualitatively and quantitatively. The latter provides resistivity models in which the layer boundaries are boundaries of geoelectrical layers but not necessarily of lithological layers. For a better correlation to the geology, geoelectrical data should be integrated with borehole logs or the results of other geophysical methods.

Sounding and profiling can be combined in a single process (2-D resistivity imaging) in order to investigate complicated geological structures with strong lateral resistivity changes. This combination provides detailed lateral and vertical informations. 2-D inversion produces a two-dimensional distribution of resistivities in the ground.

Three-dimensional (3-D) resistivity surveys and ERT measurements provide information about complex structures (Seidel and Lange, 2007).

- **Fundamentals physical basics**

A point electrode that induce an electrical current I generate a potential V_r at a distance r from the source. If both source and measuring points are at the surface of a homogeneous half-space with resistivity ρ, this potential is given by:

$$V_r = \frac{\rho I}{2\pi r}$$

In the case of a four-electrode array (Figure 2.3) consisting of two current electrodes (C_1, C_2) that introduce a current $\pm I$, the potential difference ΔV between the potential electrodes P_1 and P_2 can be calculated as:

$$\Delta V = \rho I \left[\frac{1}{2\pi}\left(\frac{1}{r_1} - \frac{1}{r_2} - \frac{1}{r_3} + \frac{1}{r_4}\right)\right]$$

where $r_1 = C_1P_1$, $r_2 = C_2P_2$, $r_3 = C_3P_3$, and $r_4 = C_4P_4$.

Replacing the factor in square brackets by $1/K$, the resistivity of the homogeneous half-space is obtained as follows:

$$\rho = K\frac{\Delta V}{I}$$

The parameter K is the configuration (or geometric) factor and be easily calculated for all practical configurations. Figure 2.4 shows K parameters for the most commonly used arrays. When inhomogeneous conditions occur, the above-mentioned equation gives the resistivity of an equivalent homogeneous half-space. For this case the apparent resistivity ρ_a is introduced, it is normally assigned to the centre of the electrode array. In a given four-electrode array, the current and potential electrodes are interchangeable. This concept, called principle of reciprocity, can be used in multi-electrode systems in order to improve the signal-to-noise ratio.

There are many different types of electrode arrays even if in practice only a few of them are used. The most common are listed in Figure 2.4.

Electrode array	Electrode configuration	Configuration factor
Wenner Wenner α Lee	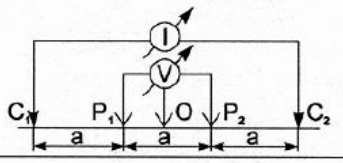	K = 2π a
Schlumberger	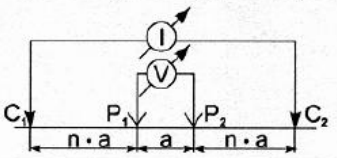	K = π n (n+1) a n > 3
dipole-dipole axial dipole Wenner β	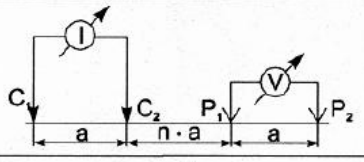	K = π n (n+1) (n+2) a
pole-dipole half Schlumberger Hummel	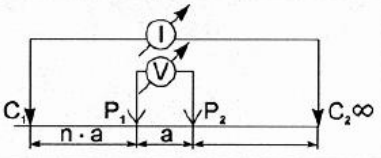	K = 2π n (n+1) a n > 3
pole-pole	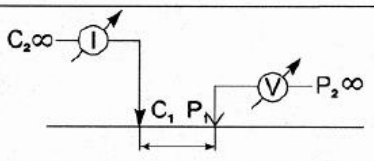	K = 2π a

Figure 2.4: Some electrode arrays for direct current resistivity measurements (Seidel and Lange, 2007).

Each array has its advantages and disadvantages with regard the depth of investigation, the resolution of horizontal and vertical structures, the sensitivity to lateral changes in resistivity, etc. It

is essential to select the most appropriate electrode array for each problem. Resolution and depth of investigation of different arrays have been investigated by several researchers. They show that both the Schlumberger array and the Wenner array have very good vertical resolution, because of their symmetric geometry, but a lower lateral resolution than asymmetric configurations, for instance pole-dipole or dipole-dipole arrays. Wenner arrays provide the best results under noisy conditions. The dipole-dipole array has the best resolution with regard to the detection of single objects (e.g., cavities, sand and clay lenses).

The investigation depth of commonly used arrays is approximately between $L/6$ to $L/4$, where L indicates the spacing between the two outer active electrodes. The dipole-dipole array offers the best depth of investigation but has the disadvantage of a comparatively low signal-to-noise ratio. Then, the electrodes must be adequately coupled to the ground and the equipment must have a high sensitivity to obtain good quality data.

Field logistical qualities are also important for a survey. The type of electrode array selected influences the resolution and the depth of investigation. Generally, the geology of interest has a 3-D resistivity distribution and would require a 3-D resistivity survey. In many practical cases the problem can be reduced to a 2-D or even a 1-D case, but it must be remember that the measurements can be influenced by objects outside the arrays. The 2-D case is based on the assumption that the resistivity of the ground varies only in the vertical and one horizontal direction, no resistivity variations are present in the second horizontal direction. Hence, survey profiles should run perpendicular to the strike of such structures. In the 1-D case, it is assumed that the ground corresponds to a horizontally layered model, requirement that is fulfilled only if the dip of the layers is less than 10° (Seidel and Lange, 2007).

- **Ambiguity of results**

The direct current resistivity method is a potential field method, so presents considerable inherent ambiguity. In the case of resistivity sounding, the ambiguity is related to layer thickness, layer resistivity and is governed by the principles of equivalence and suppression.

The principle of equivalence in the 1-D case says that it is impossible to have a unique solution for the layer parameters (thickness and resistivity): for conductive layers, only the thickness/resistivity ratio can be determined (S-equivalence), while for highly resistive layers only the product between thickness and resistivity can be determined (T-equivalence). Then, when resistivity and thickness of a layer vary within certain ranges, their product remains constant and no differences can be seen in the sounding curve. Thickness and resistivity cannot be independently determined, then there are

different equivalent layer models which all fit the sounding curve within a selected fitting error range. Is for this reason that it is important to correlate resistivity sounding data with data from boreholes.

The principle of suppression (hidden layer problem) occurs when a layer has a resistivity intermediate between the resistivities of the layers above and below. In this case, the layer has an insignificant effect on the sounding curve. In general, a layer can be detected if its thickness is greater than its depth and its resistivity differs from the cover layer. By modelling, a series of thin layers will mostly be represented by only one layer and a mean resistivity.

The determination of the confidence intervals and parameter limits of models for the 2-D and 3-D cases is problematic. In 2-D inversion, ambiguity is influenced by several factors: the structure of the grid used to approximate the geological structures, limited data avaiability, errors in the data and sensitivity distribution of the electrode configuration used (Seidel and Lange, 2007).

- **Instruments**

The basic equipment for direct current resistivity measurements consists of: transmitter, receiver, power supply, electrodes, and cables. Transmitter, receiver and power supply may be integrated in a single unit or may be separated and different types of current are used:

- direct current,
- low-frequency alternating current (ac < 30 Hz),
- pulsed square wave direct current with changing polarity (on^+ - off - on^-).

Transmitters produce either a constant voltage or a constant input current. Anyway, it is advantageous if the transmitted current and voltage are measured and the data stored together with the resistivity data. The current is automatically stabilized and the cycle timing (on^+ - off - on^- ...) is automatically controlled. In dependence on the output power to be generated, the appropriate power supply has to be chosen (battery pack, car battery or generator). A switching unit is necessary for 2-D and 3-D measurements to activate the electrodes individually. For some instruments, a laptop is necessary for data acquisition, display and storage. The acquisition software must be able to take into consideration the electrode configuration, electrode spacing and other survey parameters.

Two types of operation are frequent. The first one uses “passive” electrodes connected to a switching box via a cable containing 20 or more cores. The other type of operation use “active” electrodes: a cable containing only a few cores (which are used to transmit current and communications, as well as measure voltage) is connected to an addressable box on each electrode. The addressable box is used to switch the electrode between active and passive modes.

For 3-D resistivity surveys multichannel instruments are necessary to reduce the acquisition time (Seidel and Lange, 2007).

2.1.3 Case study

The tests performed in the study area in date 05/03/2013 are located as shown in Figure 2.5 and consist of:

- 1 active seismic line downstream the castle (MASW). The acquisition was made through a 48-channel seismograph connected to geophone spacing of 3 m for a length of 144 m of the seismic line. The energization, produced with rifle, was performed at 6 m from the first geophone. To reduce the background noise and improve the overall quality of the seismograms, more shots were performed.
- 2 electrical ERT lines, one downstream the castle (called ERT1) and one upstream (ERT2). The acquisition was made through a 72-channel acquisition device (SYSCAL-PRO IRIS georesistivimeter) with different spacing. In the ERT1 test the electrode spacing was 5 m, so 200 m long, and the acquisition was made with two electrode arrays: the dipole-dipole and the Werner-Schlumberger arrays. Concerning the ERT2 line, the electrode spacing was 2 m for a length of 96 m, and the acquisition was made only with the dipole-dipole electrode array. The acquisition device is equipped with a system for the automatic management of the electrodes, i.e. able to switch the electrodes arranged along the section to be investigated in the input current electrodes and measuring electrodes of the electric potential with all possible quadripolar combinations.
- 4 passive seismic tests, 3 downstream the castle (HVSR1, HVSR2, HVSR3) and one upstream (HVSR4), made with an instrument called tromograph (3-components seismometer with frequency range 0.1-256 Hz). Each measurement was 32 minutes long, analysed with several temporal windows with the software Grilla (Micromed), briefly described in Appendix 3, as well as others geophysical software.

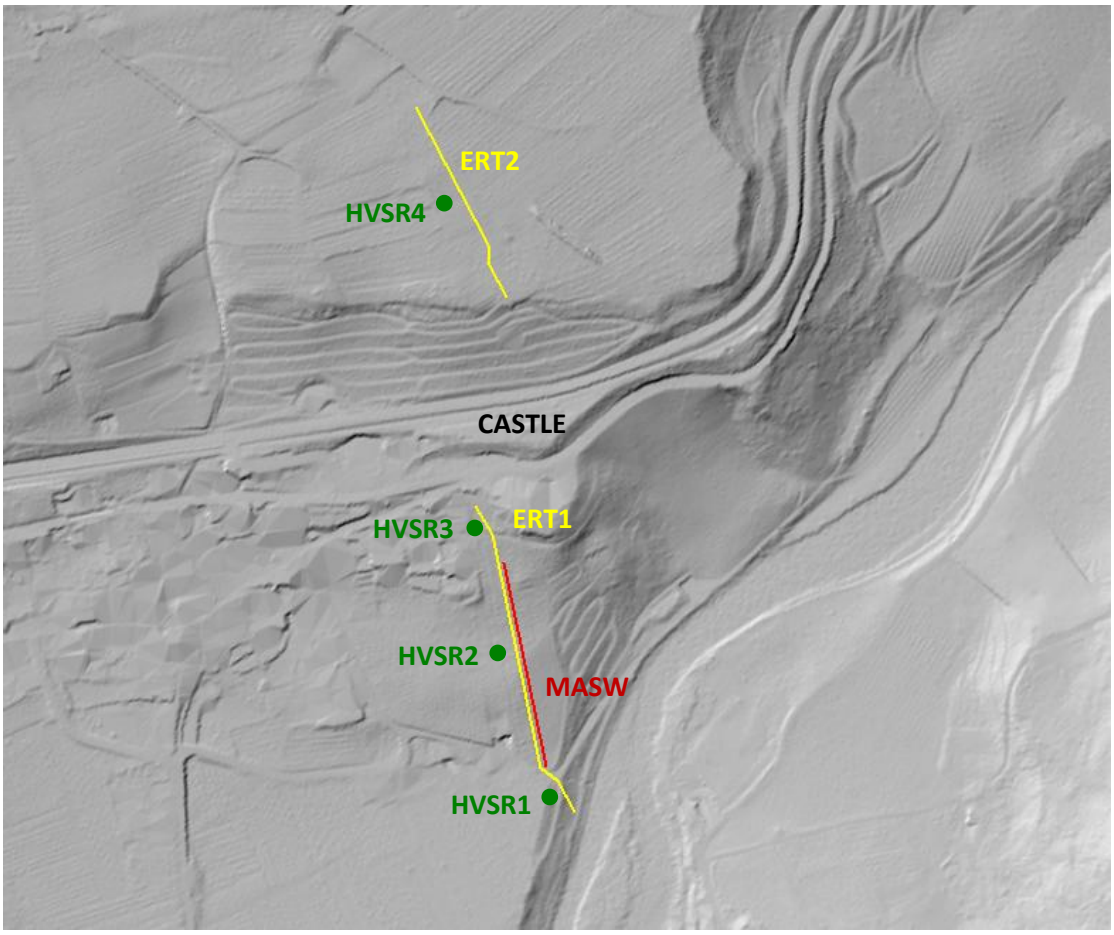

Figure 2.5. Location of the geophysical tests in the study area.

The results obtained are the following.

– MASW

The data acquired, which consist in the recording of wave trains from the instant of energization, were recorded on a laptop computer and subsequently processed. The geophysical interpretation of the data was performed with the software SWAMI for the inversion and with the software SeisImager for the spectral analysis of the surface wave contribution. The details of the software are reported in the Appendix 1 and the results in the Figure 2.6. They show that shear wave velocities are typical of unconsolidated sediments for the depth of investigation reached, enhancing no bedrock up to 31 m deep.

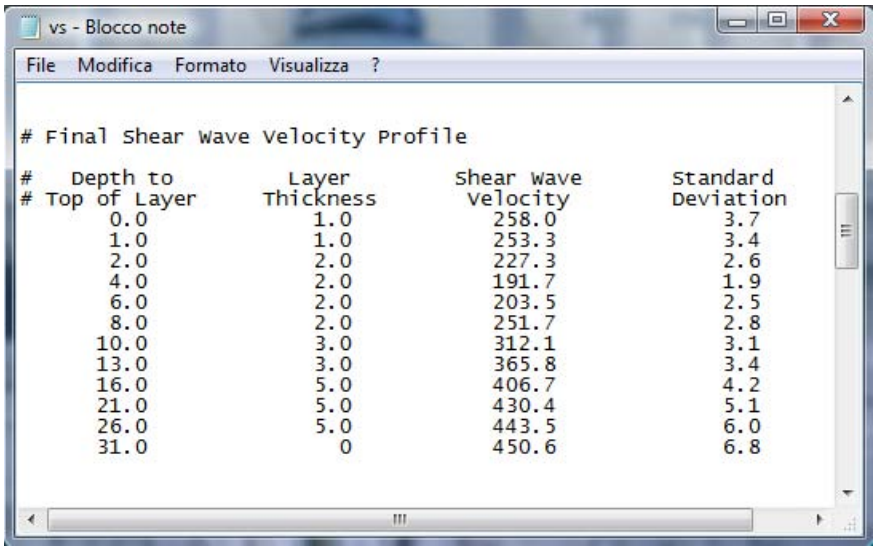

Figure 2.6. MASW results.

– ERT

The 2-D electrical resistivity tomography were obtained using the software profiler (Appendix 3) for the analysis and the software Surfer (Appendix 3) for the graphical representation. The results are shown in the Figures 2.7-2.9. In the firsts two graphs it can be seen that the resistivity is low, typical of unconsolidated sediments, meaning that there is no bedrock until the depth of the of the survey, so at least for 50 m no bedrock is detectable. The third figure, refers to Samoclevo site, instead show immediately high resistivity typical of consolidated rock, leading to the deduction that the bedrock is just below a thin layer of topsoil.

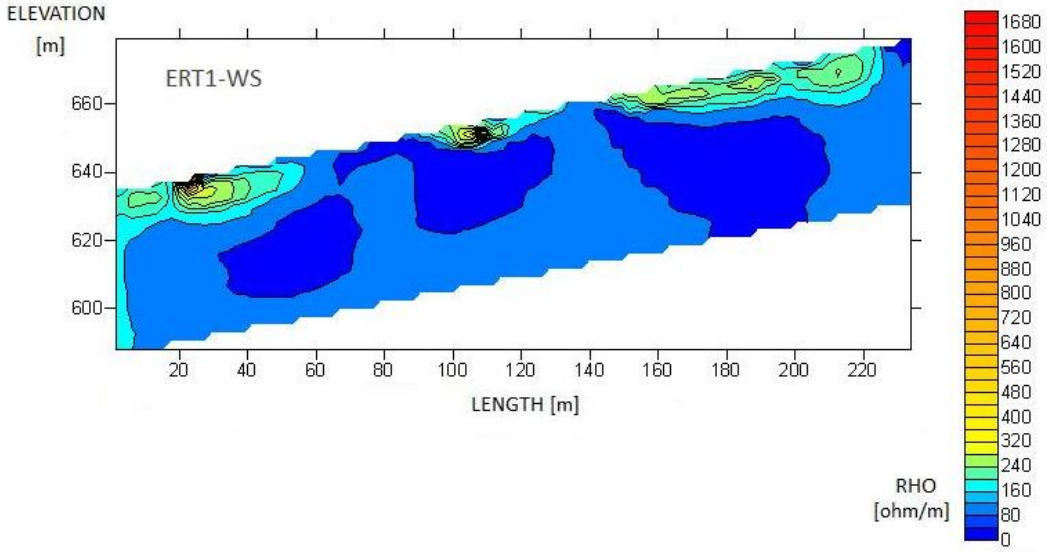

Figure 2.7. 2-D electrical resistivity tomography relative to the Werner-Schlumberger electrode array of the ERT1 line. Caldes site.

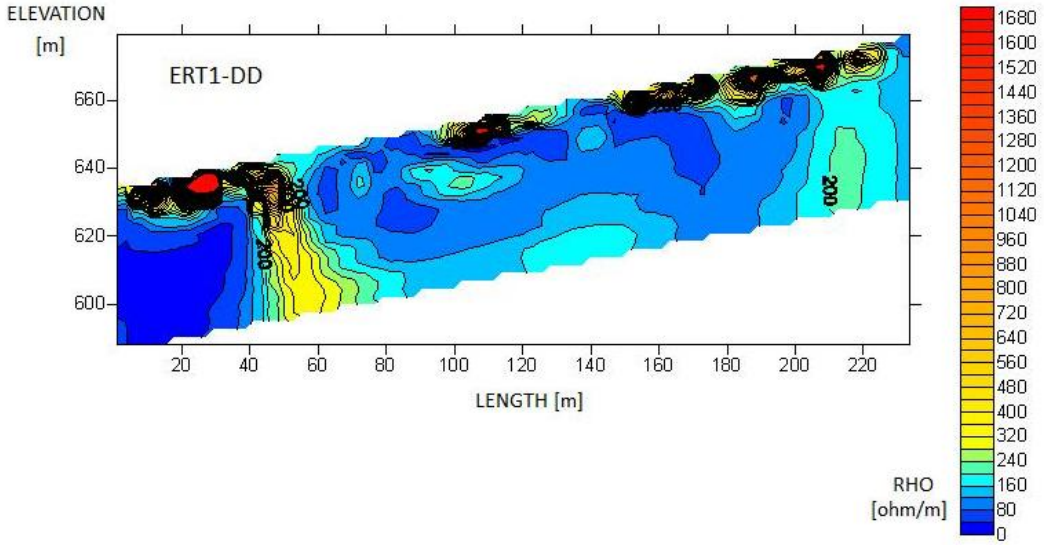

Figure 2.8. 2-D electrical resistivity tomography relative to the dipole-dipole electrode array of the ERT1 line. Caldes site.

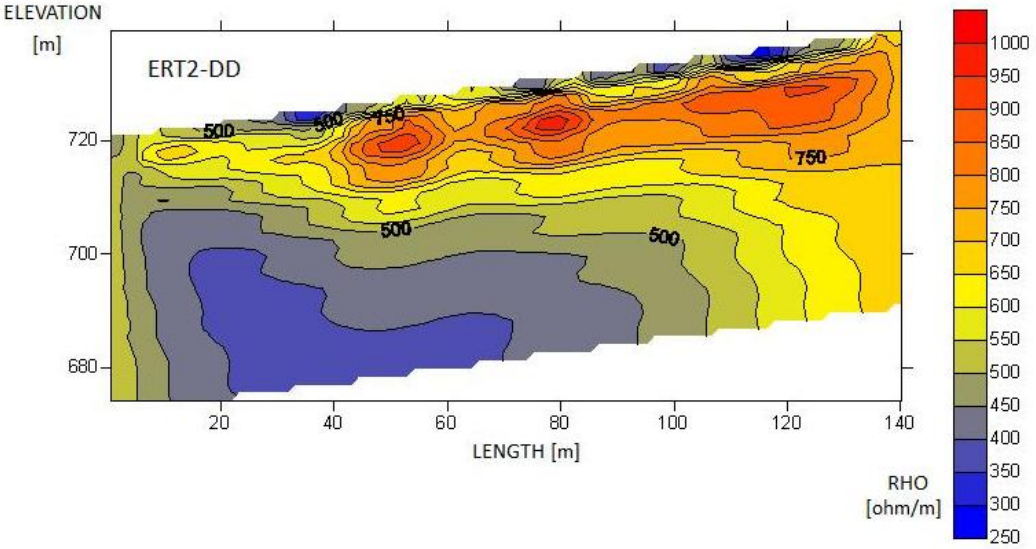

Figure 2.9. 2-D electrical resistivity tomography relative to the dipole-dipole electrode array of the ERT2 line. Samoclevo Site.

– HVSR

From recordings of seismic noise HVSR spectral curves were obtained and finally, from the inversion, the model of the subsoil was reconstructed in terms of velocity profiles. In this case, the used software is Grilla (Micromed spa) (Appendix 3).

The results are the H/V-frequency curves (NHV curves) and are represented in Figures 2.10-2.13.

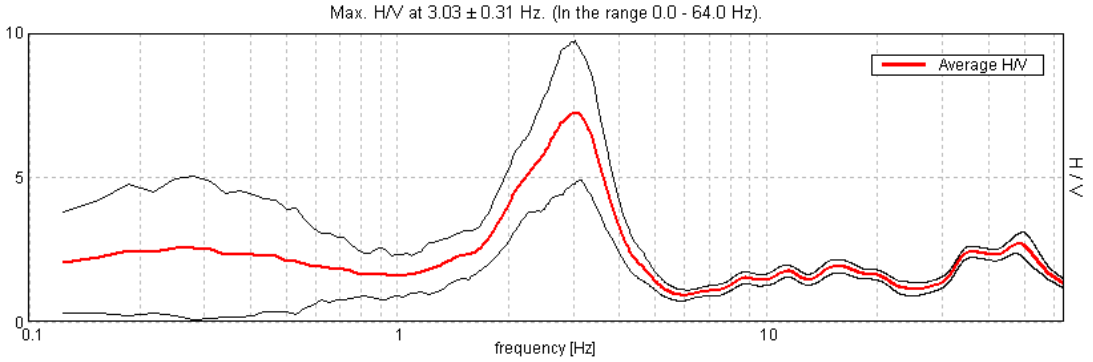

Figure 2.10. NHV curve for the test HVSR1. Caldes site.

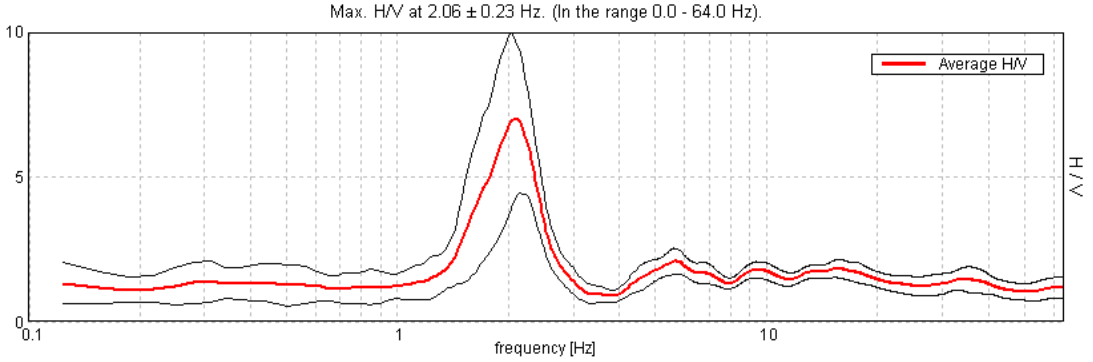

Figure 2.11. NHV curve for the test HVSR2. Caldes site.

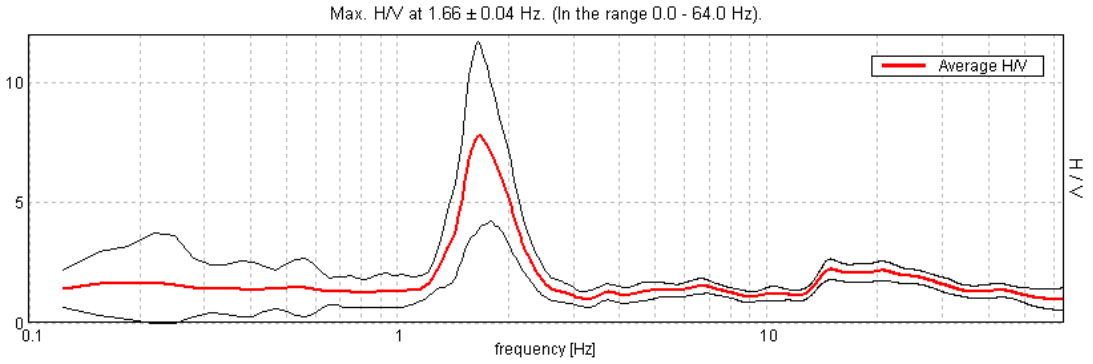

Figure 2.12. NHV curve for the test HVSR3. Caldes site.

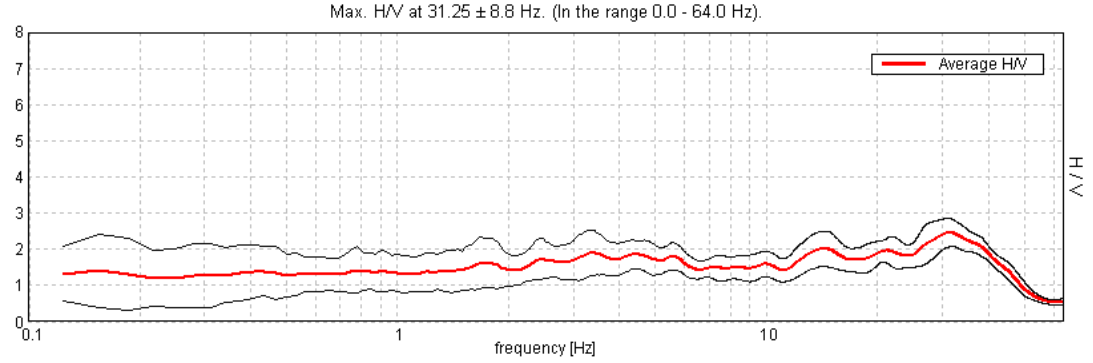

Figure 2.13. NHV curve for the test HVSR4. Samoclevo site.

The presence of a peak in the H/V ratio is directly related with the resonance frequency determined by the transition between two layers with a significant difference of the impedance contrast. Then it is possible to recognize the presence of the bedrock and its depth. In the firsts three tests the estimated bedrock depth are respectively 45 m, 50 m and 60 m.
In the last case (Figure 2.13), since the H/V ratio has not a peak, it can be deduced that the bedrock is at the surface level. These results confirm the considerations made analysing the results of the electrical surveys and allow us to determine the fundamental information about the bedrock depth. Another consideration can be made in the part downstream the castle: the slope of the bedrock is lower than the slope of the ground surface.

2.2 Borehole stratigraphies

In the area near the castle, 3 borehole stratigraphies located as shown in Figure 2.14 were made. The first survey, called S1, reaches a depth of 15 m, the other two (S2 and S3) are 25 m deep. The representation of the stratigraphies is reported in Figures 2.15-2.19. From the stratigraphies undisturbed samples of the materials constituting the subsoil were obtained, which were subsequently analysed in the laboratory. Although the stratigraphies are fairly close to each other, they show significant differences in the alternation of the layers but, despite this, as better explained in Chapter 3, the samples analysed belong to three main groups: clayey silts, sands and gravels. Being able to classify the soil into groups with similar characteristics is very useful in the next phase of modelling because it makes it easier to assign material properties to the relative layers.

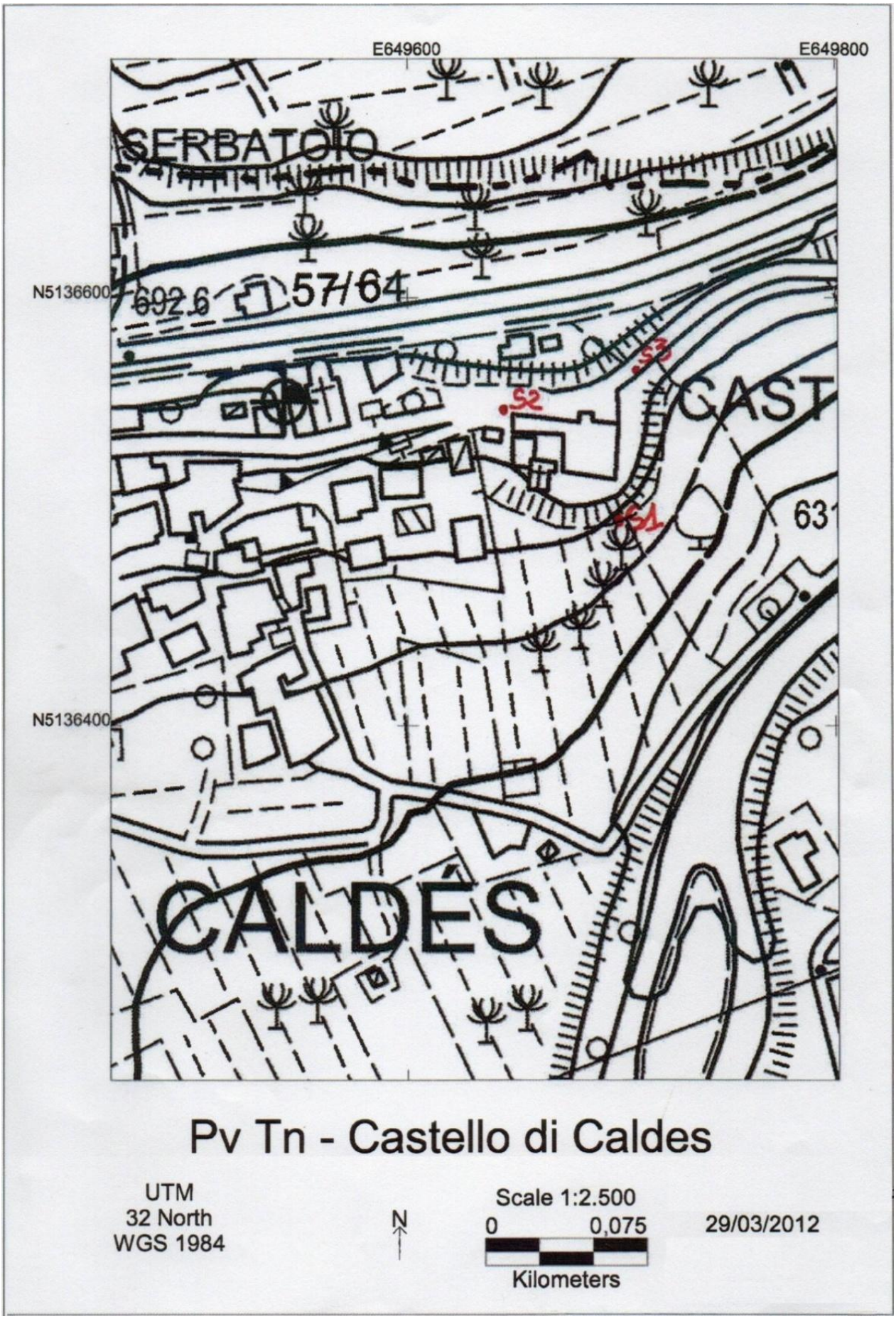

Figure 2.14. Location of borehole stratigraphies S1, S2 and S3

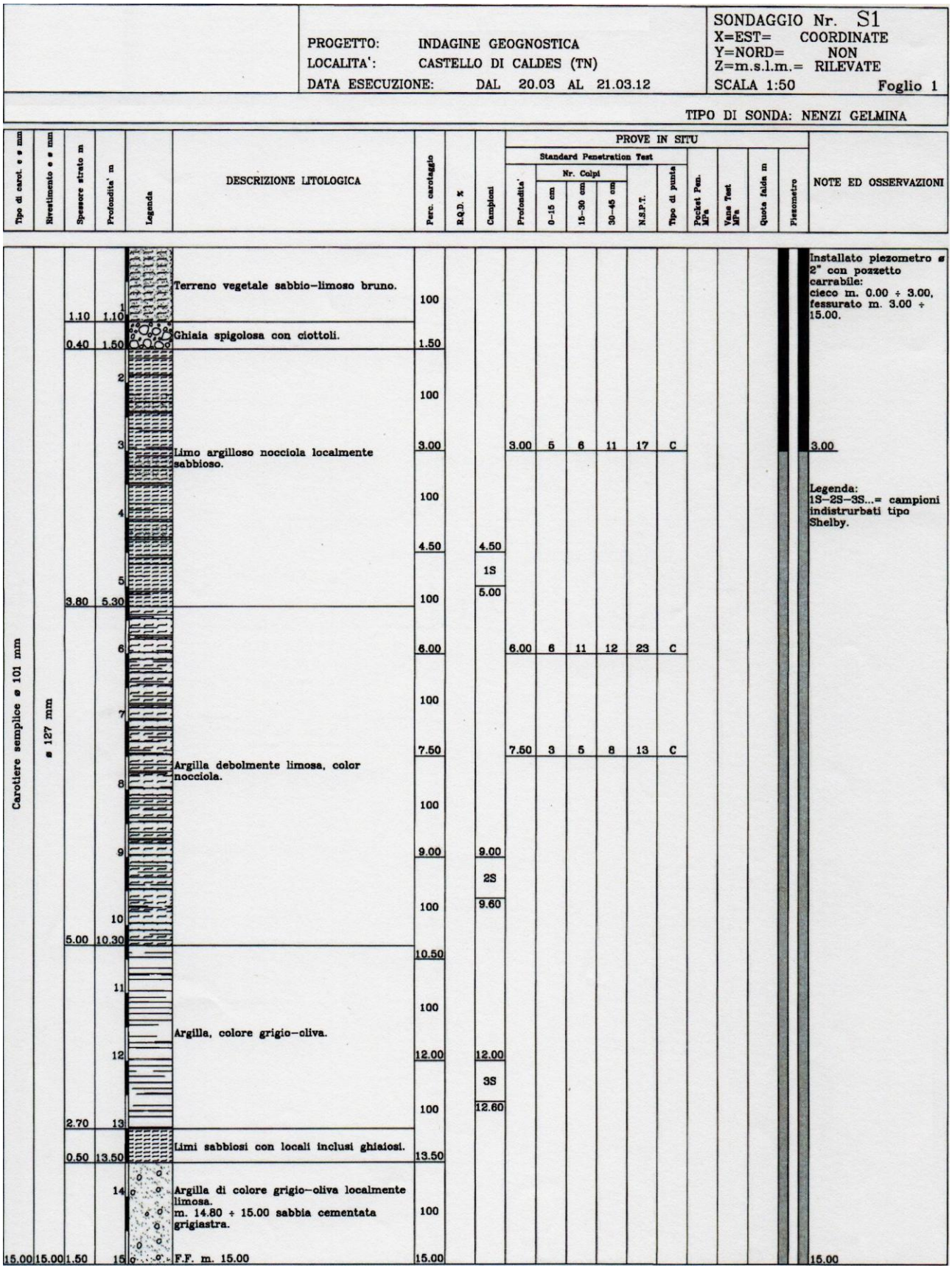

Figure 2.15. Borehole stratigraphy S1

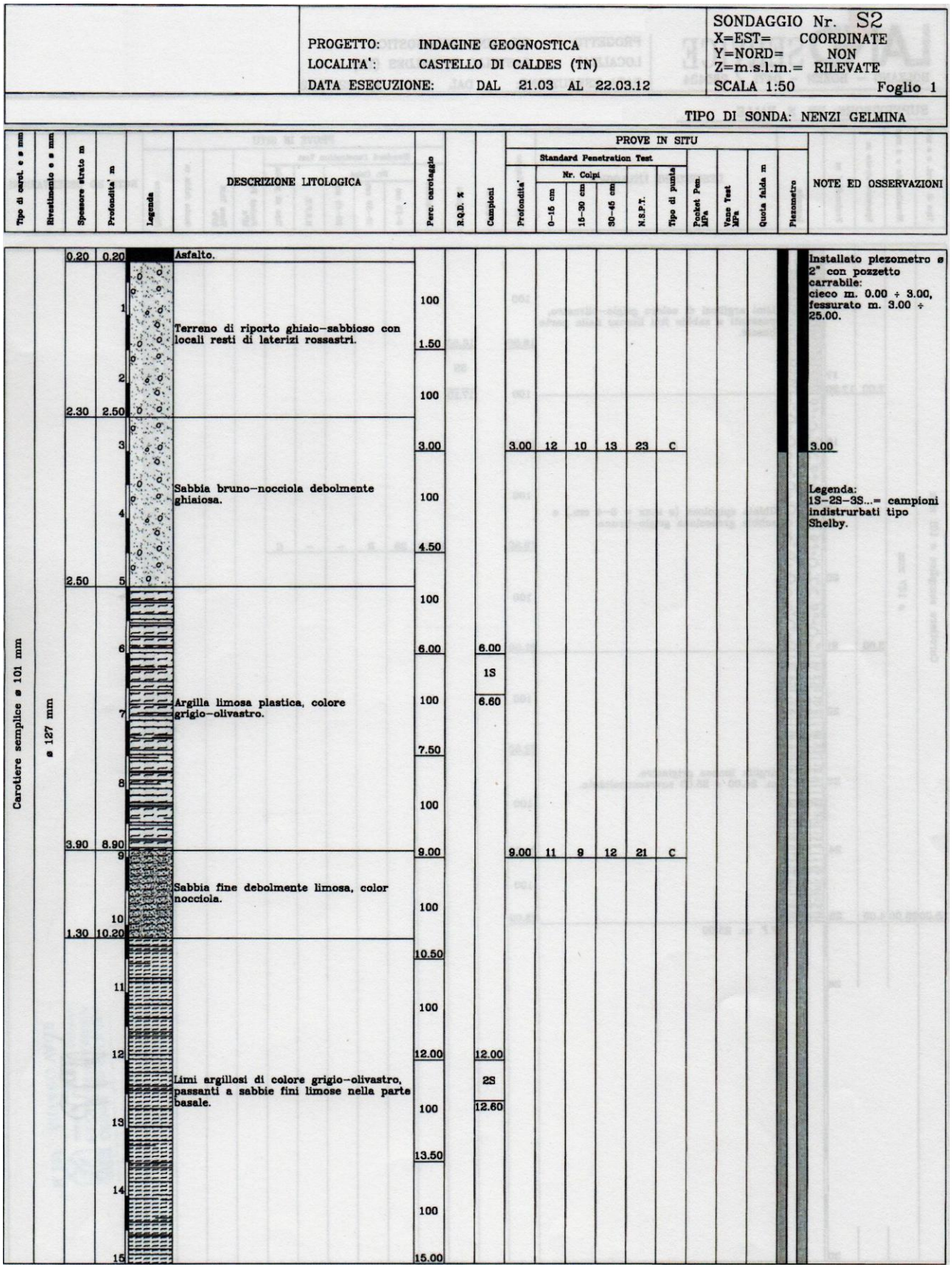

Figure 2.16. Borehole stratigraphy S2, part 1.

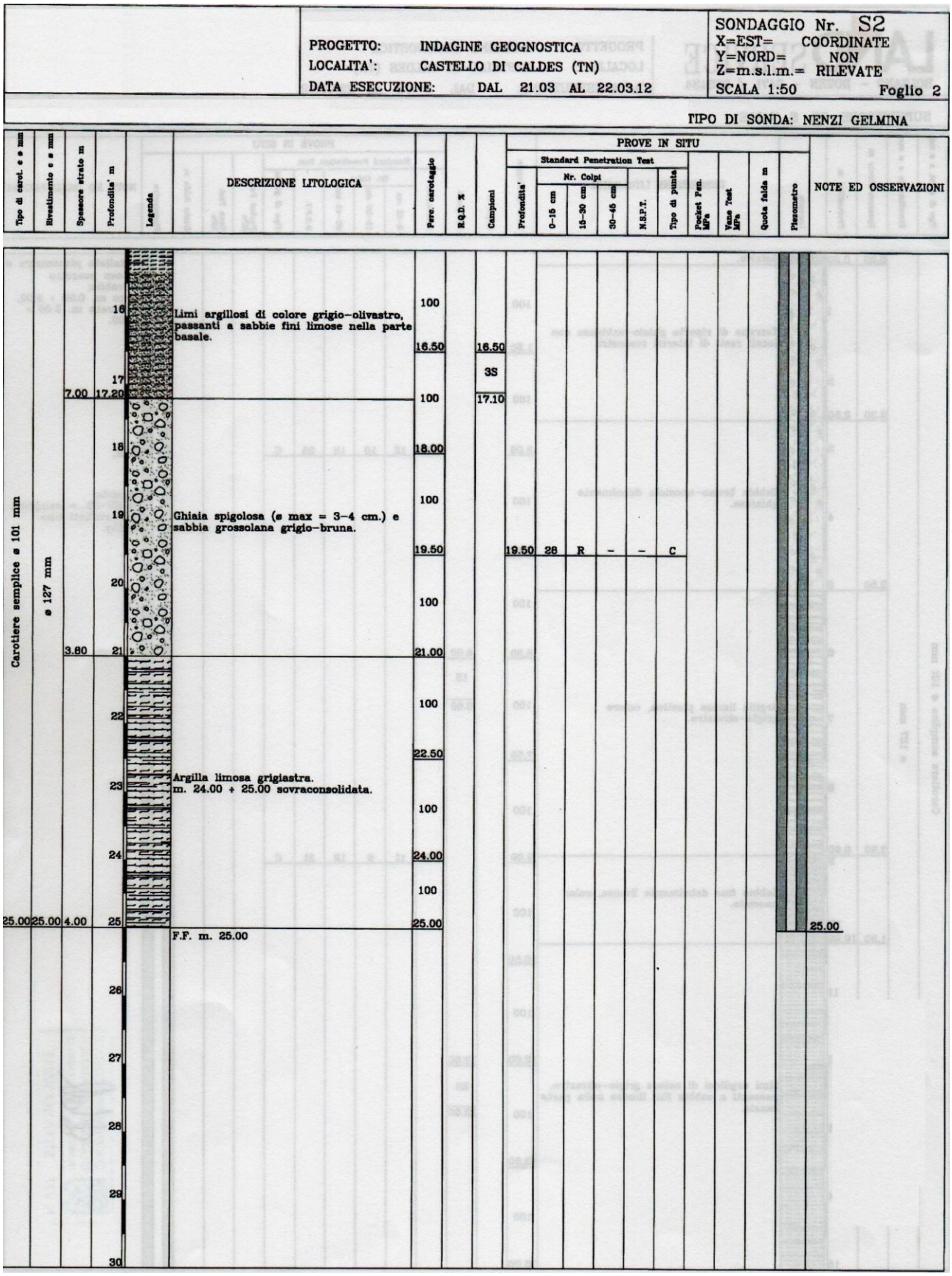

Figure 2.17. Borehole stratigraphy S2, part 2.

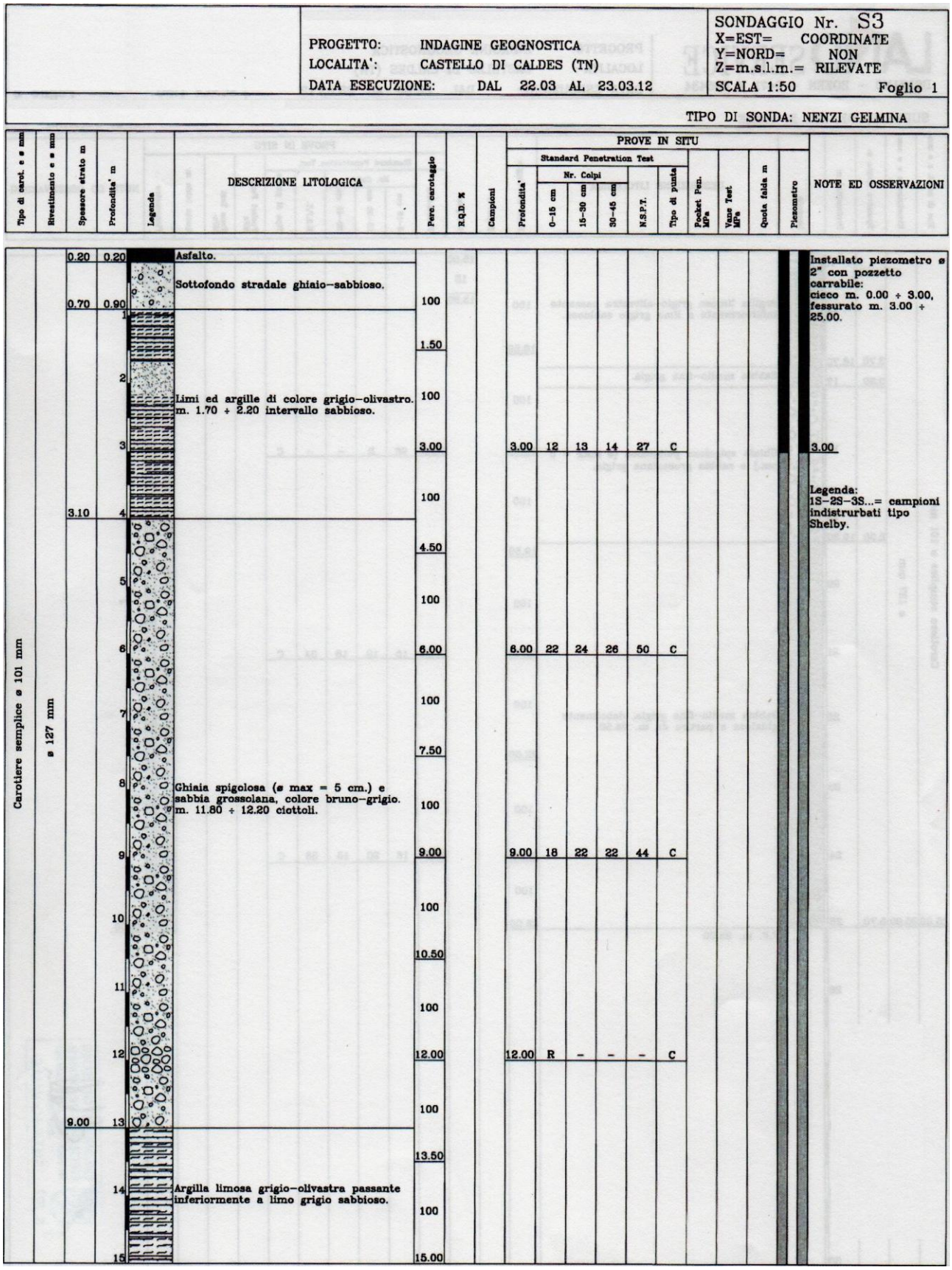

Figure 2.18. Borehole stratigraphy S1, part 1.

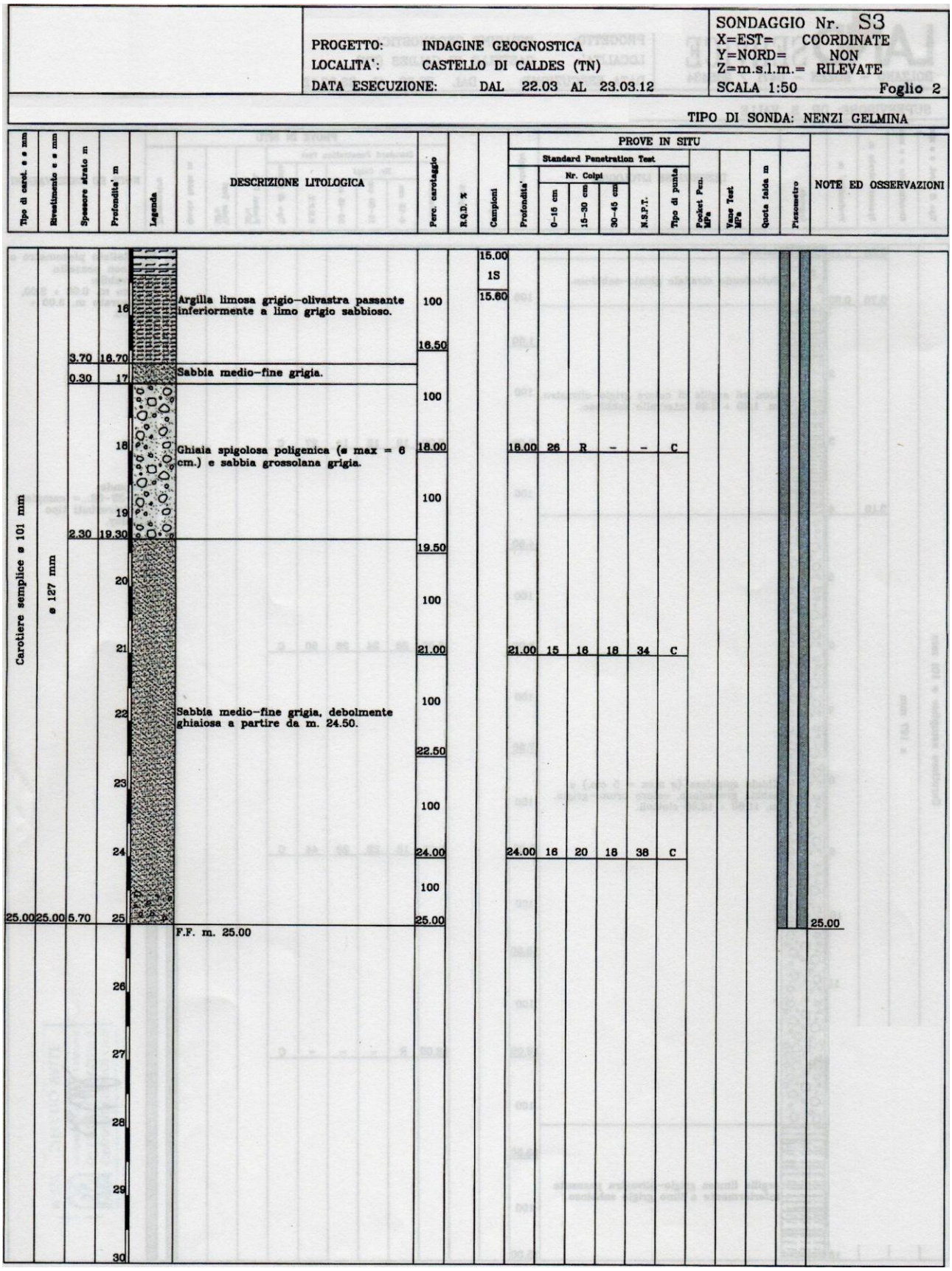

Figure 2.19. Borehole stratigraphy S3, part 2.

2.3 Subsurface models

Analysing the behaviour of the shear wave velocity with depth, a schematization of the subsurface was made. This schematization will be given in input to the numerical models and should not be too complicated. It was made grouping the strata having similar velocities in order to have a smaller number of layers. After, a mean value of the V_S for each layer was assigned and, also in accordance with the borehole stratigraphies, a material for each layer was assigned. The subsurface model obtained is reported in the table below (Table 2.1).

Table 2.1. Subsurface model.

Depth [m]	Vs [m/s]	Mean Vs [m/s]	Layer type	Assigned material
0	258	250	sand	SAND
1	253,3			
2	227,3			
4	191,7	200	silt + clay	CLAYEY SILT
6	203,5			
8	251,7			
10	312,1	350	gravel 1	GRAVEL
13	365,8			
16	406,7			
21	430,4	440	gravel 2	
26	443,5			
31	450,6			

The firsts 2 m of soil was classifies as sand, the following 6 m as clayey silt, the remaining 23 m as gravel but with different shear wave velocities. In this manner the subsurface is schematized into 4 strata with 3 different materials. The properties of these materials, which are necessary for the numerical modelling, have been determined by means of laboratory tests as described thoroughly in next chapter.

To validate the veracity of the hypothesized subsoil model, the NHV curve of the model was compared with the measured one through a direct method. Practically, at each point in which it was provided a passive seismic measurement, were manually entered for each layer values of thickness, V_S, and density. If the peaks of the measured and hypothesized curves are approximately similar, means that the model is good. Furthermore, given that the V_S profile is only up to 31 m, the thickness of the last layer was extended up to the known depth of the bedrock, with a small change in velocity to get a better fit of the curve. The shear velocity of the bedrock was assigned between 880-900 m/s because are typical velocity values for carbonate rock. This procedure was performed

for the 3 points because, being the bedrock less inclined than the surface, the layers are not parallel but are thinner near the castle and become thicker proceeding downstream. This consideration is not very important for the subsequent one-dimensional modelling because it assumes parallel layers (in fact it will be carried out on the central point considering it representative of the average behaviour), but it is important for the two-dimensional modelling which also considers the lateral variations.

In the figures below are reported the 3 subsurface models (Figures 2.20-2.22) and in the subsequent graphs (Figures 2.23-2.25) the comparison between their NHV curves and the measured ones.

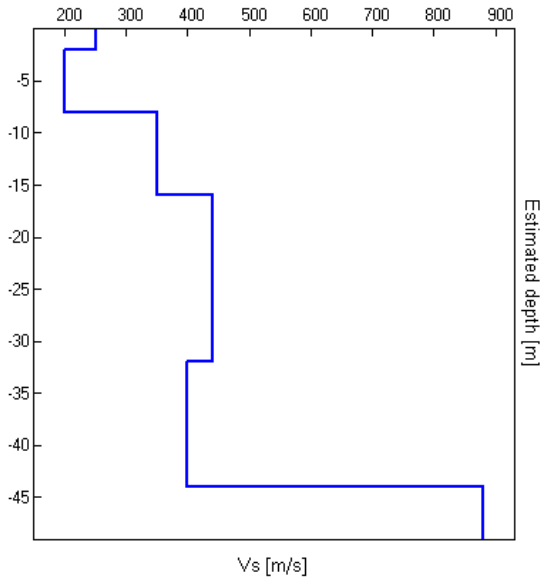

HVSR1 – downstream test		
Thickness [m]	Vs [m/s]	Density [kg/dm^3]
2	250	1,7
6	200	1,8
8	350	1,8
16	440	1,8
12	400	1,9
0	880	2
bedrock depth: 44 m		

Figure 2.20. Subsurface model for the site corresponding to the HVSR1 test.

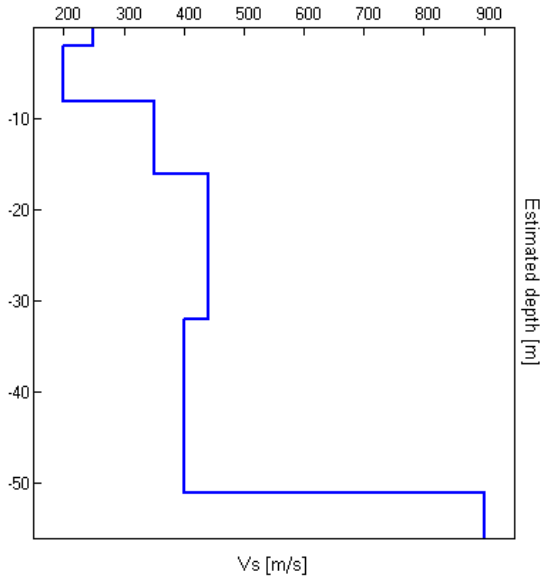

HVSR2 – intermediate test		
Thickness [m]	Vs [m/s]	Density [kg/dm^3]
2	250	1,7
6	200	1,8
8	350	1,8
16	440	1,8
19	400	1,9
0	900	2
bedrock depth: 51 m		

Figure 2.21. Subsurface model for the site corresponding to the HVSR2 test.

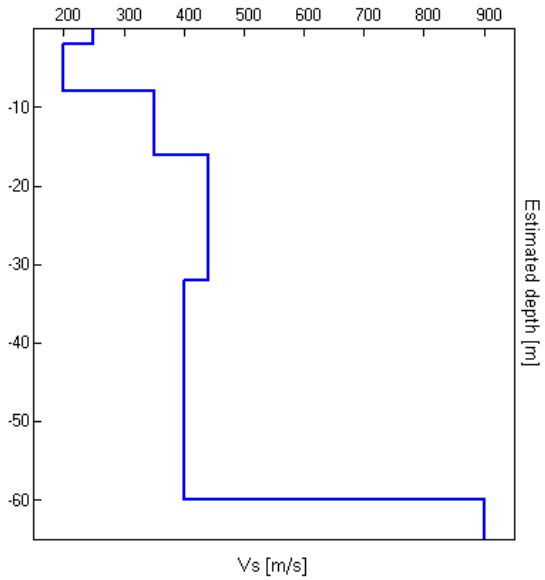

HVSR3 – upstream test		
Thickness [m]	Vs [m/s]	Density [kg/dm^3]
2	250	1,7
6	200	1,8
8	350	1,8
16	440	1,8
28	400	1,9
0	900	2
bedrock depth: 60 m		

Figure 2.22. Subsurface model for the site corresponding to the HVSR3 test.

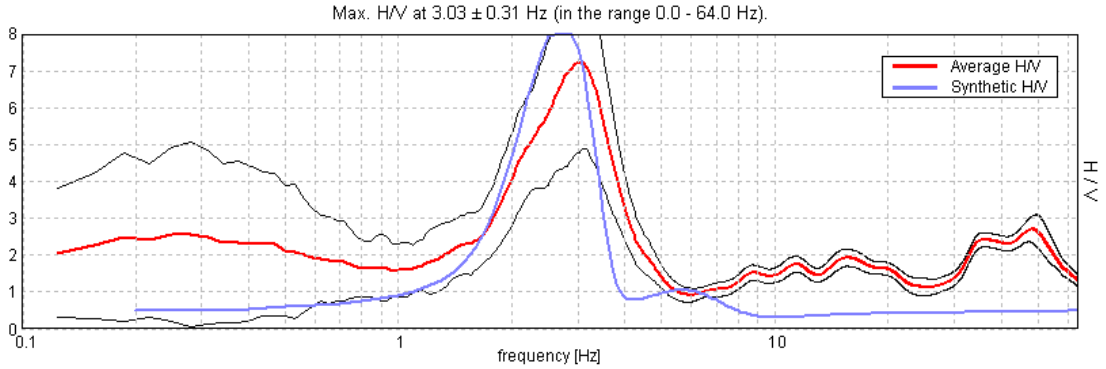

Figure 2.23. Comparison between calculated and measured NHV curve for the test HVSR1.

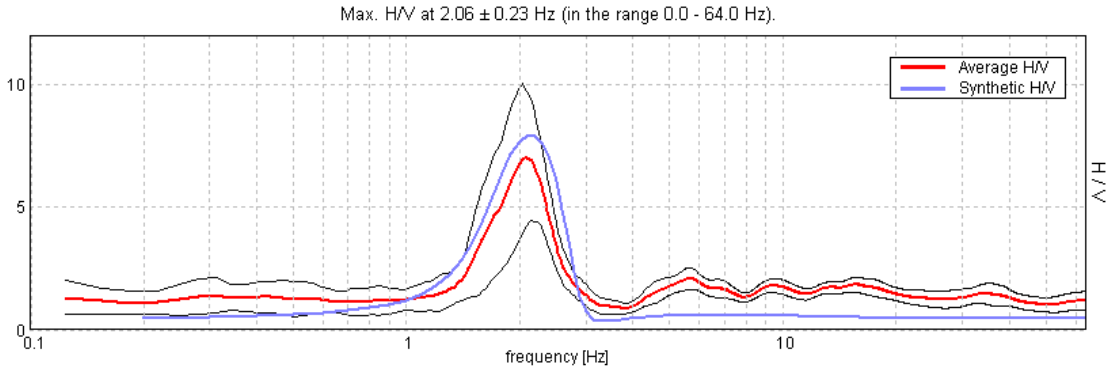

Figure 2.24. Comparison between calculated and measured NHV curve for the test HVSR2.

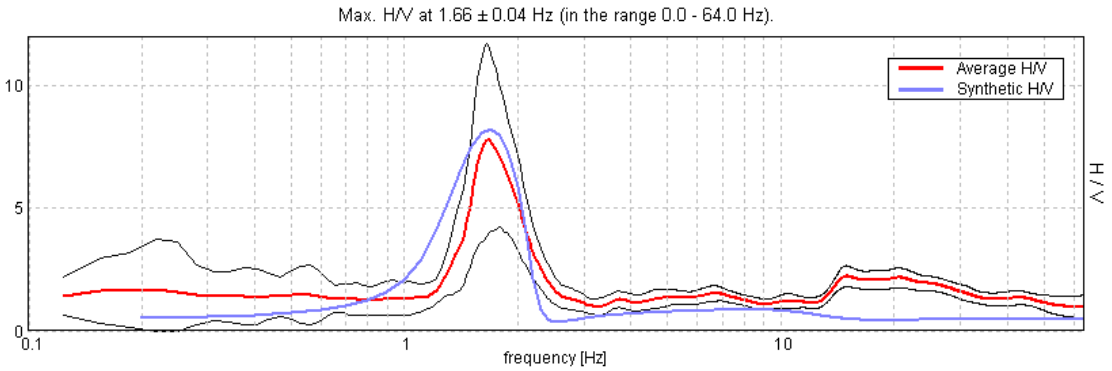

Figure 2.25. Comparison between calculated and measured NHV curve for the test HVSR3.

From the comparisons, it can be seen that the calculated and measured curves are quite similar, so the schematization of the subsurface is good.

In Figures 2.26 are reported the limit between bedrock and sediments and the trend of the layers deduced from the 3 tests.

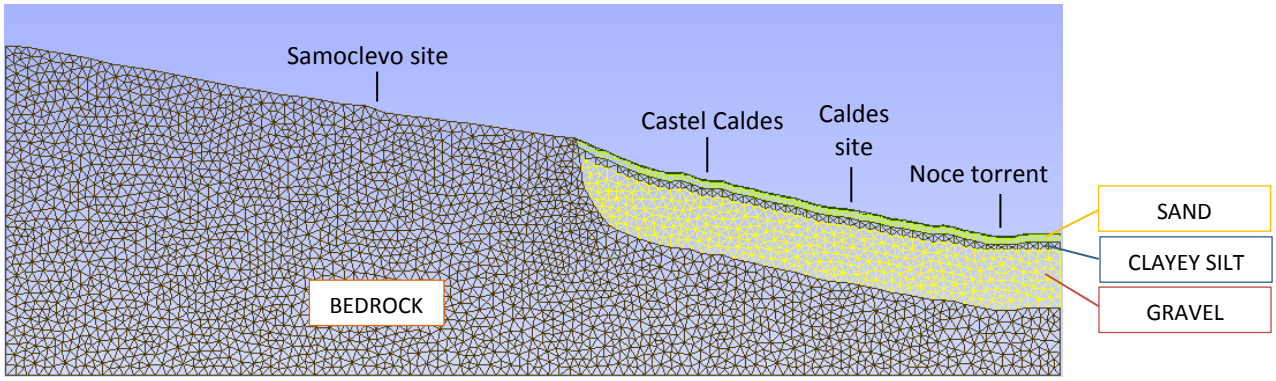

Figure 2.26. Limit between bedrock and sediments and trend of the subsurface layers.

Chapter 3

Dynamic properties of soils

The nature and distribution damage due to earthquakes is strongly influenced by the responses of soils to cyclic loading. This response is mainly controlled by the mechanical properties of the soil. For problems dominated by wave propagation effects, only low levels of strain are induced in the soil. For other important problems, for example those involving the stability of soil masses, large strains are induced in the soil. The behaviour of soils subjected to dynamic loading is governed by the *dynamic soil properties*. Different field and laboratory techniques are available for the measurement of dynamic soil properties, each with different advantages and limitations with respect to different problems. Some tests measure low strain behaviour and others soil behaviour at high strain levels. The selection of testing techniques requires careful consideration and understanding of the specific problem at hand (Kramer, 1996).

The soil properties that influence wave propagation and other low-strain phenomenal are: stiffness, damping, Poisson's ratio and density. Stiffness and damping are the most important, the others have less influence and tend to fall within relatively narrow ranges. The stiffness and damping characteristics of cyclically loaded soils are critical to the evaluation of many earthquake engineering problems at low, intermediate and high strains because soils are nonlinear materials. At high levels of strains, the influence of the rate and number of cycles of loading on shear strength may also be important. Also volume change characteristics are important at high strain levels (Kramer, 1996).

3.1 Stress-strain behaviour of cyclically loaded soils

Three wide classes of soils models can be used to represent the stress-strain behaviour of cyclically loaded soils: *equivalent linear models*, *cyclically nonlinear models*, and *advanced constitutive models*. Equivalent linear models are the simplest and most commonly used but have limited ability to represent many aspects of soil behaviour under cyclically loaded conditions. At the other hand, advanced constitutive models can represent many details, but they are complex and difficult to calibrate, so impractical for many common problems (Kramer, 1996). Below is described only the equivalent linear model because it is the one used in the numerical simulations.

For the equivalent linear model, a typical soil subjected to symmetric cyclic loading might exhibit a hysteresis loop of the type shown in Figure 3.1. This hysteresis loop can be described in two ways: (i) by the actual path of the loop itself, and (ii) by parameters that describe its general shape. Two important characteristics of the shape of hysteresis loop are its inclination and its breadth. The inclination of the loop depends on the stiffness of the soil. It can be described at any point during the loading process by the *tangent shear modulus*, G_{tan}. G_{tan} varies throughout a cycle of loading but its average value over the entire loop can be approximate by the secant shear modulus

$$G_{sec} = \frac{\tau}{\gamma}$$

where τ and γ are the shear stress and shear strain amplitudes, respectively. Hence, G_{sec} describes the general inclination of the hysteresis loop. The breadth of the hysteresis loop is related to the area, it is a measure of energy dissipation and can be described by the damping ratio

$$\xi = \frac{W_D}{A\pi W_S} = \frac{1}{2\pi}\frac{A_{loop}}{G_{sec}\gamma^2}$$

where W_D is the dissipated energy, W_S the maximum strain energy stored in the system, and A_{loop} the area of the hysteresis loop (Figure 3.1). The parameters G_{sec} and ξ are often indicated as *equivalent linear* material parameters.

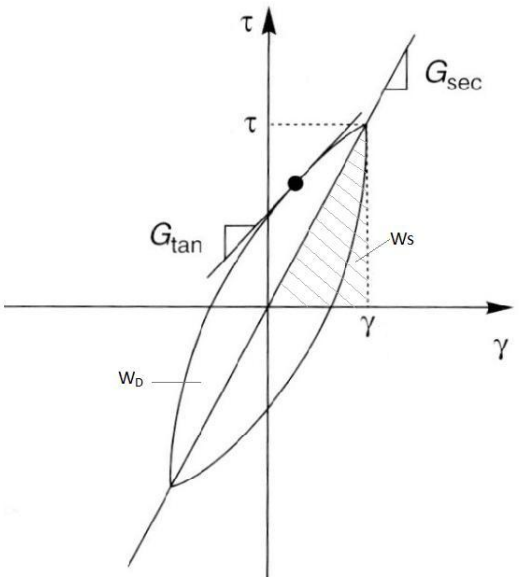

Figure 3.1. Hysteresis loop for one cycle of loading (Modified from Kramer, 1996).

Great attention has been given to the characterization of G_{sec} and ξ for different soils because some of the most commonly used methods of ground response analysis are based on the use of equivalent linear properties. The assumption of the linearity embedded in the use of equivalent linear model

has important implication when it is used for ground response analysis, as it will be discussed in Chapter 4. Moreover, equivalent linear models imply that the strain will always return to zero after cycling loading, and since a linear material has as no limiting strength, failure cannot occur (Kramer, 1996).

3.1.1 Shear modulus

Laboratory tests have shown that soil stiffness is influenced by cyclic strain amplitude, void ratio, mean principal effective stress, plasticity index, overconsolidation ratio and number of loading cycles. The secant shear modulus of an element of soil varies with cyclic shear strain amplitude: at low strain amplitudes, the secant shear modulus is high but it decreases as strain amplitude increases. The locus of points corresponding to the tips of hysteresis loops of various cyclic strain amplitudes is called a *backbone curve* (Figure 3.2a). Its slope at the origin (zero cyclic strain amplitude) represents the largest value of the shear modulus, G_0. At greater cyclic strain amplitudes, the *modulus ratio* G_{sec}/G_0 decreases to values of less than 1. Then, the characterisation of stiffness of an element of soil requires consideration of both G_0 and the manner in which the modulus ratio G/G_0 varies with a cyclic strain amplitude and other parameters. The variation of the modulus ratio with shear strain is described graphically by a modulus reduction curve (Figure 3.2b).

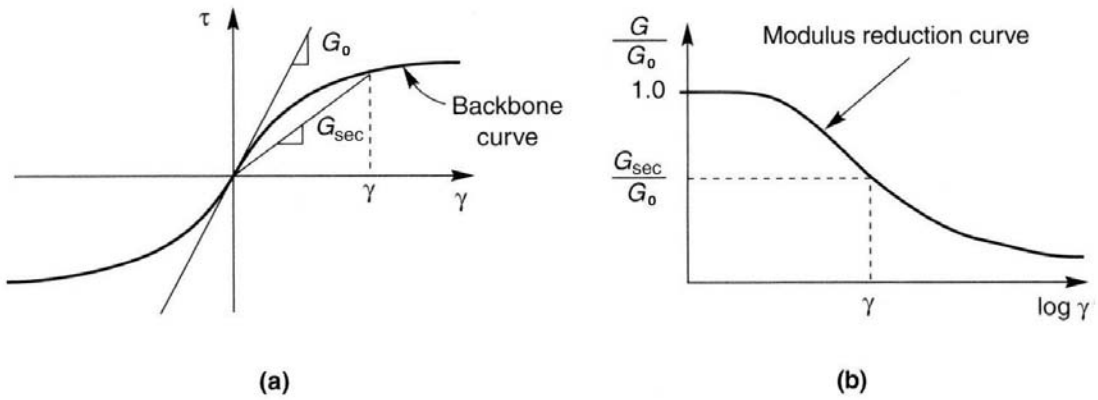

Figure 3.2. Backbone curve (a) and modulus reduction curve (b) (Modified from Kramer, 1996).

The measured shear wave velocities can be used to compute G_0 because most seismic geophysical tests induce shear strains lower than about $3 \cdot 10^{-4}\%$

$$G_0 = \rho V_S^2$$

where ρ is the mass density of soil.

The use of measured shear wave velocities is in general the most reliable means of evaluating the in situ value of G_0. When shear wave velocity measurements are not available, G_0 can be estimated in several different ways by means of laboratory tests or from in situ test parameters (Kramer, 1996).

Modulus reduction

At the beginning, the modulus reduction behaviour of coarse- and fine-grained soils where treated separately. Recent research, however, has revealed a gradual transition between the modulus reduction behaviour of nonplastic coarse-grained soil and plastic fine-grained soil.

Soil plasticity influences the shape of the modulus reduction curve: the shear modulus of highly plastic soils was observed to degrade more slowly with shear strain than did low-plasticity soils, as shown in Figure 3.3. Moreover the $PI = 0$ modulus reduction curve is very similar to the average modulus reduction curve that was commonly used for sands when coarse- and fine-grained soils were treated separately.

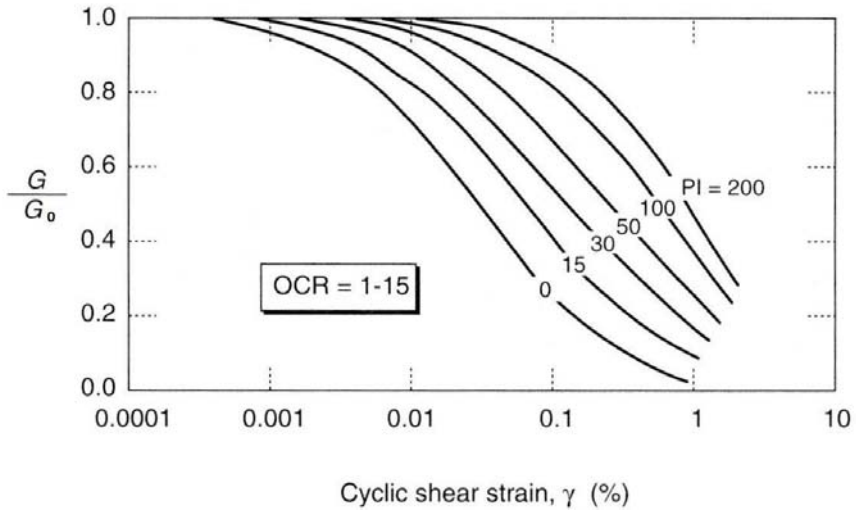

Figure 3.3. Modulus reduction curves for fine-grained soils of different plasticity (Modified from Kramer, 1996).

This similarity suggest that the modulus reduction curves of Figure 3.3 may be applicable to both fine- and coarse-grained soils. The difficulty of testing very large specimens has precluded the testing on gravelly soils in the laboratory. Available test data indicate that the average modulus reduction curve is similar to that of sand (Kramer, 1996).

Modulus reduction behaviour is also influenced by other factors, summarized in Paragraph 3.1.3.

3.1.2 Damping ratio

In theory, no hysteretic dissipation of energy takes place at strains below the linear cyclic threshold shear strain. Experimental evidence, however, shows that some energy is dissipated even at very low strain levels, so the damping ratio is never zero. Above threshold strain, the breadth of the hysteresis loops of a cyclically loaded soil increase with increasing cyclic strain amplitude. It indicates that the damping ratio increases with increasing strain amplitude.

Also the damping ratio behaviour is influenced by plasticity characteristics: damping ratios of high plastic soils are lower than those of low plasticity soils at the same cyclic strain amplitude (Figure 3.4). The $PI = 0$ damping curve is nearly identical to the average damping curve that was commonly used for coarse-grained soils when they were soils were treated separately from fine-grained.

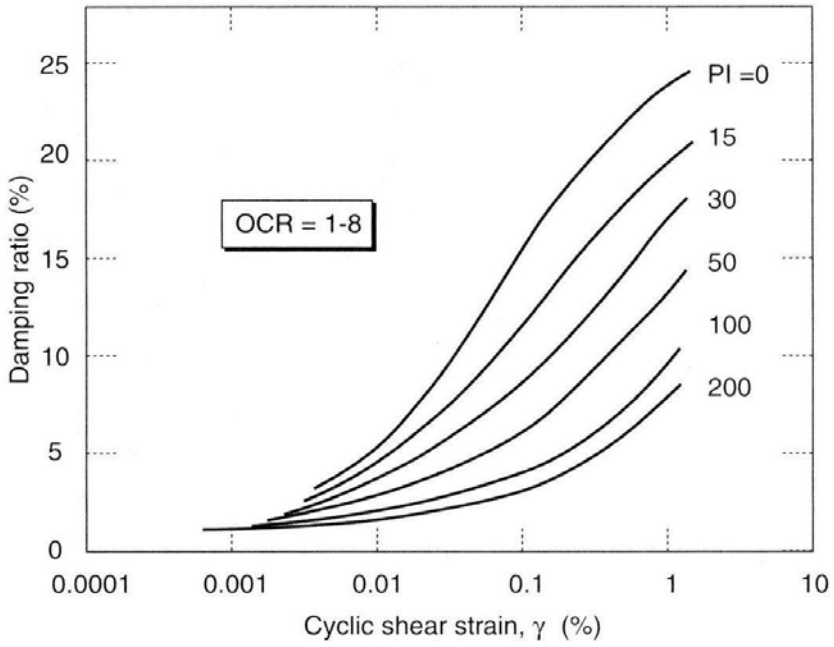

Figure 3.4. Variation of damping for fine-grained soils of different plasticity (Modified from Kramer, 1996).

This similarity suggests that the damping curves of Figure 3.4 can be applied to both fine- and coarse-grained soils. The damping behaviour of gravel is very similar to that of sand (Kramer, 1996).

Other factors that influence the damping ratio are summarized in the next Paragraph.

3.1.3 Parameters affecting shear modulus and damping

Because so many parameters regarding the environmental and loading conditions affect the shear modulus and damping of soils, Hardin and Drnevich (1972a) have thoroughly analysed the five parameters that, in general, are very important (strain amplitude, effective mean principal stress, void ratio, number of cycles of loading and degree of saturation). They have obtained the following conclusions:

1. The shear modulus decreases and damping ratio increases, very rapidly, with increasing strain amplitude. However, the rate of decrease or increase depends on many parameters and a single relationship between modulus or damping and strain amplitude is not enough. The initial rates of decrease in modulus or increase in damping are higher for:
   - lower effective mean principal stress;
   - higher void ratio;
   - lower number of cycles of loading.

   The initial rates are also higher for cohesive than for cohesionless soils.
2. The shear modulus increases and damping ratio decreases with increasing effective mean principal stress. For very small strain amplitudes the modulus varies with the 0.5 power of effective mean principal stress, but at large strain amplitudes the modulus variation is about with the 1.0 power. The damping decreases approximately with the 0.5 power of effective mean principal stress independent of strain amplitude.
3. The shear modulus decreases and damping ratio decreases with increasing void ratio in undisturbed cohesive soils.
4. The shear modulus decreases for cohesive soils and increases slightly for cohesionless soils with the number of cycles of loading. The damping ratio decreases more or less with the logarithm of the number of cycles of loading in both cohesive and cohesionless soils, up to about 50.000 cycles. Beyond this there appears to be a fatigue mechanism involved that causes the damping to increase with the number of cycles.
5. The effect of degree of saturation on the modulus and damping in cohesionless soils is small, but the modulus of cohesive soils increases rapidly with decreasing degree of saturation.

Also other parameters, such as geologic age, cementation, overconsolidation ratio, strain rate and frequency of loading, may affect the shear modulus and damping ratio, but their importance is lower.

3.2 Laboratory tests

Laboratory tests are usually performed on relatively small specimens that are assumed to be representative of a large body of soil. Their ability to provide accurate measurements of soil properties depends on their ability to replicate the initial conditions and loading condition of the problem of interest (Kramer, 1996).

Several laboratory tests measure low-strain soil properties, among these are the *resonant column test* and the *cyclic torsional shear test*, which are the two tests performed to characterize the properties of the soils belonging to the study area. The large amount of data used to produce the graphs below were provided by the Geological Survey of the Autonomous Province of Trento for this experimental study of the Castel Caldes area.

The samples analysed fall into three large granulometric families: clayey silts, sands and gravel beaches (Figure 3.5, Viganò et al., 2013b). Clayey silts and sands are well reproducible in the laboratory, the next section describes the experimental methodology used to analyse them.

The analysed samples are 8 and their particle size curves with the notation for each specimen are reported in Figure 3.6.

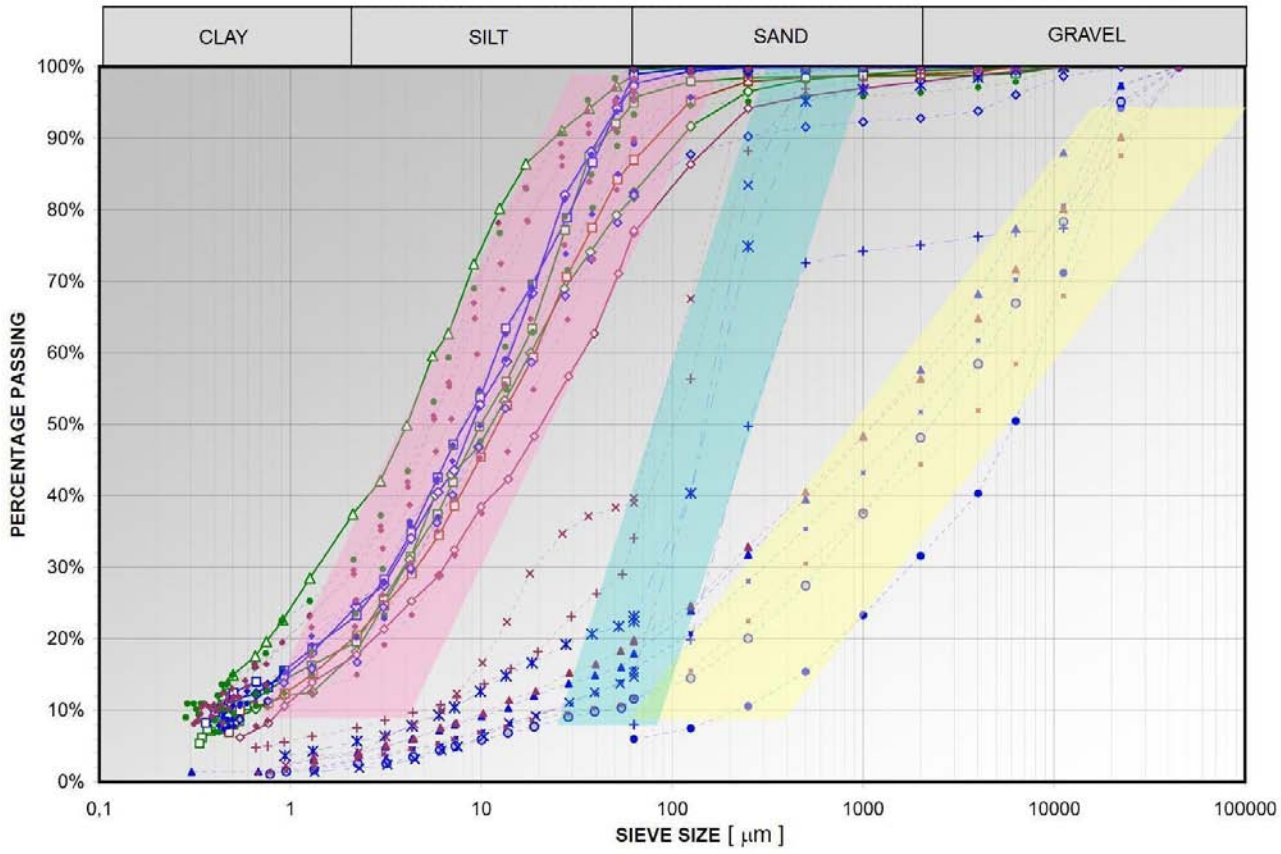

Figure 3.5. Particle size curves relative to clayey silts (pink), sand (light blue) and sandy gravel (yellow).

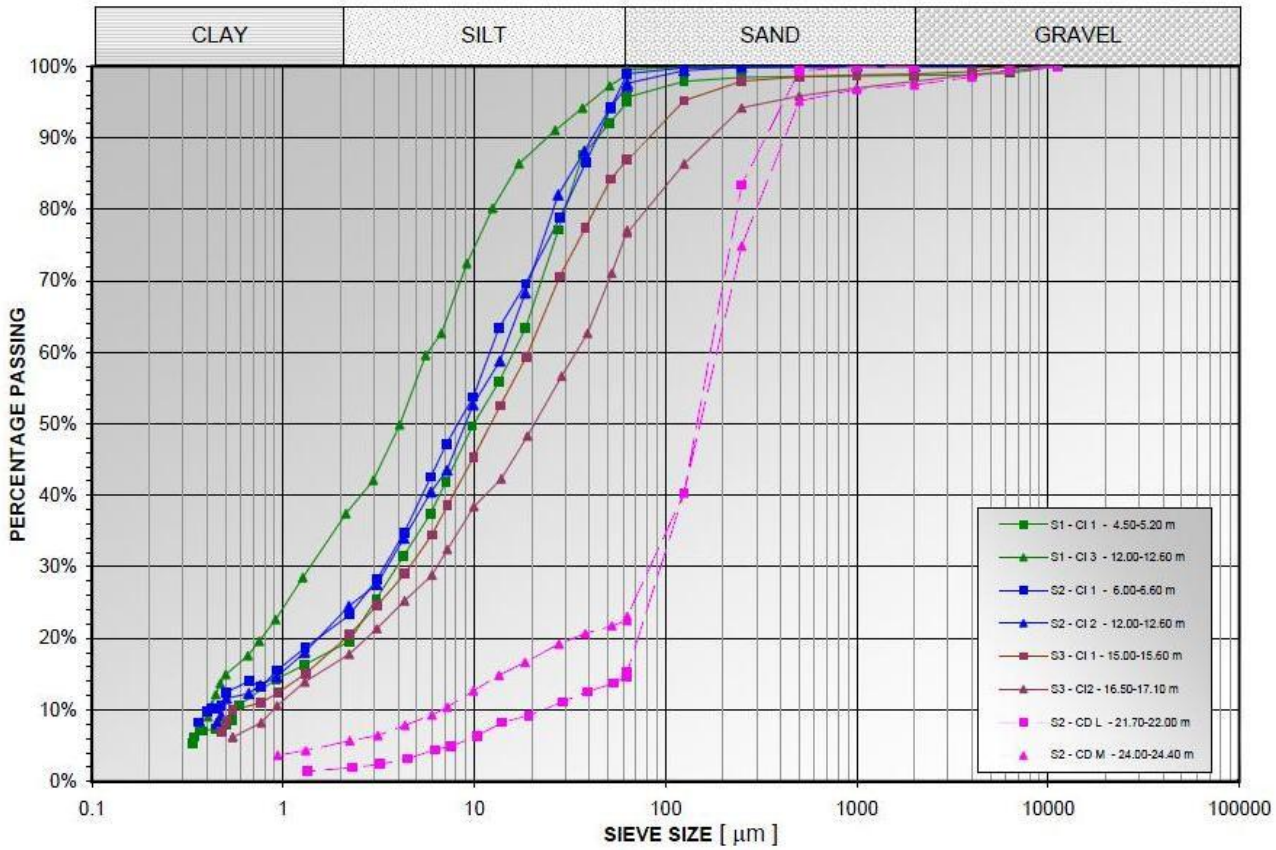

Figure 3.6. Grain size curves of the 8 analysed samples.

3.2.1 Description of the experimental method

Firstly, typical geotechnical laboratory tests were conducted, such as classification (e.g. Casagrande classification, Figure 3.7), oedometer consolidation tests, hydraulic conductivity measurements in triaxial cell and isotropically consolidated undrained triaxial tests (CIU). The laboratory tests for the determination of the dynamic soil properties were conducted through resonant column (RC) and cyclic torsional shear (CTS) devices performed according to the scheme *fixed-free* (Figure 3.8) (Viganò et al, 2013b).

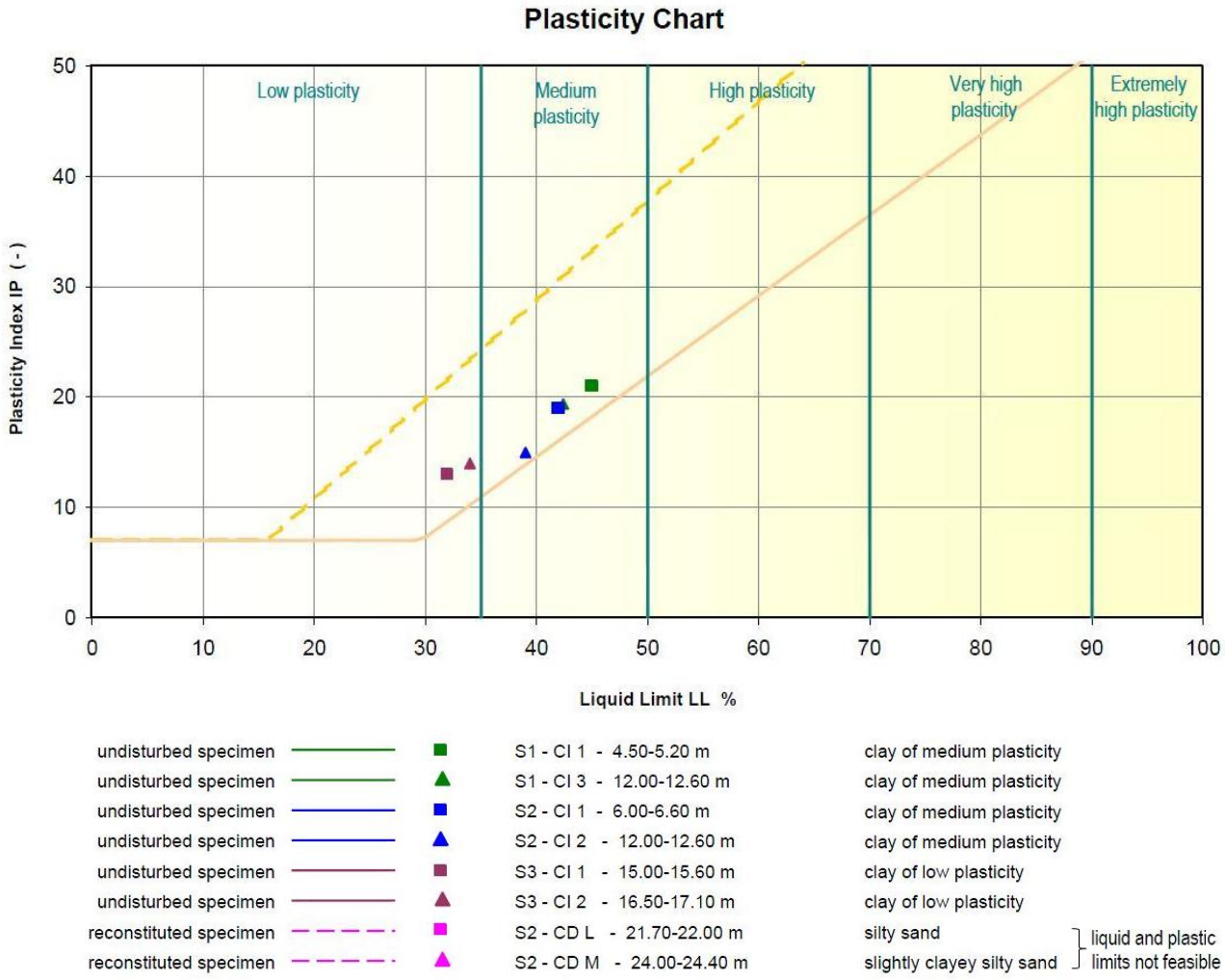

Figure 3.7. Casagrande classification for the 8 analysed samples.

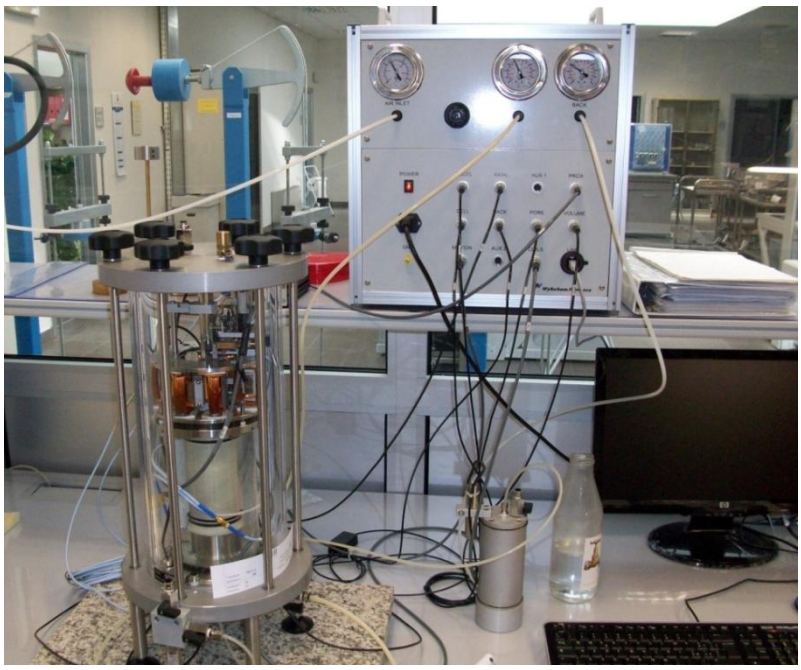

Figure 3.8. Resonant column and cyclic torsional shear devices. To the left there is the triaxial cell. In the middle, at the top, the control unit. In the middle, at the bottom, the device for measuring the volume changes of the specimen.

- **Resonant column tests**

During RC tests, the resonance frequency and the rotation of the specimen are measured. From the value of the first quantity it is possible to derive the velocity of propagation of shear waves and then the shear modulus G. The shear deformation γ is obtained from the measurement of the rotations of the specimen (Simoni, 2004).

During the tests, a sinusoidal electrical signal, variable in amplitude and frequency, is generated by a function generator and a power amplifier. The electrical signal $V(t)$ is transformed into mechanical torsional stress $M_t(t)$ by an electromagnetic motor. It consists in eight coils interacting with four permanent magnets leaning on the head of the specimen by means of a plate. The excitation frequency is varied so that the system detects the resonance condition. In resonance condition there is a relationship between the velocity of propagation of shear waves V_S and the fundamental frequency f_n of the type $V_S = f(f_n, h)$, where h is the height of the specimen and f a function that depends on the boundary conditions of the specimen. Placing an accelerometer on the free end of the specimen, it is possible to identify the resonance condition relative to the first vibration mode because varying the frequency varies the response of the specimen, and because the fundamental frequency is that at which the response is maximum. Knowing the density of the sample it is possible to determine the shear modulus through the relation $G = \rho {V_S}^2$.

By the RC device the damping ratio can be determined in two ways: considering the resonance amplification factor (*steady state method*), or by interrupting the excitation and measuring the decay of the free oscillations (*amplitude decay method*).

The experimental results obtained during RC tests are interpreted by referring to the theory of shear-waves propagation in a linear elastic medium to determine the shear modulus, or, to the theory of free or forced oscillations in an elasto-plastic medium to determine the damping ratio (Simoni, 2004).

- **Cyclic torsional shear tests**

In CTS tests a saturated and consolidated specimen is subjected to the action of a torque moment applied to the free end by means of a torsional motor, to which is sent a signal (sine or triangle) of constant and predetermined frequency with gradually increasing amplitude. By means of two non-contact transducers, which are applied in correspondence of the head of the specimen, and by means of the rotations that they have measured, it is possible to plot the hysteresis loop corresponding to

the stress amplitude imposed. Knowing the hysteresis loops for different stress amplitude, the decay laws of the shear modulus and damping ratio can be derived (Simoni, 2004).

- **Procedure**

With reference to standard RC tests, two fundamental phases can be distinguished:

1) *Multistage consolidation test* during which the measurement of G_0 is taken at three different values of the effective confinement pressure. It is incremented until the value of the effective lithostatic pressure has been reached.
2) *Large strain test* during which, varying the amplitude of the torque moment, is carried the resonance test. After that, the excitement is interrupted and the *amplitude decay test* is run (i.e. the analysis of the free vibrations). The amplitude is varied again and the test repeated, up to explore a field of deformations sufficiently extended.

Both CTS test and the resonant column test can by carried on the same specimen using the Stokoe equipment with fixed – free conditions because the preliminary stages are the same (saturation and isotropic consolidation) and the excitation is based on a torque moment.

The phases of RC and CTS tests procedures are listed below, the details for each phase can be found in Simoni, 2004:

1) equipment and of the sample preparation;
2) apparatus and specimen installation;
3) saturation;
4) consolidation;
5) decay in CTS mode;
6) reconsolidation of the specimen;
7) evaluation of pre-straining;
8) decay in RC mode;
9) disassembly of the test.

Regarding the samples analysed, this procedure was strictly followed. Precisely, each specimen was previously saturated with the application of the back-pressure and subsequently different steps of consolidation were conducted. At the end of each phase of consolidation, measurements of the dynamic shear modulus at very low deformation (G_0) in RC mode were carried out, with the aim of knowing its correlation with the effective pressure (σ'_C) for the different soils investigated (*multistage consolidation test*, Figure 3.9). Reached the desired state of stress, low-frequency cyclic torsional shear tests (0.5 Hz for 25 cycles) were carried out, using progressively increasing stresses

without invading the field of plastic deformations. To comply with this, care was taken to avoid an increase of the pore pressure and to check that there was no cyclic degradation. So were checked that strain, dynamic shear modulus (G) and the damping factor (D) of the n-th cycle were close to those of the initial cycles (Viganò et al, 2013b). The results are reported in Figure 3.10.

Resonant column tests were then conducted, modulating the frequency in a field that included the resonance frequency of the sample - loads actuator system. In resonance conditions, knowing the inertia of the specimen and of the actuator, it is possible to determine the shear modulus at a certain value of deformation. The resonant column tests were repeated for different stresses up to the maximum power of the equipment, obtaining the typical decay curve beyond the elastic threshold (*large strain test*) (Figure 3.11).

The damping values were detected in reference to the hysteretic behaviour of the material (CTS tests, interpolation of hysteresis loops, Figure 3.10) or to its viscoelastic characteristics (RC tests, *half-power method*; Figure 3.11). In addition, the damping was measured using the *free decay* technique, linked to the logarithmic decrement of the free oscillations after a stress applied at the resonance frequency (Viganò et al, 2013b).

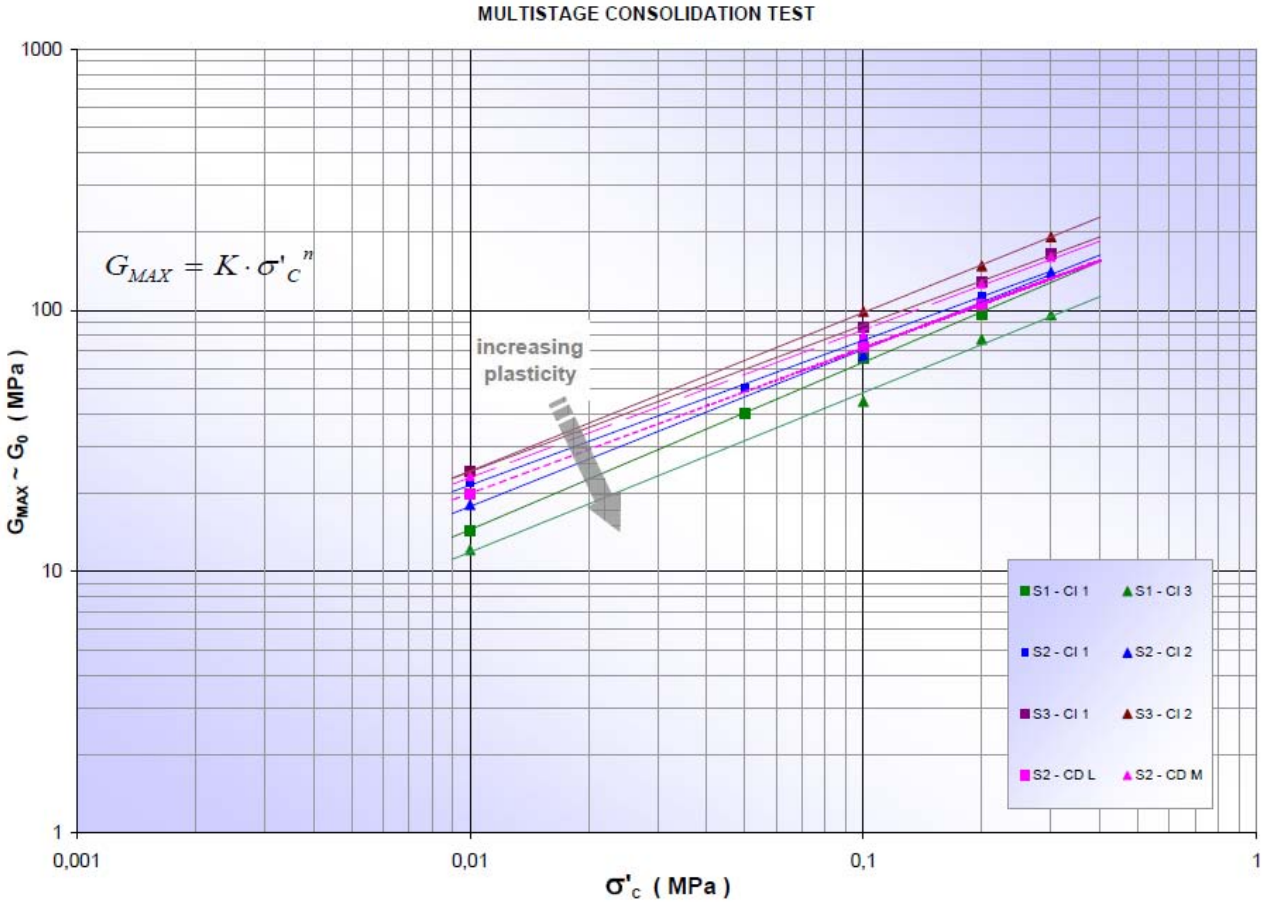

Figure 3.9. Multistage consolidation test for the 8 analysed samples.

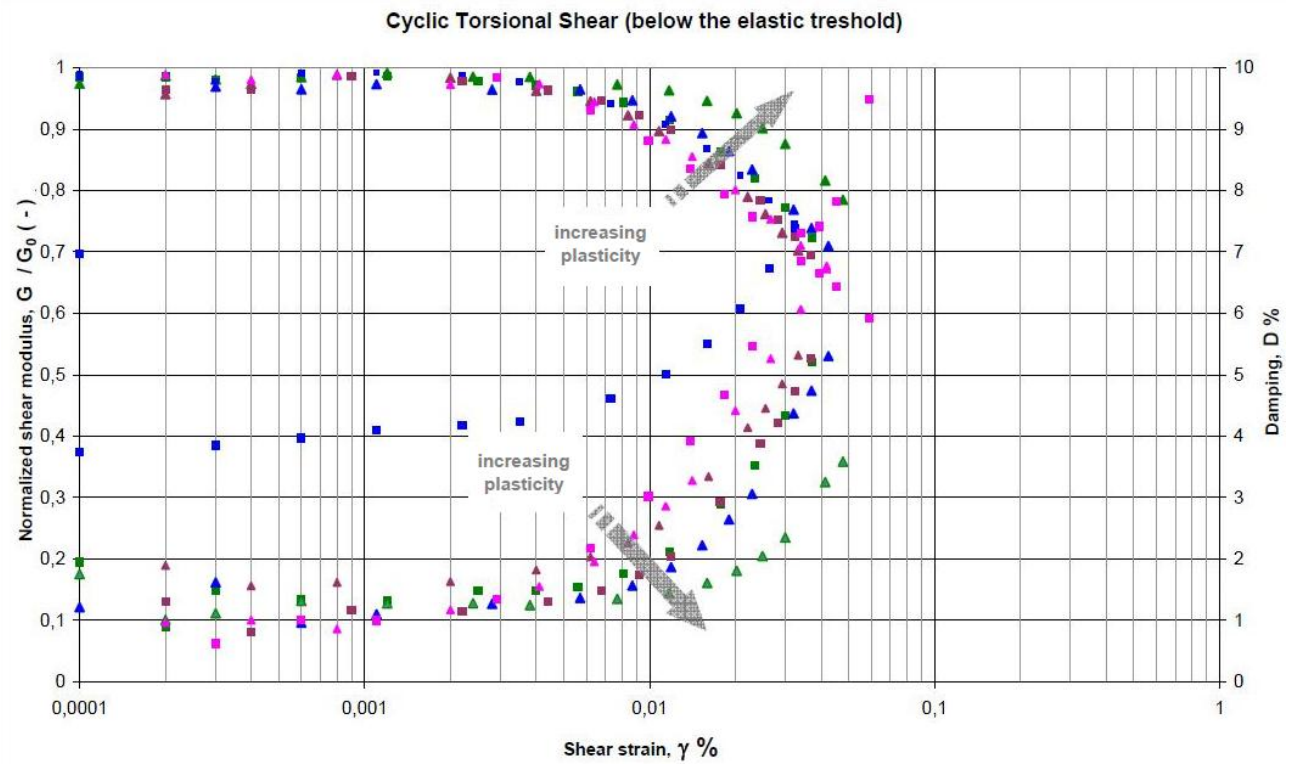

Figure 3.10. Experimental measurements carried out in cyclic torsional shear mode for the 8 analysed samples.

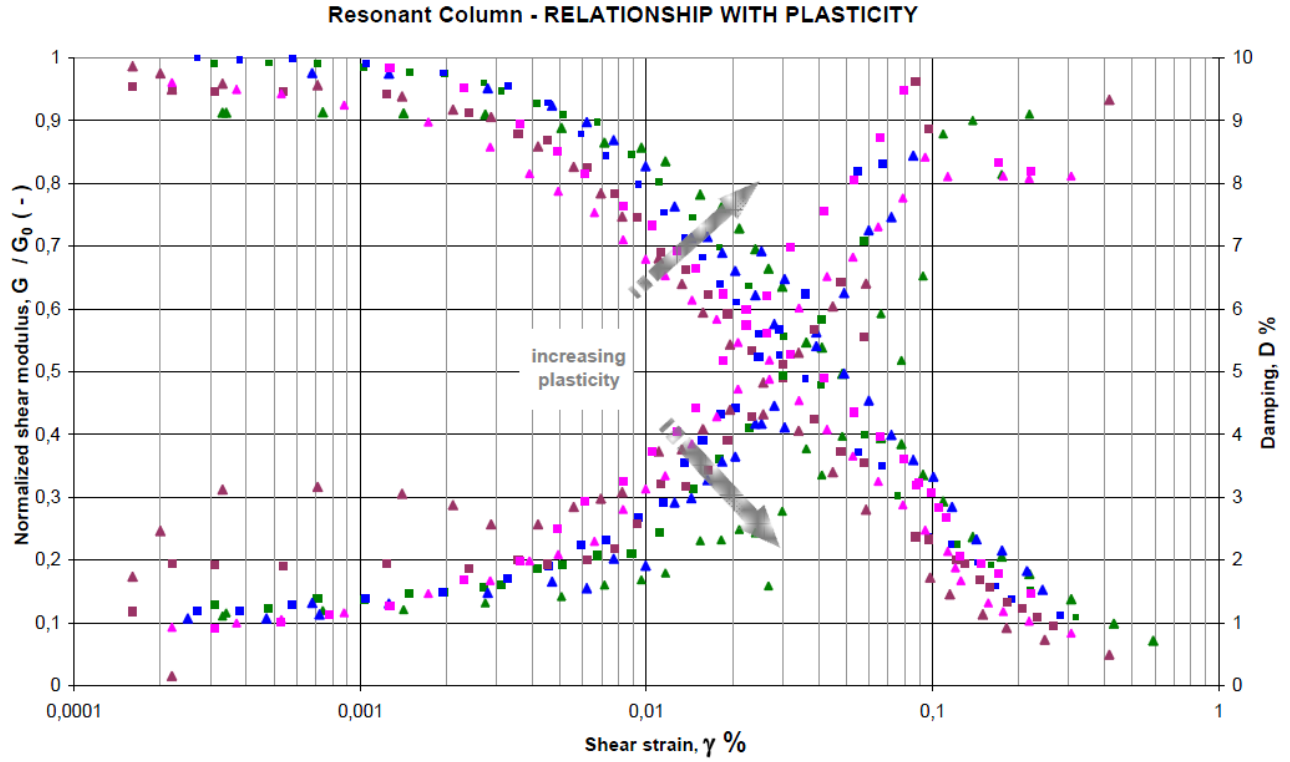

Figure 3.11. Experimental measurements carried out in resonant column mode for the 8 analysed samples.

3.2.2 Elaboration of the results

The experimental data, obtained by dynamic cyclic laboratory tests, can be used to express analytical relations that correlate stresses to deformations and damping ratio to deformations. The experimental results were processed with the aim of determining the dynamic shear modulus at very low deformation (the so-called G_0 *of laboratory*). It was used to normalize the decay curves, and the parameters of the interpolating curves of the shear modulus and damping factor. The G_0 of laboratory can be experimentally determined in correspondence of very low stress using of piezoceramic transducers or bender elements. In this case, the linear extrapolation of Hardin and Drnevich (1972b) was adopted, plotting the trend line of points determined to various stresses (Figure 3.9). In this manner the value of G_0 has the advantage of being a stronger and more reliable result as determined by a series of measures, and because they are made for progressively increasing oscillations where the instrumental errors decrease (Viganò et al, 2013b).

To interpolate the experimental data of the shear modulus the modified hyperbolic model of Yokota et al. (1981) was used. For the analytical representation of the damping factor curve, the exponential model proposed by Yokota et al. (1981) was utilized:

$$\frac{G}{G_0} = \frac{1}{1 + \alpha\gamma^{\beta}}$$

$$\frac{D}{D_{max}} = e^{\lambda\frac{G}{G_0}}$$

where α, β, D_{max} and λ are typical constants of every considered soil. The interpolated curves regarding CTS mode and RC mode are represented in Figure 3.12 and 3.13.

In Figures 3.9-3.13 it can be noted that the influence of the plasticity of the investigated soils on dynamic parameters is highlighted by the distribution of the experimental data, despite the rather narrow field of plasticity indexes determined (Figure 3.7). So there is a good correlation between plasticity (hence grain size) and the curves obtained with the dynamic tests. In Figures 3.10 and 3.11 data relating to the two samples of sandy type for which it was not possible to determine the Atterberg limits are placed close to the less plastic soils (Viganò et al, 2013b).

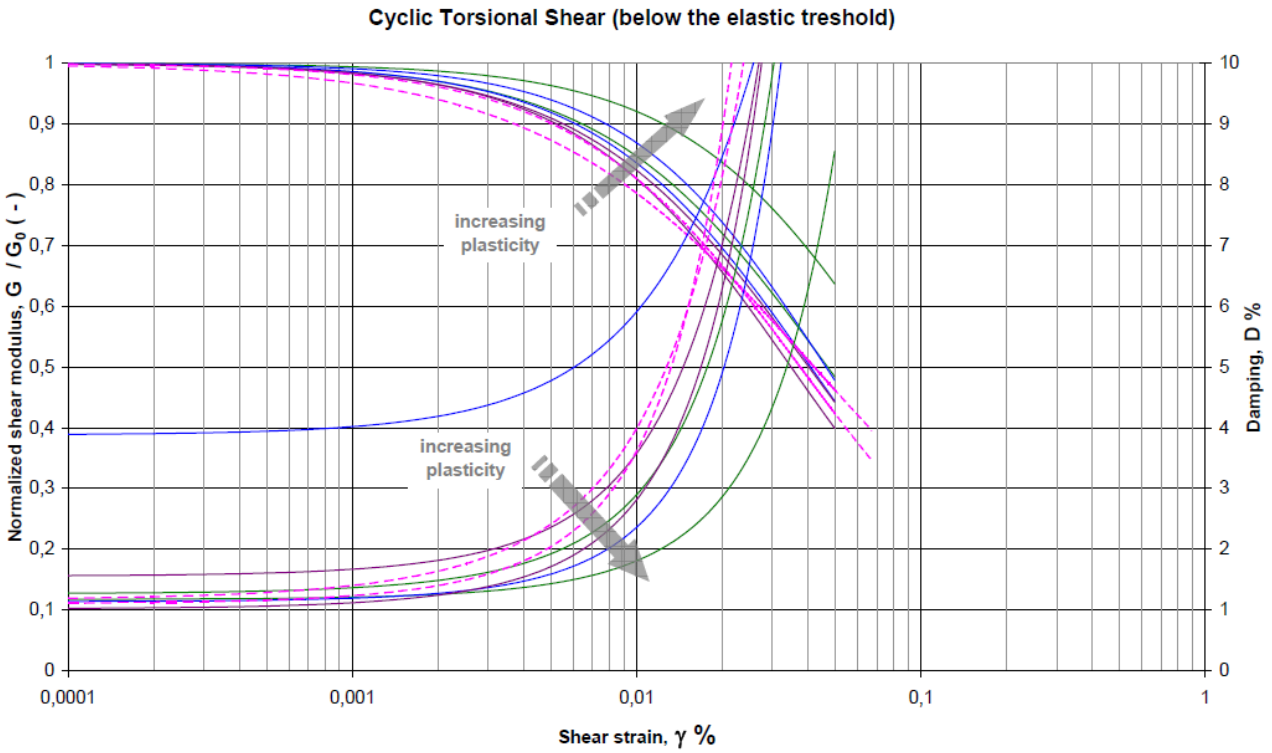

Figure 3.12. Interpolated curves in cyclic torsional shear mode for the 8 analysed samples.

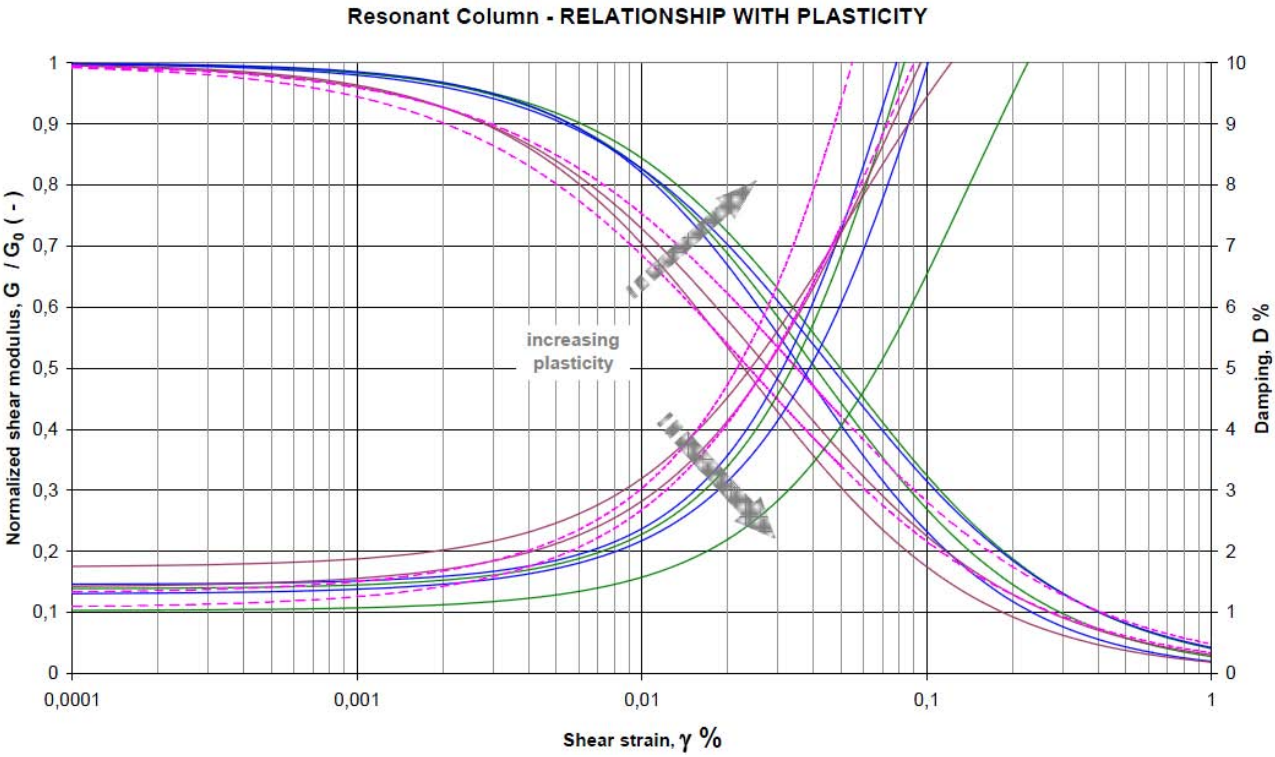

Figure 3.13. Interpolated curves in resonant column mode for the 8 analysed samples.

The data obtained by CTS and RC methods are both good, but for subsequent analyses will be used the curves obtained in RC mode for 2 reasons:

- measurements in RC mode go far beyond the elastic limit allowing to analyse a wide range of deformations. Measurements with the CTS mode instead stop before reaching the elastic limit;
- for the lowest stress RC mode seemed to be more suitable than the CTS one, due to the increased reliability of the measurements conducted at higher strain rate. In fact, for small deformations the interpolations proposed in CTS mode are based on weak experimental data judging them from a metrological point of view.

The curves must be known for points, so 16 representative points were chosen to express them. These points (normalized shear modulus – shear strain, damping – shear strain) will be given as input to numerical models. Their representation is shown in the following pages, the first concerns the sand, the second regards the clayey silt.

S

Resonant Column Tests

fitting of *Yokota et al.* (1981) model to experimental data obtained on

2 samples: **S2-CD L (21.70-22.00 m) and S2-CD M (24.00-24.40 m)**

at the effective stress of 200 kPa (S2 CD L) and 300 kPa (S2 CD M) normalized using G_0

coming from the hyperbolic relationship of *Hardin e Drnevich*

α	β	D_{max}	λ
23.3607	0.8887	19.3231	-2.5740

	$\frac{G(\gamma)}{G_0} = \frac{1}{1+\alpha\gamma(\%)^{\beta}}$	$\frac{D}{D_{max}} = e^{-\frac{\alpha}{m}}$
γ (%)	G / G_0 (-)	D (%)
0.0001	0.994	1.498
0.0002	0.988	1.519
0.0003	0.983	1.539
0.0004	0.978	1.558
0.0005	0.974	1.577
0.001	0.952	1.667
0.002	0.915	1.835
0.004	0.853	2.152
0.01	0.719	3.033
0.02	0.581	4.335
0.03	0.491	5.456
0.04	0.428	6.423
0.05	0.380	7.262
0.1	0.249	10.183
0.2	0.152	13.074
0.3	0.111	14.523

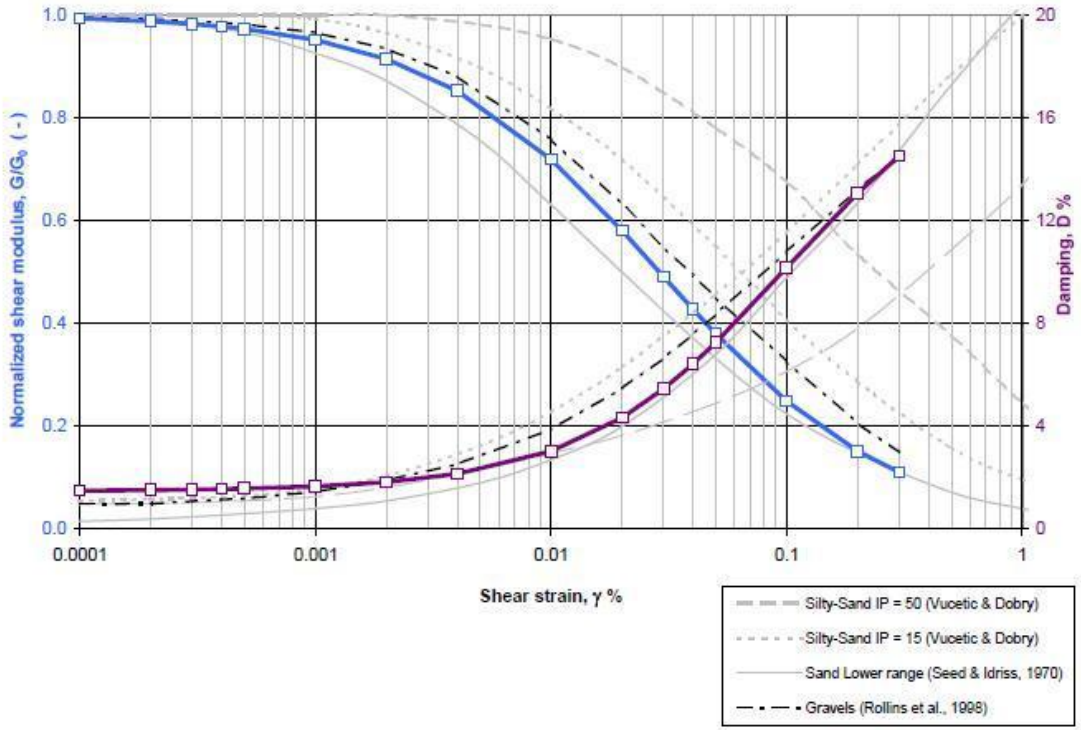

LA

Resonant Column Tests

fitting of *Yokota et al.* (1981) model to experimental data obtained on

2 samples: **S1-CI1 (4.50-5.00 m) and S2-CI1 (6.00-6.60 m)**

at the effective stress of 200 kPa normalized using G_0

coming from the hyperbolic relationship of *Hardin e Drnevich*

α	β	D_{max}	λ
43.1209	1.1548	19.5943	-2.5964

	$\frac{G(\gamma)}{G_0} = \frac{1}{1+\alpha\gamma(\%)^{\beta}}$	$\frac{D}{D_{max}} = e^{\lambda\frac{\alpha}{\pi}}$
γ (%)	G / G_0 (-)	D (%)
0.0001	0.999	1.464
0.0002	0.998	1.469
0.0003	0.996	1.475
0.0004	0.995	1.480
0.0005	0.993	1.486
0.001	0.985	1.517
0.002	0.968	1.587
0.004	0.932	1.744
0.01	0.825	2.298
0.02	0.680	3.353
0.03	0.571	4.451
0.04	0.488	5.515
0.05	0.424	6.509
0.1	0.249	10.270
0.2	0.129	14.000
0.3	0.085	15.706

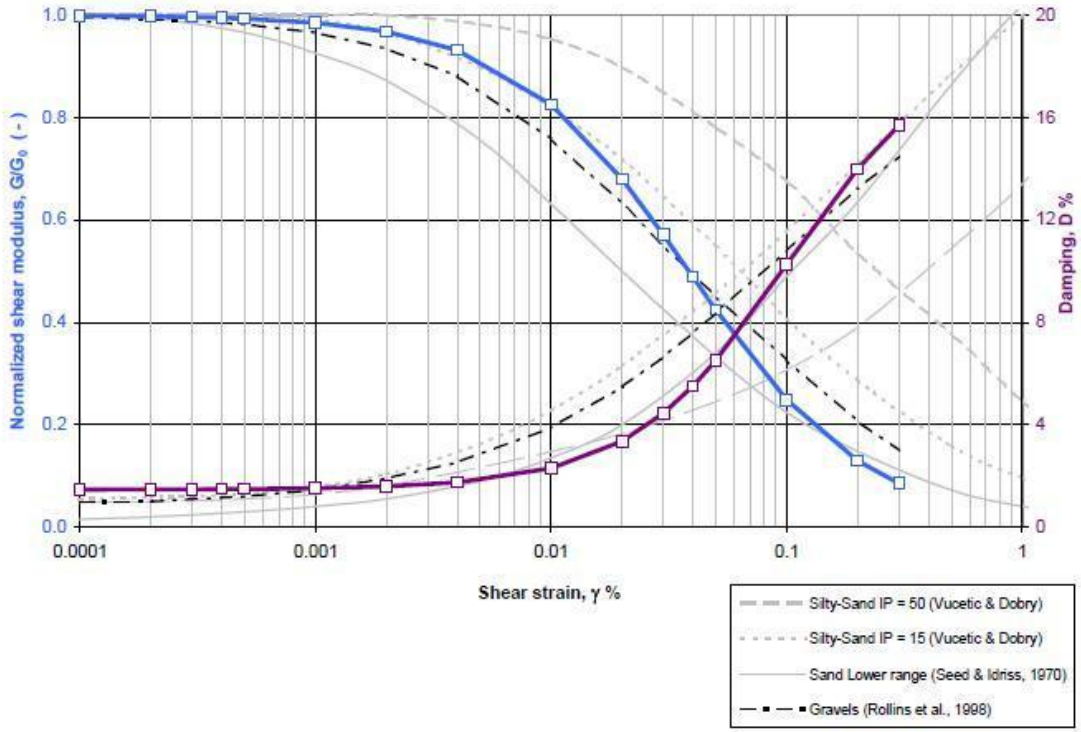

Chapter 4

Local site response

Local site response analyses are principally aimed to (i) predict ground surface motion for development of design response spectra, (ii) evaluate dynamic stress and strain for liquefaction hazard studies, and (iii) determine earthquake-induced forces responsible of potential instabilities. A complete local site response analysis requires a model regarding the rupture mechanism at the source (earthquake focus), the propagation of elastic waves through the Earth to the surface, and ground motion modifications influenced by local site geology and topography. Due to poorly-detailed information on the seismic source and the deep crustal nature, empirical relationships based on seismic recordings are generally used to predict bedrock motion at the local scale. Thus, the ground response analysis focalizes on the evaluation of specific contribution of the soil deposits to the ground motion at the surface. In fact, even if seismic waves pass through kilometres of rocks but only limited soil thicknesses (typically in the order of several tens of meters), soil plays a crucial role in determining the characteristics of surface ground motion (Kramer, 1996).

Many techniques have been developed for local site response analysis, according to three main approaches for soil evaluation effects: the seismic attenuation approach, the code-factor approach, and the site response analysis approach. Attenuation relationships or ground motion prediction equations consider local site effects, including soil conditions. The code-factor approach computes response spectra at bedrock and modifies them by generic soil amplification factors. The third approach, which is used in this study, evaluates a site-specific response analysis by a multi-disciplinary method involving geology, geophysics, geotechnics and computational science (Transportation Research Board, 2012). In particular, it provides deformation and tension time behaviours, acceleration histories and corresponding response spectra. The whole procedure can be summarized as below:

1. definition of structure and geometry of the subsurface physical model;
2. definition of the seismic input acting at the bedrock-soil interface;
3. application of the calculation code for numerical simulations.

For this purpose, a set of input data is required:

– depth of the seismic bedrock (seismic bedrock is defined as a lithostratigraphic sequence characterized by a shear wave velocity greater than or equal to $800\ m/s$; Gruppo di lavoro MS, 2008, and could or not be coincident with geologic bedrock, i.e. rock);

- number and thickness of deposits overlying the bedrock;
- material and seismic properties of bedrock and deposits (unit weight, shear-wave velocity, dynamic properties, etc.)
- depth of the aquifer;
- ground motion time histories;

All these parameters influence at different levels numerical models and results. In particular, the depth of bedrock-deposits interface and the seismic velocity structure play the main role (Barani et al., 2013).

Site response analysis methods can be classified by:

- the domain in which calculations are performed (frequency domain or time domain);
- the complexity of the constitutive employed model (linear, equivalent-linear, and/or nonlinear);
- whether effects of pore water pressure generation are neglected or not (total-stress and effective-stress analyses, respectively);
- the dimensionality of the space in which analysis is performed (1-D, quasi 2-D, 2-D, and 3-D). (Transportation Research Board, 2012).

The site response analysis method applied to the Castel Caldes study is equivalent-linear and one-dimensional (by means of EERA calculation code; Bardet et al., 2000). The application of the equivalent-linear two-dimensional approach is in progress (QUAD4M calculation code; Hudson et al., 1993).

In the next sessions the evaluation of the seismic action, the seismic input selection and the numerical modelling with results are described.

4.1 Evaluation of the seismic action through design spectra

4.1.1 Theoretical bases

- **Elastic response spectra**

Here the dynamic analysis of linear systems with a *single-degree-of-freedom* (SDOF) subjected to arbitrary dynamic forces, including earthquakes, is described. The dynamic analysis of a SDOF system is extremely important because:

- some civil structures can be modelled as SDOF systems;

- the dynamic response of SDOF systems is necessary for the determination of the response of *multiple-degrees-of-freedom* (MDOF) systems;
- spectral analysis, which is the basis of technical standards for the seismic design of structures, is based on the response spectra obtained from SDOF systems (Majorana et al., 2007).

The position of a SDOF system can be described completely by a single variable, where a rigid mass m, connected in parallel to a spring of stiffness k and a dashpot of viscous damping coefficient c, is subject to some external time-dependent load $f(t)$ (Figure 4.1).

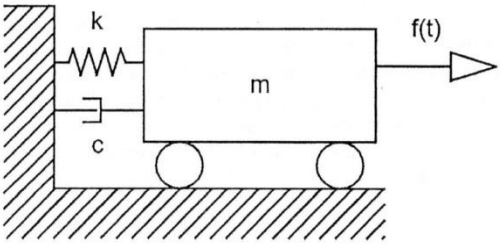

Figure 4.1. SDOF system scheme.

When a dynamic load is applied to the mass, motion is opposed by the mass inertia and by forces from dashpot and spring. Thus, the external load $f(t)$ is opposed by three forces: the *inertia force* $f_I(t)$, the *viscous damping force* $f_D(t)$, and the *elastic spring force* $f_S(t)$. The equation of motion can be expressed in terms of the dynamic equilibrium of these forces:

$$f_I(t) + f_D(t) + f_S(t) = f(t).$$

According to the Newton's second law, the inertial force acting on a mass is equal to its rate of momentum change:

$$f_I(t) = \frac{d}{dt}\left(m\frac{du(t)}{dt}\right) = m\frac{d^2u(t)}{dt^2} = m\ddot{u}(t)$$

for a viscous dashpot, the damping force is proportional to the velocity of the mass:

$$f_D(t) = c\frac{du(t)}{dt} = c\dot{u}(t)$$

and the force provided by the spring is function of stiffness and displacement:

$$f_S(t) = ku(t).$$

Substituting, the equation of motion can be written as a second-order differential equation:

$$m\ddot{u}(t) + c\dot{u}(t) + ku(t) = f(t)$$

This differential equation is linear because all of terms have constant coefficients and external load depends only by time. The linearity allows a close-form analytical solution and the application of superposition principle. The function $u(t)$ represents the response of the system, and the other kinematic parameters (velocity and acceleration) can be determined subsequently by derivation.

In order to evaluate the dynamic response of a linear SDOF system, the differential equation of motion must be solved. There are several type of conditions under which the dynamic response are commonly calculated. Here, only the case of interest for the determination of the response spectra is examined, namely the case of *damped forced vibrations in general loading conditions*.
A general loading function can be thought as a train of load pulses, each of infinitesimal duration $d\tau$ (Figure 4.2).

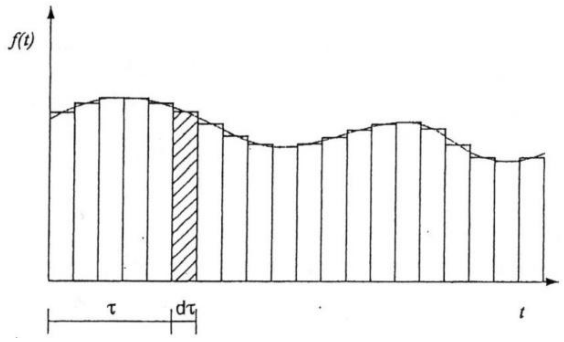

Figure 4.2. General loading function with pulse of duration dτ occurring at time t = τ (Majorana et al., 2007).

The pulse of duration $d\tau$ occurring at time $t = \tau$ causes the response at latter time $t > \tau$. The response for a single pulse is:

$$du(t) = \frac{1}{m\omega_d} f(\tau) d\tau e^{-\xi\omega(t-\tau)} sin\omega_d(t-\tau) \qquad t \geq \tau$$

where:
ω_d = damped natural circular frequency of the system;
ω = un-damped natural circular frequency of the system;
ξ = damping ratio.
The response of the system at time t is obtained by integration of the infinitesimal responses up to time t:

$$u(t) = \frac{1}{m\omega_d} \int_0^t f(\tau) e^{-\xi\omega(t-\tau)} sin\omega_d(t-\tau) d\tau$$

This equation is known as *Duhamel's integral*.

The *response spectrum* describes the maximum response of a SDOF system to a particular input motion as a function of the natural frequency (or natural period, $T = 1/\omega$) and damping ratio of the SDOF system. This response can be expressed in terms of acceleration, velocity or displacement. The maximum values of each of these parameters depend only by natural frequency and damping ratio of the SDOF system for a particular input motion. These values are called spectral acceleration (S_A), spectral velocity (S_V) and spectral displacement (S_D).

The response caused by a shaking of the ground, characterized by an acceleration $\ddot{u}_g$, can be obtained by replacing the generic external load $f(t)$ with the dynamic fictitious forcing $-m\ddot{u}_g$. For a system subject to earthquake shaking at the base the excitement is due to an inertial force resulting from the motion impressed on the base by a transitory source. So, the Duhamel's integral becomes:

$$u(t) = -\frac{1}{\omega_d}\int_0^t \ddot{u}_g(\tau)e^{-\xi\omega(t-\tau)}sin\omega_d(t-\tau)d\tau$$

Therefore, set the time history of the seismic acceleration and the damping, it is possible to obtain the displacement time history for the system and evaluate its maximum value (S_D) for different values of frequency (ω) or period. The *elastic response spectrum in terms of displacement* for any fixed damping value can be determine on a graph with natural period T and S_D values. It is a concise description of the maximum effect (in terms of displacement) of an assigned earthquake for a given level of damping, depending on the own period of the oscillator.

Similarly, spectra in terms of velocity (S_V) and acceleration (S_A) can be obtained. An example of the results is reported in Figure 4.3.

- **Design spectrum**

The *design spectrum* derives from the elastic spectra and it is used in the design. The design spectrum is always derived from a set of accelerograms, because natural earthquakes show peaks at different periods, even if detected at the same site. Therefore the design spectrum is the synthesis of the effects of multiple events (Majorana et al., 2007). Response spectra are highly irregular, their shapes reflect details of specific frequency and phase. Design spectra, on the other hand, are generally quite smooth. They are determined by smoothing, averaging, or enveloping the response spectra of multiple motions (Gruppo di lavoro MS, 2008). Their typical shape is represented in Figure 4.4.

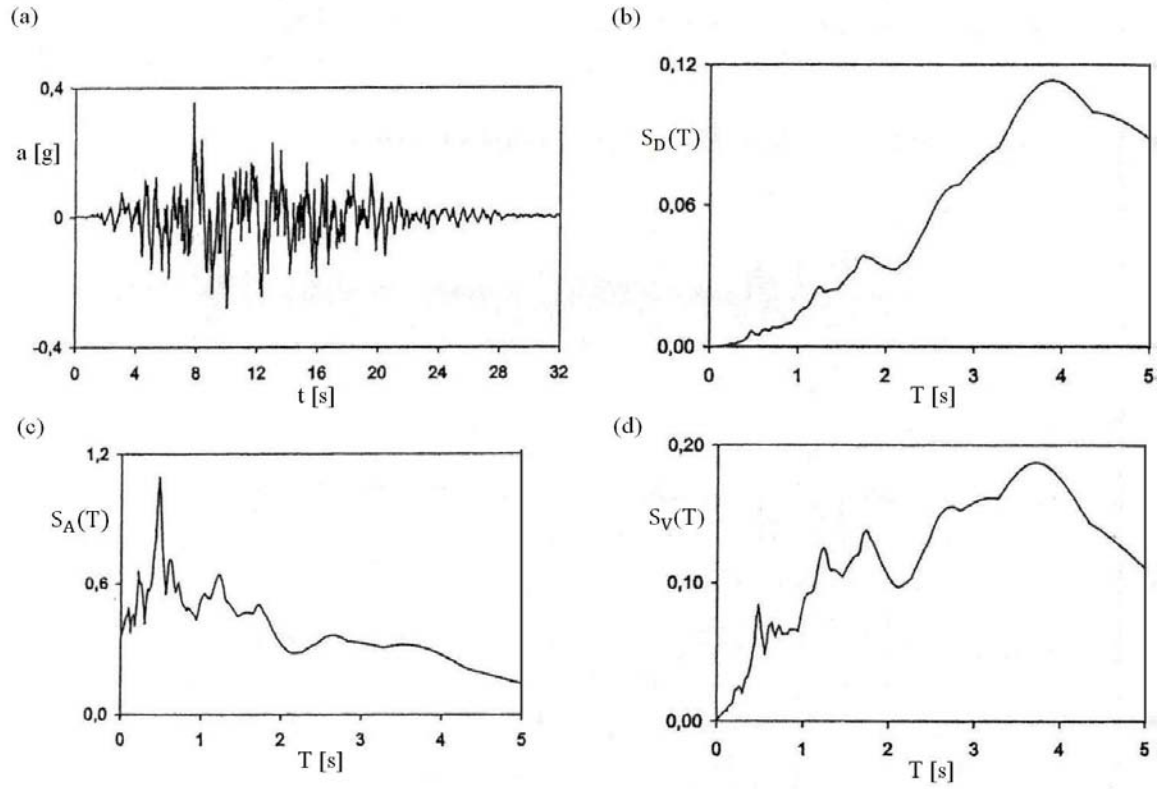

Figure 4.3. Accelerogram (a) and relative elastic response spectra (b-d) (Modified from Majorana et al., 2007).

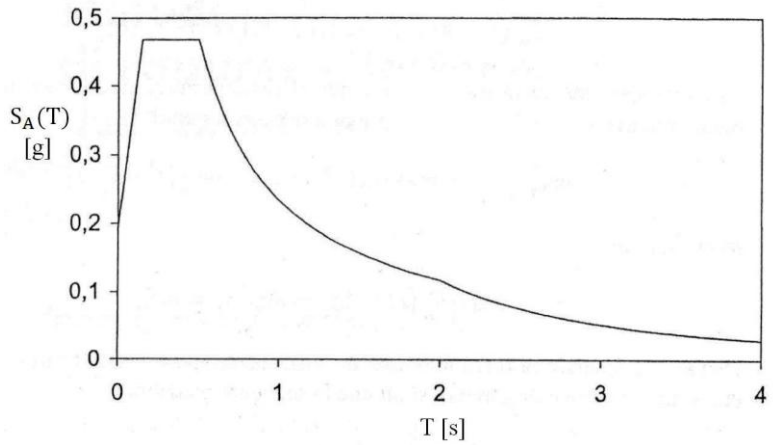

Figure 4.4. Example of design spectrum.

4.1.2 Seismic action according to the Italian building code

Here a brief summary of the Italian building code (CS.LL.PP., DM 14/01/2008) regarding the seismic action is reported. For more details refer to Section 3.2 of the Code.

The design seismic action to evaluate compliance with the various limit states considered, are defined starting from the "basic seismic hazard" of the construction site.

The seismic hazard is defined in terms of:

- maximum expected horizontal acceleration a_g, under so-called free-field conditions, on the reference "rigid" soil (A category, described later) and horizontal topography;
- ordinates of the acceleration elastic response spectrum ($S_e(T)$), with reference to the predetermined exceedance probability (P_{VR}) during the reference period (V_R).

Alternatively, it is allowed the use accelerograms, if properly suited to the site seismic hazard.

The spectral shapes are defined, for each of the exceedance probability during the reference period, from the values of the following parameters of the rigid and horizontal reference site:

- a_g: maximum horizontal acceleration at the site;
- F_0: maximum value of the amplification factor of the horizontal acceleration spectrum;
- T_C^*: period corresponding to the constant-velocity portion of the horizontal acceleration spectrum.

For the definition of the seismic design action, it is necessary to evaluate the effect of local site response using specific analysis. In fact, the motion generated by an earthquake at a site depends on the local conditions, i.e. on the topographic and stratigraphic characteristics of the deposits of soil and rock masses and on the physical and mechanical properties of the soil/rock materials. At the scale of a single construction site, the local seismic response allows to define the changes that a seismic signal undergoes, due to the aforementioned factors, as compared to that of a rigid reference site with horizontal topographic surface.

For the definition of the design seismic action in the absence of such analyses, a simplified approach based on the identification of soil categories can be used. The classification shall be made on the basis of the values of the equivalent shear wave velocity within the first 30 m of depth ($V_{S,30}$). The conventional categories are 5, from class A (outcropping rock masses or very rigid soils with $V_{S,30} > 800\ m/s$) to class E (soil of type C or D with thickness less than 20 m, places on the reference substrate) (CS.LL.PP., DM 14/01/2008). For these five categories, the seismic actions can be determined with the simplified approach described below. For soil belonging to additional 2 categories (called S1 and S2, that concern deposits of peat or highly organic clays, or deposits susceptible to liquefaction), it is necessary to provide specific analysis for the definition of the seismic action.

Regarding the topography, for simple surface configurations it is possible to use one of the topographic categories, from T1 (average slope ≤ 15°) to T4 (average slope > 30°). For complex topographical conditions instead is necessary to provide specific analysis of local seismic response.

The seismic action is characterized by 3 translational components to be considered independent one of each other, two horizontal (X and Y) and one vertical (Z). The vertical component will be

considered only where specifically noted. The components can be described by one of the following representations depending on the type of analysis:

- maximum expected acceleration at the surface;
- maximum acceleration and relative response spectrum expected at the surface;
- accelerogram.

- **Simplified approach**

- Acceleration elastic response spectrum

The acceleration elastic response spectrum is expressed by a spectral shape (normalized spectrum) in reference to a conventional damping of 5%, multiplied by the value of the maximum horizontal acceleration a_g on rigid horizontal reference site.

As an example, are shown the equations for the determination of the horizontal component of the acceleration elastic response spectrum, but in the same way it is possible to determine the vertical component, for the displacement, and so on.

$$0 \le T < T_B \qquad S_e(T) = a_g \cdot S \cdot \eta \cdot F_0 \cdot \left[\frac{T}{T_B} + \frac{1}{\eta \cdot F_0}\left(1 - \frac{T}{T_B}\right)\right]$$

$$T_B \le T < T_C \qquad S_e(T) = a_g \cdot S \cdot \eta \cdot F_0$$

$$T_C \le T < T_D \qquad S_e(T) = a_g \cdot S \cdot \eta \cdot F_0 \cdot \left(\frac{T_C}{T}\right)$$

$$T_D \le T \qquad S_e(T) = a_g \cdot S \cdot \eta \cdot F_0 \cdot \left(\frac{T_C \cdot T_D}{T^2}\right)$$

in which:

T = vibration period;

S_e = horizontal spectral acceleration;

S = coefficient that takes into account the subsoil and topographical categories;

η = factor that modifies the elastic spectrum for viscous damping coefficients ξ different from 5% through the relation $\eta = \sqrt{10/(5+\xi)} \ge 0{,}55$;

F_0 = factor that quantifies the maximum spectral amplification on the rigid horizontal reference site;

T_C = period corresponding to the beginning of the part of the spectrum with constant velocity;

T_B = period corresponding to the beginning of the part of the spectrum with constant acceleration;

T_B = period corresponding to the beginning of the part of the spectrum with constant displacement.

The influence of the stratigraphy and topography is considered in the coefficients S and T_C, and is quantified by specific expressions for each category.

– Design spectrum

The design spectrum to be used for the serviceability limit state is the corresponding elastic spectrum, both for the horizontal components that for the vertical component.

For the ultimate limit state, the dissipative properties of the structures can be put into account through a reduction of the elastic forces. It takes into account, in a simplified way, the inelastic energy dissipation capacity of the structure, its overstrength and the increase of his own period as a result of plasticization. In this case, the corresponding elastic spectrum with ordinates reduced is used, where coefficient η is replaced by $1/q$ (where q is the *structure factor*) both for horizontal and vertical components (CS.LL.PP., DM 14/01/2008).

- **Site-specific analysis**

The evaluation of local seismic response using specific analysis permits to obtain a realistic seismic response. This approach is considered by the Italian building code the official way for the determination of the seismic action. Neverthless, the alternative simplified approach described above is usually used by practitioners. The codes, in general, consider site effect in a simplify way, so design spectra developed from code previsions are usually more conservative than those developed with site-specific analyses. This provide an economic incentive that implicitly encourages the development of site-specific analyses (Kramer, 1996).

Spectra defined with the simplified approach can be used for structures with fundamental period less than or equal to 4.0 s. For structures with greater fundamental periods, the spectrum should be defined by appropriate analysis, i.e. the seismic action must be described by accelerograms. Similarly, in the presence of soil category S1 or S2.

The Italian building code provides that limit states can be verified through the use of accelerograms, artificial or simulated or natural. Each accelerogram describes a component, horizontal or vertical, of the seismic action. The characteristics that must have the natural accelerograms are explained in the paragraph 4.2.1 that concerns the choice of the seismic input.

The seismic action in the Castel Caldes area will be determined by means of site-specific analyses.

4.2 Seismic input selection

4.2.1 Seismic input according to Italian building code

Three is the minimum number of records to use, and seven allows the consideration of the mean effects on the structure as design values (rather than the maxima). Selected real records have to be scaled in order to approximate the elastic response spectrum in a range of periods of interest for the structure.

Disaggregation of the seismic hazard in terms of magnitude and distance is often used to assess the contribution to the seismic hazard of a site by the various seismic sources. The Istituto Nazionale di Geofisica e Vulcanologia (INGV) provides disaggregation values for peak acceleration, even if it is today acknowledged that disaggregation should be performed for those ranges of the response spectrum more relevant for the behaviour of the structure (for example, close to the fundamental period). On the other hand, some studies have shown that in most of the cases some of the variables dominating the hazard (i.e., magnitude and distance) may be not particularly relevant for a correct estimation of the structural response if the spectral shape is the parameter driving record selection (Iervolino et al., 2010).

4.2.2 REXEL software

In order to choose the seismic input, the REXEL software (Iervolino et al., 2010, freely available at http://www.reluis.it) was used. REXEL allows to define the design spectra according to the Eurocode 8, the Italian building code or completely user-defined. Based on these spectra, the software allows to search for sets of 7 on-average compatible records. Records may also reflect the seismogenetic features of the sources (in terms of magnitude and epicentral distance), ground motion intensity measures, and soil conditions. The datasets contained in REXEL are the *European Strong-motion Database* (ESD), the I*talian Accelerometric Archive* (ITACA) and the *Selected Input Motions for displacement-Based Assessment and Design* (SIMBAD).

The procedure implemented for record selection consists in four steps:

1. definition of the design (reference) horizontal and/or vertical spectra;
2. list and plot of the records embedded in REXEL which fall into the magnitude and distance bins specified by the user for a specific site class;
3. definition of the period range where the average spectrum is requested to be compatible with the reference spectrum, and of tolerances in this compatibility;

4. search for combinations of seven records that, on average, match the design spectrum with parameters specified in step 3. They may include one, two of all three components of motion.

How the code works and the explanation of the data required are reported in Appendix 4, here are only listed the steps carried out to find the combination for the study area.

The screenshot of the software with the inserted data regarding the Castel Caldes area is shown in Figure 4.5.

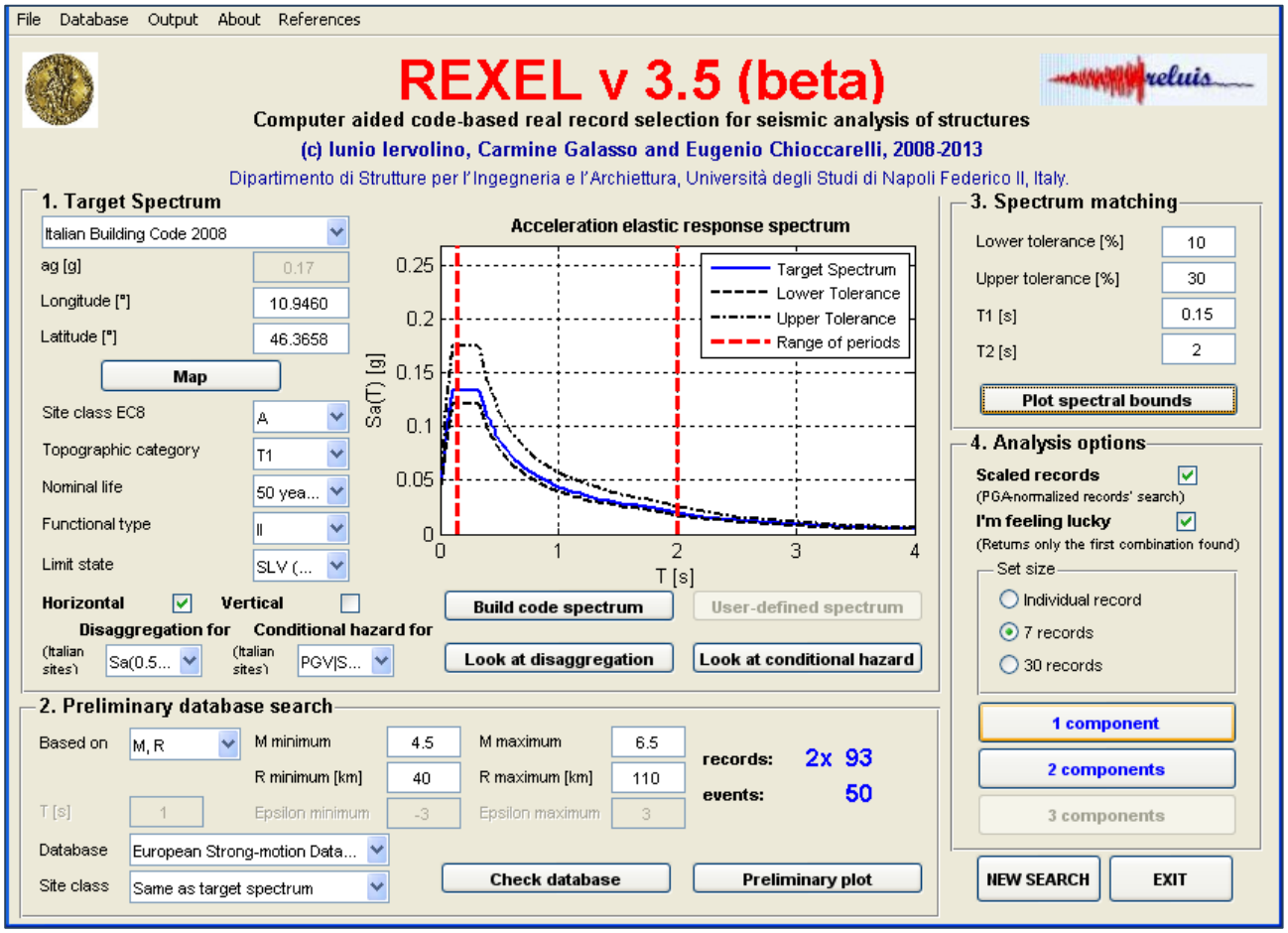

Figure 4.5. Castel Caldes data.

The *Target (Reference) Spectrum* is determined with reference to the Italian building code with the following characteristics:

- Coordinates of the site: Longitude 10.9460°N and Latitude 46.3658°E;
- Soil category: A (reference rigid site);
- Topographic category: T1 (horizontal topographic surface);
- Nominal life: 50 years (normal works);
- Functional type: II (structures with normal crowd);

– Limit state: SLV (ultimate limit state concerning the safety of people).

The spectrum component considered is only the *Horizontal* one since the successive analyses are one-dimensional.

For the extraction of the input accelerograms the data of the disaggregation have to be known (variability in terms of magnitude and distance). They can be obtained from website of the INGV (http://esse1-gis.mi.ingv.it) or directly from the REXEL program. The disaggregation was made in both ways, obtaining the results showed in Figures 4.6 and 4.7. The magnitude and distance intervals selected are $[M_{min}, M_{max}] = [4.5, 6.5]$ and $[R_{min}, R_{max}] = [40, 110]$ km.

Regarding the database, the *European Strong-motion Database* with the site class *Same as target spectrum* was chosen (to get seismic input whose average adheres to the spectrum of A category). After that, by means of the command *Check database*, the list containing the inventory of records in which to search for seven spectra in average compatible with the code spectrum can be extracted. These spectra may also be plotted (command *Preliminary plot*) along with the reference spectrum to have a picture of the spectra in which REXEL will search among (Figure 4.8).

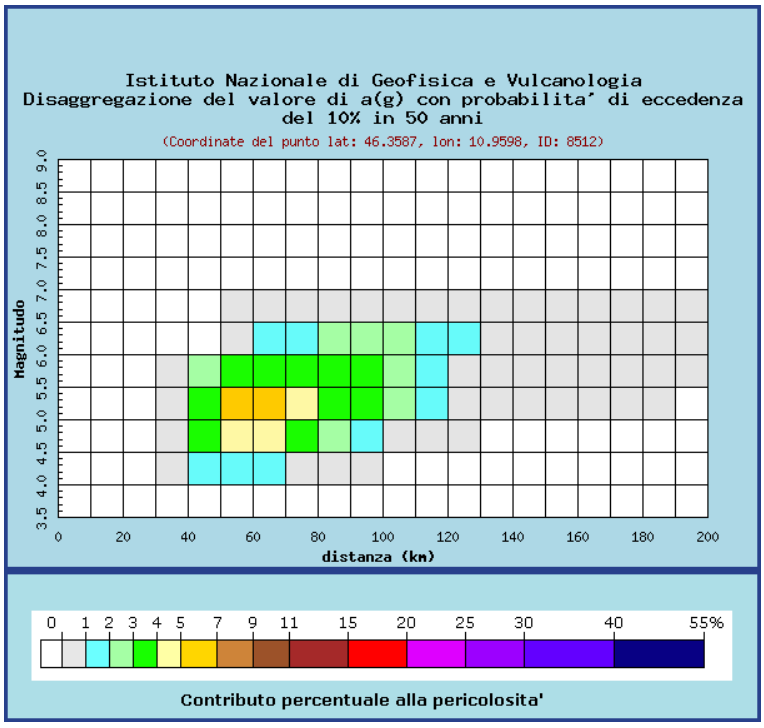

Figure 4.6. Disaggregation obtained from INGV website.

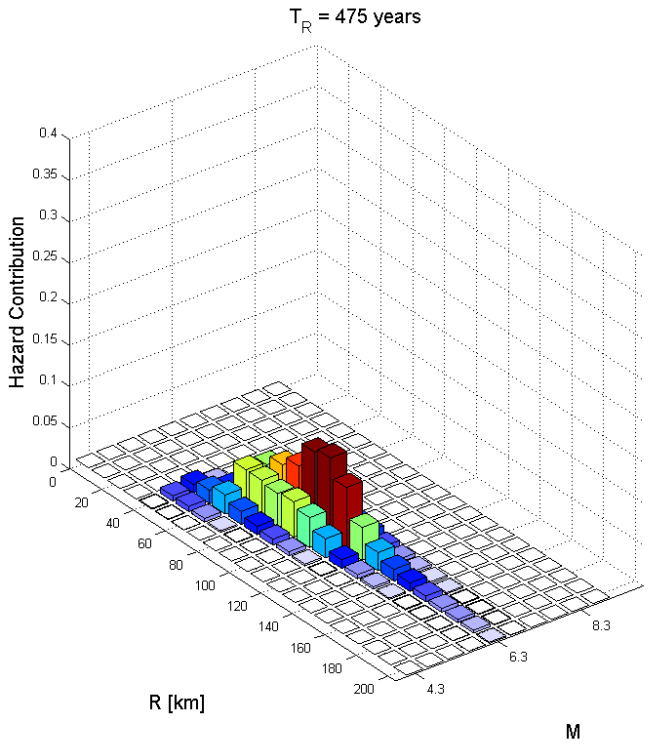

Figure 4.7. Disaggregation obtained from REXEL.

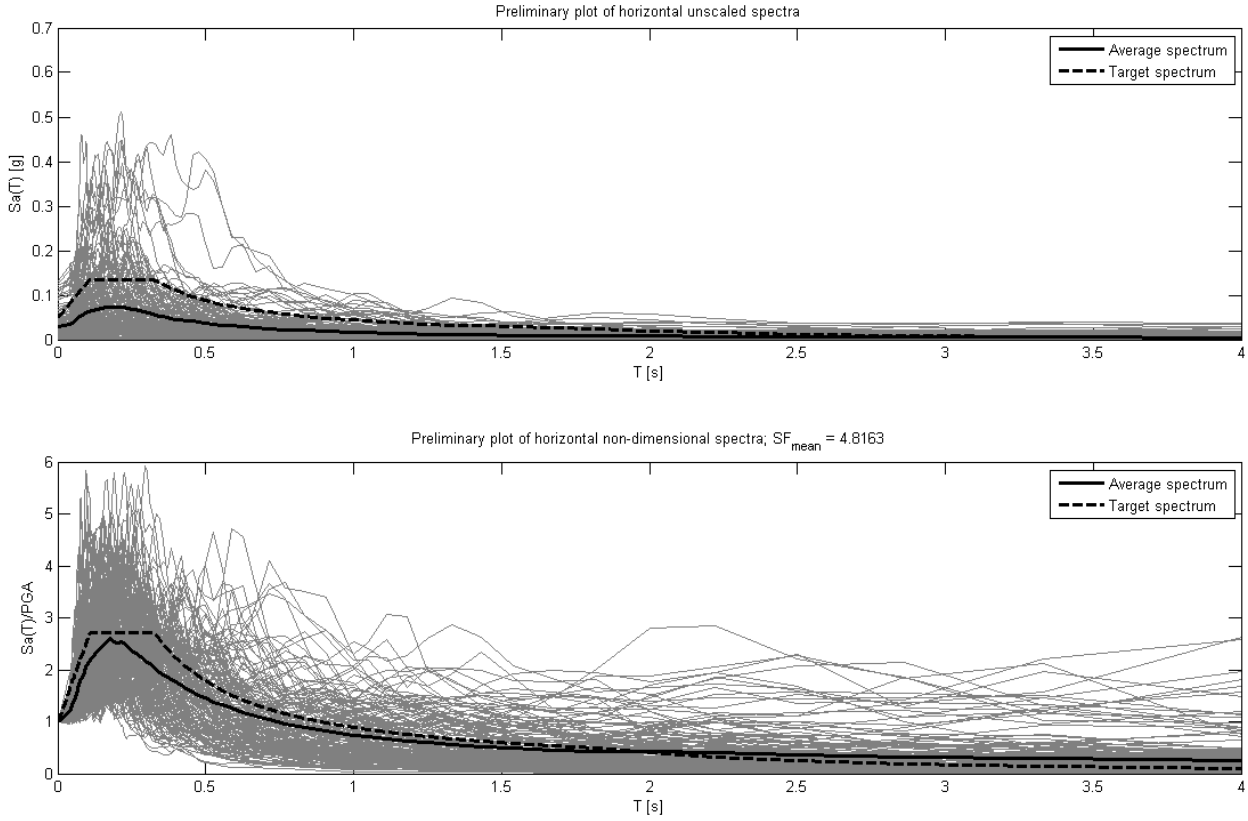

Figure 4.8. Preliminary plots of horizontal unscaled spectra (up) and of horizontal non-dimensional spectra (down).

In the section *Spectrum Matching* the parameters related to the spectral compatibility (period range and tolerances) are defined. The default parameters were left, namely:

- Upper tolerance: 30%
- Lower tolerance: 10%
- Period range: [0.15 – 2] s.

Finally, *7 records* of *one component* and *scaled* with maximum mean scale factor equal to 5 (default value) were sought, using the option *I'm feeling lucky*. The chosen combination of 7 spectra with their scale factor (SF) is reported in Figure 4.9. REXEL returns both spectra and accelerograms in text format.

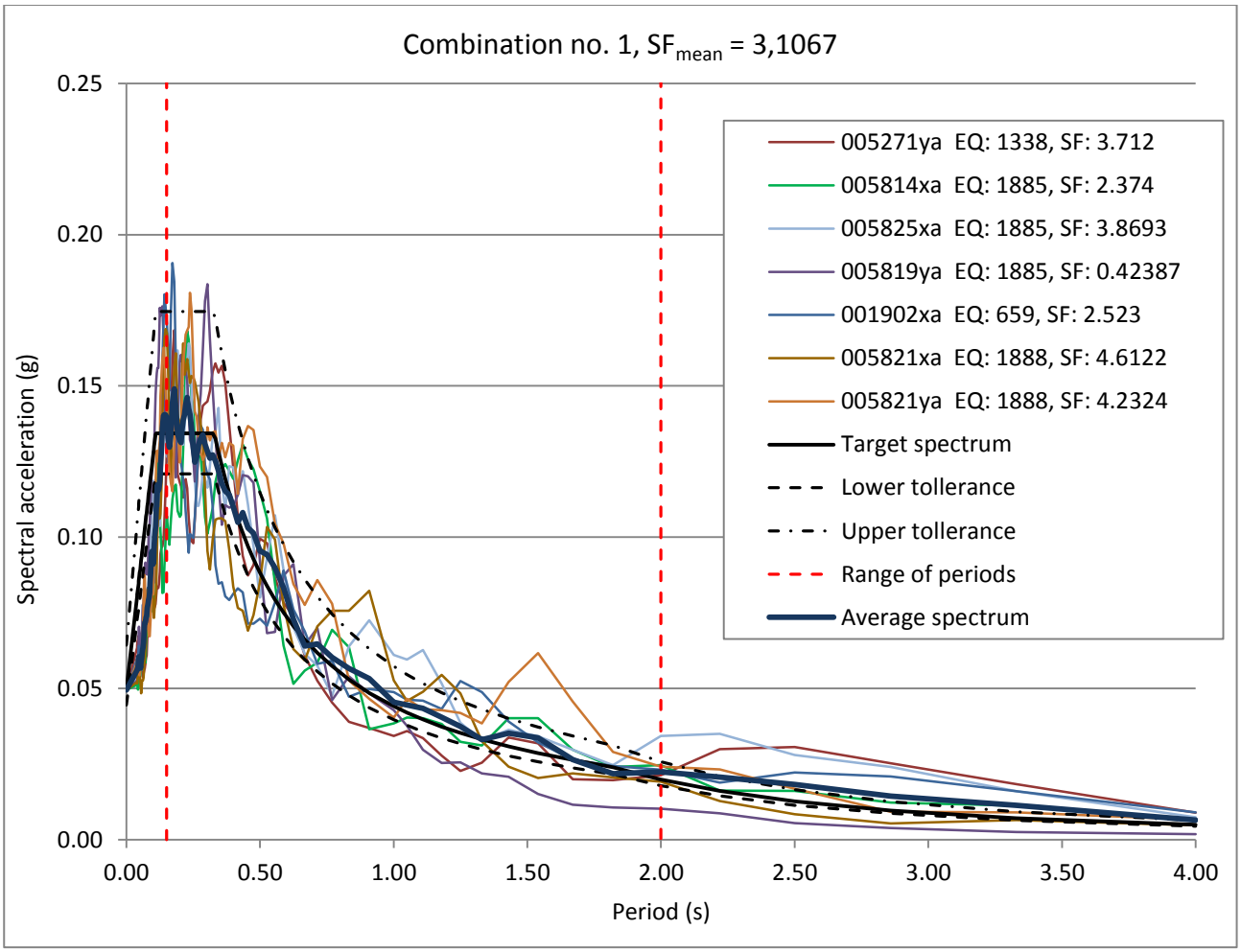

Figure 4.9. Combination of the 7 compatible spectra.

For each earthquake, in order to simplify its identification, progressive numbers instead of the code provided by REXEL were assigned. The correspondence is indicated in the table below (Table 4.1). Hereafter these identification names will be used.

Table 4.1. Denominations of earthquakes.

REXEL code	Identification name
005271ya	Earthquake 1
005814xa	Earthquake 2
005825xa	Earthquake 3
005819ya	Earthquake 4
001902xa	Earthquake 5
005821xa	Earthquake 6
005821ya	Earthquake 7

In Table 4.2 are reported some information about the individual records returned by REXEL, that are: earthquake ID, recording station ID, earthquake name, date, magnitude, fault mechanism, epicentral distance, peak ground accelerations. Also the mean values of the combination are presented.

Table 4.2. Information about records (simplified).

Earth-quake ID	Station ID	Earthquake Name	Date	Mw	Fault Mechanism	Epicentral Distance [km]	PGA_X [m/s^2]	PGA_Y [m/s^2]
1338	ST2483	Mt. Vatnafjoll	25/05/1987	6	oblique	42	0.1378	0.1308
1885	ST1309	Kalamata	13/10/1997	6.4	thrust	61	0.2046	0.2014
1885	ST1323	Kalamata	13/10/1997	6.4	thrust	103	0.1255	0.1127
1885	ST1321	Kalamata	13/10/1997	6.4	thrust	48	1.1845	1.1459
659	ST1324	Anchialos	30/04/1985	5.6	normal	55	0.1925	0.1585
1888	ST1321	Strofades (aftershock)	18/11/1997	6	strike slip	93	0.1053	0.1148
1888	ST1321	Strofades (aftershock)	18/11/1997	6	strike slip	93	0.1053	0.1148
mean:				6.1		70,7	0.2936	0.2827

Once known the seismic input is possible proceed with the modelling.

4.3 Numerical modelling: one-dimensional approach

After earthquake nucleation seismic waves travel away from the source at depth in all directions within the crust. When they reach different geologic materials in depth and also upper soils near the surface seismic reflection and refraction always occur. One-dimensional local site response analyses assume that all geologic boundaries are horizontal and the response of soil deposits is predominantly caused by waves propagating vertically from the underlying bedrock (Kramer, 1996). So, one-dimensional calculation codes are valid for modelling plane-parallel layers along a vertical column, assuming laterally-homogeneous stratigraphy.

Under these assumptions, the main factors responsible for seismic motion amplifications are: (i) impedance contrasts between ground layers, particularly with bedrock and (ii) resonance effects due to the closeness between the frequencies of the motion at the substrate and the natural vibration of the deposit.

Calculation procedures consider, in the solution of the dynamic equilibrium of the system, the non-linear relation through two types of analyses: *equivalent linear* and *nonlinear analyses*.

The *equivalent linear analysis* consists in the execution of a sequence of complete linear analysis with subsequent update of the parameters of stiffness and damping until the satisfaction of a predetermined convergence criterion. There parameters depend on the state of deformation of the ground.

The *nonlinear analysis* consists in the integration step-by-step of the equations of motion, simultaneously changing the parameter values of stiffness and damping.

The first analysis provides satisfactory results at not excessive deformation of the ground, less than 1%, for higher deformation is necessary to use non-linear incremental analysis.

Among the programs that adopt the equivalent linear analysis the best known and most frequently used is the computer code SHAKE (Schnabel et al., 1972; Idriss and Sun, 1992) and later revisions like EERA (Bardet et al., 2000), which is used in this study.

They work in the total stresses field using the Kelvin-Voigt physical model (continuous and homogeneous layers with linearized viscoelastic behaviour). It consists of n flat and parallel layers of infinite horizontal extension on an outcropping half-space corresponding to the bedrock, on which the input motion is applied. Each layer is considered to be homogeneous and isotropic and characterized by the thickness h, the density ρ, the shear modulus G and the damping ratio ξ. The input motion is constituted by shear waves which propagate in the direction perpendicular to the

free surface. The equation used in the model is the dynamic equilibrium equation expressed as a function of the displacement:

$$\bar{G}\frac{\delta^2 u}{\delta z^2} = \rho\frac{\delta^2 u}{\delta t^2}$$

where:

z = depth;

ρ = density;

t = time;

u = horizontal displacement;

$\bar{G}$ = complex shear modulus expresses as: $\bar{G} = \rho\bar{V_S}^2 \quad \bar{V_S} = V_S\sqrt{1+2i\xi}$

V_S = shear wave velocity;

ξ = damping ratio.

Any function of time can be decomposed into a sum of harmonic waves of circular frequency ω through the Fourier transform. Then the solution is found for the single wave and after all the solutions are combined using the inverse Fourier transform. So, the code works in the so-called frequency domain.

In Figure 4.10 is shown the calculation scheme: there are N groups of four known soil properties: density ρ, shear modulus G (or equivalently the velocity V_S), damping ratio ξ and thickness h of the layers. Amplitude of incident and reflected waves in each layer, and reflected waves F_n at the bedrock are unknown. The incident wave E_n at the bedrock is given and unknowns are $2N+1$.

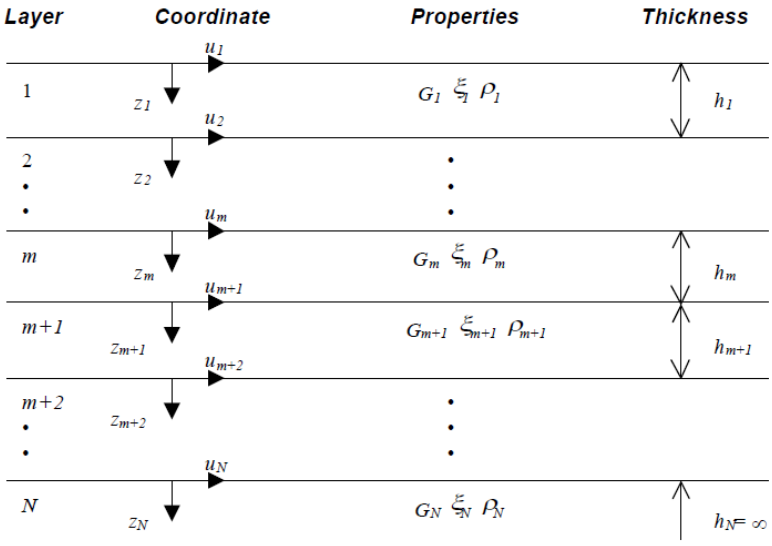

Figure 4.10. One-dimensional layered soil deposit system (Bardet et al., 2000).

The calculation method consists in writing the solution of the equations of motion in each layer and in imposing two conditions: (i) congruence of displacements and stresses at the interfaces, and (ii) equality of the incident and reflected waves at the surface. In this way, the number of equations is equal to the number of unknowns. The resolution of the resulting equations is done taking into account the damping of the ground, in order to express the shear wave velocity V_S as function of the damping ratio ξ through the relation (Schnabel et al., 1972):

$$\bar{V_S} = V_S\sqrt{1 + 2i\xi}$$

The soil behaviour is not linear, it varies with the strain induced by the earthquake. It is taken into account by the shear modulus and damping ratio behaviours. Figure 4.11 shows an example of shear modulus G (dimensionless with G_0) and damping ratio ξ behaviours, as a function of shear strain γ. G_0 is the shear modulus at very low shear strain ($\gamma = 10^{-6}$) (Chapter 3.1.2; Gruppo di lavoro MS, 2008).

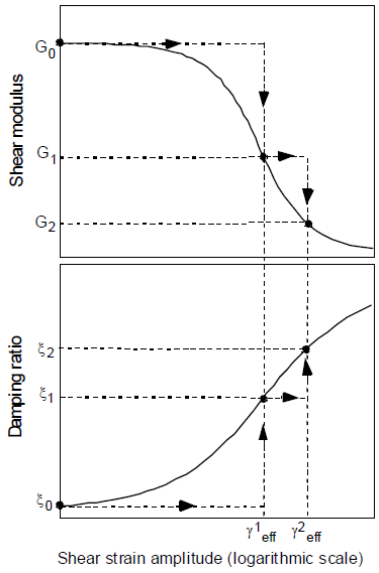

Figure 4.11. Iteration of shear modulus and damping ratio with shear strain in equivalent linear analysis (Bardet et al., 2000).

Since the computed strain level depends on the values of the equivalent linear properties, an iterative procedure is required to ensure that the properties used in the analysis are compatible with the computed strain levels in all layers. The iterative procedure operate as follows:

1. Initial estimation of G and ξ are made for each layer.
2. These values are used to compute the ground response, including time histories and of shear strain for each layer.
3. The effective shear strain is determined from the maximum shear strain.

4. From this effective shear strain, new equivalent linear values of G and ξ are chosen for the next iteration.
5. Iteration on steps 2 to 4 until differences between computed shear modulus and damping ratio values of two consecutive iterations fall below some predetermined value in all the layers.

Results are provided in terms of accelerograms, their response spectra and Fourier spectra in any layer and at the surface. Even though the nonlinear soil behaviour is approximated, it is important to remember that this method is still a linear method of analysis. The strain-compatible soil properties are constant throughout the duration of the earthquake so the method is not able to represent changes in soil stiffness (Kramer, 1996).

The one-dimensional analysis was carried out in two sites, Caldes and Samoclevo, because they have different stratigraphic conditions (Paragraph 2.1.3). One dimensional analysis in fact does not consider the spatial heterogeneity but only the vertical one, so to evaluate the effect of the same seismic action on two different sites the analysis must repeated.

4.3.1 EERA's implementation

EERA stands for *Equivalent-linear Earthquake site Response Analyses* and it is fully integrated with the spreadsheet program Excel. The description of the equations and the assumptions on which it is based are explained in Appendix 5, here are just treated the input data.
EERA is made of nine types of worksheets, 3 input and 6 output, their contents are summarized in Table 4.3.

Table 4.3. Types of worksheets in EERA and their contents (Bardet et al., 2000, modified).

	Worksheet	Contents
Input	*Earthquake*	Earthquake input time history
	Profile	Vertical profile of layers (geometry and soil properties)
	Mat i	Material curves (shear modulus and damping ratio versus strain for material type i)
Output	*Iteration*	Results of main calculation
	Acceleration	Time history of acceleration/relative velocity/relative displacement at a selected sub-layer
	Strain	Time history of stress, strain and dissipated energy
	Ampli	Amplification factor between two sub-layers
	Fourier	Fourier amplitude spectrum of acceleration for a selected sub-layer
	Spectra	Response spectra for a selected sub-layer in terms of acceleration/velocity/displacement

As shown in Figure 4.12, worksheet *Earthquake* is used to define the earthquake input motion. In this worksheet the input accelerogram obtained by means of REXEL is inserted. The maximum frequency cut-off is used to filter the high frequencies from the input acceleration. The chosen value is 20 Hz, which correspond to a period of 0,05 s, because it makes no sense to consider higher frequencies (i.e. lower periods) in the context of building.

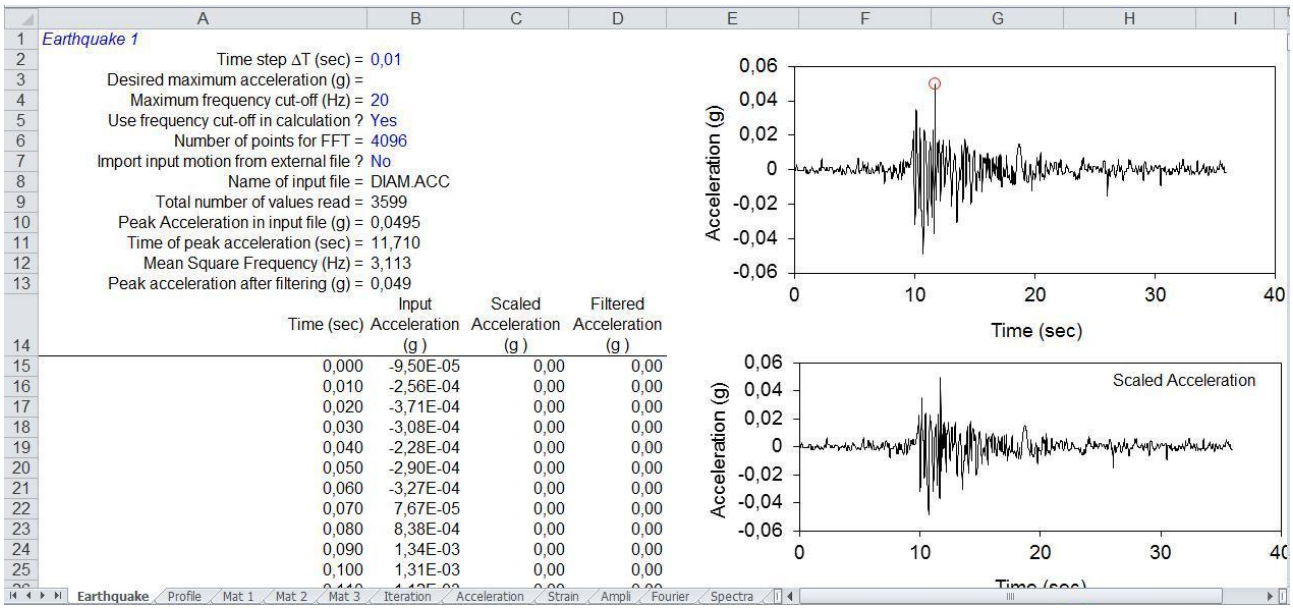

Figure 4.12. Worksheet Earthquake.

Worksheet *Profile* (Figure 4.13) is used to define the geometry and properties of the soil profile. The data required are:

- soil material type, each material type is defined in a separate worksheet called *Mat i*. In this model, number 1 means clayey silt, 2 means sand and 3 means gravel.
- thickness of each layer. Each layer may be subdivided in several sub-layers. This feature improves the accuracy of calculation (for this reasons that the number of layer is 17 instead of 4).
- total unit weight of each layer.
- shear-wave velocity of each layer, determined by geophysical surveys (Paragraph 2.1.3).

The other data, for example the maximum shear modulus, are calculated by the code from the inserted data.

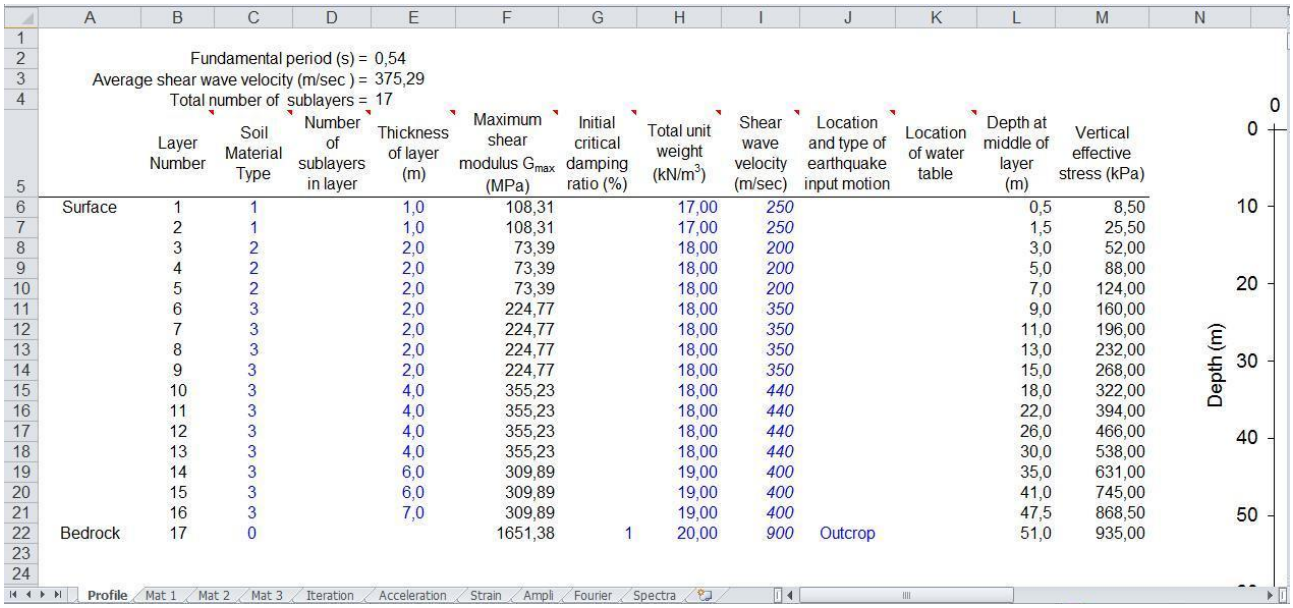

Fundamental period (s) = 0,54
Average shear wave velocity (m/sec) = 375,29
Total number of sublayers = 17

	Layer Number	Soil Material Type	Number of sublayers in layer	Thickness of layer (m)	Maximum shear modulus G_{max} (MPa)	Initial critical damping ratio (%)	Total unit weight (kN/m^3)	Shear wave velocity (m/sec)	Location and type of earthquake input motion	Location of water table	Depth at middle of layer (m)	Vertical effective stress (kPa)
Surface	1	1		1,0	108,31		17,00	*250*			0,5	8,50
	2	1		1,0	108,31		17,00	*250*			1,5	25,50
	3	2		2,0	73,39		18,00	*200*			3,0	52,00
	4	2		2,0	73,39		18,00	*200*			5,0	88,00
	5	2		2,0	73,39		18,00	*200*			7,0	124,00
	6	3		2,0	224,77		18,00	*350*			9,0	160,00
	7	3		2,0	224,77		18,00	*350*			11,0	196,00
	8	3		2,0	224,77		18,00	*350*			13,0	232,00
	9	3		2,0	224,77		18,00	*350*			15,0	268,00
	10	3		4,0	355,23		18,00	*440*			18,0	322,00
	11	3		4,0	355,23		18,00	*440*			22,0	394,00
	12	3		4,0	355,23		18,00	*440*			26,0	466,00
	13	3		4,0	355,23		18,00	*440*			30,0	538,00
	14	3		6,0	309,89		19,00	*400*			35,0	631,00
	15	3		6,0	309,89		19,00	*400*			41,0	745,00
	16	3		7,0	309,89		19,00	*400*			47,5	868,50
Bedrock	17	0			1651,38	1	20,00	*900*	Outcrop		51,0	935,00

Figure 4.13. Worksheet Profile.

In worksheet *Mat i* stress-strain and damping-strain curves can be defined, one for every material type (in this case 3, *Mat 1 Mat 2* and *Mat 3*). Worksheet *Mat 1* corresponds to clayey silt and the inserted curves are the ones described in the Paragraph 3.2. Worksheet *Mat 2* corresponds to sand, and also for sand the curves are determined in the laboratory. Worksheet Mat 3 correspond to gravel and in the absence of measured data, a literature curve of Aghaei Araei, 2008 was used. The graphical representation of these curves is reported in Figures 4.14-4.16.

clayey silt

Strain (%)	G/G_{max}	Strain (%)	Damping (%)
0,0001	0,994	0,0001	1,498
0,0002	0,988	0,0002	1,519
0,0003	0,983	0,0003	1,539
0,0004	0,978	0,0004	1,558
0,0005	0,974	0,0005	1,577
0,001	0,952	0,001	1,667
0,002	0,915	0,002	1,835
0,004	0,853	0,004	2,152
0,01	0,719	0,01	3,033
0,02	0,581	0,02	4,335
0,03	0,491	0,03	5,456
0,04	*0,428*	*0,04*	*6,423*
0,05	*0,38*	*0,05*	*7,262*
0,1	*0,249*	*0,1*	*10,183*
0,2	*0,152*	*0,2*	*13,074*
0,3	*0,111*	*0,3*	*14,523*

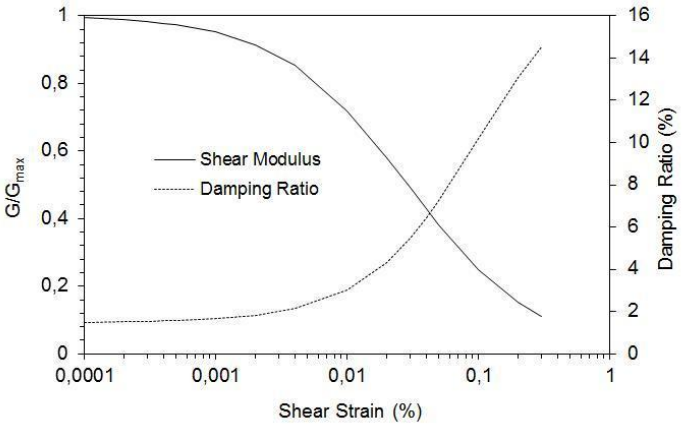

Figure 4.14. Worksheet Mat 1 – clayey silt.

sand

Strain (%)	G/G_{max}	Strain (%)	Damping (%)
0,0001	0,999	0,0001	1,464
0,0002	0,998	0,0002	1,469
0,0003	0,996	0,0003	1,475
0,0004	0,995	0,0004	1,48
0,0005	0,993	0,0005	1,486
0,001	0,985	0,001	1,517
0,002	0,968	0,002	1,587
0,004	0,932	0,004	1,744
0,01	0,825	0,01	2,298
0,02	0,68	0,02	3,353
0,03	0,571	0,03	4,451
0,04	*0,488*	*0,04*	*5,515*
0,05	*0,424*	*0,05*	*6,509*
0,1	*0,249*	*0,1*	*10,27*
0,2	*0,129*	*0,2*	*14*
0,3	*0,085*	*0,3*	*15,706*

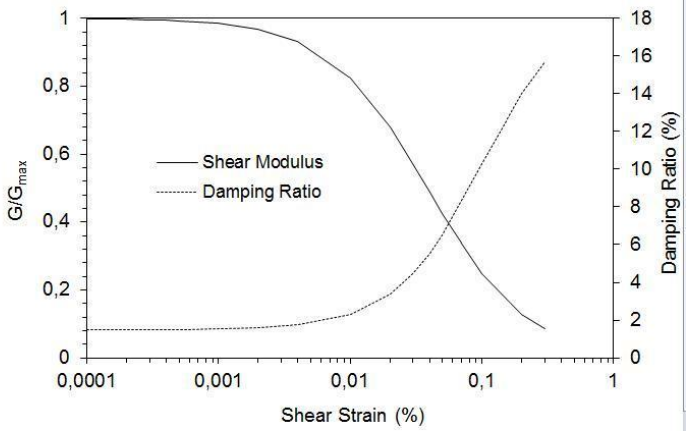

Figure 4.15. Worksheet Mat 2 – sand.

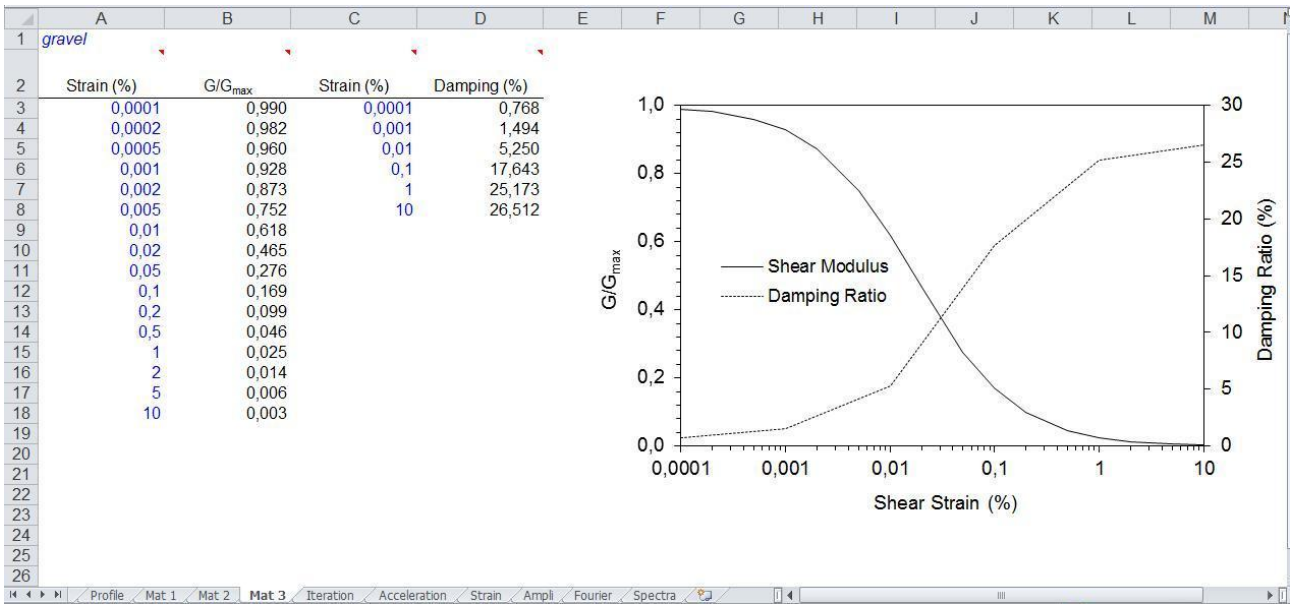

Figure 4.16. Worksheet *Mat 3* – gravel.

By running EERA a series of results may be obtained, as briefly displayed in Table 4.3. In this work results are shown as *acceleration response spectra* and *amplification factors* (section 4.4).

4.4 Results and discussion

The calculation codes allow to determine the expected seismic motion and to express it in different manners: (i) in time domain (time history of the acceleration or velocity), (ii) in frequency domain (through Fourier spectrum, or response spectra) or (iii) summarizing the seismic contents using parameters. The problem is to determine which is the best form to represent the seismic motion at the surface and then quantify the possible effects of amplification, given the objective of the study.
Often the results of the seismic response analysis are shown comparing accelerograms obtained at the surface and at the bedrock-sediment interface. Seismic content is described using maximum peak accelerations, expressed as the ratio between the value at the surface and at the basal layer (i.e., amplification factor). Amplification factors greater than one means amplification phenomena, otherwise attenuation phenomena.
However, the amplification factor defined above does not take into account frequency contents of the seismic motion and how it is eventually modified. In order to consider the complete seismic signal, possibly in the frequency domain, the amplification ratio function can be considered. It not only provides information on the maximum expected amplification and on the corresponding frequency, but also on the values of amplification or attenuation related to the frequency ranges of interest. Even more widespread is the comparison made in terms of the response spectrum, which can be synthesized with only one parameter, for example the Housner spectral intensity.
The Housner amplification factor ($H_{T_1 \div T_2}$) is a seismic parameter computed as the ratio between the Housner spectral intensity calculated at the surface and the one calculated at the bedrock. The Housner spectral intensity SI (Housner, 1952) is a parameter that describes very well the energy content of the earthquake, so it is directly connectable to the damage suffered by the structures. In numerical terms it represents the integral of the pseudo-velocity response spectrum $PSV(\xi, T)$, calculated in a given range of periods $[T_1 \div T_2]$, at 5% of structural damping:

$$SI_{T_1 \div T_2}(\xi) = \int_{T_1}^{T_2} PSV(\xi, T)dT$$

As previously mentioned, EERA software provides different type of results, but here are discussed only the ones in terms of *acceleration response spectra* and *amplification*. The amplification is presented both in terms of *amplification ratio function* and of *Housner amplification factor*. Also the *time history of acceleration* (accelerograms) are represented, but only in a qualitative way. In this manner, the expected seismic motion is characterized in time domain, in frequency domain and using seismic content parameters.

In Figure 4.17 is represented the subsurface model of the Caldes site with bedrock and surface seismic responses in terms of accelerogram, acceleration response spectrum and amplification.

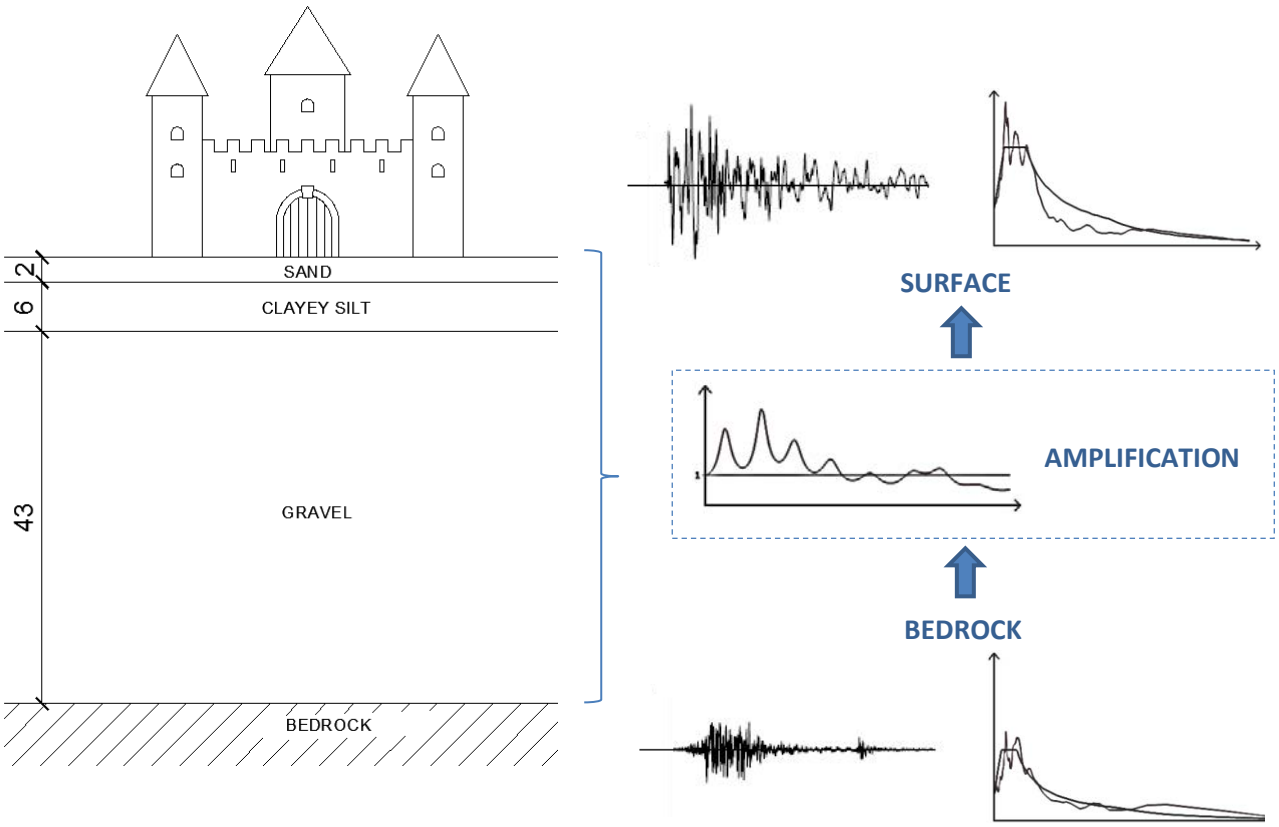

Figure 4.17. Subsurface model of the Caldes site with bedrock and surface seismic responses.

Acceleration response spectra referred to a 5% damping factor provided by EERA are compared with response spectra obtained using the simplified approach of the Italian building code. The last ones are built by means of the computer program Spettri-NTCver1.0.3 (freely available at website of Consiglio Superiore dei lavori Pubblici). C soil category ($V_{S,30}$ equal to 314 m/s, so between 180 and 360 m/s) and T1 topographic category (mean slope equal to 11.6°, so lower than 15°) are considered.

The amplification ratio functions are given directly by EERA as ratio between the amplitudes of the Fourier spectra at the surface and at the base of the deposit, as function of frequency. For easy comparison with the Housner amplification factors, the amplification ratio function is also expressed in terms of period.

The interval of integration in the Housner original definition is $[0.1 - 2.5]\ s$, which includes the effects caused on all typology of civil structures. Here, we consider four range of periods:

- the original interval $[0.1 - 2.5]\ s$;
- $[0.1 - 0.5]\ s$, which is typical for rigid structures (for example masonry buildings);

- $[0.5 - 1.5]\ s$, which is typical for flexible structures;
- $[1.5 - 2.5]\ s$, which is typical for seismically isolated structures.

These Housner amplification factors will subsequently be indicated by the notation $H_{0.1-2.5}$, $H_{0.1-0.5}$, $H_{0.5-1.5}$ and $H_{1.5-2.5}$, respectively.

EERA was run 7 times, one for each input motion chosen by means of REXEL, and one time more considering the Merano earthquake of 2001. Also Merano is considered, in a separate way, because it represents a relevant earthquake near the study area. The obtained response spectra were compared with the response spectrum calculated according to the Italian building code corresponding to the soil category to which belongs the subsurface stratigraphic column analysed (defined via the $V_{S,30}$ parameter).

Figures 4.18-4.38 show results for each seismic input, while Figures 4.39-4.41 show average outputs, considering the 7 earthquakes from REXEL. The Merano earthquake results are not considered together with the average results and are shown in Figures 4.42-4.44.

Figures 4.18-4.44 are related to the area identified as *Caldes site*, located downstream of the castle, Figures 4.45-4.48 to the area upstream of the castle, indicated as *Samoclevo site*.

EARTHQUAKE 1 – Caldes site

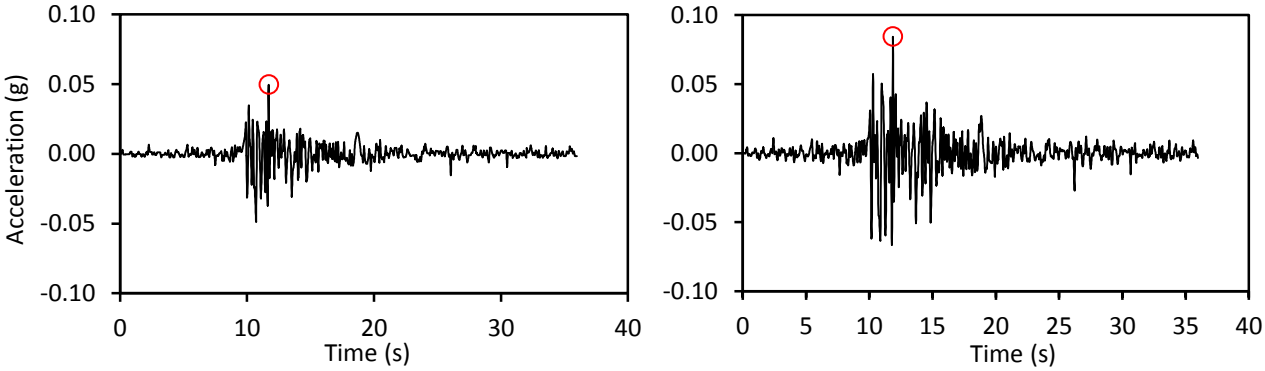

Figure 4.18. Accelerograms at bedrock (left) and at surface (right).

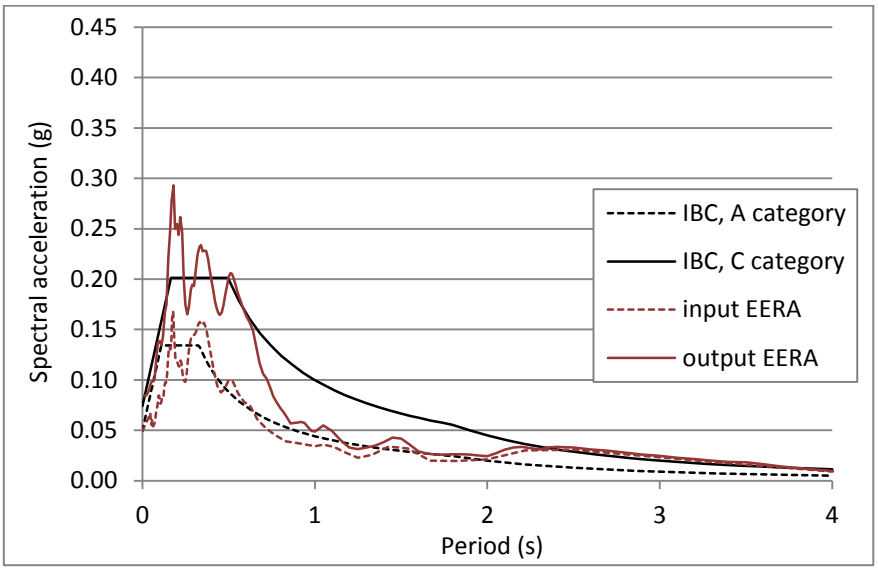

Figure 4.19. Comparison among EERA and IBC input and output spectra.

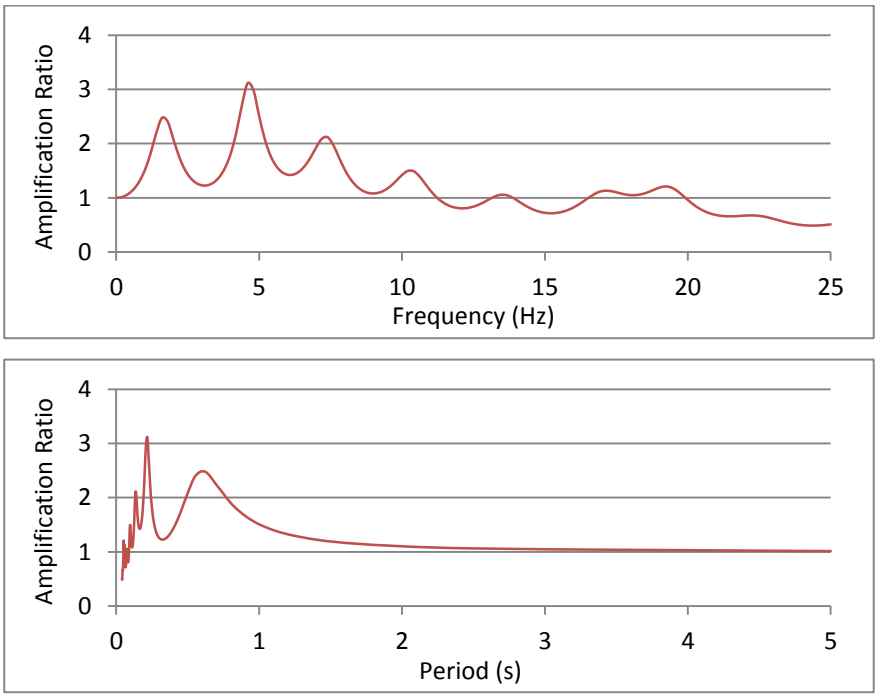

Housner amplification factors	
$H_{0.1-2.5}$	1.47
$H_{0.1-0.5}$	1.62
$H_{0.5-2.5}$	1.74
$H_{1.5-2.5}$	1.25

Figure 4.20. Amplification ratio function in terms of frequency and period (left) and Housner amplification factors (right).

EARTHQUAKE 2 – Caldes site

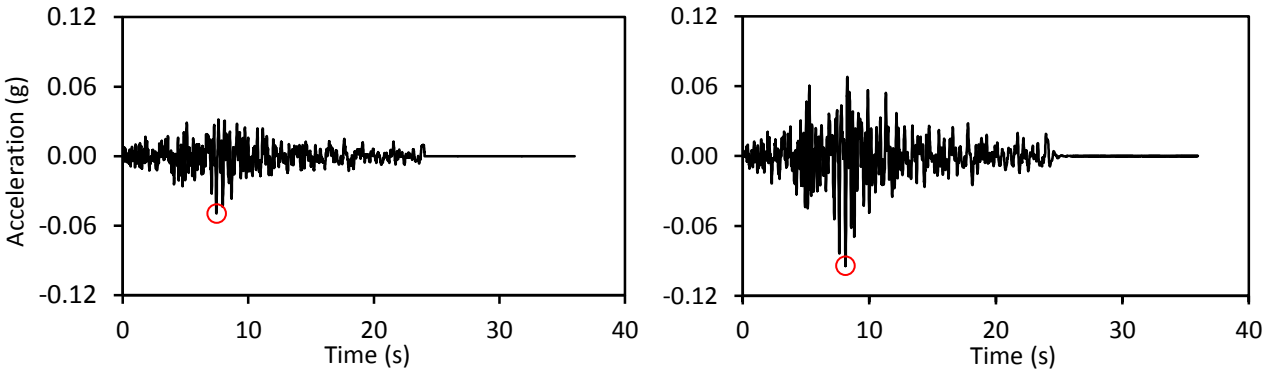

Figure 4.21. Accelerograms at bedrock (left) and at surface (right).

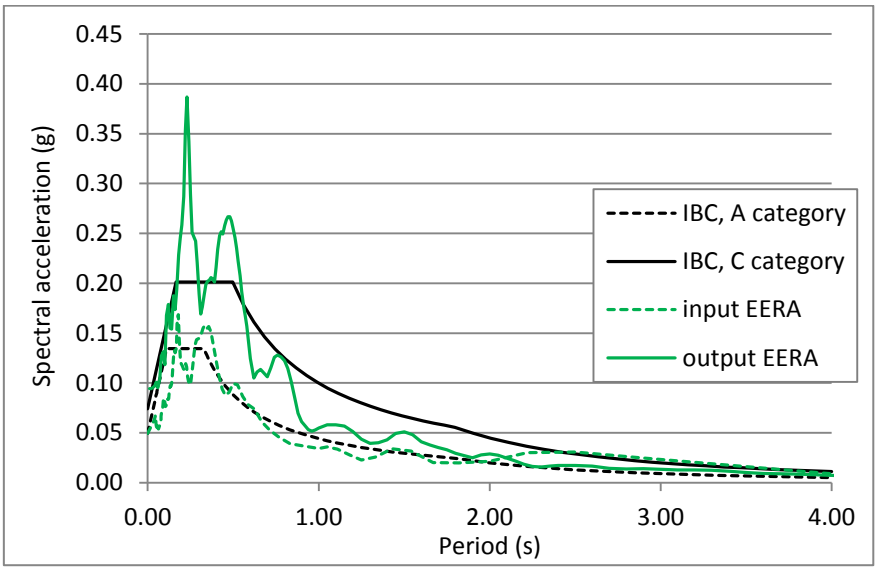

Figure 4.22. Comparison among EERA and IBC input and output spectra.

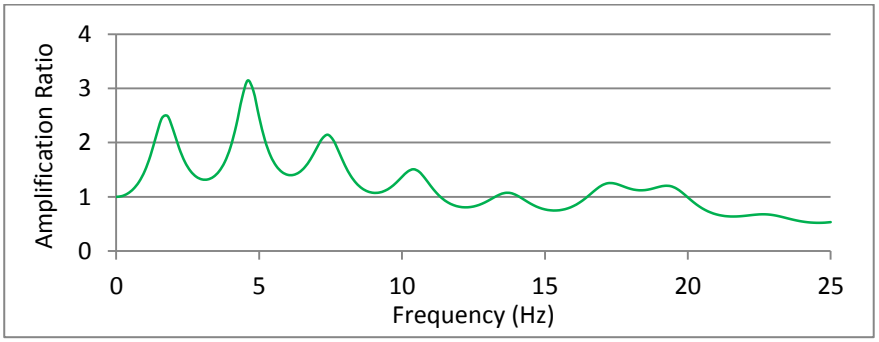

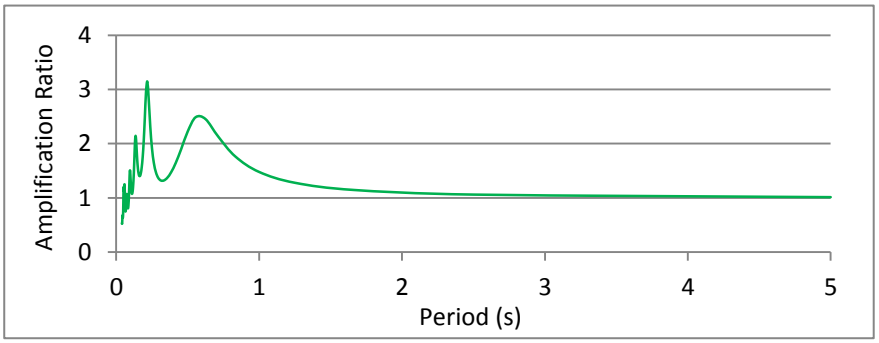

Housner amplification factors	
$H_{0.1-2.5}$	1.52
$H_{0.1-0.5}$	1.91
$H_{0.5-2.5}$	1.67
$H_{1.5-2.5}$	1.27

Figure 4.23. Amplification ratio function in terms of frequency and period (left) and Housner amplification factors (right).

EARTHQUAKE 3 – Caldes site

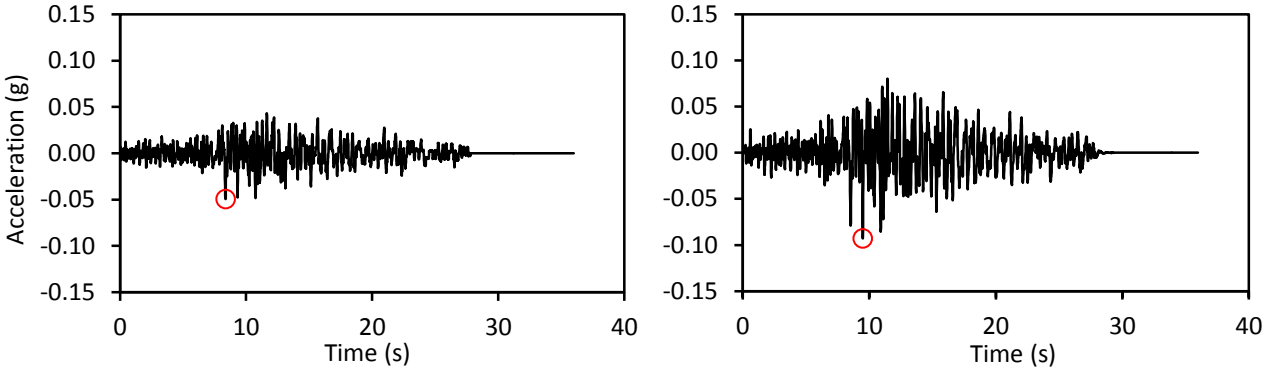

Figure 4.24. Accelerograms at bedrock (left) and at surface (right).

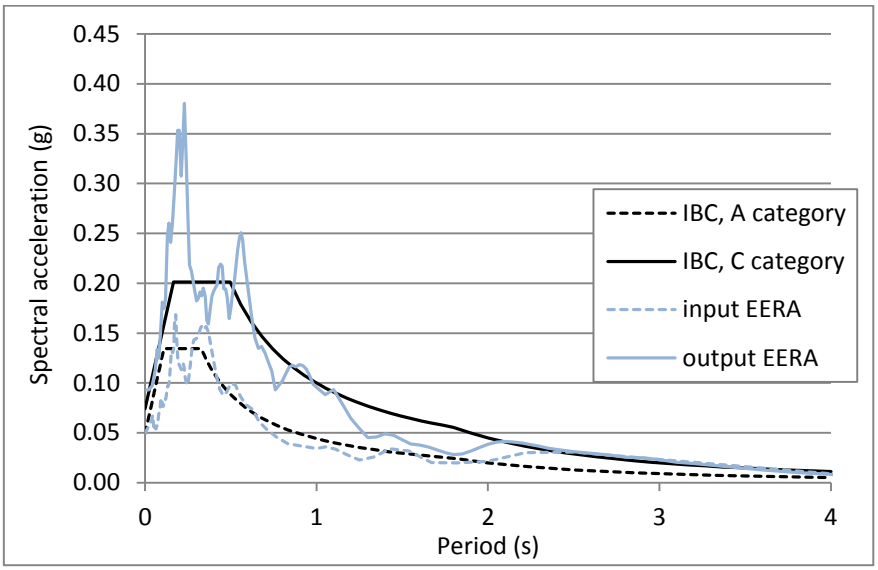

Figure 4.25. Comparison among EERA and IBC input and output spectra.

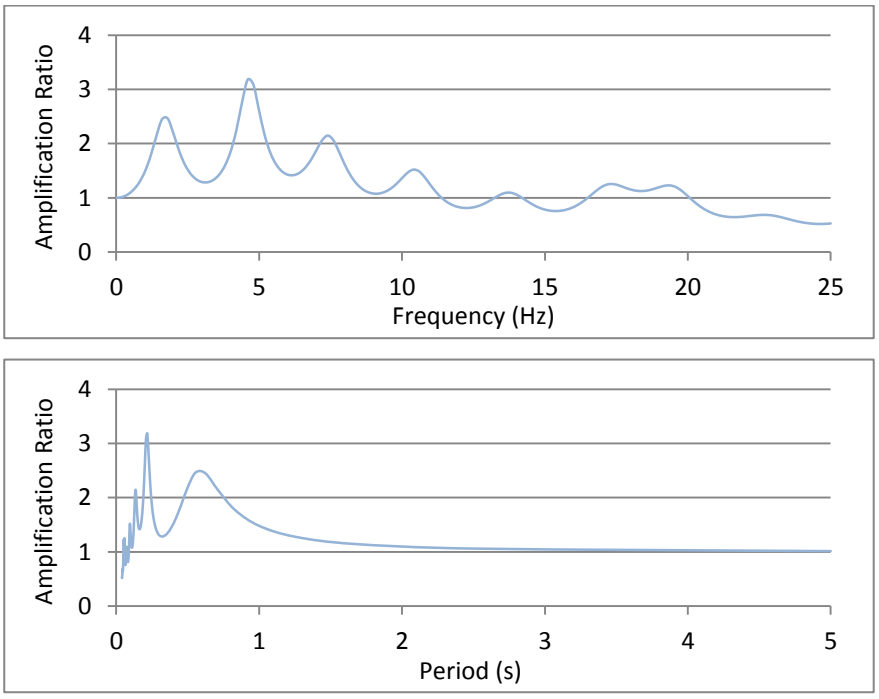

Housner amplification factors	
$H_{0.1-2.5}$	1.51
$H_{0.1-0.5}$	1.78
$H_{0.5-2.5}$	1.70
$H_{1.5-2.5}$	1.30

Figure 4.26. Amplification ratio function in terms of frequency and period (left) and Housner amplification factors (right).

EARTHQUAKE 4 – Caldes site

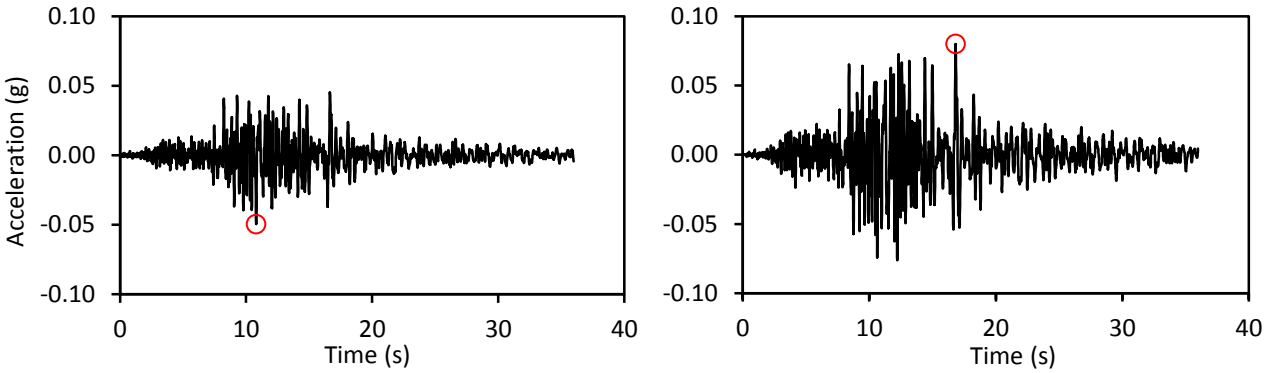

Figure 4.27. Accelerograms at bedrock (left) and at surface (right).

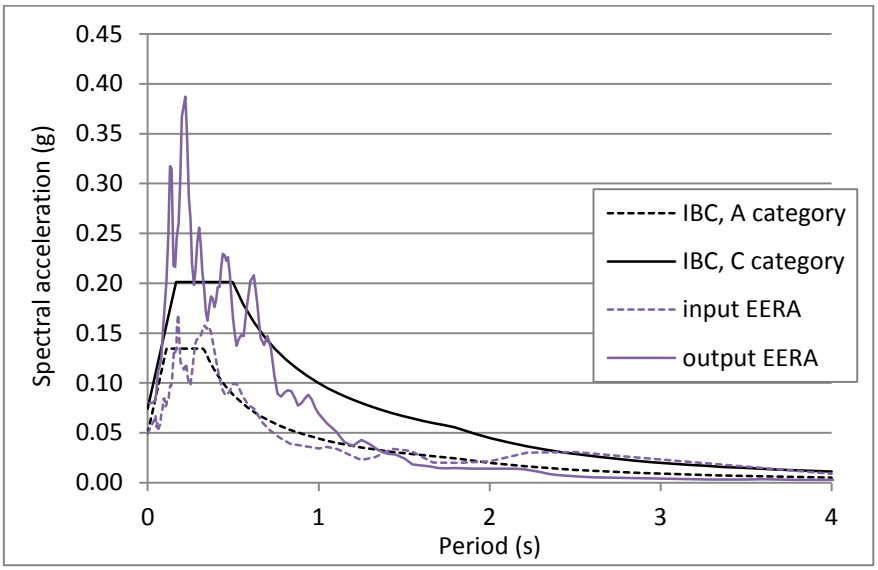

Figure 4.28. Comparison among EERA and IBC input and output spectra.

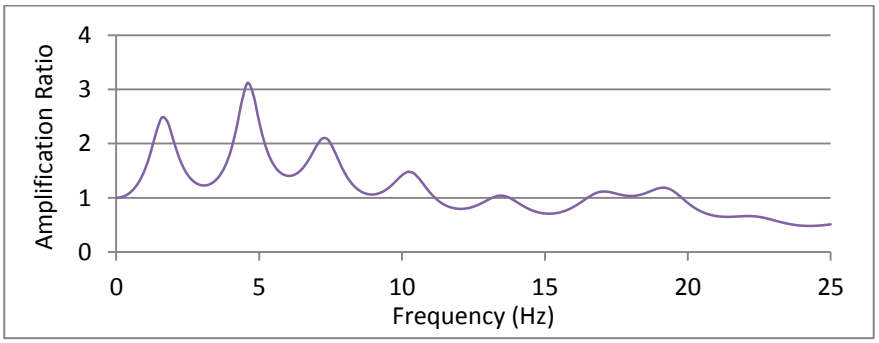

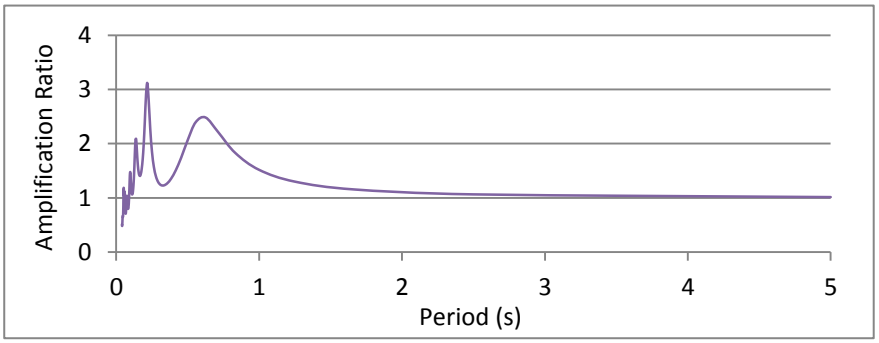

Housner amplification factors	
$H_{0.1-2.5}$	1.77
$H_{0.1-0.5}$	1.71
$H_{0.5-2.5}$	1.83
$H_{1.5-2.5}$	1.69

Figure 4.29. Amplification ratio function in terms of frequency and period (left) and Housner amplification factors (right).

EARTHQUAKE 5 – Caldes site

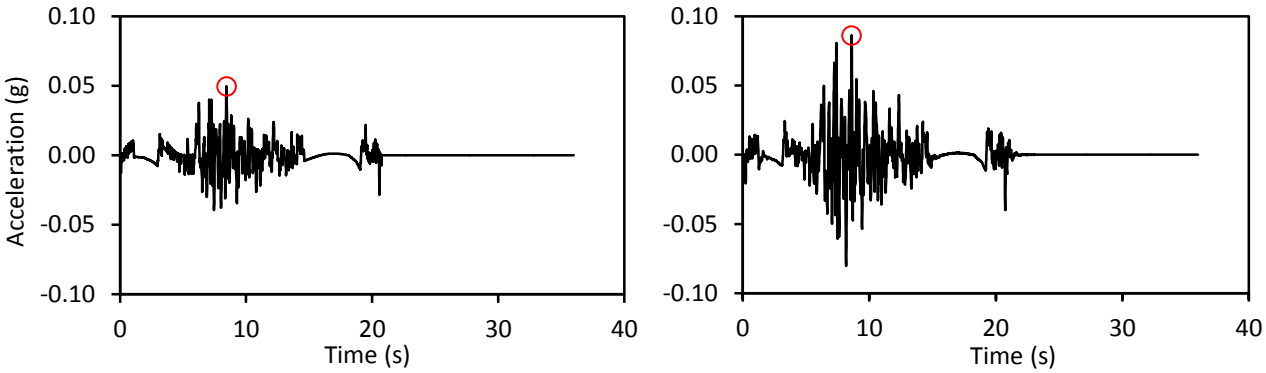

Figure 4.30. Accelerograms at bedrock (left) and at surface (right).

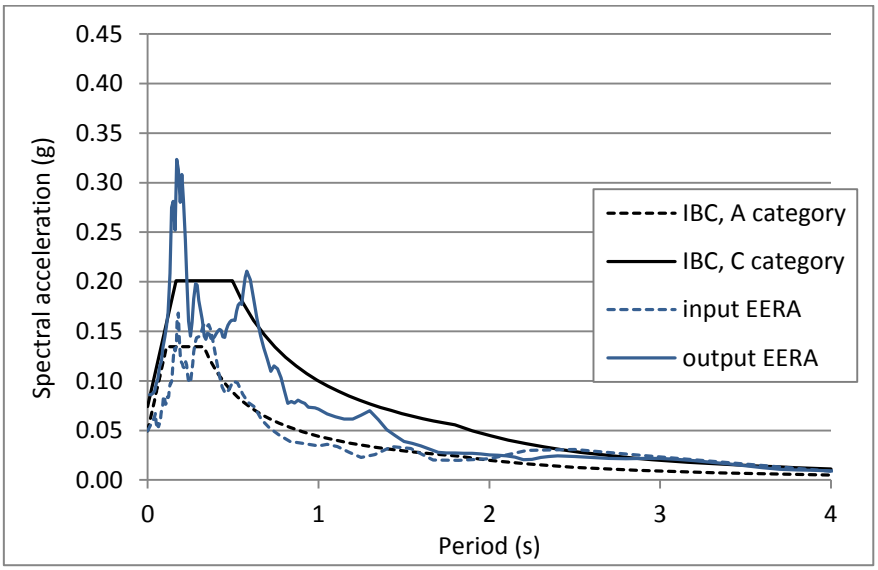

Figure 4.31. Comparison among EERA and IBC input and output spectra.

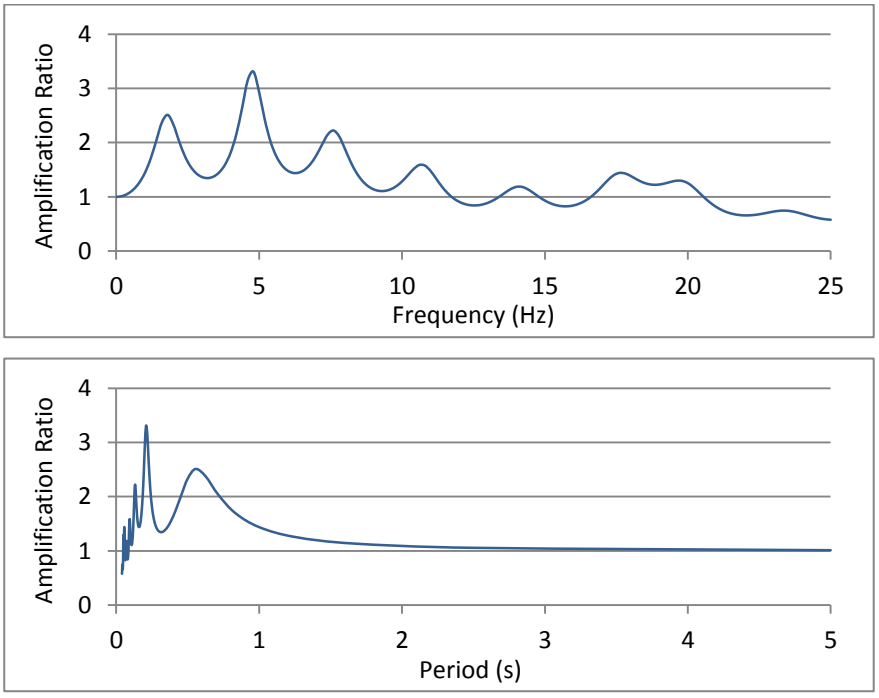

Housner amplification factors	
$H_{0.1-2.5}$	1.46
$H_{0.1-0.5}$	1.80
$H_{0.5-2.5}$	1.65
$H_{1.5-2.5}$	1.19

Figure 4.32. Amplification ratio function in terms of frequency and period (left) and Housner amplification factors (right).

EARTHQUAKE 6 – Caldes site

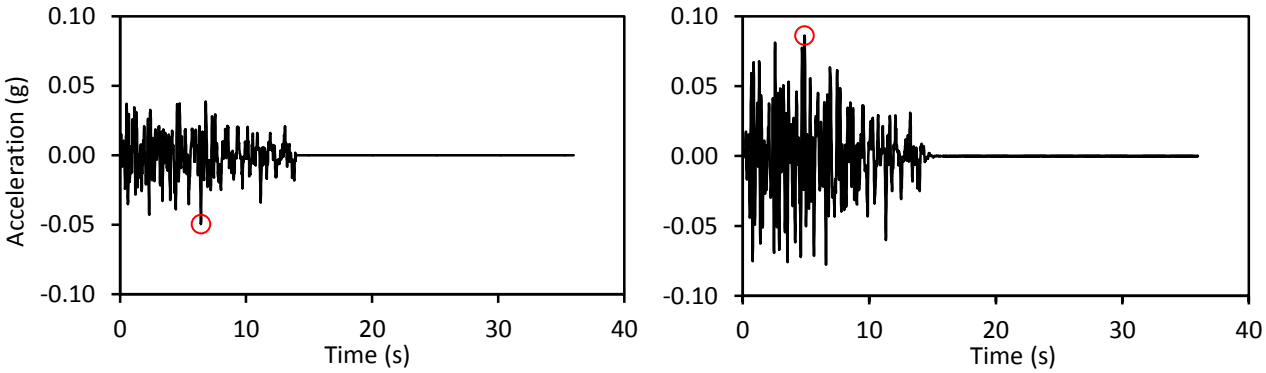

Figure 4.33. Accelerograms at bedrock (left) and at surface (right).

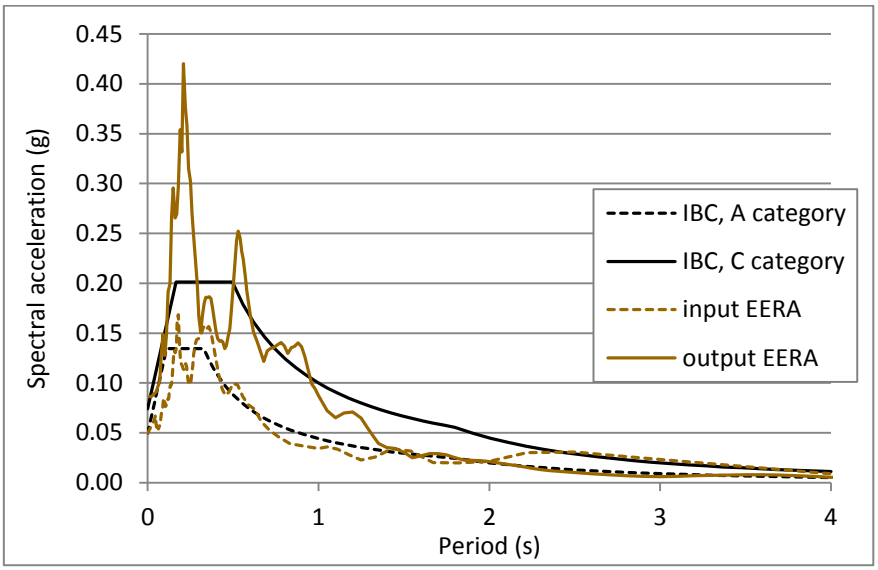

Figure 4.34. Comparison among EERA and IBC input and output spectra.

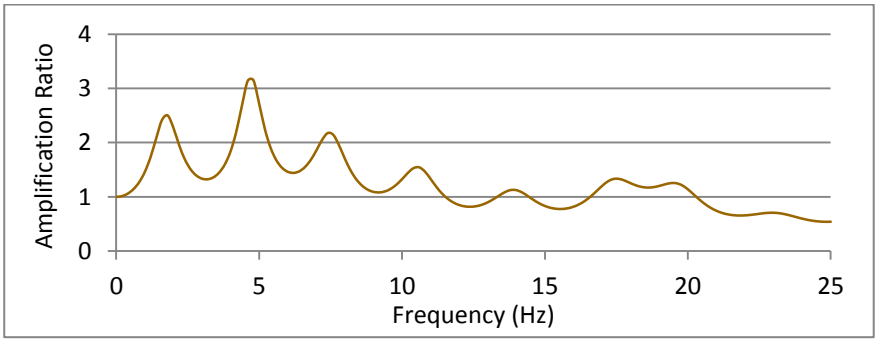

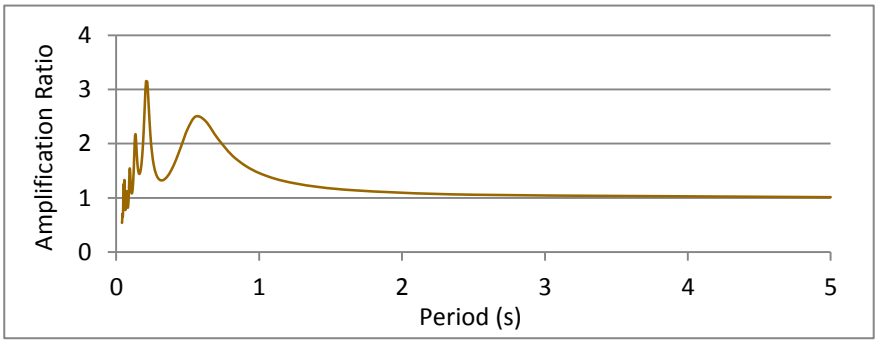

Housner amplification factors	
$H_{0.1-2.5}$	1.62
$H_{0.1-0.5}$	1.93
$H_{0.5-2.5}$	1.66
$H_{1.5-2.5}$	1.46

Figure 4.35. Amplification ratio function in terms of frequency and period (left) and Housner amplification factors (right).

EARTHQUAKE 7 – Caldes site

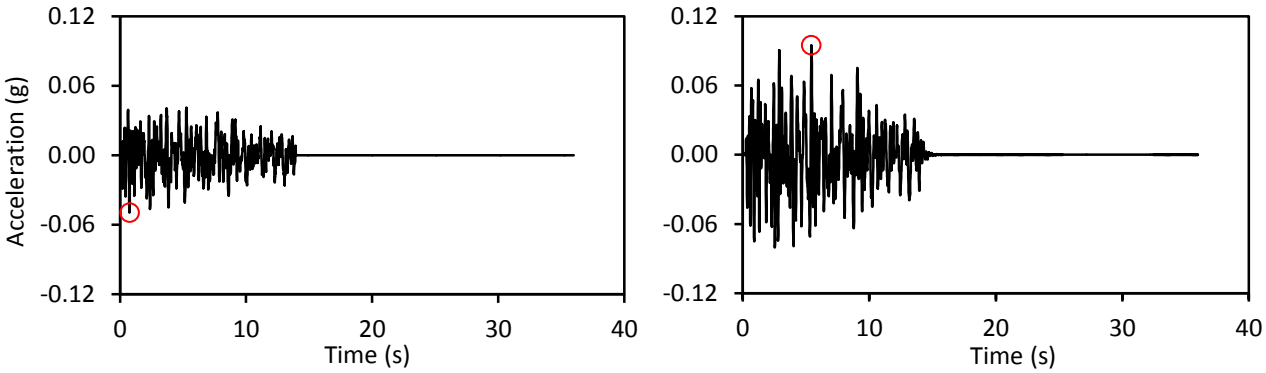

Figure 4.36. Accelerograms at bedrock (left) and at surface (right).

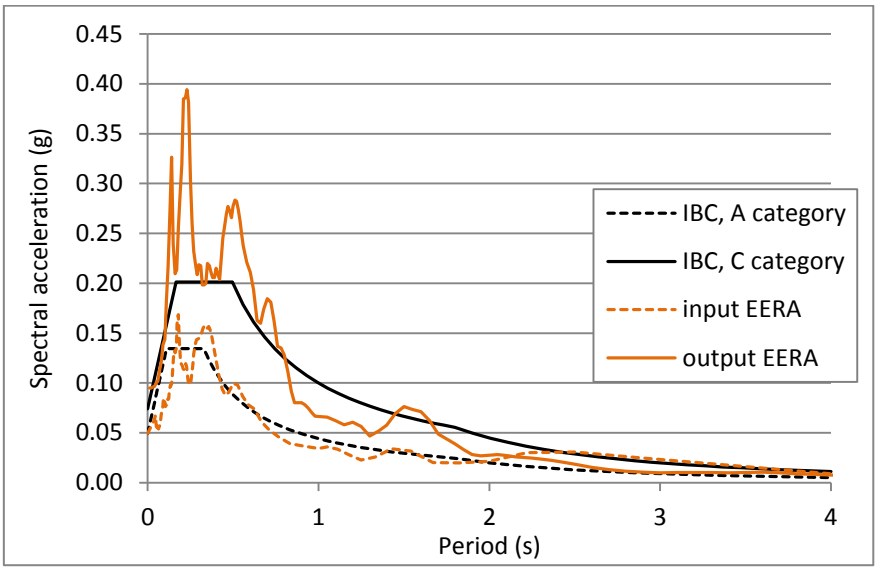

Figure 4.37. Comparison among EERA and IBC input and output spectra.

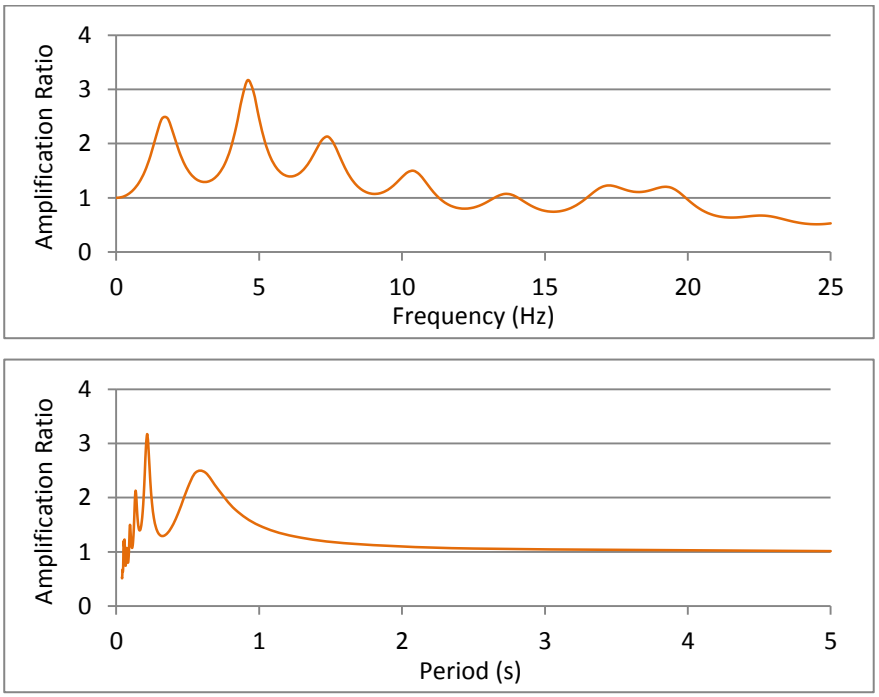

Housner amplification factors	
$H_{0.1-2.5}$	1.53
$H_{0.1-0.5}$	1.87
$H_{0.5-2.5}$	1.68
$H_{1.5-2.5}$	1.33

Figure 4.38. Amplification ratio function in terms of frequency and period (left) and Housner amplification factors (right).

AVERAGE RESULTS – Caldes site

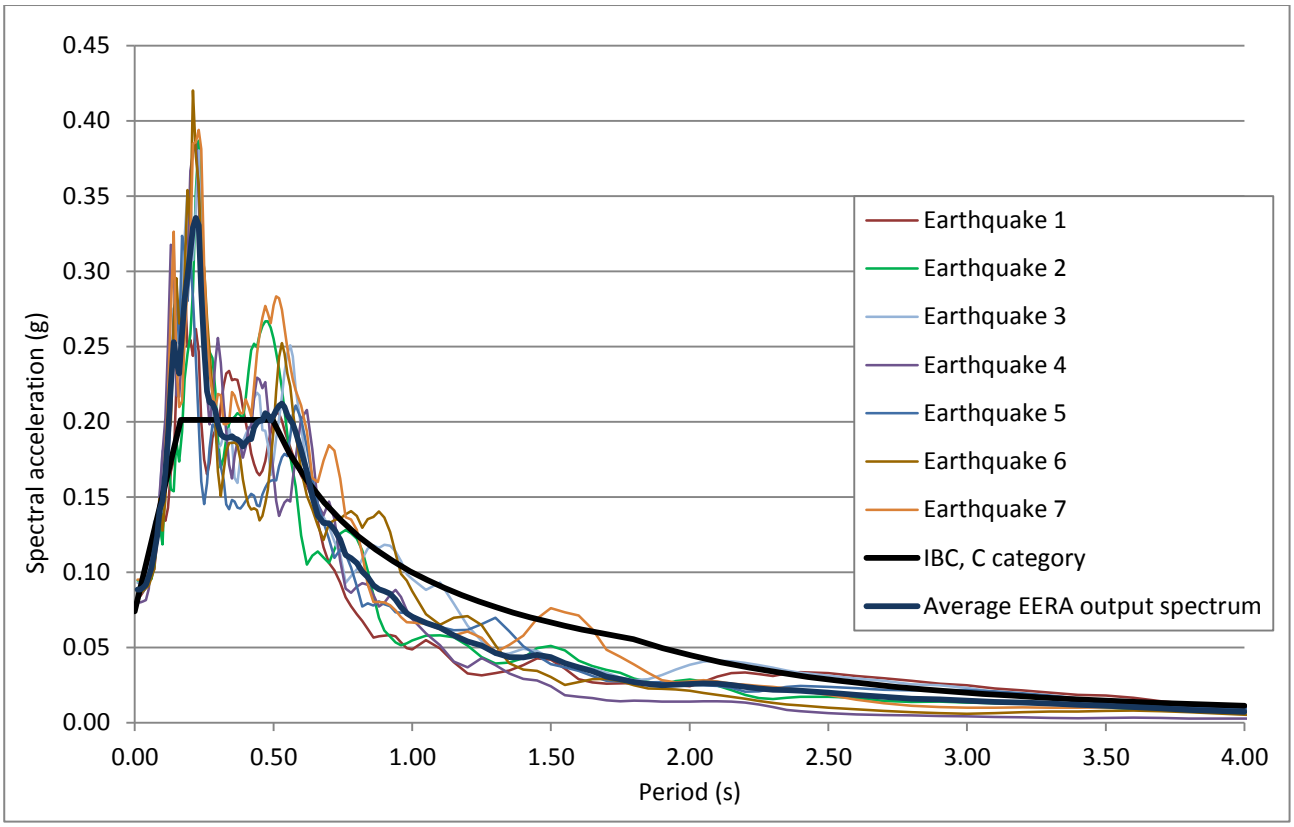

Figure 4.39. Comparison among the output spectra of the 7 earthquakes, the average one, and the spectrum calculated according to the Italian building code.

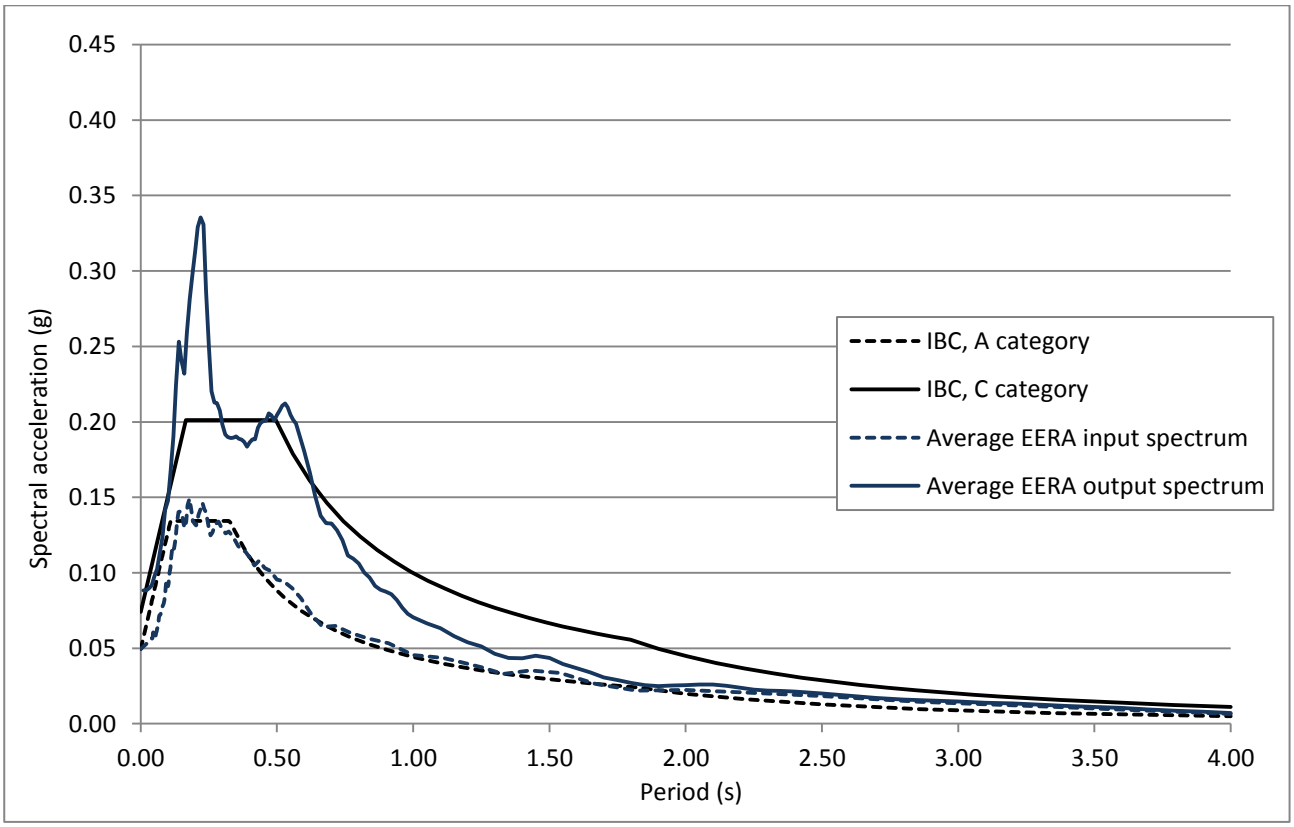

Figure 4.40. Comparison among average input and output spectra calculated with EERA and according to the Italian building code.

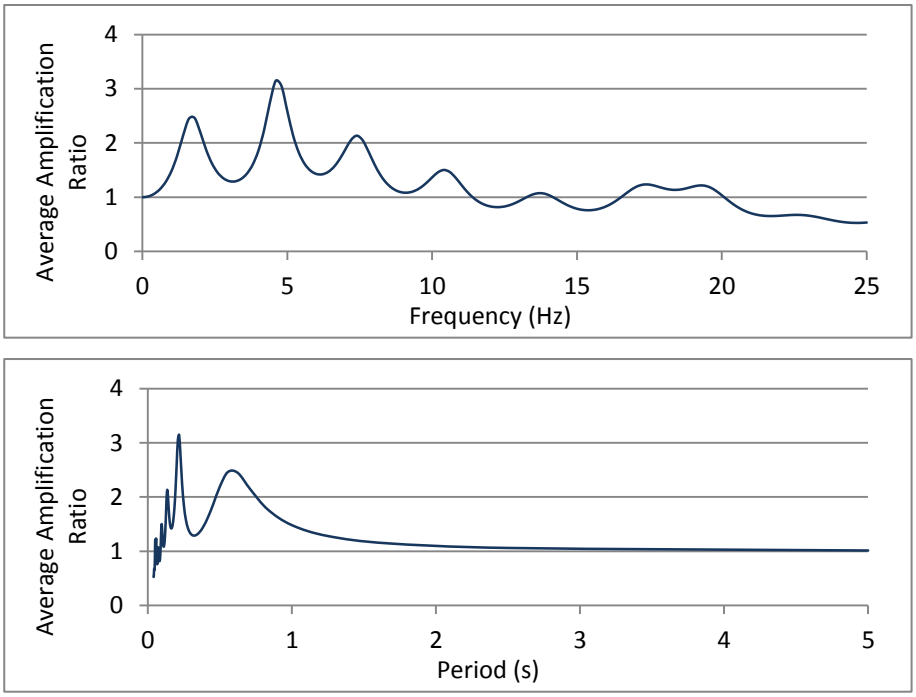

Average Housner amplification factors	
$H_{0.1-2.5}$	1.55
$H_{0.1-0.5}$	1.80
$H_{0.5-2.5}$	1.71
$H_{1.5-2.5}$	1.36

Figure 4.41. Average amplification ratio function in terms of frequency and period (left) and average Housner amplification factors (right).

The structure of the pages that list the results case by case (Earthquake 1, Earthquake 2, etc.) is as follows:

- Upper part: accelerograms. Input accelerogram at the bedrock obtained with the program REXEL on the left and output accelerogram at the surface (from EERA) on the right. The red circles indicate the maximum acceleration.
- Middle part: comparison between response spectrum at the bedrock and at the surface. These graphs also show the spectra calculated with the simplified approach proposed by the Italian building code (indicated in the legends with *IBC*) to see the differences.
- Lower part: amplification. In terms of amplification ratio function on the left and of Housner amplification factors on the right.

Already from the accelerograms it is possible to see that there is a considerable increase of the peak acceleration, on average of about $0.4\ g$.

The graphs of the response spectra show that the spectral acceleration varies with the period and is maximal at low periods (between 0.10 and 0.40 s). The maximal value of the spectra acceleration ranges from 0.29 g (earthquake 1) to 0.42 g (earthquake 6). The differences between EERA and Italian building code spectra are significant in fact the spectrum of the legislation strongly underestimates the spectral acceleration at low periods. In the case of earthquake 6 (Figure 4.34) the spectral acceleration calculated with EERA is more than double of the one determined with the simplified approach ($0.42\ g$ versus $0.20\ g$ at the period $0.21\ s$). For periods higher than 0.40 s, sometimes is more cautelative the spectrum obtained with EERA, other times the one of the Italian building code.

The amplification ratio functions confirm that the amplification is greater at low periods (between 0.1 and 0.4 s). Also the Housner factors are in agreement in fact they assume the maximum value in the interval 0.1-0.5 s.

The average results (Figures 4.39-4.41) can be considered representative of the area under consideration and therefore can be used for the design. In Figure 4.39 the response spectra of all the 7 earthquake and the average spectrum are reported. Figure 4.40 instead shows only the average spectrum and its comparison with the Italian building code spectrum. The maximum spectral acceleration of the average spectrum is $0.33\ g$ at the period $0.21\ s$. It shows 2 peaks, one at $0.21\ s$ and one in $0.55\ s$. Both exceed the maximum spectral acceleration expected according to the Italian building code, the excess is respectively of $0.15\ g$ and $0.02\ g$. For periods greater than $0.7\ s$, the Italian building code spectrum is more cautelative than EERA spectrum. The average amplification ratio functions (Figure 4.41) confirm what has already been said about the individual cases. The peak of the amplification is at $0.21\ s$ with a value equal to 3.15. The amplification is maximum in

the range of periods between 0.1 and $0.5\,s$ in which the Housner amplification factor is 1.80 (Figure 4.41).

The Merano earthquake results are quite similar to those obtained with the other input earthquakes (Figures 4.42-4.44).

MERANO EARTHQUAKE – Caldes site

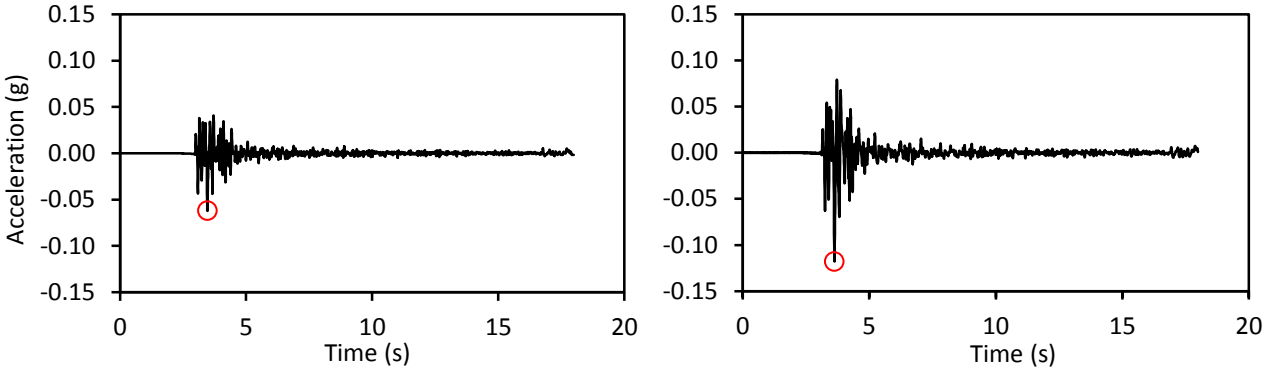

Figure 4.42. Accelerograms at bedrock (left) and at surface (right).

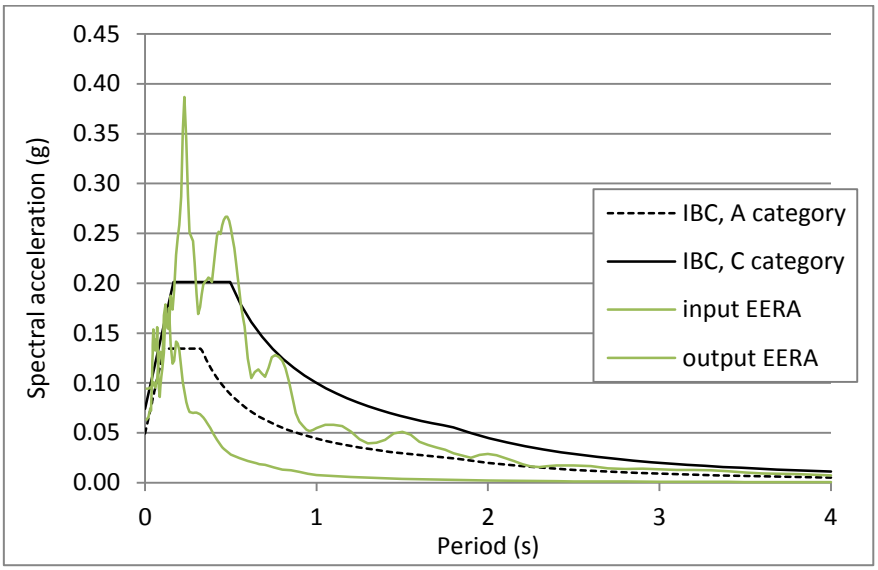

Figure 4.43. Comparison among EERA and IBC input and output spectra.

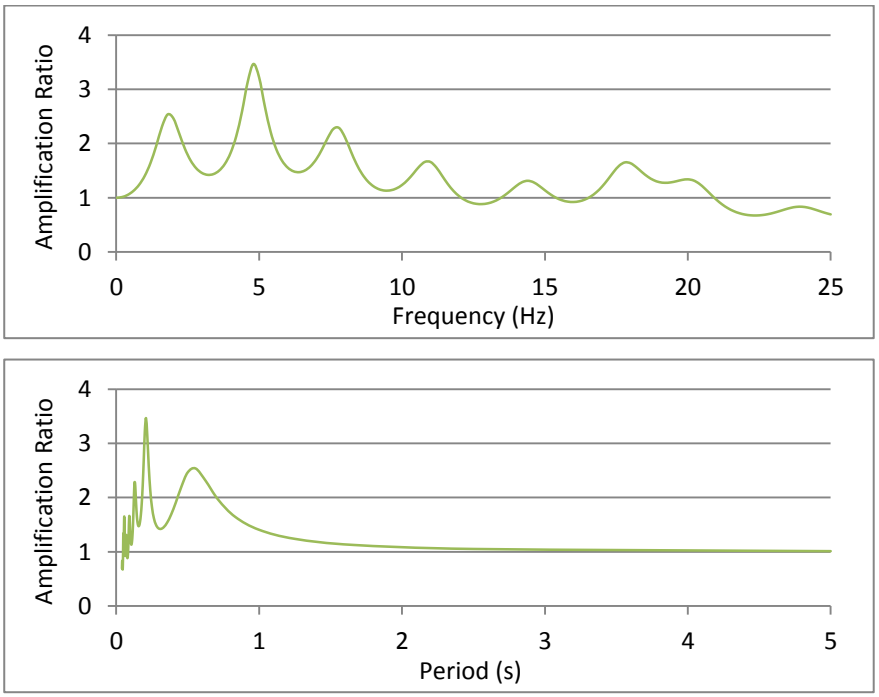

Housner amplification factors	
$H_{0.1-2.5}$	1.98
$H_{0.1-0.5}$	2.08
$H_{0.5-2.5}$	2.01
$H_{1.5-2.5}$	1.88

Figure 4.44. Amplification ratio function in terms of frequency and period (left) and Housner amplification factors (right).

The same work is performed also for the Samoclevo site, located north of the castle. Here only the graphs related to the average results are shown (Figures 4.45-4.48; Appendix 6 for specific results).
The Samoclevo site is characterized by a limited layer of soil (about 0.5 m) above the bedrock (Paragraph 2.1.3). Absence of amplification (soil of type A according to the Italian building code) is confirmed by:

- superimposition of input and output spectra of the one-dimensional simulation (Figure 4.46);
- amplification ratio function and Housner factors equal to 1 (Figure 4.47).

Seismic response at the Samoclevo site (no amplification) is totally different from the Caldes site (relevant amplification) due to different shallow geologic characters, as also evidenced in Figure 4.48.

AVERAGE RESULTS – Samoclevo site

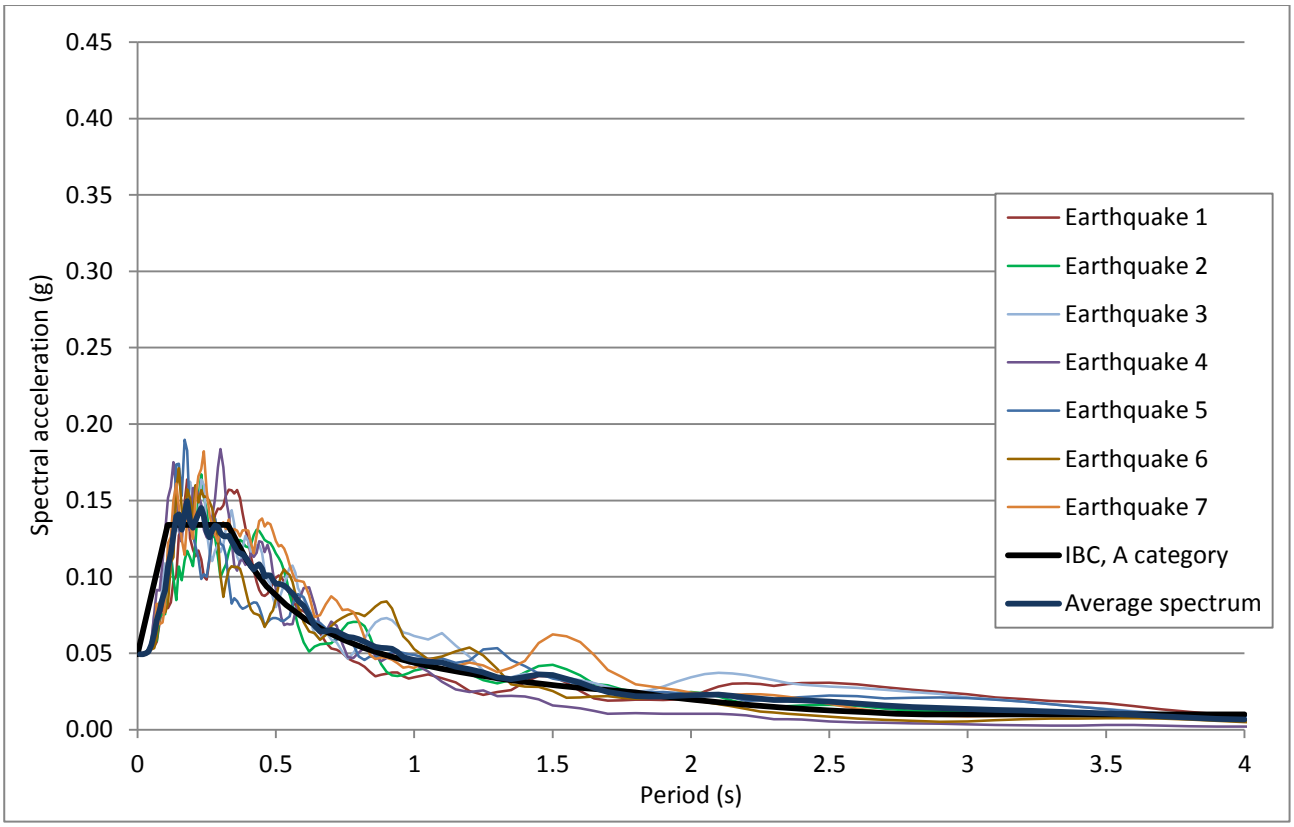

Figure 4.45. Comparison among the output spectra of the 7 earthquakes, the average one, and the spectrum calculated according to the Italian building code.

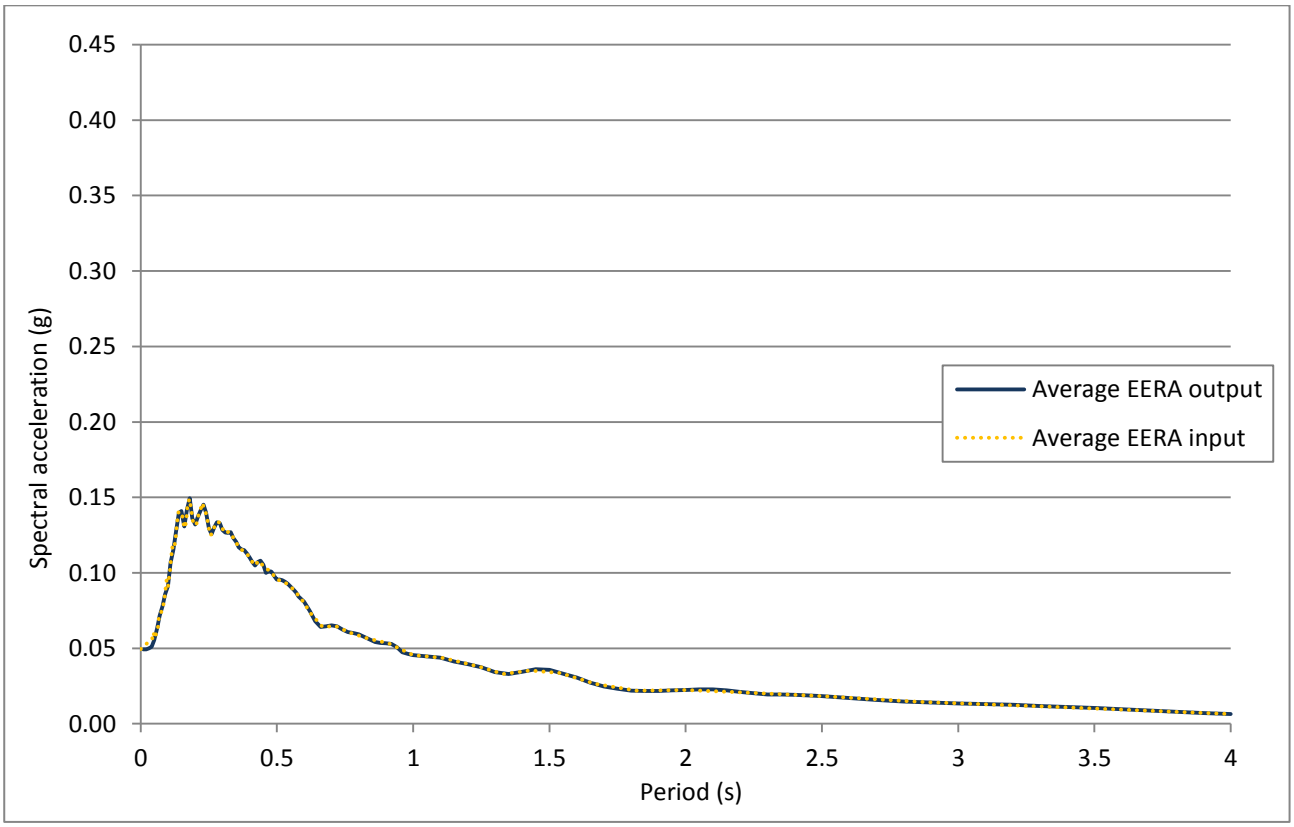

Figure 4.46. Comparison between EERA input and output spectra.

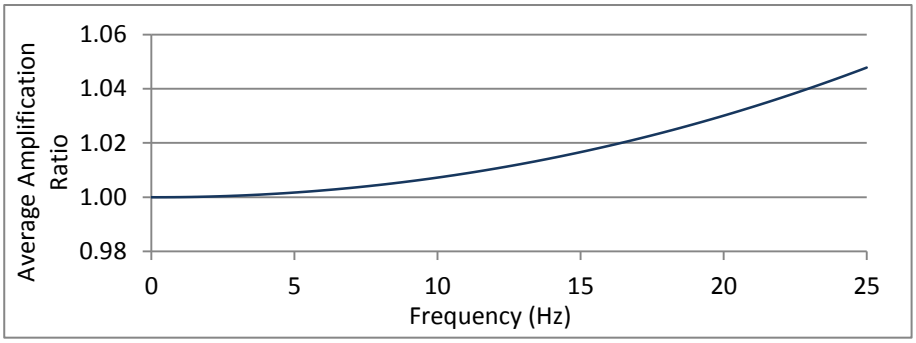

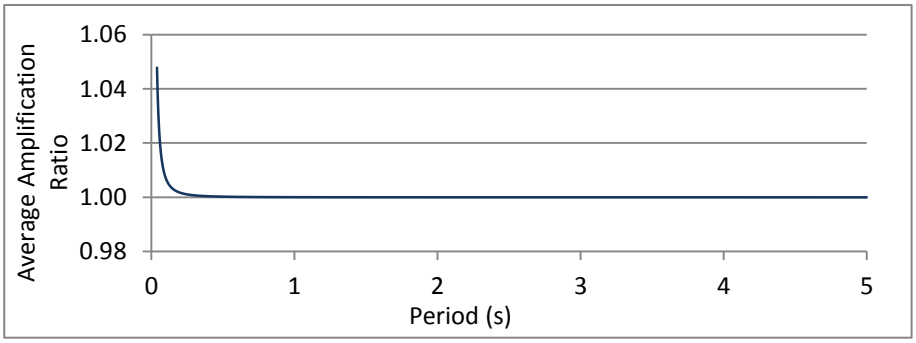

Average Housner amplification factors	
$H_{0.1-2.5}$	1.00
$H_{0.1-0.5}$	1.00
$H_{0.5-2.5}$	1.00
$H_{1.5-2.5}$	1.00

Figure 4.47. Average amplification ratio function in terms of frequency and period (left) and average Housner amplification factors (right).

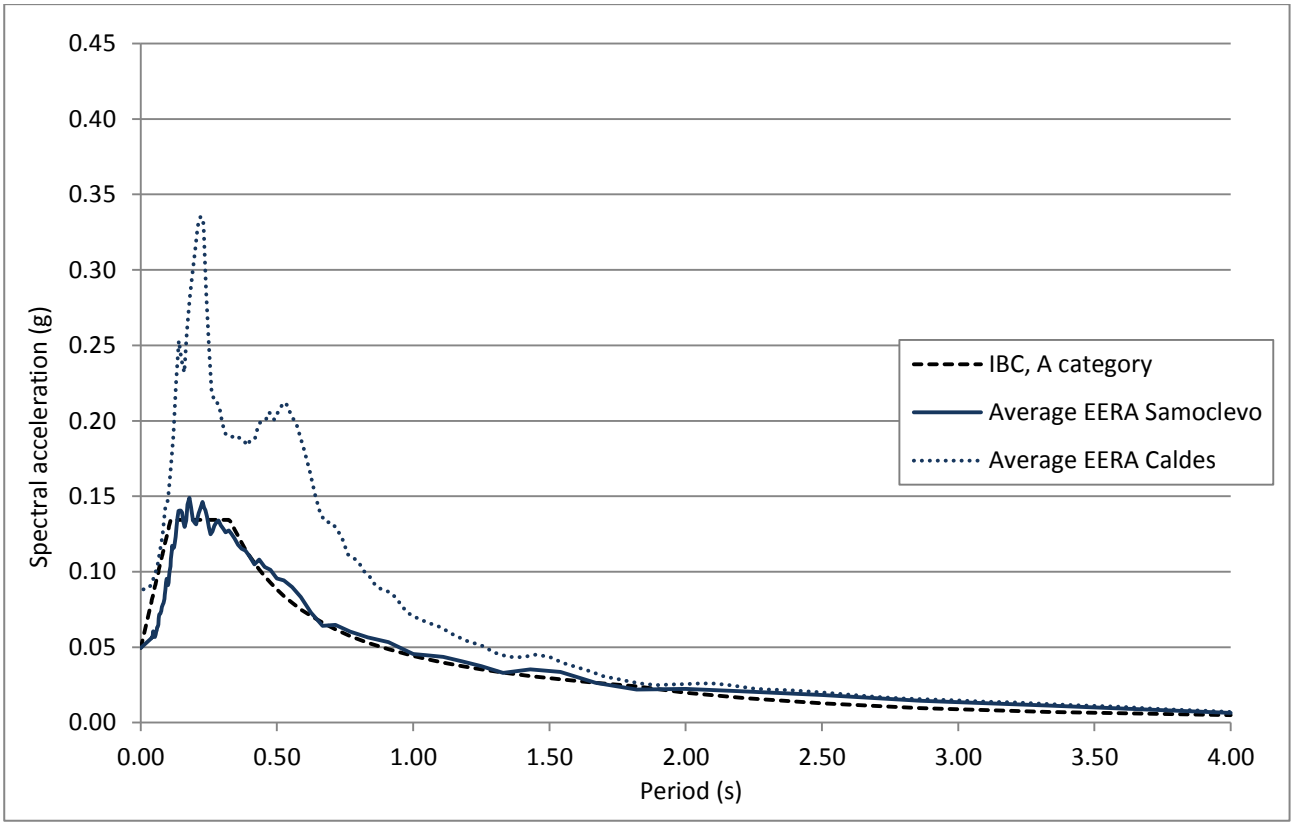

Figure 4.48. Comparison between average output spectra calculated with EERA and according to the Italian building code for Samoclevo site, and comparison with EERA output spectra of Caldes site.

4.4.1 Third level seismic microzonation map

One-dimensional models are not able to model the response along the whole transect between Samoclevo and Caldes, because the hypothesis of parallel layers in the physical model is not valid. However, on the basis of the data obtained from the one-dimensional analyses, a tentative *third level seismic microzonation map* is drafted (Figure 4.49 and 4.50). Three different zones are recognized: *Caldes*, *Samoclevo* and a *transition zone*.

In particular, for each zone the average response spectra and the average Housner amplification factors are shown. In the Samoclevo zone, where there is immediately rock under few centimetres of soil, there is not amplification of the spectrum and the amplification factors are equal to 1.00. In the Caldes zone, the amplification of the spectrum is evident and it is confirmed by the amplification factors. In the transition zone there are no quantitative applicable results because this domain cannot be analysed with a one-dimensional approach.

4.4.2 Future research: two-dimensional approach

Two-dimensional models are divided according to the mathematical method used to discretize the dynamic equilibrium equations. QUAD4M (Hudson et al., 1993) is the code that my working group and I are implementing the site of Castel Caldes in order to see the differences with respect to the one-dimensional analysis and to determine the response also in the transition zone. It belongs to the group of the Finite Element methods (FEM).

The equations at the base of QUAD4M code are given in Appendix 7, here is only briefly described how it works. The code operates in the time domain with equivalent non-linear constitutive law for the materials. The numerical procedure requires the discretization of the domain in a mesh of triangular and/or quadrilateral elements, with dimensions that must satisfy precise relations in order to optimize the discretization. The input motion takes into account both vertical and horizontal components. The code solves the discretized system, described by the equations of motion, using step-by-step integration in the time domain. The required parameters are the geometry of the domain (i.e. coordinates of the nodes and description of the finite elements) and, for each element, density, Poisson's ratio, initial shear modulus G_0, initial damping, shear modulus and damping ratio curves (Gruppo di lavoro MS, 2008).

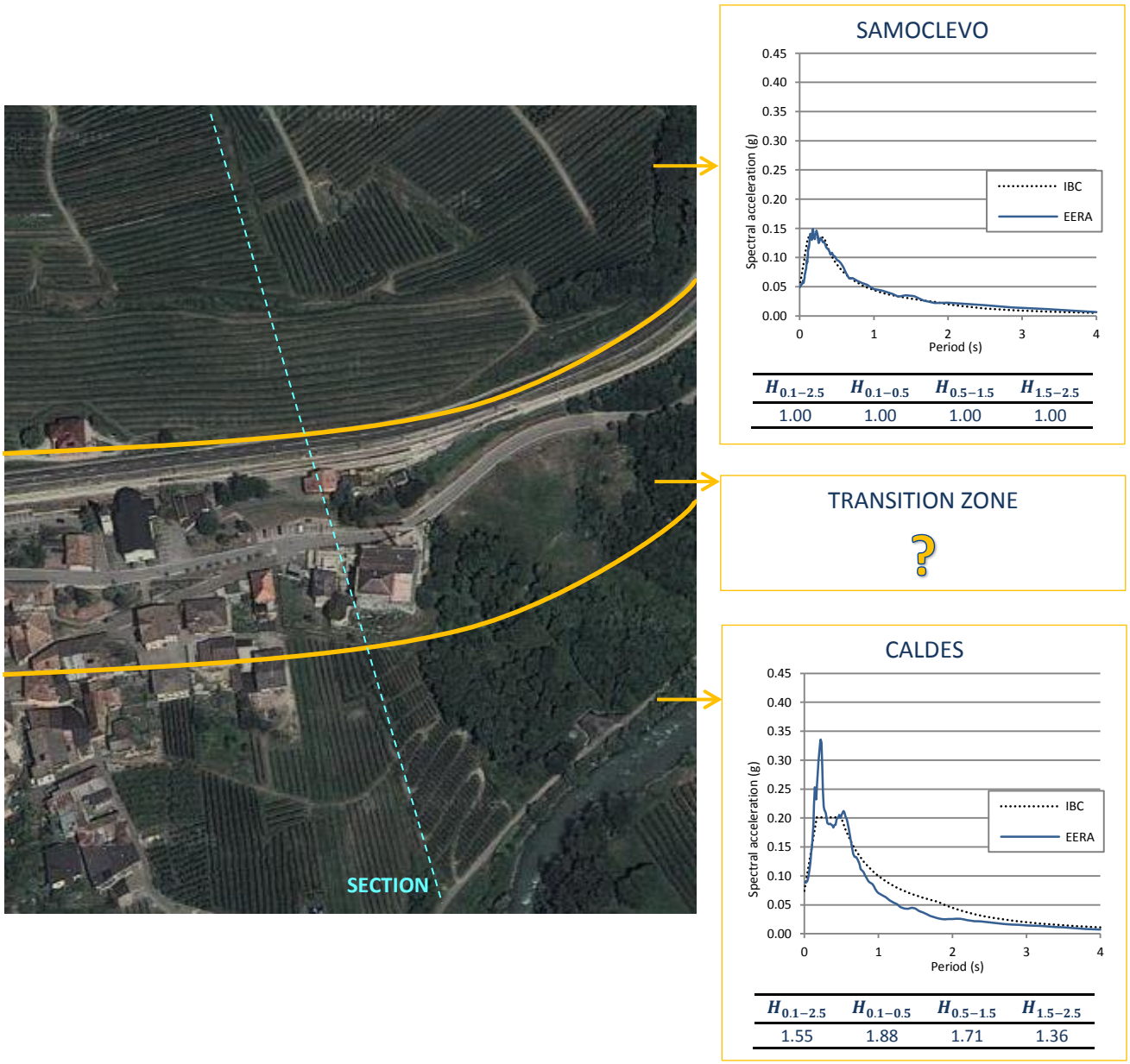

Figure 4.49. Third level Seismic microzonation map of the Castel Caldes area.

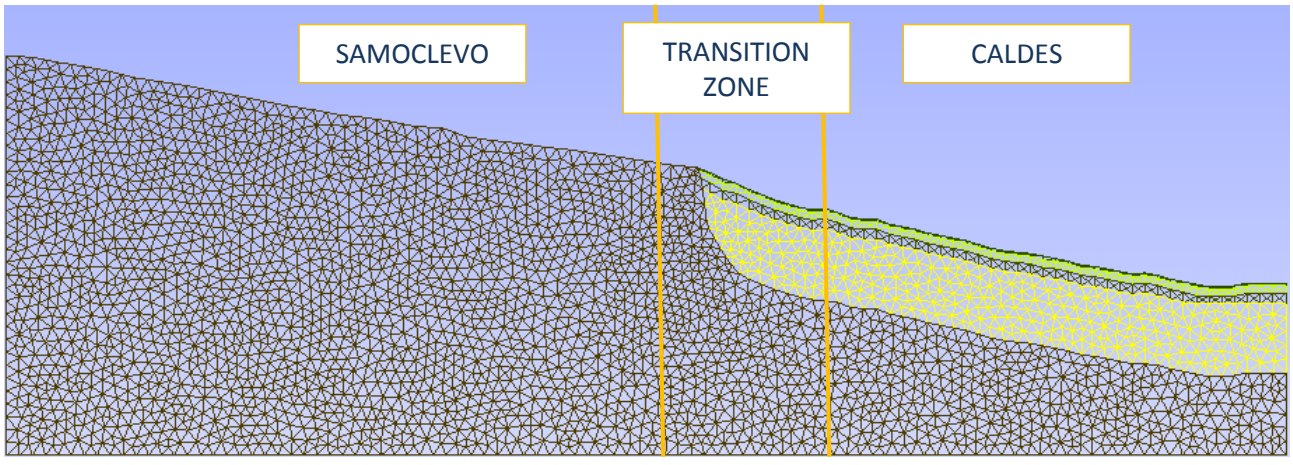

Figure 4.50. Section with indication of the three zones.

Chapter 5
Conclusions

This thesis describes methodology, data and results about the Castel Caldes area seismic microzonation. Given the large amount of data available, a multi-disciplinary approach that integrates results from different disciplines (geology, geomorphology, geophysics and geotechnics) was adopted.

Summarized here are the main results:

- Two sites with different stratigraphic characters (Caldes and Samoclevo) were analysed by means of one-dimensional analysis (EERA code).
- Two sub-surface physical models for Caldes and Samoclevo were obtained by analysing borehole stratigraphies and the shear-wave velocity profile along depth. The Caldes site is characterized by 2 m of sand, 6 m of clayey silt and 23 m of gravel (up to the bedrock depth at 51 m). The Samoclevo site is characterized by a very limited layer of soil (about 0.5 m) above the bedrock.
- Clayey silts and sands were analysed in the laboratory for the determination of their dynamic properties (normalized shear modulus and damping ratio curves) by using resonant column tests. For gravel, in the absence of measured data, literature curves were used.
- The site-specific seismic input was chosen using the REXEL software. The reference seismic motion derives from averaging of 7 natural accelerograms compatible with the acceleration spectrum of the Italian building code.
- The amplifications obtained by numerical simulations are different for the two studied sites. In Caldes, the amplification is high and maximum in the range of periods between 0.1 and $0.5\,s$, where the Housner amplification factor is 1.80. In Samoclevo, there is no amplification.
- Considering the results about Caldes, the reference acceleration spectrum determined by simplified approach (Italian building code) underestimates spectral accelerations in the period range $0.1 - 0.7\,s$. The maximum value of the spectral acceleration obtained from the specific analyses is $0.33\,g$ at the period $0.21\,s$, exceeding the reference spectrum by 0.15 g.

References

Aghaei-Araei, A., Tabatabaei, S.H. and Ghalandarzadeh, A., 2008, *Assessment of shear modulus and damping ratio of gravelly soils*, Research Project, No. 3-4469-2007, BHRC, Iran.

Avanzini, M., Bargossi, G. M., Borsato, A., Cucato, M., Morelli, C., Picotti, V. and Selli, M., 2010, *Note illustrative della Carta Geologica d'Italia alla scala 1:50,000, foglio 043 Mezzolombardo*, Provincia Autonoma di Trento and Provincia Autonoma di Bolzano.

Barani, S., De Ferrari, R. and Ferretti, G., 2013, *Influence of Soil Modeling Uncertainties on Site Response*, Earthquake Spectra: August 2013, Volume 29, Issue 3, pp: 705-732.
doi: http://dx.doi.org/10.1193/1.4000159

Bardet, J. P., Ichii, K. and Lin, C. H., 2000, *EERA: A Computer Program for Equivalent-linear Earthquake site Response Analyses of Layered Soil Deposits*, Department of Civil Engineering, University of Southern California.

Binley, A., 2003, *ProfileR*, Lancaster University.

CS.LL.PP., DM 14/01/2008, *Norme tecniche per le costruzioni*, Gazzetta Ufficiale della Repubblica Italiana, 29.

Dal Piaz, V. G., Castellarin, A., Martin, S., Selli, L., Carton, A., Pellegrini, G. B., Casolari, E., Daminato, F., Montresor, L., Picotti, V., Prosser, G., Santuliana, E. and Cantelli, L., 2007, *Note illustrative della Carta Geologica d'Italia alla scala 1:50,000, foglio 042 Malè*, Provincia Autonoma di Trento.

Foti, S., 2005, "Surface Wave Testing for Geotechnical Characterization", in Lai, C.G and Wilmanski, K., *Surface Waves in Geomechanics: Direct and Inverse Modelling for Soils and Rocks*, Springer, pp: 47-71.

Foti, S., Parolai, S., Albarello, D. and Picozzi, M., 2011, *Application of Surface wave methods for seismic site characterization*, Surveys in Geophysics, Springer, Vol. 32, pp: 777-825.

Gabriels, P., Sneider, R. and Norlet, G., 1987, *In situ measurements of shear-wave velocity in sediments with higher-mode Rayleigh waves*, Geophysical Prospecting, Volume 35, Issue 2, pp: 187-196.

Gruppo di lavoro MS, 2008, *Indirizzi e criteri per la microzonazione sismica*, Conferenza delle Regioni e delle Province autonome - Dipartimento della protezione civile, Roma, 3 vol. e Dvd.

Hardin, B. O., Drnevich, V. P., 1972a, *Shear modulus and damping in soils: Measurement and parameter effects*, Journal of the Soil Mecanics and Foundation Division, ASCE 98(6), pp: 603–624.

Hardin, B. O., Drnevich, V. P., 1972b, *Shear modulus and damping in soils: Design equations and curves*, Journal of the Soil Mecanics and Foundation Division, ASCE 98(7), pp: 667–692.

Housner, G.W., 1952, *Spectrum intensities of strong-motion earthquakes*, Proc. Symp. On Earthquake and Blast Effects Structures, Los Angeles.

Hudson, M. B., Idriss, I. M. and Beikae, M., 1993, *QUAD4M: a computer program for evaluating the seismic responses of soil structures by variable damping finite element procedure*, Report No. EERC-73/13, Earthquake Engineering Research Center, University of California, Berkeley.

Idriss, I. M., Lysmer, J., Hwang, R., and Seed, H. B., 1973, *QUAD-4: a computer program for evaluating the seismic responses of soil structures by variable damping finite element procedure*, Report No. EERC-73/13, Earthquake Engineering Research Center, University of California, Berkeley.

Idriss, I. M. and Sun, J. I., 1992, *User's Manual for SHAKE91*, Center for Geotechnical Modeling, Department of Civil Engineering, University of California, Davis.

Iervolino, I., Galasso, C., Cosenza, E., 2010, *REXEL: computer aided record selection for code-based seismic structural analysis*, Bulletin of Earthquake Engineering, Volume 8, Issue 2, pp: 339-362.

Knödel, K. and Voigt, H. J., 2007, *Environmental Geology: Handbook of Field Methods and Case Studies*, Springer, pp: 1195-1318.

Kramer, S.L., 1996, *Geotechnical Earthquake Engineering*, Prentice Hall.

Majorana, C., Modena, C., Franchetti, P., Grendene, M. and Secchi, S., 2007, *Fondamenti di dinamica e di ingegneria sismica*, The McGraw-Hill Companies.

Martin, S. and Zambotti, P., 2012, *Caratterizzazione geologica della Val di Sole ai fini della valutazione della potenzialità geotermica a bassa entalpia del territorio da Ossana a Caldes e all'utilizzo di fonti energetiche rinnovabili*.

Martino, S., Minutolo, A., Paciello, Rovelli, A., Scarascia Mugnozza, G. and Verrubbi, V., *Evidence of Amplification Effects in Fault Zone Related to Rock Mass Jointing*, Natural Hazards, Volume 39, pp: 419–449.

Marzorati, S., Ladina, C., Falcucci, E., Gori, S., Saroli, M., Ameri, G. and Galadini, F., 2011, *Site effects "on the rock": the case of Castelvecchio Subequo (L'Aquila, central Italy)*, Bulletin of Earthquake Engineering, Volume 9, pp: 841-868.

Robinson, E. S. and Coruh, C., 1988, *Basic exploration geophysics*, Wiley.

Schnabel, P. B., Lysmer, J., and Seed, H. B.,1972, *SHAKE: A Computer Program for Earthquake Response Analysis of Horizontally Layered Sites*, Report No. UCB/EERC-72/12, Earthquake Engineering Research Center, University of California, Berkeley.

SeisImager/2D^{TM} Manual, 2009.

Socco, L.V. and Strobbia, C., 2004, *Surface-wave method for near-surface characterization: a tutorial*, Near Surface Geophysics, pp: 165-185.

Seidel, K. and Lange, G., 2007, "Direct Current Resistivity Methods", in Knödel, K., Voigt, Lange, G., H. J., *Environmental Geology: Handbook of Field Methods and Case Studies*, Springer, pp: 205-237.

Simoni, G., 2004, *Prove dinamiche di laboratorio colonna risonante e taglio torsionale ciclico*, Appunti della lezione de corso di Geotecnica II, Università degli studi di Firenze.

Transportation Research Board, 2012, *NCHRP Synthesis 428: Practices and Procedures for Site-Specific Evaluations of Earthquake Ground Motions*, National Academies Press.

Viganò, A., Groaz, O., Froner, L., Fedrizzi, F. and Franceschini, A., 2013a, *Monitoraggio sismico, microzonazione sismica e studi sismologici in Trentino*.

Viganò, A., Scafidi, D., Martin, S. and Spallarossa, D., 2013b, *Structure and properties of the Adriatic crust in the central-eastern Southern Alps (Italy) from local earthquake tomography*, Terranova, pp: 1-9, DOI: 10.1111/ter.12067.

Yokota, K., Imai, T. and Konno, M., 1981, *Dynamic deformation characteristics of soils determined by laboratory tests*, OYO Technical Rep., 3, pp. 13-37.

Appendix

1. Geological Map of Italy, Malè sheet (scale 1:50,000)
2. First level seismic microzonation map of Trentino
3. Geophysical software
4. REXEL software
5. EERA code basics
6. Samoclevo results
7. QUAD4M code basics

Appendix 1

Geological Map of Italy, Malè sheet (scale 1:50,000)

Appendix 2

First level seismic microzonation map of Trentino

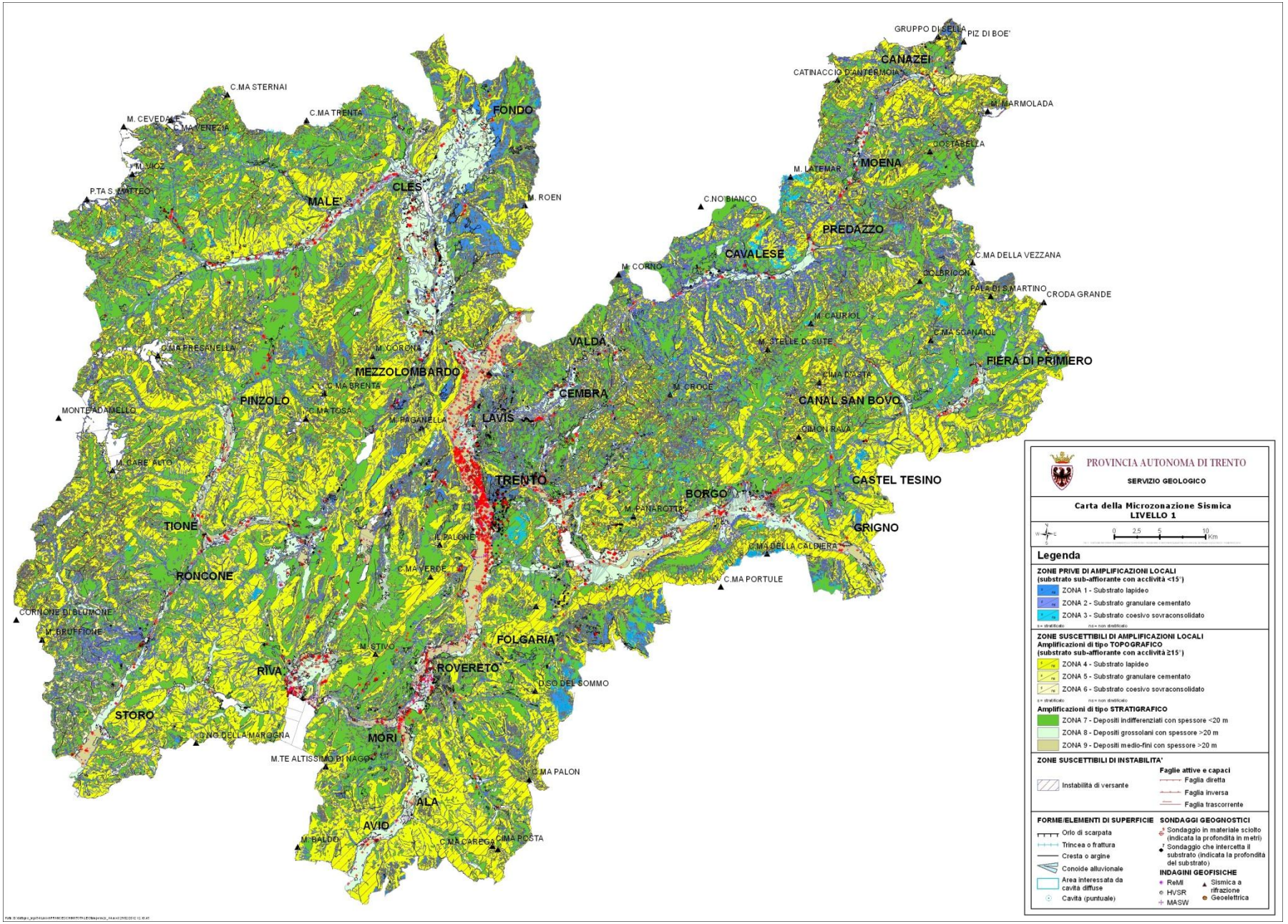
GRUPPO DI SELLA
PIZ DI BOE'
CANAZEI
CATINACCIO D'ANTERMOIA
M. MARMOLADA
C.MA STERNAI
C.MA TRENTA
FONDO
M. CEVEDALE
C.MA VENEZIA
COSTABELLA
MOENA
M. VIOZ
M. LATEMAR
P.TA S. MATTEO
MALE'
CLES
M. ROEN
C.NO BIANCO
PREDAZZO
CAVALESE
C.MA DELLA VEZZANA
M. CORNO
DOLOMIEU
PALA DI S.MARTINO
CRODA GRANDE
M. CAURIOL
C.MA FRESANELLA
M. CORONA
VALDA
M. STELLE D. SUTE
C.MA SCANAIOL
FIERA DI PRIMIERO
MEZZOLOMBARDO
CIMA D'ASTA
C.MA BRENTA
CEMBRA
M. CROCE
PINZOLO
CANAL SAN BOVO
MONTE ADAMELLO
C.MA TOSA
M. PAGANELLA
LAVIS
CIMON RAVA
M. CARE' ALTO
TRENTO
CASTEL TESINO
BORGO
M. PANAROTTA
TIONE
GRIGNO
IL PALONE
C.MA DELLA CALDIERA
C.MA VERDE
RONCONE
C.MA PORTULE
CORNONE DI BLUMONE
M. BRUFFIONE
FOLGARIA
M. STIVO
RIVA
ROVERETO
D'SO DEL SOMMO
STORO
C.NO DELLA MAROGNA
MORI
M.TE ALTISSIMO DI NAGO
C.MA PALON
ALA
AVIO
M. BALDO
C.MA CAREGA
CIMA POSTA
PROVINCIA AUTONOMA DI TRENTO
SERVIZIO GEOLOGICO
Carta della Microzonazione Sismica
LIVELLO 1
0 2,5 5 10 Km
Legenda
ZONE PRIVE DI AMPLIFICAZIONI LOCALI
(substrato sub-affiorante con acclività <15°)
ZONA 1 - Substrato lapideo
ZONA 2 - Substrato granulare cementato
ZONA 3 - Substrato coesivo sovraconsolidato
s= stratificato ns= non stratificato
ZONE SUSCETTIBILI DI AMPLIFICAZIONI LOCALI
Amplificazioni di tipo TOPOGRAFICO
(substrato sub-affiorante con acclività ≥15°)
ZONA 4 - Substrato lapideo
ZONA 5 - Substrato granulare cementato
ZONA 6 - Substrato coesivo sovraconsolidato
s= stratificato ns= non stratificato
Amplificazioni di tipo STRATIGRAFICO
ZONA 7 - Depositi indifferenziati con spessore <20 m
ZONA 8 - Depositi grossolani con spessore >20 m
ZONA 9 - Depositi medio-fini con spessore >20 m
ZONE SUSCETTIBILI DI INSTABILITA'
Instabilità di versante
Faglie attive e capaci
Faglia diretta
Faglia inversa
Faglia trascorrente
FORME/ELEMENTI DI SUPERFICIE
Orlo di scarpata
Trincea o frattura
Cresta o argine
Conoide alluvionale
Area interessata da cavità diffuse
Cavità (puntuale)
SONDAGGI GEOGNOSTICI
Sondaggio in materiale sciolto (indicata la profondità in metri)
Sondaggio che intercetta il substrato (indicata la profondità del substrato)
INDAGINI GEOFISICHE
ReMI
HVSR
MASW
Sismica a rifrazione
Geoelettrica

Appendix 3

Geophysical software

A3.1 Grilla (Micromed)

Grilla is the software to archive, organize and analyze the recordings of TROMINO® and SoilSpy Rosina.

Some Grilla capabilities:

- Spectral analyses (time, space, directivity)
- H/V analysis following the international and national guide lines
- Constrained fit of the H/V curve to obtain subsoil V_S profiles and seismic site classifications (forward modeling and automatic fit)
- Multichannel analysis of surface waves, both Rayleigh and Love (SASW, MASW, ReMi™, ESAC, SPAC, other spatial correlation techniques)
- Forward modeling of surface wave dispersion curves to obtain subsoil V_S profiles and seismic site classifications
- Joint fit of H/V and surface wave dispersion curves
- Vibration analysis according to UNI 9916, DIN 4150 (effects of strong vibrations on structures)
- Modal analysis of structures (mode frequencies, mode shapes)

Grilla produces automatic reports for the different analyses, completed with images. Recordings of non-proprietary instruments can also be imported into the database and analysed with Grilla. Grilla is constantly upgraded following the state of the art according to the leading international peer-reviewed geophysical journals.

Website: http://www.tromino.eu/prodsel.asp?cat=3&prod=4

A3.2 SWAMI

Computer Programs for Surface Wave Analysis

SWAMI (Surface WAve Modal Inversion) solves the nonlinear inverse problem of estimating the shear wave velocity profile given a surface wave dispersion curve (i.e., phase velocity vs. frequency) and associated uncertainties, which are assumed to represent the fundamental mode of propagation. The medium is assumed to be elastic and the solution of the inverse problem is uncoupled from the related problem of estimating the shear damping ratio profile from surface wave attenuation data.

The inversion algorithm is based on:

Constable, S. C., Parker, R. L., and Constable, G. G., 1987, *Occam's Inversion: A Practical Algorithm for Generating Smooth Models from Electromagnetic Sounding Data*, Geophysics, 52, pp: 289-300.

The strategy of the algorithm is as follows: given an experimental dispersion curve and associated uncertainties, find the smoothest shear wave velocity profile subject to the constraint of a specified misfit between experimental and theoretical data. Convergence is defined as achieving a root-mean-square (rms) error of 1.0 or less (i.e., the specified misfit) or a negligible change in the shear wave velocity profile from one iteration to the next. A maximum of 10 iterations is allowed. The user may change these parameters as desired. For a detailed description of the inversion algorithm, see Lai and Rix (1998).

The forward algorithm used to calculate theoretical dispersion curves and partial derivatives of the phase velocity with respect to the shear wave velocity of each layer is based on:

Hisada, Y., 1994, *An Efficient Method for Computing Green's Functions for a Layered Half-Space with Sources and Receivers at Close Depths*, Bulletin of the Seismological Society of America, 84(5), pp: 1456-1472.

Lai, C. G. and Rix, G. J., 1998, *Simultaneous Inversion of Rayleigh Phase Velocity and Attenuation for Near-Surface Site Characterization*, Report No. GIT-CEE/GEO-98-2, School of Civil and Environmental Engineering, Georgia Institute of Technology, 258 pp.

An estimate of the uncertainty of the final shear wave velocity profile is calculated based on:

Lai, C. G., Foti, S., and Rix, G. J., 2005, *Propagation of Data Uncertainty in Surface Wave Inversion*, Journal of Environmental and Engineering Geophysics, 10(2), pp: 219-228.

Website: http://geosystems.ce.gatech.edu/soil_dynamics/research/surfacewavesanalysis/

A3.3 SeisImager

Refraction Data Analysis Software

SeisImager/2D is a robust and comprehensive package including three methods for refraction data analysis, including time-term inversion, the reciprocal method, and tomography. It also includes modeling, filtering, and a host of other features.

SeisImager/2D is an easy-to-use, yet powerful program that allows you to:

- Read in and display your refraction data.
- Control how your data is displayed.
- Make changes/corrections to your data files and save them.
- Pick first breaks and save them.
- Invert your data for a velocity section.
- Output a travel-time plot, velocity section, and other graphics.

SeisImager™ is the master program that consists of four modules for refraction and surface wave data analysis. The individual modules are Pickwin™, Plotrefa™, WaveEq™, and GeoPlot™. The Surface Wave Analysis Wizard™ is not a separate module but automatically calls on specific functions from Pickwin, WaveEq, and GeoPlot. Pickwin and Plotrefa are the modules used for refraction analysis, making up the program called SeisImager/2D™. Pickwin is the first break picking module and Plotrefa is the main analysis program.

SeisImager/2D is a very powerful refraction package. It offers three separate inversion techniques: the time-term method, the reciprocal method, and tomography. Both the time-term and reciprocal methods are based on "delay times". The main difference between the two is the method by which the delay times are calculated. In the time-term method, the delay times are calculated automatically (via a linear least-squares inversion technique). In the reciprocal time method, the delay times are calculated manually. Each technique is different, and which technique you should use depends on the goals of the survey and the character of the data. SeisImager/2D also contains many ancillary tools (SeisImager/2D™ Manual, 2009).

Website: http://www.geometrics.com/geometrics-products/seismographs/

A3.4 ProfileR

Resistivity inversion software

ProfileR has been designed for surface array resistivity profile imaging. ProfileR is an inverse solution for a 2-D resistivity distribution based on computation of 3-D current flow using a quadrilateral finite element mesh. The inverse solution is based on a regularised objective function combined with weighted least squares (an 'Occams' type solution).

ProfileR requires very little input for generation of the finite element mesh. The minimum the user must specify is the number of electrodes and the co-ordinates of the end electrodes. ProfileR can account for variation in topography by user specification of position of intermediate electrode positions and elevation. The spacing of electrodes does not need to be uniform.

The mesh that is generated consists of a foreground region and a background region. The foreground region is the area investigated by the survey and it will be the resistivity variation in this area that will be output by ProfileR. The background region is transparent to the user and is employed to account for the infinite boundary conditions. The mesh is generated with two finite elements between electrodes in the horizontal in the foreground region. In the background region the mesh is extended to the left and right of the electrode array using exponentially increasing elements. In the vertical elements increase in size with depth. The region is parameterised in terms of resistivity blocks by grouping patches of elements. In the foreground region a parameter block is defined as a 2 by 2 block of elements (Binley, 2003).

ProfileR has no built in graphical interface. The user can use his/her own software for graphical output (e.g. Surfer).

Website: http://www.es.lancs.ac.uk/people/amb/Freeware/Profiler/Profiler.htm

A3.5 Surfer

Surfer is a full-function 3D visualization, contouring and surface modeling package that runs under Microsoft Windows. Surfer is used extensively for terrain modeling, bathymetric modeling, landscape visualization, surface analysis, contour mapping, watershed and 3D surface mapping, gridding, volumetrics, and much more.

Surfer's sophisticated interpolation engine transforms your XYZ data into publication-quality maps. Surfer provides more gridding methods and more control over gridding parameters, including customized variograms, than any other software package on the market. You can also use grid files

obtained from other sources, such as USGS DEM files or ESRI grid files. Display your grid as outstanding contour, 3D surface, 3D wireframe, watershed, vector, image, shaded relief, and post maps. Add base maps and combine map types to create the most informative display possible.

Website: http://www.goldensoftware.com/products/surfer

Appendix 4
REXEL software

A4.1 Reference (design) spectrum

To build the elastic acceleration response spectrum for the site of interest according to the Italian building code is necessary specify:

- geographical coordinates of the site (*longitude* and *latitude* in decimal degrees);
- *Site Class* (A, B, C, D or E);
- *Topographic Category* (T1, T2, T3 or T4);
- *Nominal Life* of the structure;
- *Functional Type* of the structure;
- *Limit State* of interest.

Then the software automatically generates the spectrum accordingly.
Finally, it is necessary to specify the component of the spectrum to consider; i.e., horizontal and/or vertical. The two orthogonal independent components that describe the horizontal motion (X and Y) are characterized by the same elastic response spectrum, while the component that describes the vertical motion (Z) is characterized by a specific spectrum. It is possible to select X/Y and Z separately or contemporarily, depending on the number of components of ground motion (1, 2 or 3) desired to be included in the set.

A4.2 Design earthquake (source) parameters

The software has built-in the records of the ESD database (in terms of three components corrected acceleration waveforms and 5% damping spectra) which are from free field instruments and from events of magnitude larger than 4. The soil type is decided in step 1 and this choice automatically limits the search of the combinations to the records belonging to this specific site class. Moreover, the user can choose to search for combinations coming from specific magnitude and distance (M and R) ranges. Therefore, can specify the magnitude and distance intervals, $[M_{min}, M_{max}]$ and $[R_{min}, R_{max}]$, in which the records have to fall. The software returns the number of records (and the corresponding number of originating events) available in the intervals. This list constitutes the

inventory of records in which to search for suites of seven which are in the average compatible with the code spectra of step 1.

A4.3 Spectrum matching parameters and analysis options

In this step the parameters related to the spectral compatibility are defined, namely the period range $[T_1, T_2]$ in which the reference spectrum has to be matched and the tolerances allowed in spectral matching. This means the user has to specify the tolerated deviations (*lower* and *upper* limits) in percentage terms that the average spectrum can have with respect to the reference one in the specified period range. It is economically viable to reduce as much as possible the overestimation of the spectrum.

In this phase it is possible to select the *Non-dimensional* option, which corresponds to choose whether to search for *unscaled* or *scaled* record sets. The user can also select the option *I'm feeling lucky* in order to stop the analysis after the first compatible combination is found. In the most of cases this option allows to immediately get a single combination compatible with the reference spectrum, otherwise, the search may take a very long time. Alternatively, the *maximum number of compatible combinations to find* after which the search has to stop can be specified.

A4.4 Combinations search

At this point the initial list of records and the analysis parameters are set and it is possible to decide which kind of search to perform. The software searches for combinations of:

a) Seven 1-component accelerograms (horizontal and/or vertical). The found combinations can be applied in one direction for plane analysis of structures.
b) Seven pairs of accelerograms which include the two horizontal components of seven recordings (i.e., 14 records which are the *X*, *Y* components of seven recording). Used for cases in which horizontal motion has to be applied in both directions of a 3D structure.
c) Seven groups of accelerograms which include the two horizontal and the vertical component of seven recordings (i.e., 21 records which are the *X*, *Y* and *Z* components of seven recording) for full 3D analysis.

An important feature of REXEL is that the list of records are ordered in ascending order of a parameter which takes into account the deviation of the spectrum of an individual record from the reference spectrum. This allows to analyse first the records which have a similar spectral shape with

respect to the reference. This ensures the first combinations (e.g., the one found with the *I'm feeling lucky* option) to be those with the smallest individual scattering in respect to the reference spectrum.

A4.5 Post-analysis

After the analysis has finished, REXEL returns a list of combinations whose average spectrum respects compatibility with the reference one in the chosen range of periods and with the assigned tolerances. The results of the analysis are sorted so that the combinations with the smallest deviation from the reference spectrum are at the beginning of the output list. Combinations returned are uniquely identified by a serial number.

If a specific combination is chosen, REXEL also returns the mean value of M and R of the combination and the information about the individual records. In the case of non-dimensional sets, the scale factors of the individual records and the mean scale factor of the combination are given. For all the combinations found, it is possible to calculate the deviation of each accelerogram, and the deviation of the average spectrum.

Appendix 5
EERA code basics

A5.1. Introduction

During past earthquakes, the ground motions on soft soil sites were found to be generally larger than those of nearby rock outcrops, depending on local soil conditions. These amplifications of soil site responses were simulated using several computer programs that assume simplified soil deposit conditions such as horizontal soil layers of infinite extent. One of the first computer programs developed for this purpose was SHAKE (Schnabel et al., 1972). SHAKE computes the response in a horizontally layered soil-rock system subjected to transient and vertical travelling shear waves. SHAKE assumes that the cyclic soil behavior can be simulated using an equivalent linear model.
In 1998, the computer program EERA was developed in FORTRAN 90 starting from the same basic concepts as SHAKE. EERA stands for Equivalent-linear Earthquake Response Analysis. EERA is a modern implementation of the well-known concepts of equivalent linear earthquake site response analysis. EERA's implementation takes full advantages of the dynamic array dimensioning and matrix operations in FORTRAN 90. EERA's input and output are fully integrated with the spreadsheet program Excel.

A5.2. Equivalent linear model for soil response

A5.2.1 One-dimensional Stress-Strain Relationship

The equivalent linear model represents the soil stress-strain response based on a Kelvin-Voigt model as illustrated in Figure A5.1.
The shear stress τ depends on the shear strain γ and its rate $\dot{\gamma}$ as follows:

$$\tau = G\gamma + \eta\dot{\gamma} \qquad (1)$$

where G is shear modulus and η the viscosity. In a one-dimensional shear beam column, the shear strain and its rate are defined from the horizontal displacement $u(z,t)$ at depth z and time t as follows:

$$\gamma = \frac{\partial u(z,t)}{\partial z}$$

$$\dot{\gamma} = \frac{\partial \gamma(z,t)}{\partial t} = \frac{\partial^2 u(z,t)}{\partial z \partial t} \qquad (2)$$

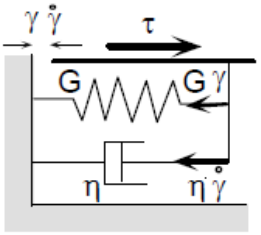

Figure A5.1. Schematic representation of stress-strain model used in equivalent-linear model.

In the case of harmonic motion, the displacement, strain and strain rate are:

$$u(z,t) = U(z)e^{i\omega t}$$

$$\gamma(z,t) = \frac{dU}{dz}e^{i\omega t} = \Gamma(z)e^{i\omega t} \qquad (3)$$

$$\dot{\gamma}(z,t) = i\omega\gamma(z,t)$$

where $U(z)$ and $\Gamma(z)$ are the amplitude of displacement and shear strain, respectively. Using these equations, the stress-strain relation (Eq. 1) becomes in the case of harmonic loadings:

$$\tau(z,t) = \Sigma(z)e^{i\omega t} = (G + i\omega\eta)\frac{dU}{dz}e^{i\omega t} = G^*\frac{dU}{dz}e^{i\omega t} = G^*\gamma(z,t) \qquad (4)$$

where G^* is the complex shear modulus and $\Sigma(z)$ is the amplitude of shear stress. After introducing the critical damping ratio ξ so that $\xi = \omega\eta/2G$, the complex shear modulus G^* becomes:

$$G^* = G + i\omega\eta = G(1 + 2i\xi) \qquad (5)$$

The energy dissipated W_d during a complete loading cycle is equal to the area generated by the stress-strain loop, i.e.:

$$W_d = \oint_{\tau_c} \tau d\gamma \qquad (6)$$

In the case of strain-controlled harmonic loading of amplitude γ_c (i.e., $\gamma(t) = \gamma_c e^{i\omega t}$), Eq. 6 becomes:

$$W_d = \int_t^{t+2\pi/\omega} Re[\tau(t)] Re\left[\frac{d\gamma}{dt}\right] dt \qquad (7)$$

where only the real parts of the stress and strain rate are considered. Using Eq. 4, the real parts of stress and strain rate are:

$$Re[\tau(t)] = \gamma_c(G\cos\omega t - \omega\eta \sin\omega t)$$

$$Re\left[\frac{d\gamma}{dt}\right] = -\gamma_c\omega \sin\omega t \qquad (8)$$

Finally, Eq. 7 becomes:

$$W_d = \frac{1}{2}\omega\gamma_c^2 \int_t^{t+2\pi/\omega} [-G\, sin\, 2\omega t + \omega\eta(1-\cos 2\omega t)]dt = \pi\omega\eta\gamma_c \qquad (9)$$

The maximum strain energy stored in the system is:

$$W_s = \frac{1}{2}\tau_c\gamma_c = \frac{1}{2}G\gamma_c^2 \qquad (10)$$

The critical damping ratio ξ can be expressed in terms of W_d and W_s as follows:

$$\xi = \frac{W_d}{4\pi W_s} \qquad (11)$$

A5.2.2 Equivalent Linear Approximation of Nonlinear Stress-strain Response

The *equivalent linear* approach consists of modifying the Kelvin-Voigt model to account for some types of soil nonlinearities. The nonlinear and hysteretic stress-strain behavior of soils is approximated during cyclic loadings as shown in Figure A5.2. The equivalent linear shear modulus, G, is taken as the secant shear modulus G_s, which depends on the shear strain amplitude γ. As shown in Figure A5.2a, G_s at the ends of symmetric strain-controlled cycles is:

$$G_s = \frac{\tau_c}{\gamma_c} \qquad (12)$$

where τ_c and γ_c are the shear stress and strain amplitudes, respectively. The equivalent linear damping ratio, ξ, is the damping ratio that produces the same energy loss in a single cycle as the hysteresis stress-strain loop of the irreversible soil behavior.

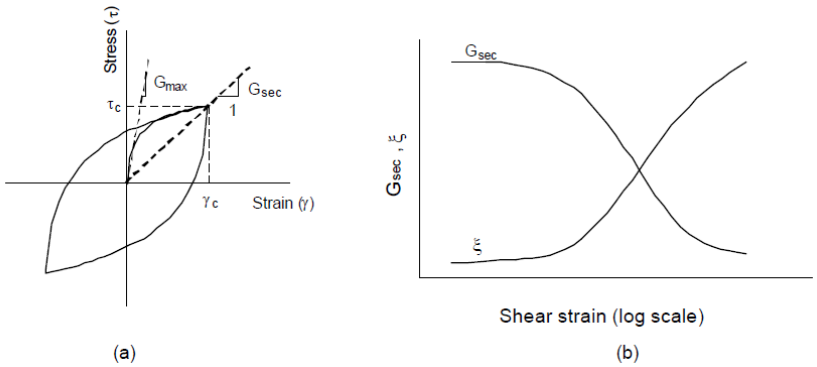

Figure A5.2. Equivalent-linear model: (a) Hysteresis stress-strain curve; and (b) Variation of secant shear modulus and damping ratio with shear strain amplitude.

In site response analysis, the material behavior is generally specified as shown in Figure A5.2b. The $G_s - \gamma$ curves cannot have arbitrary shapes as they derive from $\tau - \gamma$ stress-strain curves. For instance, the exclusion of strain-softening from the $\tau - \gamma$ curves imposes some restrictions on the corresponding $G_s - \gamma$ curves. The exclusion of strain-softening implies that:

$$\frac{d\tau}{d\gamma} = G_s(\gamma) + \frac{dG_s}{d\gamma}\gamma \geq 0 \qquad (13)$$

In the case of $G_s - \gamma$ curves specified with discrete points (G_i, γ_i), Eq. 13 becomes:

$$\frac{\Delta G_s}{G_{max}} \geq -\frac{G_s(\gamma)}{G_{max}}\frac{\Delta\gamma}{\gamma} \qquad (14)$$

where ΔG_s is the decrease in G_s corresponding to the increase $\Delta\gamma$ in, and G_{max} is the maximum value of G_s. Eq. 14 is equivalent to:

$$\frac{G_{i+1}}{G_i} \geq 2 - \frac{\gamma_{i+1}}{\gamma_i} \qquad (15)$$

As shown in Fig. 2b, the equivalent linear model specifies the variation of shear modulus and damping ratio with shear strain amplitude. Additional assumptions are required to specify the effects of frequency on stress-strain relations. For this purpose, two basic models have been proposed.

Model 1

Model 1 is used in the original version of SHAKE (Schnabel et al., 1972). It assumes that ξ is constant and independent of ω, which implies that the complex modulus G^* is also independent of ω. The dissipated energy during a loading cycle is:

$$W_d = 4\pi W_s \xi = 2\pi G \xi \gamma_c^2 = \pi\eta\gamma_c^2\omega \qquad (16)$$

The dissipated energy increases linearly with ξ, and is independent of ω, which implies that the area of stress-strain loops is frequency independent. The amplitudes of complex and real shear modulus are related through:

$$|G^*| = G\sqrt{(1+4\xi^2)} \qquad (17)$$

which implies that $|G^*|$ increases with ξ.

Model 2

Model 2 is used in SHAKE 91 (Idriss and Sun, 1992). It assumes that the complex shear modulus is a function of ξ:

$$G^* = G\left\{(1-2\xi^2) + 2\xi\sqrt{1-\xi^2}\right\} \qquad (18)$$

The assumption above is a constitutive assumption that pertains to the description of material behavior. It implies that the complex and real modulus have the same amplitude, i.e.:

$$|G^*| = G\{(1-2\xi^2) + 4\xi^2(1-\xi^2)\} = G \qquad (19)$$

The energy dissipated during a loading cycle is:

$$W_d = \frac{1}{2}\omega\gamma_c^2 \int_t^{t+2\pi/\omega} 2G\xi\sqrt{1-\xi^2}\,dt = 2\pi G\xi\sqrt{1-\xi^2}\gamma_c^2 \qquad (20)$$

For practical purposes, ξ is usually less than 25%. Under these conditions, the energies dissipated by Models 1 and 2 are similar.

A5.3. One-dimensional ground response analysis

Figure A5.3 schematizes the assumptions of one-dimensional equivalent linear site response analysis. As shown in Fig. A5.4, a vertical harmonic shear wave propagates in a one-dimensional layered system. The one-dimensional equation of motion for vertically propagating shear waves is:

$$\rho\frac{\partial^2 u}{\partial t^2} = \frac{\partial \tau}{\partial z} \qquad (21)$$

where ρ is the unit mass in any layer. Assuming that the soil in all layers behaves as a Kelvin-Voigt solid (i.e., Eq. 1), Eq. 22 becomes:

$$\rho\frac{\partial^2 u}{\partial t^2} = G\frac{\partial^2 u}{\partial z^2} + \eta\frac{\partial^3 u}{\partial z^2 \partial t} \qquad (22)$$

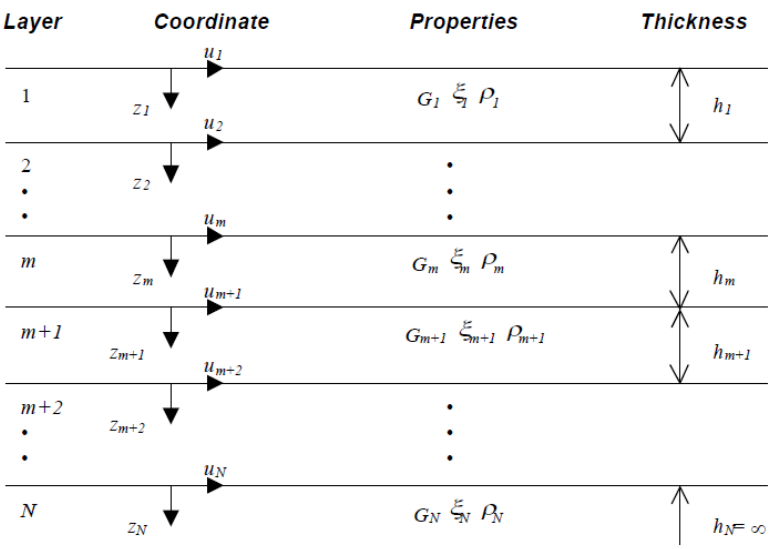

Figure A5.4. One-dimensional layered soil deposit system.

For harmonic waves, the displacement can be written as:

$$u(z,t) = U(z)e^{i\omega t} \qquad (23)$$

Using Eq. 23, Eq. 22 becomes:

$$(G + i\omega\eta)\frac{d^2U}{dz^2} = \rho\omega^2 U \qquad (24)$$

and admits the following general solution:

$$U(x) = Ee^{ik^*z} + Fe^{-ik^*z} \qquad (25)$$

where $k^* = \frac{\rho\omega^2}{G+i\omega\eta} = \frac{\rho\omega^2}{G^*}$ is the complex wave number. After introducing the critical damping ratio ξ so that $\xi = \omega\eta/2G$, the complex shear modulus G^* becomes:

$$G^* = G + i\omega\eta = G(1 + 2i\xi) \qquad (26)$$

The solution of Eq. 24 is:

$$u(z,t) = \left(Ee^{ik^*z} + Fe^{-ik^*z}\right)e^{i\omega t} \qquad (27)$$

and the corresponding stress is:

$$\tau(z,t) = ik^*G^*\left(Ee^{ik^*z} + Fe^{-ik^*z}\right)e^{i\omega t} \qquad (28)$$

The displacements at the top ($z = 0$) and bottom ($z = h_m$) of layer m of thickness h_m are:

$$u_m(0,t) = u_m = (E_m + F_m)e^{i\omega t}$$

$$u_m(h_m,t) = \left(E_m e^{ik^*h_m} + F_m e^{-ik^*h_m}\right)e^{i\omega t} \qquad (29)$$

The shear stresses at the top and bottom of layer m are:

$$\tau_m(0,t) = ik^* G_m^* (E_m - F_m) e^{i\omega t}$$

$$\tau_m(h_m,t) = ik^* G_m^* \left(E_m e^{ik_m^* h_m} - F_m e^{-ik_m^* h_m}\right) e^{i\omega t} \qquad (30)$$

At the interface between layers m and $m+1$, displacements and shear stress must be continuous, which implies that:

$$u_m(h_m,t) = u_{m+1}(0,t)$$

$$\tau_m(h_m,t) = \tau_{m+1}(0,t) \qquad (31)$$

Using Eqs. 29 to 31 the coefficients E_m and F_m are related through:

$$E_{m+1} + F_{m+1} = E_m e^{ik_m^* h_m} + F_m e^{-ik_m^* h_m} \qquad (32)$$

$$E_{m+1} - F_{m+1} = \frac{k_m^* G_m^*}{k_{m+1}^* G_{m+1}^*} \left(E_m e^{ik_m^* h_m} - F_m e^{-ik_m^* h_m}\right) \qquad (33)$$

Eqs. 32 and 33 give the following recursion formulas for amplitudes E_{m+1} and F_{m+1} in terms of E_m and F_m:

$$E_{m+1} = \frac{1}{2} E_m (1 + \alpha_m^*) e^{ik_m^* h_m} + \frac{1}{2} F_m (1 - \alpha_m^*) e^{-ik_m^* h_m} \qquad (34)$$

$$F_{m+1} = \frac{1}{2} E_m (1 - \alpha_m^*) e^{ik_m^* h_m} + \frac{1}{2} F_m (1 + \alpha_m^*) e^{-ik_m^* h_m} \qquad (35)$$

where α_m^* is the complex impedance ratio at the interface between layers m and $m+1$:

$$\alpha_m^* = \frac{k_m^* G_m^*}{k_{m+1}^* G_{m+1}^*} = \sqrt{\frac{\rho_m G_m^*}{\rho_{m+1} G_{m+1}^*}} \qquad (36)$$

The recursive algorithm is started at the top free surface, for which there is no shear stress:

$$\tau_1(0,t) = ik_1^* G_1^* (E_1 - F_1) e^{i\omega t} = 0 \qquad (37)$$

which implies:

$$E_1 = F_1 \qquad (38)$$

Eqs. 34 and 35 are then applied successively to layers 2 to m. The transfer function A_{mn} relating the displacements at the top of layers m and n is defined by

$$A_{mn}(\omega) = \frac{u_m}{u_n} = \frac{E_m + F_m}{E_n + F_n} \qquad (39)$$

The velocity $\dot{u}(z,t)$ and acceleration $\ddot{u}(z,t)$ are related to displacement through:

$$\dot{u}(z,t) = \frac{\partial u}{\partial t} = i\omega u(z,t)$$

$$\ddot{u}(z,t) = \frac{\partial^2 u}{\partial t^2} = -\omega^2 u(z,t) \qquad (40)$$

Therefore A_{mn} is also the transfer function relating the velocities and displacements at the top of layers m and n:

$$A_{mn}(\omega) = \frac{u_m}{u_n} = \frac{\dot{u}_m}{\dot{u}_n} = \frac{\ddot{u}_m}{\ddot{u}_n} = \frac{E_m + F_m}{E_n + F_n} \qquad (41)$$

The shear strain at depth z and time t can be derived from Eq. 25:

$$\gamma(z,t) = \frac{\partial u}{\partial t} = ik^* G^* \left(Ee^{ik^* z} + Fe^{-ik^* z}\right) e^{i\omega t} \qquad (42)$$

The corresponding shear stress at depth z and time t is:

$$\tau(z,t) = G^* \gamma(z,t) \qquad (43)$$

A5.3.1 Free surface, bedrock outcropping and rock outcropping motions

Figure A5.5 defines four terms used in site response analysis. The *free surface motion* is the motion at the surface of a soil deposit. The *bedrock motion* is the motion at the base of the soil deposit. The *rock outcropping motion* is the motion at a location where bedrock is exposed at the ground surface.

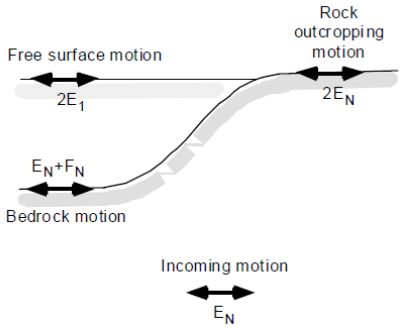

Figure A5.5. Terminology used in site response analysis.

As shown in Figure A5.5, the incoming shear wave that propagates vertically upward has for amplitude E_N through the bedrock. The bedrock motion has for amplitude $E_N + F_N$ at the top of the bedrock under the soil layers. The bedrock outcropping motion is $2E_N$, because there is no shear stress (i.e., $E_N = F_N$) on free surfaces. Therefore the transfer function relating the bedrock motion and bedrock outcropping motion is:

$$A_{NN}(\omega) = \frac{2E_N}{E_N + F_N} \qquad (44)$$

When it is assumed that $E_N = F_N = 1$ on free surface, then the transfer function relating the free surface motion and rock outcropping motion is:

$$A'_{1N}(\omega) = \frac{1}{E_N} \qquad (45)$$

A5.3.2 Transient Motions

The theory above for the one-dimensional soil column response was presented for steady state harmonic motions, i.e., in the frequency domain. It can be extended to the time histories of transient motions using Fourier series. A real-valued or complex-valued function $x(t)$ can be approximated by a discrete series of N values as follows:

$$x_n = \sum_{k=0}^{N-1} X_k e^{i\omega_k t_n} = \sum_{k=0}^{N-1} X_k e^{i\omega_k n\Delta t} = \sum_{k=0}^{N-1} X_k e^{2\pi ikn/N} \quad n = 0, \dots, N-1 \qquad (46)$$

The values x_n correspond to times $t_n = n\Delta t$ where Δt is the constant time interval (i.e., $x(n\Delta t) = x_n$ for $n = 0, \dots, N-1$). The discrete frequencies ω_k are:

$$\omega_k = 2\pi \frac{k}{N\,\Delta t} \quad k = 0, \dots, N-1 \qquad (47)$$

The Fourier components are:

$$X_m = \frac{1}{N} \sum_{k=0}^{N-1} x_n e^{-2\pi ikn/N} \quad m = 0, \dots, N-1 \qquad (48)$$

The coefficients X_m are calculated by the Fast Fourier Transform algorithm. The number of operations scales as $N\ logN$, which justifies the name of Fast Fourier Transform (i.e., FFT).

A5.3.3 Iterative Approximation of Equivalent Linear Response

As previously described, the equivalent linear model assumes that the shear modulus and damping ratio are functions of shear strain amplitude. In SHAKE, the values of shear modulus and damping ratio are determined by iterations so that they become consistent with the level of strain induced in each layer. As shown in Figure A5.6, the values of G_0 and ξ_0 are initialized at their small strain

values, and the maximum shear strain γ_{max} and effective shear strain γ_{eff1} are calculated. Then the compatible values G_1 and ξ_1 corresponding to γ_{eff}^1 are found for the next iteration. The equivalent linear analysis is repeated with new values of G and ξ until the values of G and ξ are compatible with the strain induced in all layers.

The iteration procedure for equivalent linear approach in each layer is as follows:

1. Initialize the values of G^i and ξ^i at their small strain values.
2. Compute the ground response, and get the amplitudes of maximum shear strain γ_{max} from the time histories of shear strain in each layer.
3. Determine the effective shear strain γ_{eff} from γ_{max}:

$$\gamma_{eff}^i = R_\gamma \gamma_{max}^i \qquad (49)$$

where R_γ is the ratio of the effective shear strain to maximum shear strain, which depends on the earthquake magnitude. R_γ is specified in input; it accounts for the number of cycles during earthquakes. R_γ is the same for all layers.

4. Calculate the new equivalent linear values G^{i+1} and ξ^{i+1} corresponding to the effective shear strain γ_{eff}.
5. Repeat steps 2 to 4 until the differences between the computed values of shear modulus and damping ratio in two successive iterations fall below some predetermined value in all layers.

Generally 8 iterations are sufficient to achieve convergence.

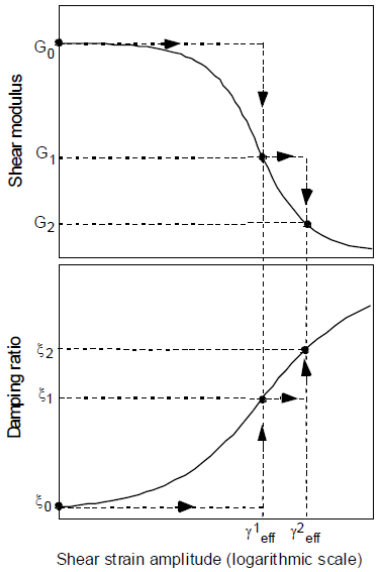

Figure A5.6. Iteration of shear modulus and damping ratio with shear strain in equivalent linear analysis.

Appendix 6

Samoclevo results

EARTHQUAKE 1

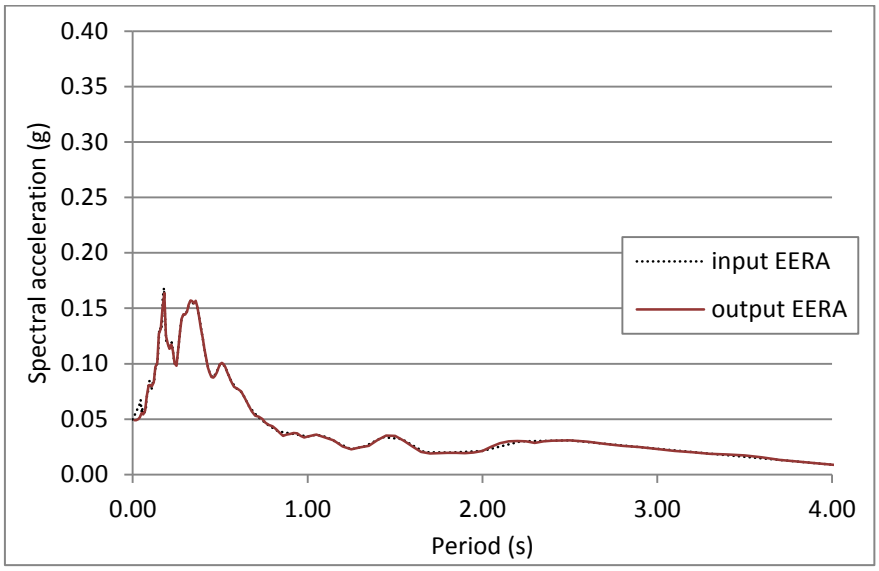

Figure A6.1. Comparison between EERA input and output spectra.

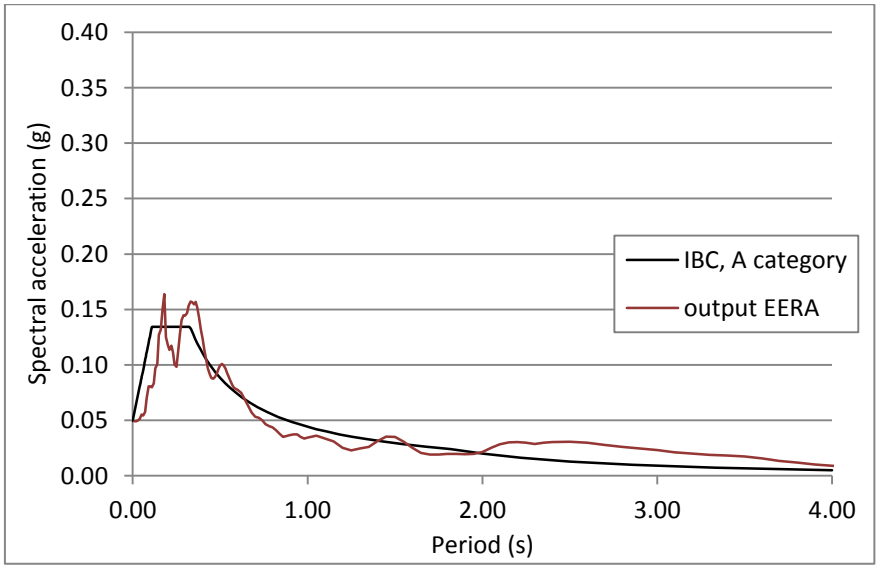

Figure A6.2. Comparison between the spectra determined with EERA and according to the Italian building code.

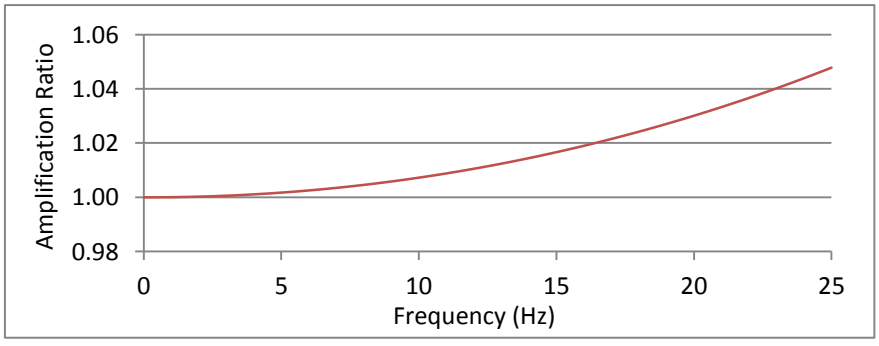

Figure A6.3. Amplification ratio function.

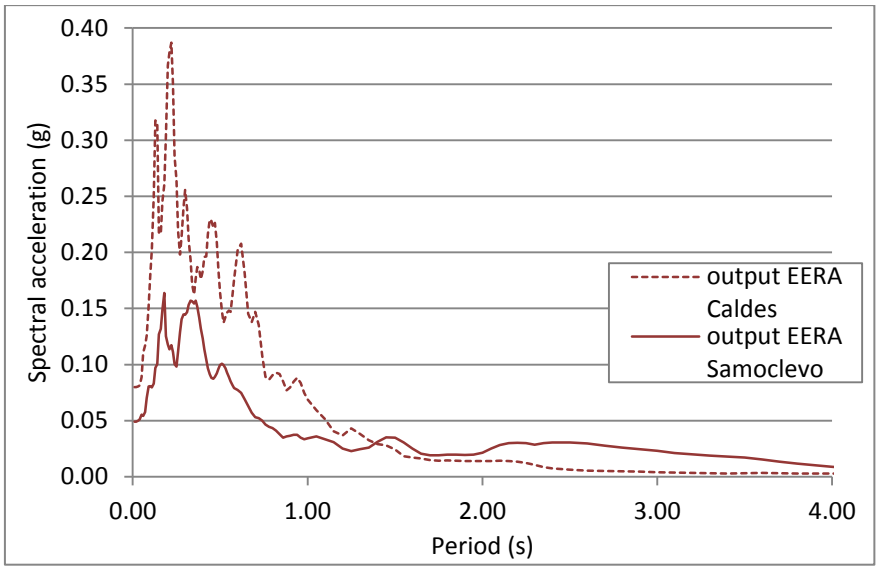

Figure A6.4. Comparison between the spectra of Caldes and Samoclevo sites.

EARTHQUAKE 2

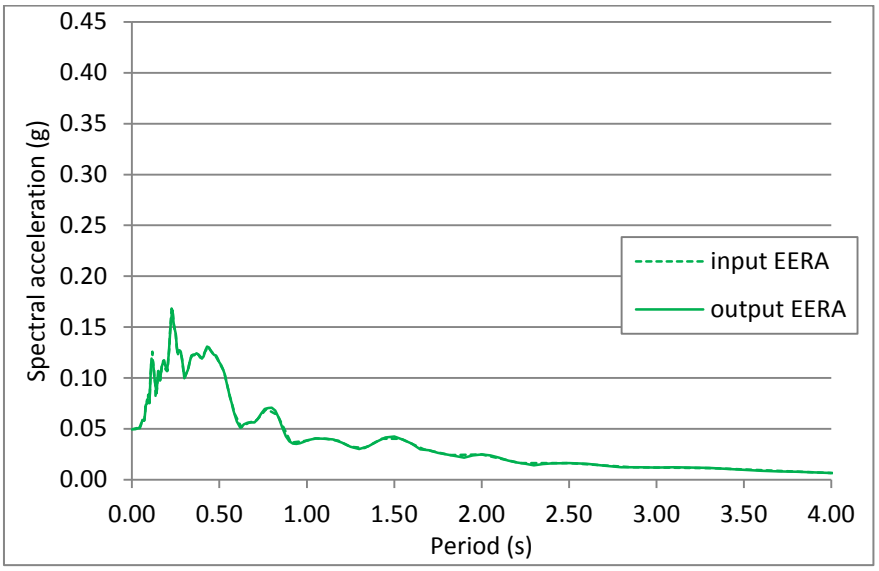

Figure A6.5. Comparison between EERA input and output spectra.

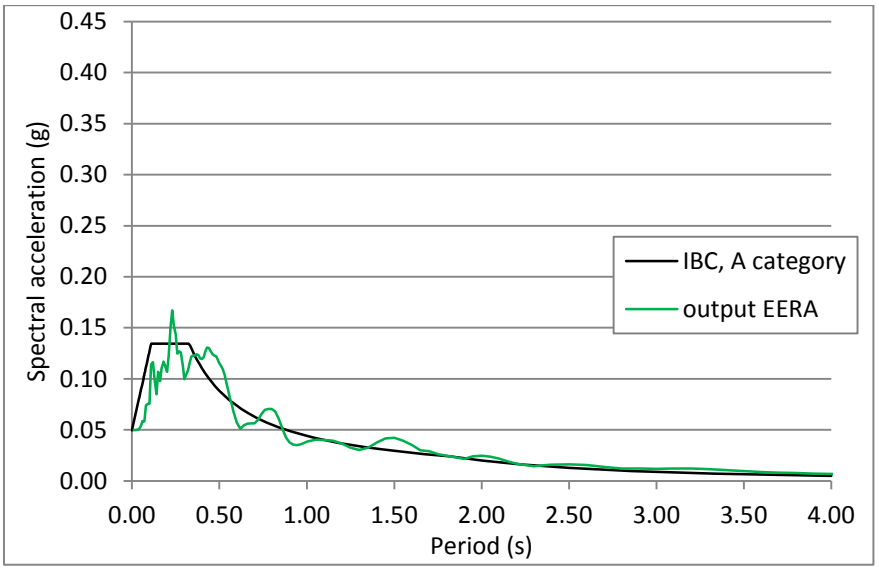

Figure A6.6. Comparison between the spectra determined with EERA and according to the Italian building code.

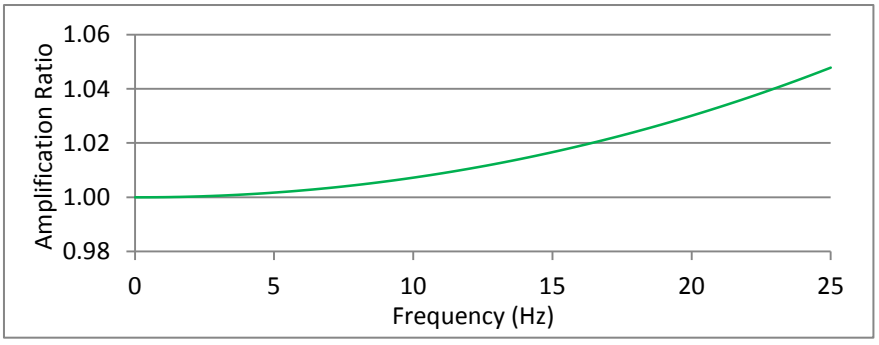

Figure A6.7. Amplification ratio function.

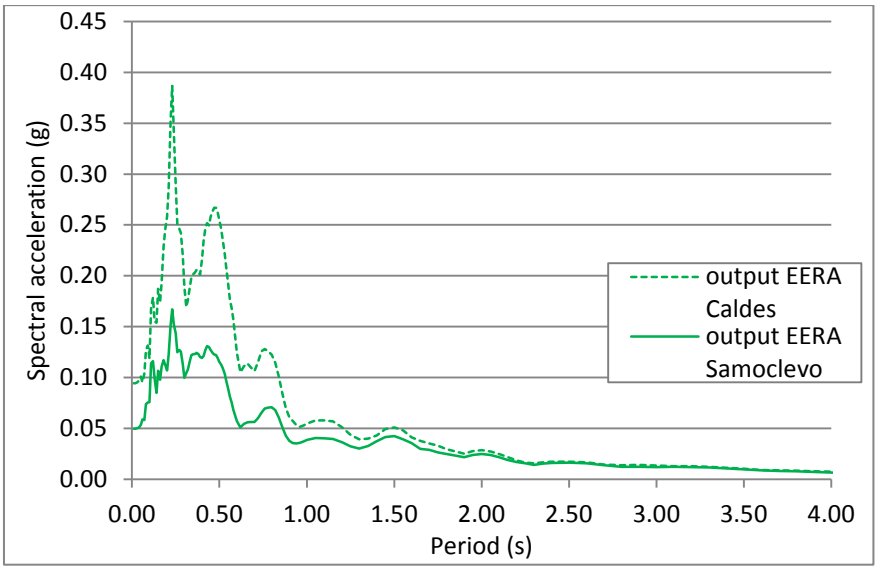

Figure A6.8. Comparison between the spectra of Caldes and Samoclevo sites.

EARTHQUAKE 3

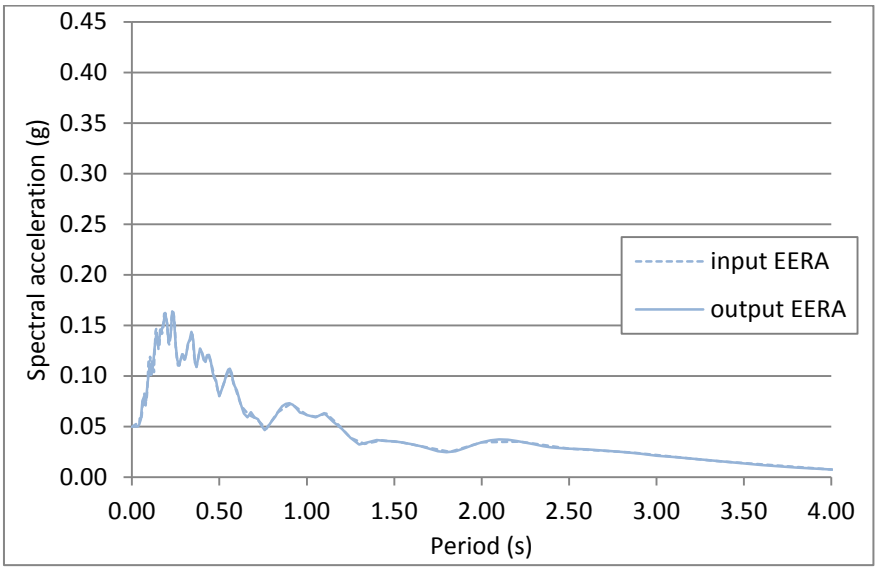

Figure A6.9. Comparison between EERA input and output spectra.

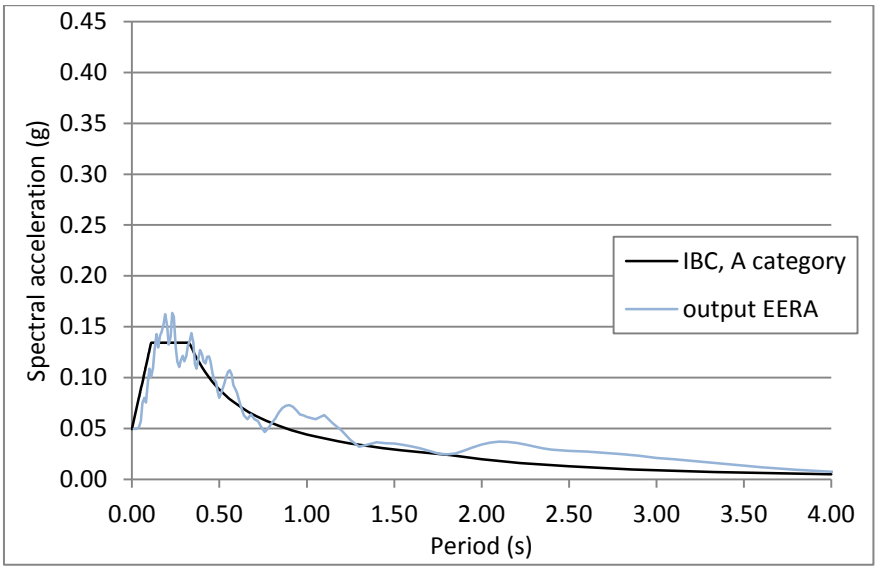

Figure A6.10. Comparison between the spectra determined with EERA and according to the Italian building code.

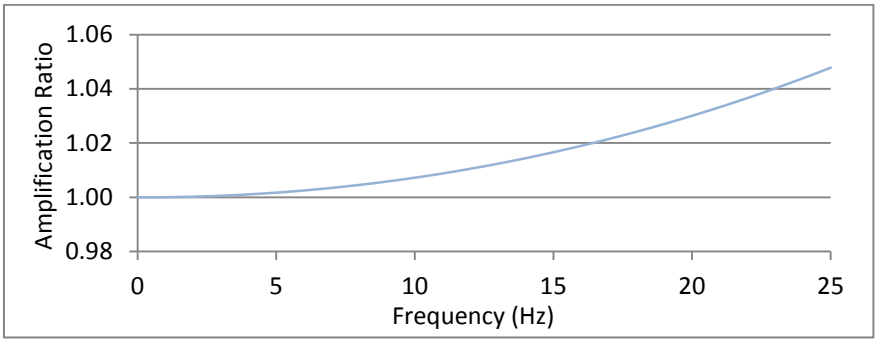

Figure A6.11. Amplification ratio function.

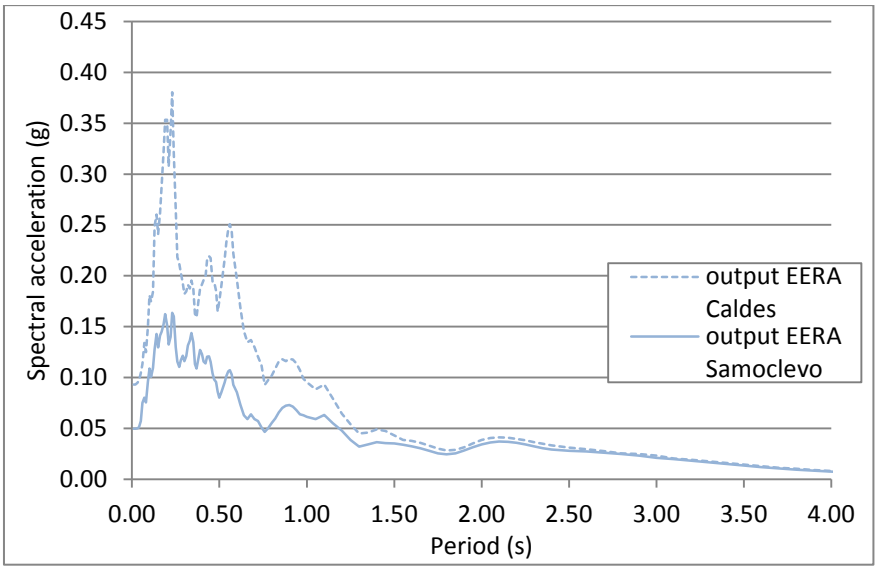

Figure A6.12. Comparison between the spectra of Caldes and Samoclevo sites.

EARTHQUAKE 4

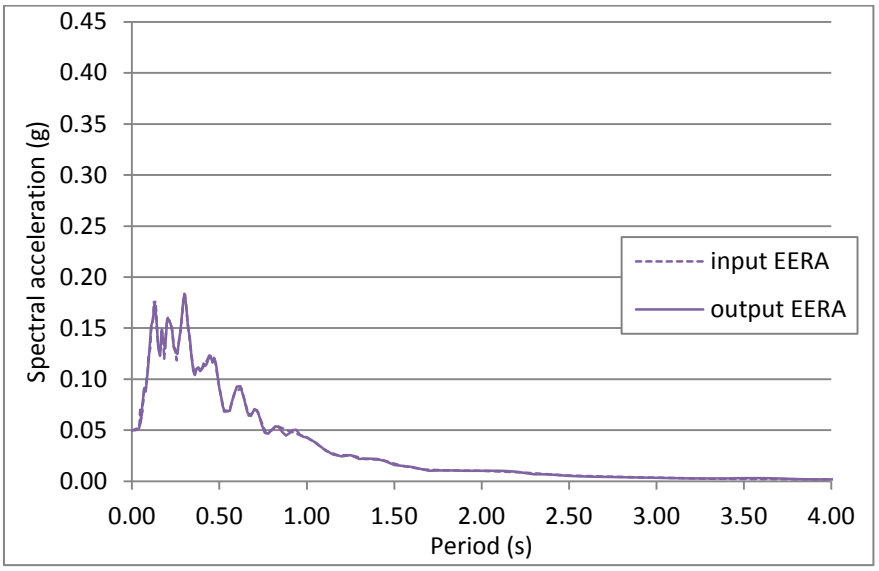

Figure A6.13. Comparison between EERA input and output spectra.

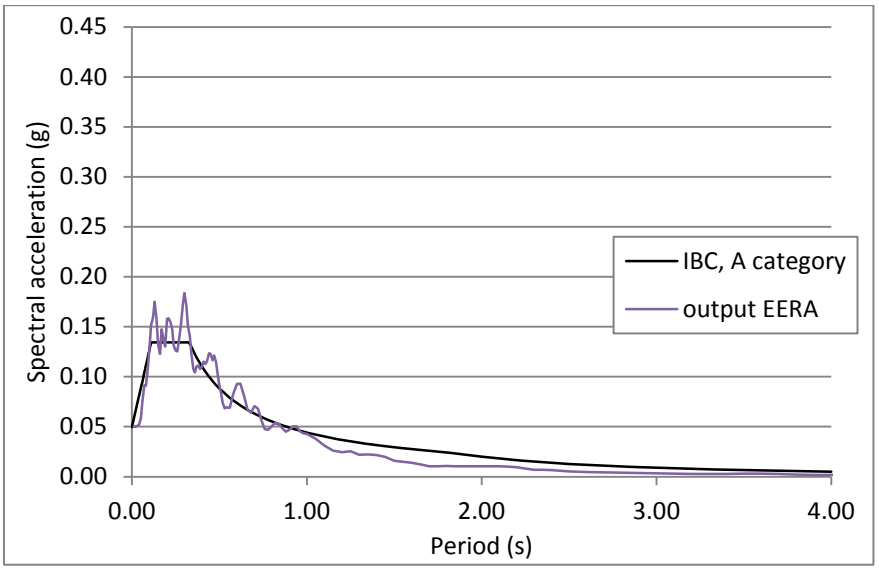

Figure A6.14. Comparison between the spectra determined with EERA and according to the Italian building code.

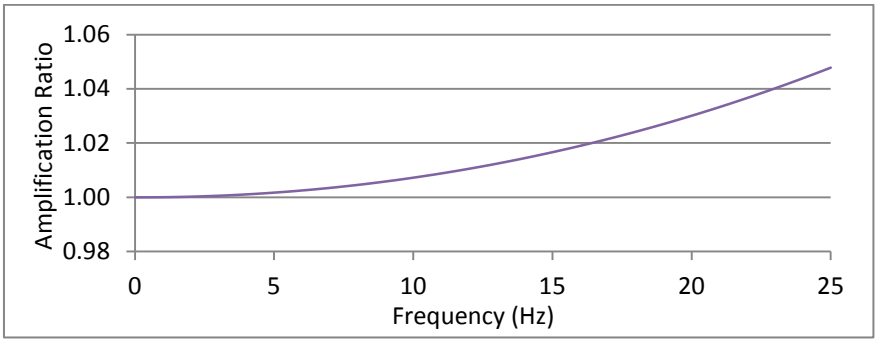

Figure A6.15. Amplification ratio function.

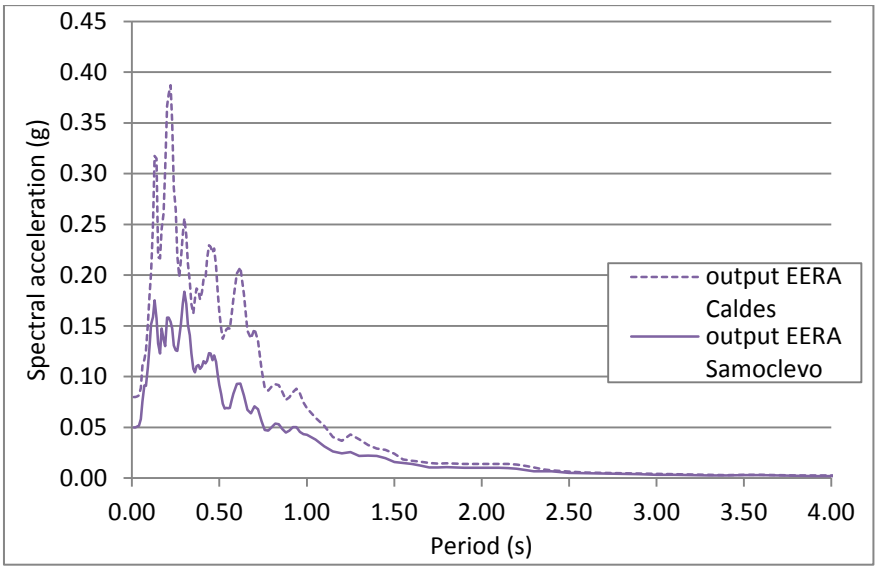

Figure A6.16. Comparison between the spectra of Caldes and Samoclevo sites.

EARTHQUAKE 5

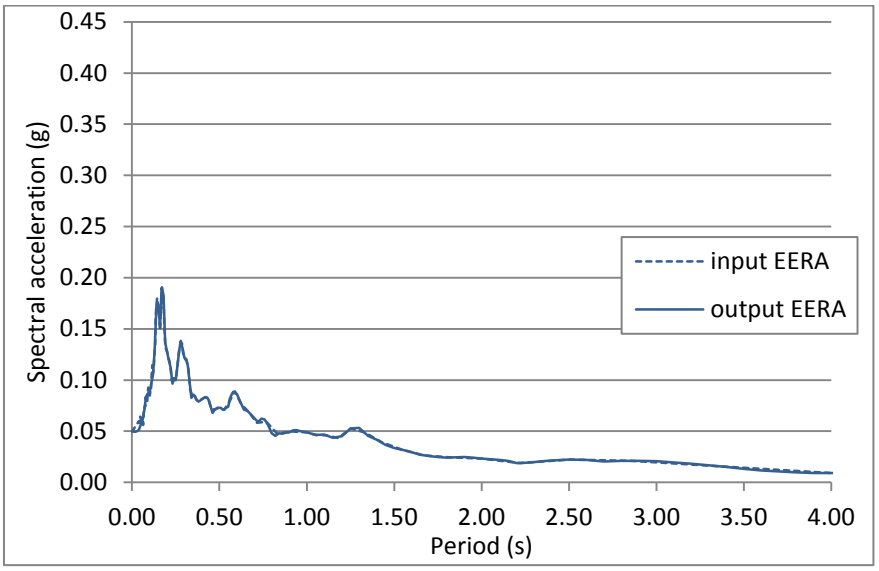

Figure A6.17. Comparison between EERA input and output spectra.

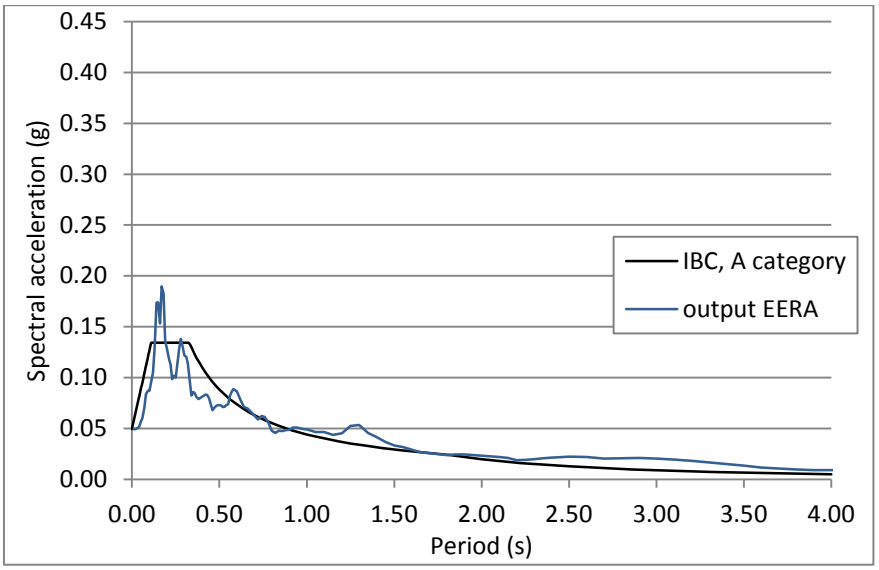

Figure A6.18. Comparison between the spectra determined with EERA and according to the Italian building code.

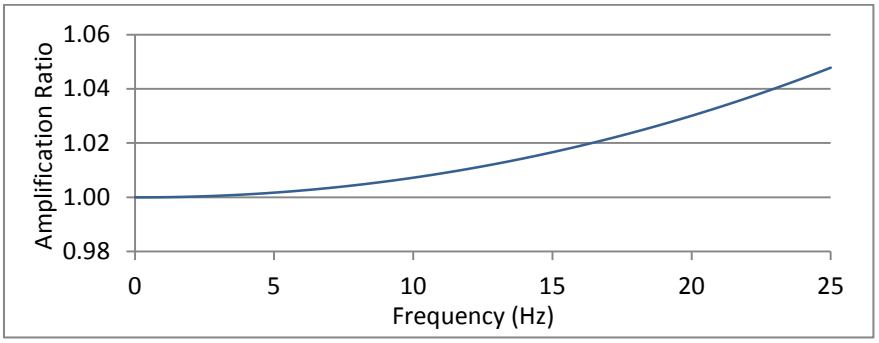

Figure A6.19. Amplification ratio function.

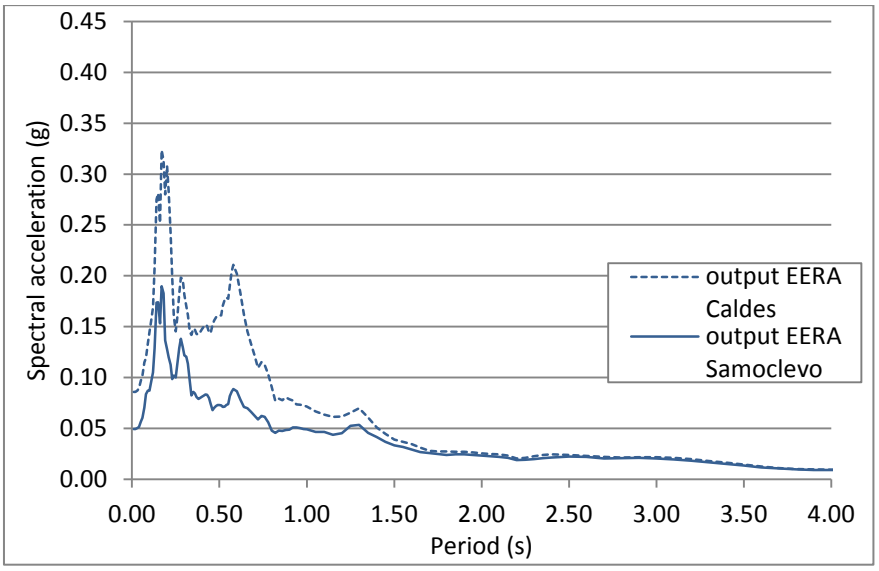

Figure A6.20. Comparison between the spectra of Caldes and Samoclevo sites.

EARTHQUAKE 6

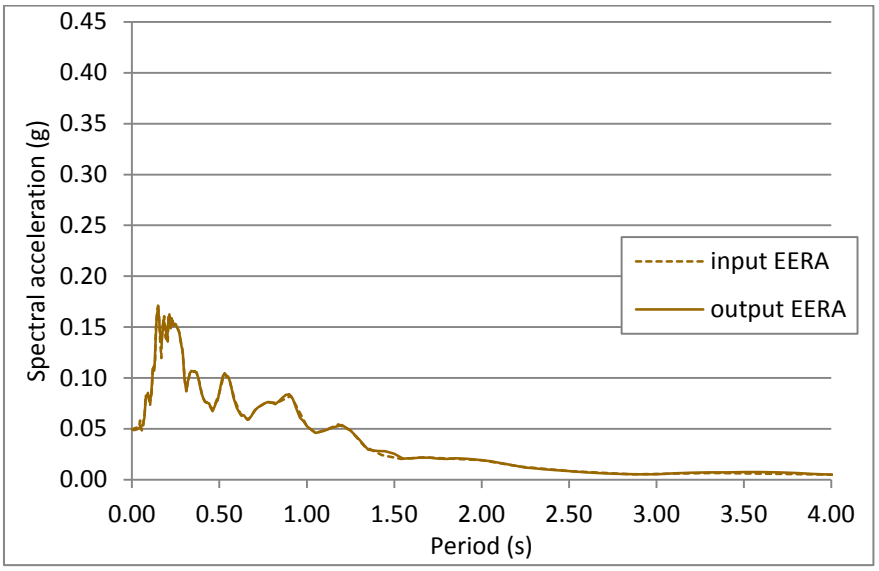

Figure A6.21. Comparison between EERA input and output spectra.

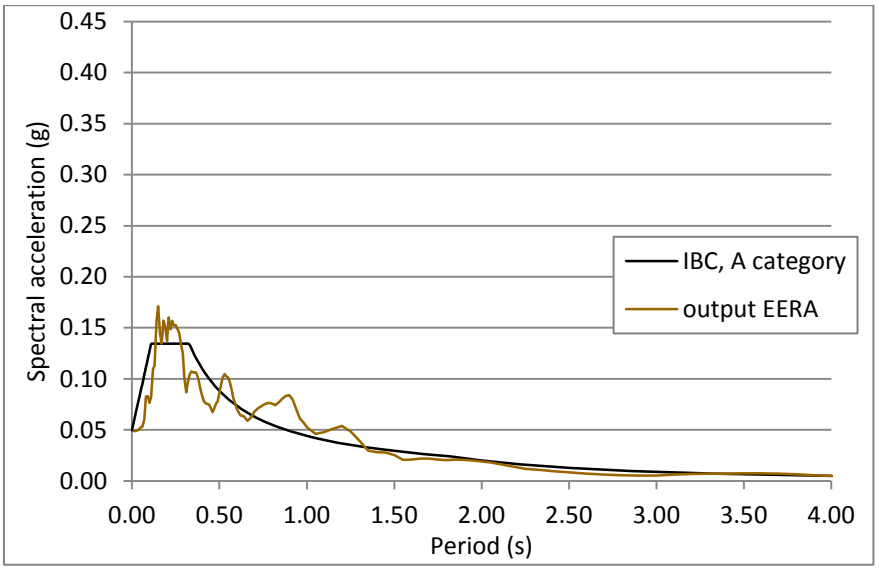

Figure A6.22. Comparison between the spectra determined with EERA and according to the Italian building code.

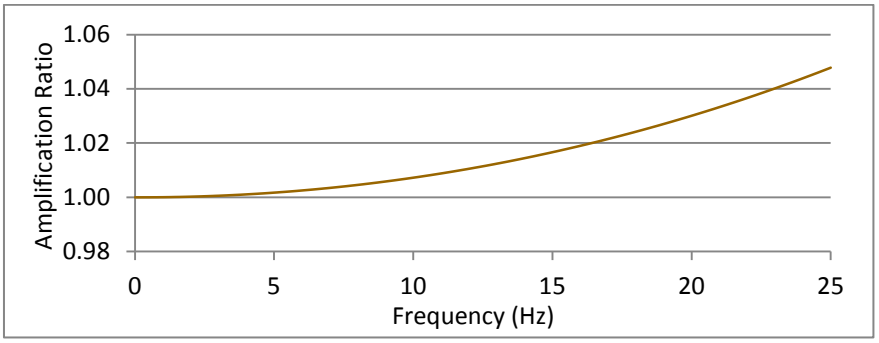

Figure A6.23. Amplification ratio function.

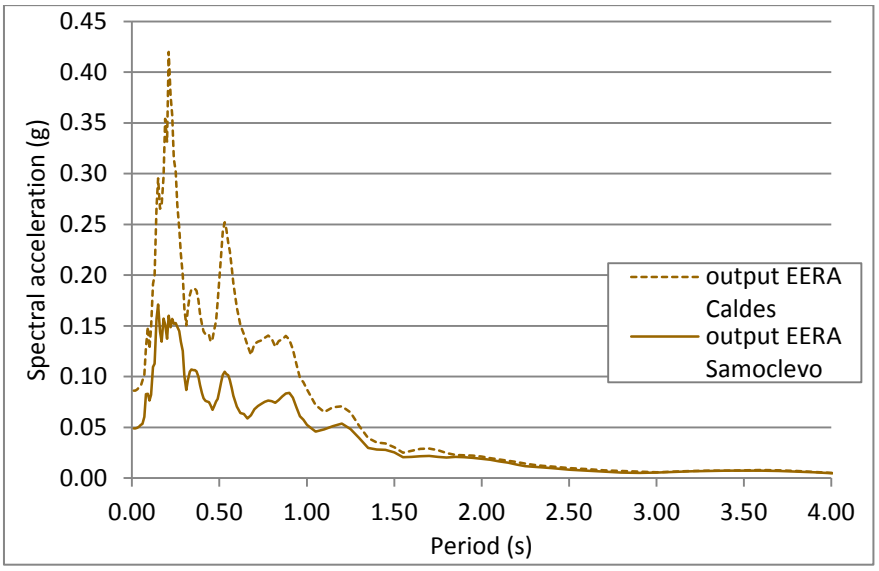

Figure A6.24. Comparison between the spectra of Caldes and Samoclevo sites.

EARTHQUAKE 7

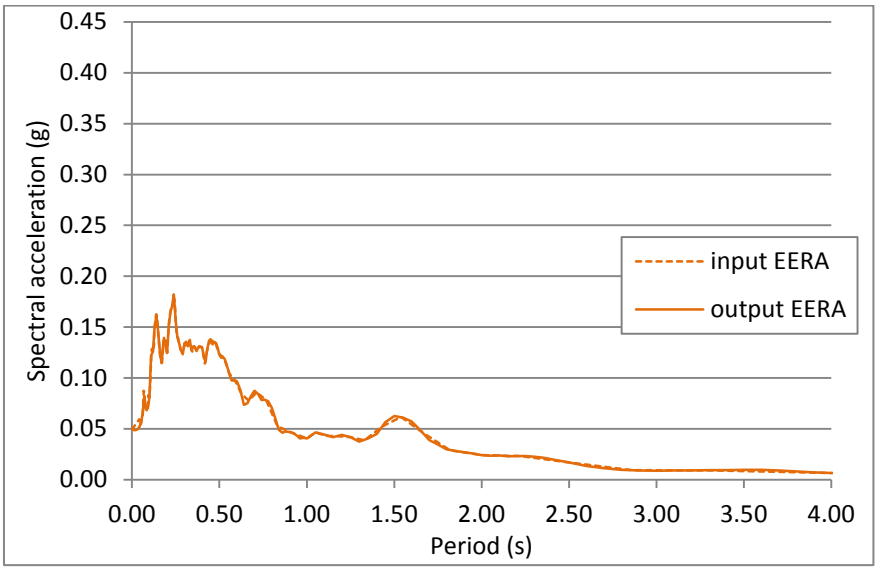

Figure A6.25. Comparison between EERA input and output spectra.

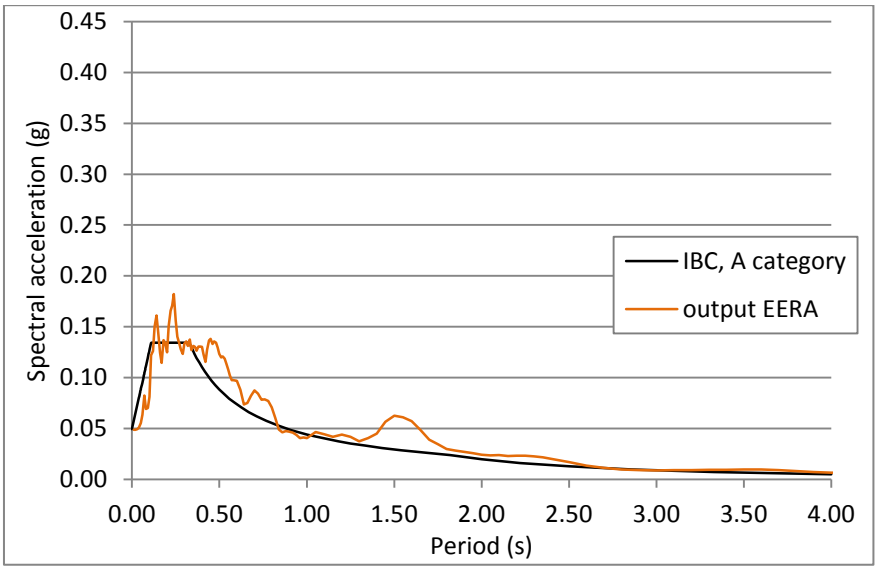

Figure A6.26. Comparison between the spectra determined with EERA and according to the Italian building code.

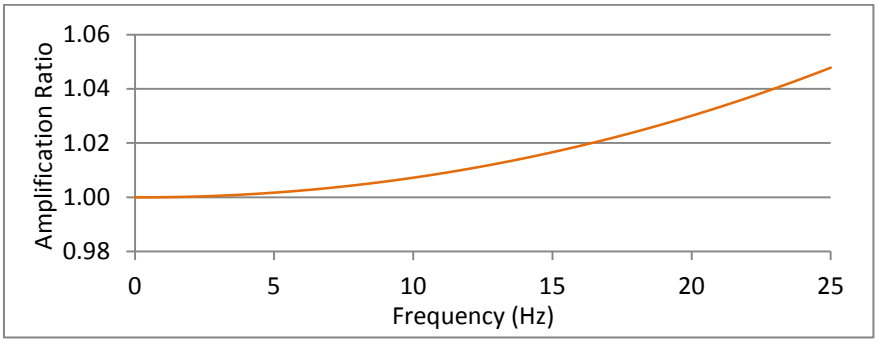

Figure A6.27. Amplification ratio function.

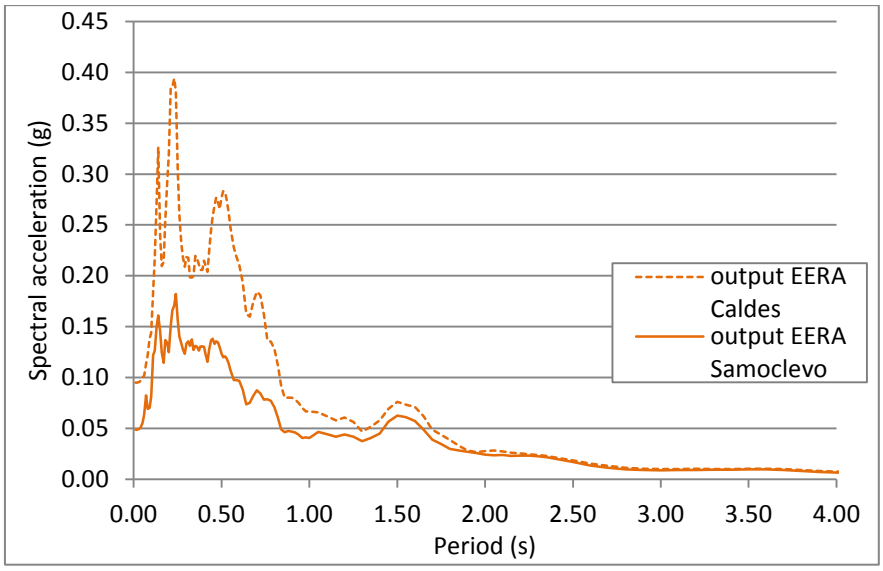

Figure A6.28. Comparison between the spectra of Caldes and Samoclevo sites.

MERANO EARTHQUAKE

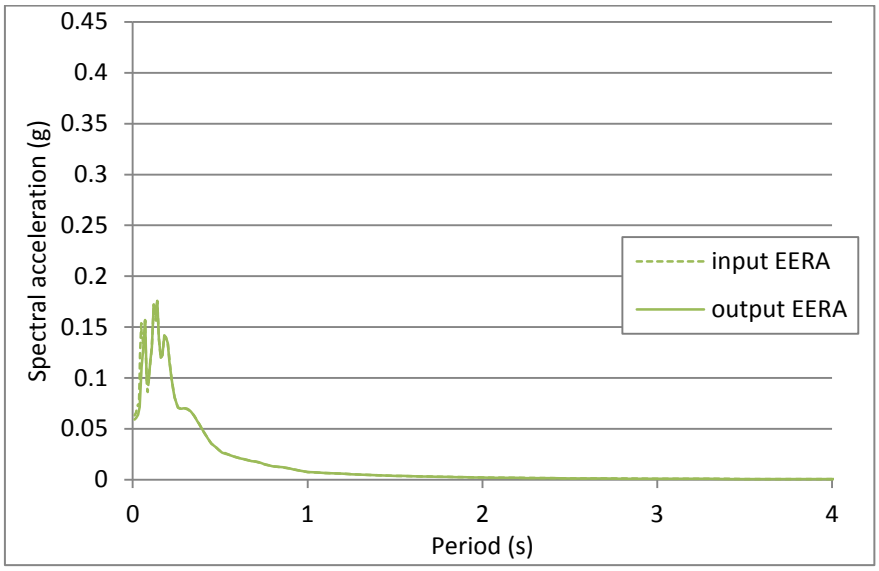

Figure A6.29. Comparison between EERA input and output spectra.

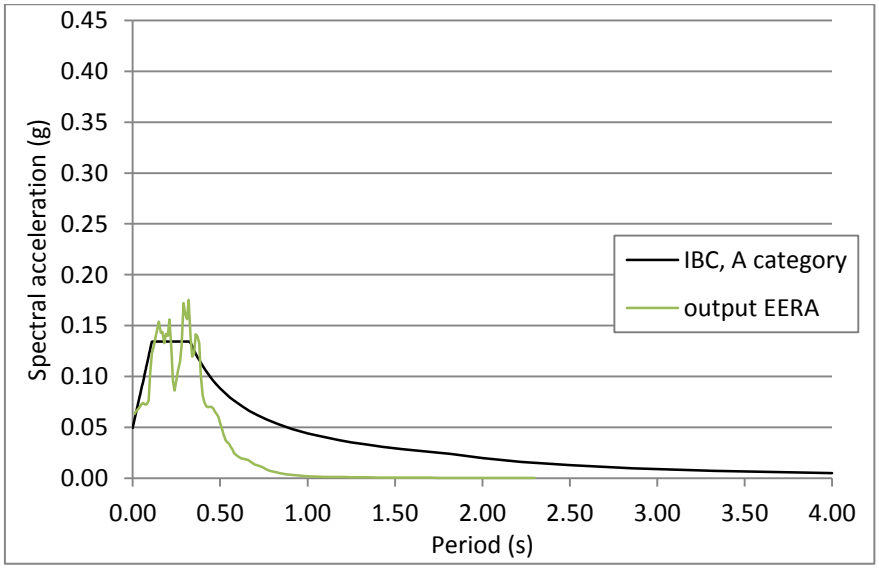

Figure A6.30. Comparison between the spectra determined with EERA and according to the Italian building code.

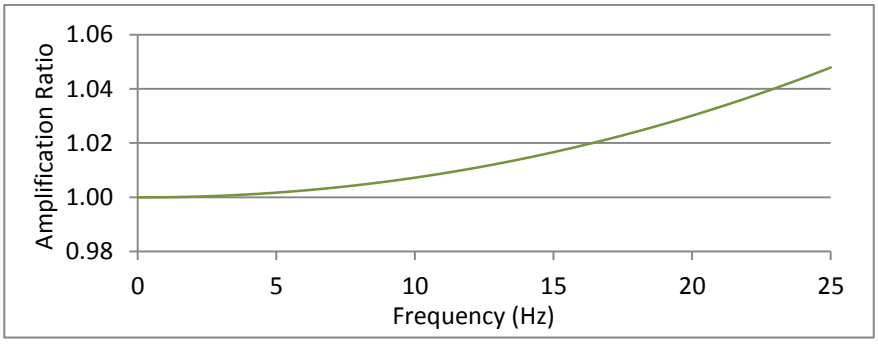

Figure A6.31. Amplification ratio function.

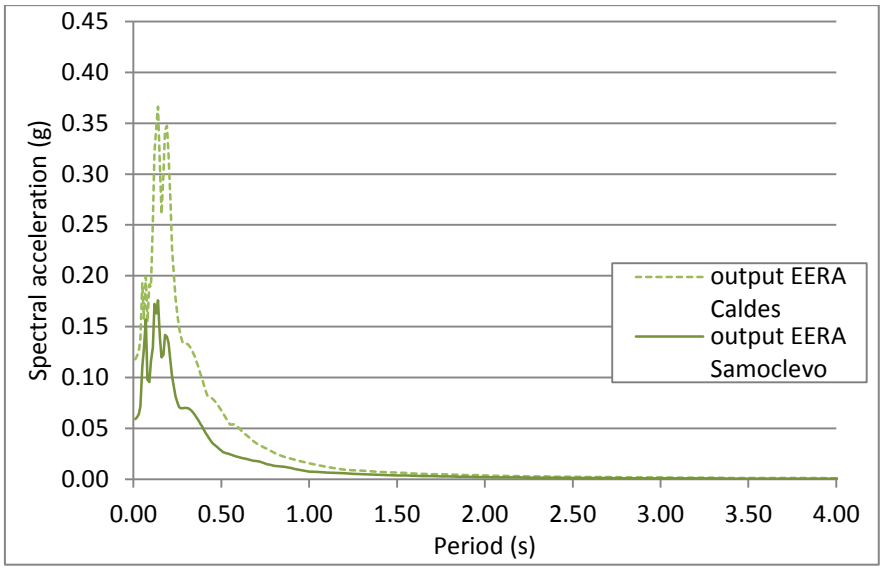

Figure A6.32. Comparison between the spectra of Caldes and Samoclevo sites.

Appendix 7

QUAD4M code basics

A7.1 Introduction

The finite element method of analysis is a widely used computational procedure for the solution of problems in continuum mechanics, as well as many other fields. The procedure has been found very powerful for modeling the seismic response of soli deposits and earth structures. Programs to solve such response have been written using time domain solutions as well as frequency domain solutions.

QUAD4 (Idriss, Lysmer, Hwang, and Seed, 1973) was written as a two-dimensional, time domain solution to dynamic response. It incorporated for the first time independent damping in each element in the continuum. QUAD4M incorporates into QUAD4 a transmitting base so that the half-space beneath a mesh can be modeled and the need to assume a rigid foundation can be eliminated. The shear and compression wave velocities and the unit weight for the material underlying the mesh can be entered, and the response of the mesh on top of that half-space can now be modeled with greater accuracy. In addition, seismic coefficients have been added in this version of the program. This feature is particularly useful in the formation analyses. The program also has a restart capability. This feature is useful for changing material properties during the shaking event. Finally, QUAD4M incorporates a new method for the formulation of damping matrices which results in a significant reduction of the damping of higher frequencies commonly associated with the use of a Rayleigh formulation.

A7.2 Evaluation of the seismic response using the finite element procedure

It consists of numerically modeling a continuum with a finite number of elements interconnected at their common nodes. The finite element procedure uses a system of equation represented in matrix form as:

$$[M]\underline{\ddot{u}} + [C]\underline{\dot{u}} + [K]\underline{u} = \underline{R} \tag{1}$$

where:

[M] = mass matrix (in this case using the assumption of a lumped mass formulation);

[C] = damping matrix;

[K] = stiffness matrix;

R = load vector, which is given by: $\underline{R} = [M]\underline{\ddot{u}_g}$

$\underline{u}$ = relative displacement vector; and dots represent differentiation with respect to time;

$\underline{\ddot{u}_g}$ = outcrop acceleration.

The damping matrix is formulated using the assemblage of element damping matrices constructed using the Rayleigh formulation (1945):

$$[C]_q = \alpha_q[M]_q + \beta_q[K]_q \tag{2}$$

for each element q.

The values of α_q and β_q are chosen as described in the section on damping. The entire solution is iterated upon the number of times specified by the user, in order to obtain strain compatible damping and modulus values. To solve equation (1), it is necessary to introduce equations relating $\underline{u}$, $\underline{\dot{u}}$, and $\underline{\ddot{u}}$. The Newmark family of methods uses the following equation to fulfill the above requirement:

$$\underline{\dot{u}_N} = \underline{\dot{u}_{N-1}} + \Delta t\left[(1-\gamma)\underline{\ddot{u}_{N-1}} + \gamma\underline{\ddot{u}_N}\right]$$
$$\underline{u_N} = \underline{u_{N-1}} + \Delta t\underline{\dot{u}_{N-1}} + \frac{\Delta t^2}{2}\left[(1-2\beta)\underline{\ddot{u}_{N-1}} + 2\beta\underline{\ddot{u}_N}\right] \tag{3}$$

where N is the current time step (quantities unknown), and $N-1$ is the previous time step (quantities known). The use of equation (3) with $\gamma = 0{,}5$ and $\beta = 0{,}25$ is called the trapezoidal rule and provides a time-stepping algorithm with unconditional stability, quadratic convergence, and no numerical damping of any frequencies. Using the Trapezoidal rule the following equation are obtained for solving the displacement, velocity, and acceleration at each time step:

$$\underline{u_{N+1}} = [\bar{K}]^{-1}[\bar{R}]_{N+1} \tag{4a}$$

$$\underline{\ddot{u}_{N+1}} = \frac{4}{\Delta t^2}\left(\underline{u_{N+1}} - \underline{u_N}\right) - \frac{4}{\Delta t^2}\underline{\dot{u}_N} - \underline{\ddot{u}_N} \tag{4b}$$

$$\underline{\dot{u}_{N+1}} = \underline{u_N} \cdot \frac{\Delta t}{2}\left(\underline{\ddot{u}_N} + \underline{\ddot{u}_{N+1}}\right) \tag{4c}$$

$$[\bar{K}] = \frac{4}{\Delta t^2}[M] + \frac{2}{\Delta t}[C] + [K] \tag{4d}$$

(4e)

$$[\bar{R}]_{N+1} = [R]_{N+1} + [M]\underline{A_{N+1}} + [C]\underline{B_{N+1}} + [K]\alpha\underline{u_N}$$

$$\underline{A_{N+1}} = \frac{4}{\Delta t^2}\left(\underline{u_N} + \Delta t\underline{\dot{u}_N} + \frac{\Delta t^2}{4}\underline{\ddot{u}_N}\right) \quad (4f)$$

$$\underline{B_{N+1}} = \frac{2}{\Delta t}\underline{u_N} + \underline{\dot{u}_N} \quad (4g)$$

A7.3 Transmitting boundaries

In order for a two-dimensional finite mesh to represent the response of an infinite field condition, the artificial reflection of seismic waves from side boundaries, as well as from the underlying half-space, should be minimized. Lyzmer and Kuhlemyer (1969) introduced a simple procedure to accomplish this.

The implementation of these dampers involves adding damping at each of the nodes that make up the base and sides of the finite model. For the present study only the base dampers have been implemented. The base dampers are more essential to incorporate than the side dampers because the finite element system. Under consideration will always be placed over a half-space. The effects of side boundaries can be readily minimized by increasing the extent of the finite element mesh. To mathematically implement these dampers, the part of the applicable element matrices have the transmitting boundaries damping term added to the diagonal terms. This produces an adjustable force in the x and y direction proportional to the velocity of the specified nodes. The coefficients added onto the diagonal terms are obtained as:

$$Term\ for\ direction\ perpendicular\ to\ boundary: pV_pL$$

$$Term\ for\ direction\ parallel\ to\ boundary:\ pV_sL$$

The velocity of the P or S waves is used for the material in the half-space below the finite element model, as is the density ρ. the "tributary width" of the nodes, L is that length corresponding to half of the distance to the next node on both sides. When a transmitting base is used, the input motion is a function of the material properties of the half-space below the mesh, and the properties and the geometry of the mesh. This is the correct choice for a boundary condition when the input motion represents an outcrop acceleration, recorded at an outcrop of the half-space material. If an infinitely stiff $(V_S \rightarrow \infty)$ rock is specified under the underlying stratum, then the input motion will not be affected by the mesh above.

A7.4 Seismic coefficient computation

A seismic coefficient is the ratio of the force induced by an earthquake in a block of the mesh, over the weight of that block. The forces acting on the block are computed by multiplying the shear and normal stresses acting on an element by the width of that element. Since the surface of the block is specified as going through the nodes (between elements) in QUAD4M, the average stress is found between the elements on either side of the interface. The summation of forces acting on a block is computed as a function time. The seismic coefficient is then computed for each time step.

A7.5 Restart capability

A feature has been added in QUAD4M whereby at the conclusion of the calculations, the acceleration, velocity, and displacement of every node is saved. This can then be used to restart the program. Before the program is restarted, the soil properties can be changed.

A7.6 Damping

The damping matrix is formulated using the assemblage of element damping matrices constructed in this manner:

$$[C]_q = \alpha_q [M]_q - \beta_q (K)_q \tag{5}$$

For each element q. the use of Rayleigh damping is this manner results in a frequency dependent damping applied to the problem, with

$$\lambda_q = \frac{1}{2}\left(\frac{\alpha_q}{\omega} + \beta_q \times \omega\right) \tag{6}$$

The damping in soil is not frequency dependent. Therefore, the choice of $\alpha_q \; and \; \beta_q$ must be made that provides for damping values that have minimum variations over the range of frequencies of interest. In QUAD4M, the constants were chosen in such a way that the damping was minimized at the fundamental frequency of the entire finite element model ω_1. The justification for this is that the first mode of vibration has the highest participation factor of all the modes. Using this criterion, the values of $\alpha_q \; and \; \beta_q$ are chosen as follows for each element:

$$\alpha_q = \lambda_q \times \omega_1$$
$$\beta_q = \lambda_q \times \omega_1 \quad (7)$$

As is the case with all procedures that utilize a Rayleigh Damping formulation, the higher frequencies are
overdamped. Therefore, in QUAD4M, a new scheme for setting damping is employed. Instead of using a single frequency (the fundamental frequency of the model), and a slope (0 at the fundamental frequency of the model) to establish the constants in equation 6, two are used to establish these constants. One frequency is chosen at the fundamental frequency of the model, as in QUAD4. The second frequency is establish as:

$$\omega_2 = n\omega_1 \quad (8)$$

where n is an odd integer. This choice was guided by the response of a shear beam in which the frequencies of higher modes are odd multiples of the frequency of the fundamental mode of the beam. The parameter n is chosen such that:

$$n = closet\ odd\ integer\ greater\ than\ \omega_i/\omega_1 \quad (9)$$

where ω_i is the predominant frequency of the input earthquake motion. To set damping at two frequencies, the values of $\alpha_q\ and\ \beta_q$ are then given by the following expression for each element:

$$\alpha_q = 2\lambda_q \frac{\omega_1\omega_2}{\omega_1+\omega_2}$$
$$\beta_q = 2\lambda_q \frac{1}{\omega_1+\omega_2} \quad (10)$$

The use of this two-frequency scheme results in under-damping between $\omega_1\ and\ \omega_2$, and the over-damping outside that range. This scheme allows the model to respond to the predominant frequencies of the input motion without experiencing significant over-damping. The element damping ratios, λ_q , are chosen based upon the average strain developed in the element. The value of the ω_1, the fundamental frequency system, is internally calculated by solving system equation:

$$K\underline{\phi}^1 = \omega_1^2 M\underline{\phi}^1 \quad (11)$$

where the first mode shape is represented by ϕ^1.

A7.7 Implementation of finite element model

The finite element computational procedure described previously was implemented by modifying program QUAD4 as presented in Idriss, Lysmer, Hwang, and Seed (1973). The revisions consisted of changing the time-stopping algorithm, incorporating transmitting base elements, incorporating the calculation of seismic coefficients fir selected potential sliding blocks, adding restart capability, modifying the damping computation, and modifying some computational procedures. All other features of QUAD4 are still intact in the new program. The time stepping method was changed from the Wilson-θ method to the trapezoidal rule as described previously. The transmitting base elements ware incorporated as described above and the user must now specify the P and S wave velocities and the unit weight of the half-space below the base elements. Seismic coefficients can now be computed. The user specifies elements witting the block, and the nodes bounding the block. The restart feature is utilized by specifying a switch in the input file, and providing a file name to which the restart input file is recorded. the new damping scheme is controlled by specifying the predominant period of the input motion, obtained from the response spectrum. The output file records the two frequencies at which the damping is set.